Multiple-scale analysis of transport phenomena in porous media with biofilms

Yohan Davit

Université de Toulouse

THÈSE

En vue de l'obtention du

DOCTORAT DE L'UNIVERSITÉ DE TOULOUSE

Délivré par *l'Institut National Polytechnique de Toulouse*

Spécialité : *Hydrologie, Hydrochimie, Sol, Environnement*

Présentée et soutenue par *Yohan Davit*
Le *3 décembre 2010*

Sujet de la thèse :
Multiple-scale analysis of transport phenomena in porous media with biofilms

Analyse multi-échelles des phénomènes de transport dans des milieux poreux colonisés par des biofilms

---

JURY

B. Goyeau	Professeur d'Université, EM2C	Rapporteur
E. Paul	Professeur d'Université, LISBP	Rapporteur
M. Quintard	Directeur de Recherche, IMFT	Examinateur
S. Sauvage	Ingénieur de Recherche, ECOLAB	Examinateur
R. Escudié	Chargé de Recherche, LBE	Examinateur
F. Delay	Professeur d'Université, HYDRASA	Président du jury
M. Gerino	Professeur d'Université, ECOLAB	Directeur de thèse
G. Debenest	Maître de conférences, IMFT	Directeur de thèse

Ecole doctorale : *Sciences de l'Univers, de l'Environnement et de l'Espace*
Unités de recherche : *Institut de Mécanique des Fluides de Toulouse, ECOLAB*

Directeurs de Thèse : *G. Debenest, M. Gerino*

Yohan Davit: *Multiple-scale analysis of transport phenomena in porous media with biofilms,* Ph.D. thesis, © December 2010

ABSTRACT

This dissertation examines transport phenomena within porous media colonized by biofilms. These sessile communities of microbes can develop within subsurface soils or rocks, or the riverine hyporheic zone and can induce substantial modification to mass and momentum transport dynamics. Biofilms also extensively alter the chemical speciation within freshwater ecosystems, leading to the biodegradation of many pollutants. Consequently, such systems have received a considerable amount of attention from the ecological engineering point of view. Yet, research has been severely limited by our incapacity to (1) directly observe the microorganisms within real opaque porous structures and (2) assess for the complex multiple-scale behavior of the phenomena. This thesis presents theoretical and experimental breakthroughs that can be used to overcome these two difficulties.

An innovative strategy, based on X-ray computed microtomography, is devised to obtain three-dimensional images of the spatial distribution of biofilms within porous structures. This topological information can be used to study the response of the biological entity to various physical, chemical and biological parameters at the pore-scale. In addition, these images are obtained from relatively large volumes and, hence, can also be used to determine the influence of biofilms on the solute transport on a larger scale. For this purpose, the boundary-value-problems that describe the pore-scale mass transport are volume averaged to obtain homogenized Darcy-scale equations. Various models, along with their domains of validity, are presented in the cases of passive and reactive transport. This thesis uses the volume averaging technique, in conjunction with spatial moments analyses, to provide a comprehensive macrotransport theory as well as a thorough study of the relationship between the different models, especially between the two-equation and one-equation models. A non-standard average plus perturbation decomposition is also presented to obtain a one-equation model in the case of multiphasic transport with linear reaction rates. Eventually, the connection between the three-dimensional images and the theoretical multiple-scale analysis is established. This thesis also briefly illustrates how the permeability can be calculated numerically by solving the so-called closure problems from the three-dimensional X-ray images.

RÉSUMÉ

Cette thèse se propose d'examiner les phénomènes de transport dans des milieux poreux colonisés par des biofilms. Ces communautés sessiles se développent dans les sols ou les roches souterraines, ou dans la zone hyporhéique des rivières et peuvent influencer significativement le transport de masse et de quantité de mouvement. Les biofilms modifient également très largement la spéciation chimique des éléments présents dans le milieu, menant à la biodégradation de nombreux polluants. Par conséquent, ces systèmes ont reçu une attention considérable en ingénierie environnementale. Pourtant, la recherche dans ce domaine a été très fortement limitée par notre incapacité à (1) observer directement les microorganismes dans des milieux poreux opaques réels et (2) prendre en compte la complexité multi-échelles des différents phénomènes. Cette thèse présente des avancées théoriques et expérimentales permettant de surmonter ces deux difficultés.

Une nouvelle stratégie, basée sur la microtomographie à rayons X assistée par ordinateur, a été utilisée pour obtenir des images en trois dimensions de la distribution spatiale du biofilm dans la structure poreuse. Ces informations topologiques peuvent être utilisées pour étudier la réponse de l'entité biologique à différents paramètres physiques, chimiques et biologiques à l'échelle du pore. De plus, ces images sont obtenues sur des volumes relativement importants et peuvent donc être utilisées pour étudier l'influence du biofilm sur le transport de solutés à plus grande échelle. Pour cela, les problèmes aux conditions limites décrivant le transport de matière à l'échelle du pore peuvent être moyennés en volume pour obtenir des équations homogénéisées à l'échelle de Darcy. Différents modèles, ainsi que leurs domaines de validité, sont présentés dans les cas réactifs et non-réactifs. Cette thèse se base sur la technique de prise de moyenne volumique, en conjonction avec des analyses utilisant les moments spatiaux, pour présenter une théorie complète de transport macroscopique ainsi qu'une analyse détaillée des relations entre les différents modèles, tout particulièrement entre les modèles à une et deux équations. Une décomposition non standard en terme de moyenne plus perturbation est présentée dans le but d'obtenir un modèle à une équation dans le cas du transport multiphasique avec des taux de réactions linéaires en fonction de la concentration. Finalement, la connexion entre l'analyse théorique et l'imagerie en trois dimensions est établie. Cette thèse illustre aussi brièvement comment la perméabilité peut être calculée numériquement en résolvant des problèmes de fermeture à partir des images en trois dimensions.

REMERCIEMENTS

Ce travail s'est déroulé en grande partie à l'institut de mécanique des fluides de Toulouse (IMFT) dans le groupe d'étude des milieux poreux (GEMP), ainsi qu'au laboratoire d'écologie fonctionnelle de Toulouse (ECOLAB). J'ai également eu la chance de collaborer avec des chercheurs des universités de l'Oregon et du Montana. J'aimerais saluer tous ceux qui, de près ou de loin, ont participé à l'élaboration et à la réussite de ce projet.

En particulier, je tiens à remercier Michel Quintard, qui a été pour moi un modèle d'excellence dans bien des domaines. Il fait partie de ces quelques personnes qui ont marqué ma vie. Je n'oublierai pas les longues heures passées à griffonner des moyennes volumiques, à discuter de la vie ou à explorer les gouffres de l'Aveyron. Merci également à Guilhem et Brigitte Quintard pour leur amitié lors de ces week-end spéléo, qui je l'espère vont pouvoir continuer.

Je voudrais exprimer mes plus sincères remerciements à Gérald Debenest pour m'avoir toujours soutenu et pour avoir été parfait dans son rôle de directeur de thèse, surtout dans les moments difficiles. Gérald m'a permis de m'épanouir scientifiquement, m'a fait confiance et n'a pas hésité a m'envoyer aux quatres coins du monde. Merci!

I would like to thank Brian Wood for teaching me so much about science, for making my trips to Corvallis so amazing and, more than anything, for his friendship. I also want to emphasize how much I liked working with Gabriel Iltis, Ryan Armstrong, Dorthe Wildenschild, James Connolly and Robin Guerlach. I hope our collaborations will be long and fruitful. I was very lucky to work with such brilliant scientists. Toujours dans les collaborations, j'ai eu énormément de plaisir à travailler avec Yoan Pechaud et Etienne Paul au LISBP à l'INSA de Toulouse. Merci de m'avoir accueuilli dans votre laboratoire, et pour tous les échanges que l'on a pu avoir.

Je tiens à exprimer toute ma gratitude à Frédéric Delay, Benoît Goyeau, Etienne Paul, Renaud Escudié, Sabine Sauvage, Gérald Debenest, Michel Quintard et Magali Gerino, pour avoir accepté de faire partie de mon jury de thèse et d'évaluer mon travail.

Pour continuer, je vais faire un tour rapide de mes compagnons de route à ECOLAB et à l'IMFT. Un énorme merci à tous mes amis GEMPiens: Stéphanie Veran, Alexandre Lapene, Arnaud Pujol, Cyprien Soulaine, Yohann Le Gac, Marion Musielak, Florent Hénon, Clément Louriou, Antoine Mallet, Pelforth et Ian Billanou. Je tiens également à remercier Suzy Bernard, Marc Prat, Manuel Marcoux, Sylvie Lorthois, Rachid Ababou et Lionel Lefur parce-que c'est un véritable plaisir de les croiser tous les jours. Je salue également Sabine Sauvage, Karine Dedieu, Yvan Aspa, Frédéric Julien et Franck

Gilbert que j'ai eu le plaisir de cotoyer à ECOLAB. C'est aussi l'occasion de remercier tous mes amis et toute ma famille, qui ont participé à mon bien être en dehors du laboratoire, en particulier Julia, Philippe, Sophie, Mij et évidemment mon père, ma mère et Jean-Claude.

J'aimerais finir par la plus importante de tous, Janna. Merci pour ton amour, pour ta patience et pour ton soutien.

CONTENTS

Part I

MICROORGANISMS IN POROUS MEDIA: A COMPLEX AND HIGHLY HETEROGENEOUS FRAMEWORK

1

CONTEXT: BIODEGRADATION IN POROUS MEDIA

Freshwater is a key component to life in general, and to human beings in particular. Human activities already require a considerable amount of water and, obviously, the consumption has the tendency to increase with population growth. Unfortunately, unfrozen freshwater is relatively rare on Earth (about 1% of the total water) and the quantity of contaminants released within aquatic ecosystems is also positively correlated with human growth. Examples of one such pollution include:

- Agriculture which releases considerable quantities of organic and inorganic pollutants such as insecticides, herbicides, nitrates or phosphates.
- Chemicals, such as solvents, detergents, heavy metals, oils which are present on (unauthorized) dumping sites and can reach groundwater resources. For instance, a huge quantity of European and American used electronic devices end up in African countries [228, 185]. These are rarely treated and release considerable amounts of extremely toxic compounds (lead, mercury, arsenic and others). This electronic waste (e-waste) represents a significant pollution and is a direct threat to human health [102].
- Medications are found in high concentrations within freshwater ecosystems. For example, hormones present in birth-control pills, in particular estrogens, deeply affect fish leading to feminization and intersex species [136].

As a direct consequence, water resources management requires specific attention. Knowledge regarding the behavior of pollutants within these freshwater ecosystems has become a matter of utmost importance. The contaminated area, that is, the original pollution site and the area that has been polluted through transport phenomena must be clearly identified because they require special treatments. To this end, it is fundamental to

1. understand the principal processes that are involved in these transport phenomena. One may think of this pollution as toxic molecules flowing through rivers and lakes, but this is a very inaccurate picture. Freshwater is mostly hidden within soil and subsurface zones. The transport of pollutants through these geological formations involves complex phenomena including molecular diffusion, convection, sorption, heterogeneous reactions and dispersion.

2. design and optimize techniques for the removal of the pollutants. For example, organic pollutants can be degraded by a number of endogenous or exogenous microorganisms. This phenomenon, usually termed biodegradation, refers to the ability of microbes, especially bacteria, to modify the chemical speciation of the elements present in the medium. Minute organisms can break toxic compounds to produce different chemical species. When the resulting chemicals are inert or less toxic, the microbes can be directly used to purify the water. For example, petroleum oils, containing toxic aromatic compounds, can be degraded by hydrocarbonoclastic bacteria (HCB) [292]. On the other hand, the biodegradation can also produce extremely toxic compounds and this must be considered very carefully. For example, anaerobic biodegradation of perchloroethylene (PCE) can lead to a substantial production of trichloroethene (TCE), dichloroethene (DCE) and vinyl chloride (VC).

To succeed in this, the transport processes require a quantitative description in terms of mathematical modeling. Some basic approximations are often made in order to undertake this description of the transport processes. In this thesis, pollutants are treated as solutes. In essence, this means that they are always water-miscible, albeit slightly and that the significant processes, in terms of transport, are those associated with the miscible portion. For example, dense non-aqueous phase liquids (NAPLs) form persistent blobs, trapped within the porous media, that dissolve slowly into the water-phase. In addition, the solutes will be considered as tracers, potentially non-conservative. This means that the contaminant is present in relatively small concentrations and thus, does not significantly modify the density or the viscosity of the fluid. This is generally the case for a large proportion of pollutants (for example the NAPLs).

One also needs to characterize the aquifers themselves. For example, this can be performed using specific non-reactive tracers. This solute can be introduced within the aquatic medium, and breakthrough curves can be observed in wells spatially distributed around the initial introduction area. The information collected from these experiments can help in determining the direction of the flow and the general organization of the medium. However, proper interpretation of these data and theoretical development of models often require topological information on a lower scale. For example, X-ray computed microtomography can been used for this purpose, that is, one can obtain a 3-D image of the porous structure at the microscale for a relatively large volume.

The remainder of this part is organized as follows. First, we introduce the concept of biofilm. This section, without being fully exhaustive, provides an up-to-date description of the biological entity and an overview of the fundamental principles regarding the biofilm mode of growth. Secondly, we describe the significance of biofilms in the context of porous media and particularly focus on the multiscale analysis of such media. Finally, we describe the scope of this thesis, the global strategy and develop its structure.

2

BIOFILMS

2.1 A BIT OF HISTORY

Microorganisms have been known to exist for centuries and yet, these are still triggering our scientific minds. Antoni van Leeuwenhoek (1632-1723) Fig (1a) was the first to directly observe microbes through a homemade microscope Fig (1b). In 1674, he describes, in letters to the Royal Society, the freshwater alga *Spirogyra*, and various ciliated protozoa. In 1676, following the same line, he discusses the behavior of diverse "little animals by him observed in rain-well-sea and snow-water" [157]. He also analyzed plaque bacteria collected from the surface of his teeth, in 1683. These were the first insights into the world of microbes, and the first rebuttals against the theory of spontaneous generation, synthesized by Aristotle and ultimately dismantled by Louis Pasteur's experiments in the 19th century. Antoni van Leeuwenhoek is now widely referred to as the father of microbiology and bacteriology for his contribution to our collective knowledge in these branches of science.

Global interest in microorganisms started later on, in the 19th century, in the "fetid fever hospitals of Europe in the mid-1880s [...] when millions were dying of plague and children were suffocating with diphtheria" [60]. In these morbid times, the science of microbes imposed itself as a necessity and research focused on methodical eradication more than on a general understanding of their behavior. Specific rules, known as Koch's postulates, were devised to establish a systematic causal connection between a given microbe and a disease. The picture that one may formerly have had of microbes was probably quite simple: weird shaped, free-floating minute organisms that need to be eradicated.

One must wait until late 1920's to early 1930's to get a glimpse of the actual complexity and intricacy of these microorganisms. Pioneering works by Hilen [127], Hentschel [126], Thomasson [253], Zobell [296], Winogradsky [281], Cholodny [50], Conn [56] and Henrici [125] showed that microbes can grow together attached on surfaces. They also noticed that, when attached, they seem to differ from their free-floating planktonic form. Hilen (1923) described "slimes on ships", Hentschel (1925) and Thomasson (1925) reported algae and diatoms behaviors on surfaces. The work undertaken by Zobell to describe sessile communities of bacteria was the real first step toward a comprehensive description of their collective behavior on surfaces. His

(a) (b)

Figure 1: (a) Antoni van Leeuwenhoek (1632-1723) and (b) Leeuwenhoek's microscope.

contributions are detailed by Hilary M. Lappin-Scott in [152]. At the same time, engineers in wastewater treatment also realized that most of the microorganisms that removed organic pollutants from water formed "slime" but also that, interestingly, mixed species "show an obvious virility by far superior to that of pure culture" [15]. While the use of the word "virility" is opened to debate, the idea that these communities were in fact complex interacting consortia of microorganisms is a reality that started to be encountered. After marine and freshwater organisms, the microbes of the dental plaque have also received a lot of early attention [110, 60, 26, 267]. In the 1980s, the "slime" concept was put forth with the work by Characklis in [42] and by Costerton in [132]. Characklis showed that "cities of microbes" colonizing surfaces are extremely tenacious and resistant to biocides. Along this path, Geesey et al. in [106] proved that most of the microorganisms in rivers live attached on rocks and Costerton [132] unified the different researches. He proposed a comprehensive "biofilm" framework regarding the ability of microbes to adhere to surfaces and the advantages of this ecological niche. Nowadays, biofilms have been shown to be extremely versatile and found virtually everywhere a minimal amount of water and nutrients is available, from your shower head to Yellowstone's springs.

Further understanding of these sessile communities has come with two major technical breakthroughs within the last decades:

- Knowledge regarding biofilms architecture has considerably improved with the arrival of 3-D optical sectioning [155], that is, confocal laser scanning microscopy (*CLSM is a depth selective microscopy technique, that can be used to obtain three-dimensional information within non-opaque biological specimens, by scanning the medium point-by-point and then reconstructing it with a computer*). Previously, most studies used light microscopy to resolve spatially cells embedded into a sticky matrix, which was still a fuzzy concept. Unfortunately, biofilm examinations based on light micrographs were found to be of limited use because of their resolution and the two-dimensional projection

analysis. Some early attempts were performed using transmission electron microscopy (TEM) and scanning electron microscopy (SEM) but the matrix was severely affected by the process leading to dehydration artifacts [60, 156]. Nowadays, significant improvements have been made regarding the preparation of biofilms samples, for example using environmental scanning electron microscopy, but CLSM remains the preferred technique, probably because it captures a three-dimensional information and can measure a relatively large volume.

- The development of molecular biology, proteomics and gene-sequence-based analysis has also revolutionized our understanding of biofilms at the molecular level. For example, various genes associated with the expression of the biofilm phenotype can be functionally identified. In addition, microbes can be forced to express a variety of exogenous proteins, through the incorporation of a specific plasmid, to trigger different behaviors, or to improve imaging, for example, using green fluorescent proteins (GFPs) [25, 214, 146].

All this collected information has lead to the realization that biofilms have a huge sanitary, ecological and economic impact. Effects can be desirable (wastewater processes, bioremediation, industrial and drinking water treatment, sequestration of CO_2) or undesirable and, potentially, harmful (paper manufacture, contamination in the food industry, medical infections, diseases, sustainability of water supply networks, microbially influenced corrosion (MIC) in pipelines, within heat exchangers or on ships). The following are examples:

- Biofilms are responsible for approximately 65% of infections treated in the developed world [117].
- 20% of corrosion inside heat exchangers is generated or influenced by biofilms [99]. MIC can generate deeper corrosion and faster propagation than other abiotic causes. In the United States, the daily cost of nuclear plants being idled for maintenance of MIC within pipes is estimated at a million dollar a day [34, 162].
- More than 99% of microbes cells in freshwater ecosystems live within biofilms [59].

2.2 INSIGHTS INTO THE WORLD OF MICROBES: A PICTURE TOUR

The true naturalists among us have already explored the surfaces of our day-to-day life objects, spending hours in contemplation of the animalcules that live there. These explorations, using a simple camera, optical microscopy or more sophisticated imaging techniques, are the cornerstone of the conception we have developed of microorganisms. Hence, we start this introduction on biofilms with a picture tour,

which aimes to demonstrate at least a glimpse of their intricacy, their diversity and even their beauty.

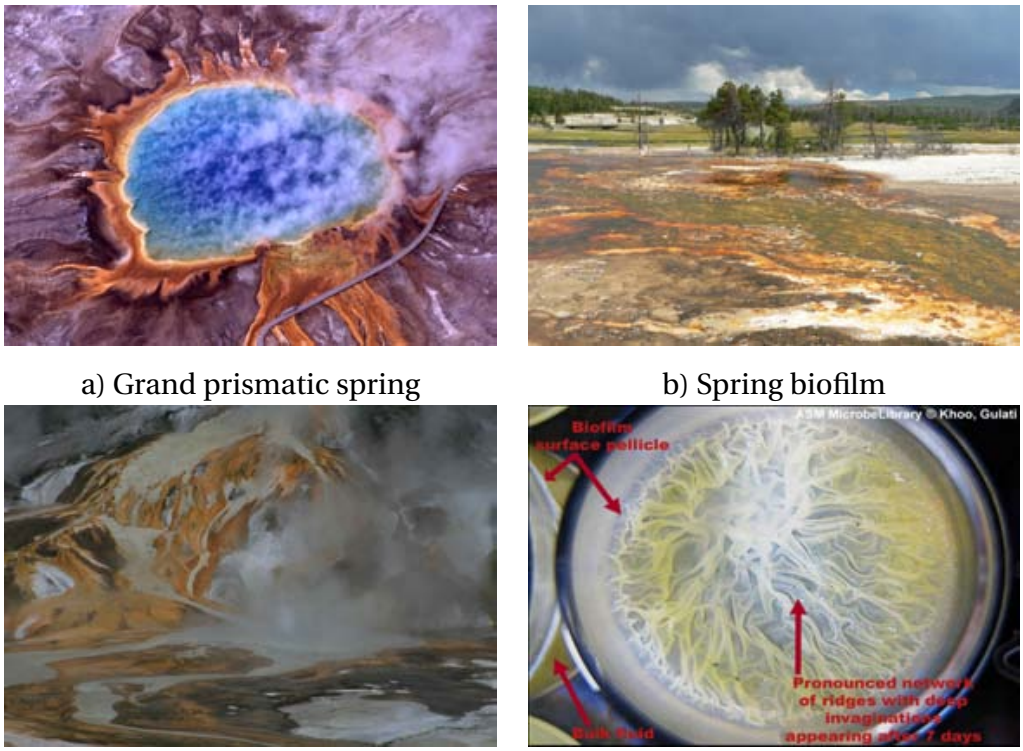

a) Grand prismatic spring b) Spring biofilm

c) Spring biofilm d) *Mycobacterium smegmatis* biofilm

Figure 2: Macroscopic manifestations of biofilms. Figure a) and b) source `www.wikipedia.com`. Figure c) courtesy of S. Veran. Figure d) source `www.microbelibrary.org`.

Figure 2 shows examples of different manifestations of biofilms visible with the naked eye. Figure (2a, b and c) illustrate the presence of biofilms around springs where hot water and high concentrations of nutrients favorable the development of microorganisms. In Figure (2a), the bacterial and algal mat, in the grand prismatic spring in Yellowstone's park (USA), is responsible for the beautiful orange, red and yellow colors during summer (low chlorophyll concentrations). Figure (2b) was taken near the grand prismatic spring and shows an outstanding amount of biofilms within the water, green colored in the middle, where phototrophic organisms are in high concentration. Figure (2c) exhibits the same color range, but was taken in the geothermal sources in Orakei Korako (New Zealand). In Figure (2d), mature *Mycobacterium smegmatis* biofilm (7 days old), a pellicle of microorganisms developing at the fluid-air interface and primarily constituted of mycolic acids (waxes), makes strange patterns.

Figure 3 shows various scanning electron micrographs, exhibiting amazing details on a nanometer scale. Figure (3a) is a colored scanning electron micrograph of an acidophilic bacterial biofilm from a sample collected in a 75-m-deep borehole located at the Kempton Mine complex in Maryland. In Figure (3b), *Bacillus subtilis* cells grow

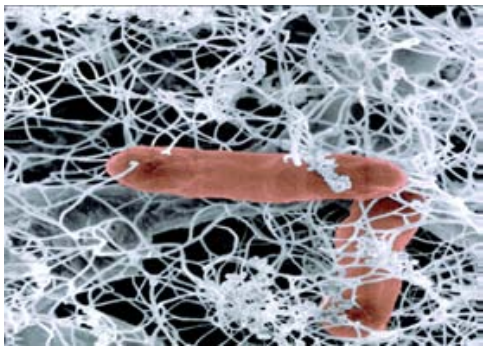

a) Acidophilic bacterial biofilm

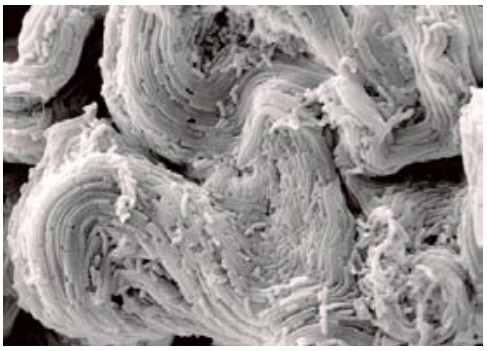

b) *Bacillus subtilis*

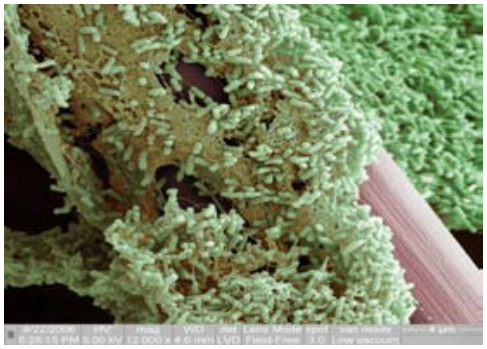

c) Bacterial biofilm

d) *Salmonella typhimurium* (red)

Figure 3: Microscale images (scanning electron micrographs). Image a) (G. Bowles, P. Piccoli, P. Candela, M. Seufer, and S. K. Lower), cover photograph (2008) of *Applied and environmental microbiology*. Image b) (B. Hatton and J. Aizenberg) source Wyss Institute website. Image c) (P. Gunning, Smith and Nephew) source `www.fei.com`. Image d) source `www.ozonefreshsystems.com`.

closely packed in parallel chains. In Figure (3c), various channels are visible within the bacterial biofilm structure, growing on a micro-fibrous material and Figure (3d) shows *Salmonella typhimurium* invading cultured human cells.

Figure 4 shows a strain of *Shewanella oneidensis* forming a biofilm under different nutrient conditions. Confocal laser scanning microscopy is, nowadays, the most utilized, and probably the most powerful, method to image biofilms on plane surfaces, as it reveals fundamental structural details such as mushroom like colonies Figure (4a).

Figure 5 represents a biofilm of *Streptococcus mutans* growing on a plane surface, imaged using a new confocal technique (CRM) with an acquisition every 12 hours. Such images give a really good idea of the heterogeneities inherent to the biofilm lifestyle and make it possible to collect non-destructive precise dynamic information about the growth of biofilms within microfluidic devices.

Very different types of microorganisms (bacteria, fungi, algae, archaea in interaction with protists) are known to produce biofilms. For instance, fungal biofilms can develop on medical implants and can cause severe complications. However,

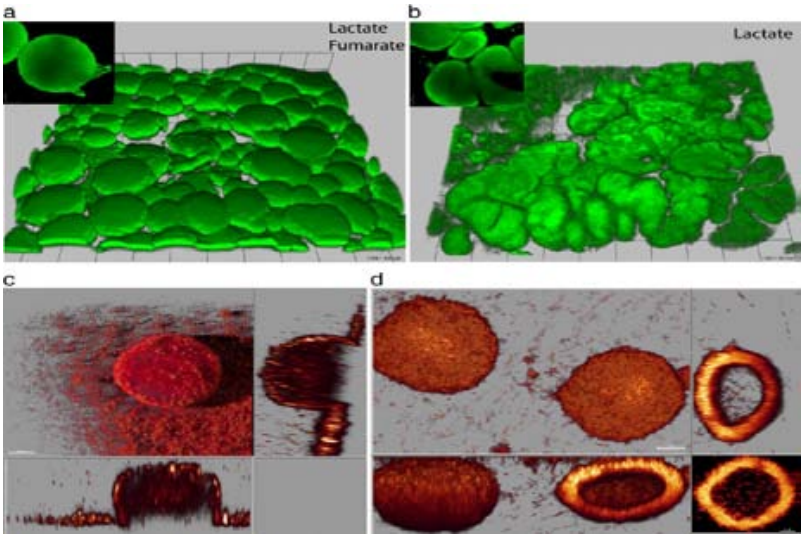

Shewanella oneidensis

Figure 4: Confocal microscopy images of biofilms growth in different environmental conditions [169].

one may have noticed that most of the above microscopic figures focus on bacterial biofilms. In a more general way, scientific interest has mainly focused on bacterial biofilms. The reasons this are diverse. First, bacteria are the most abundant organisms on Earth, meaning that, most of the time, they are the predominant species within natural and engineered biofilms. Secondly, bacteria are probably the most versatile microorganisms, and, hence, are particularly interesting for engineering applications or biomimicry. Finally, bacteria are very ancient organisms that appeared on Earth approximately 3.25 billion years ago (in comparison to Earth's formation 4.6 billion years ago) and thus, have played a very special role in the evolution of life.

2.3 THE MICROBIAL MODES OF GROWTH

Historically, the planktonic (lifestyle 1), or free-floating, phenotype has been the most studied vegetative mode of bacterial development. For example, *Escherichia Coli*, a Gram-negative bacterium (*Gram staining is a procedure used to discriminate between structural differences of bacterial cell walls. Gram-positive cell walls typically lack the outer membrane found in Gram-negative bacteria*) usually part of the mammals intestinal biota, has received a lot of attention and often serves as a model of flagellated bacteria. Planktonic microbes play a crucial role in the elaboration of antibiotics and biocides, as these are usually designed to be effective against the free-floating phenotype.

As a a dormant non-reproductive response to tough environmental conditions, some Gram-positive bacteria can also exhibit the bacterial spore, or endospore phe-

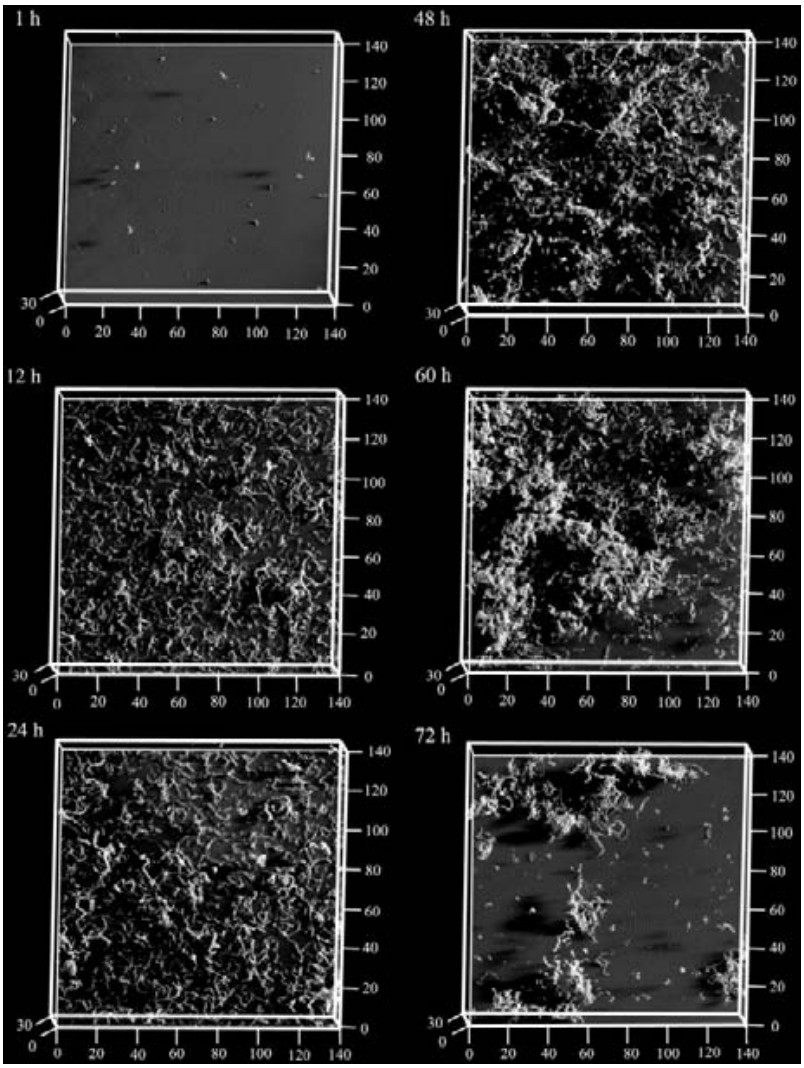

Streptococcus mutans

Figure 5: Microscale three-dimensional image obtained using confocal reflection microscopy (CRM) [293].

notype (lifestyle 2). The cell coats itself with a thick protective outer wall, and goes back to its normal vegetative state when conditions are favorable.

Even though lifestyles 1 and 2 have been examined for decades, the ultramicrobacterial or starvation form (lifestyle 3) is much less known. The realization that bacteria could express such a phenotype is a recent discovery [141], their extremely small sizes leading to difficulties of observation. Nowadays, ultramicrobacteria (UMB) are recognized as a fundamental dormant bacterial state and have been found in groundwater as deep as 1500 m below the Earth's surface and in the abyssal areas of the oceans [60]. Similarly to lifestyle 2, it activates in response to a variety of environmental stresses, such as starvation. Bacteria exhibit a huge amount of physiological mod-

ifications and can become significantly smaller, with a diameter of approximately 0.2 micrometer and a volume of about 0.02 cubic micrometer, than their normal size (not to be confused with nanobacteria or nanobes which have an even smaller normal vegetative size, i.e., 0.02 to 0.128 micrometer in diameter [265]). Remarkably, when exposed to favorable conditions and nutrients, the UMB can also return to their normal vegetative state [66]. Engineers have used these properties to develop biobarriers technology that can contain pollutants within a restricted area (see Figure 6 adapted from [60]) [90].

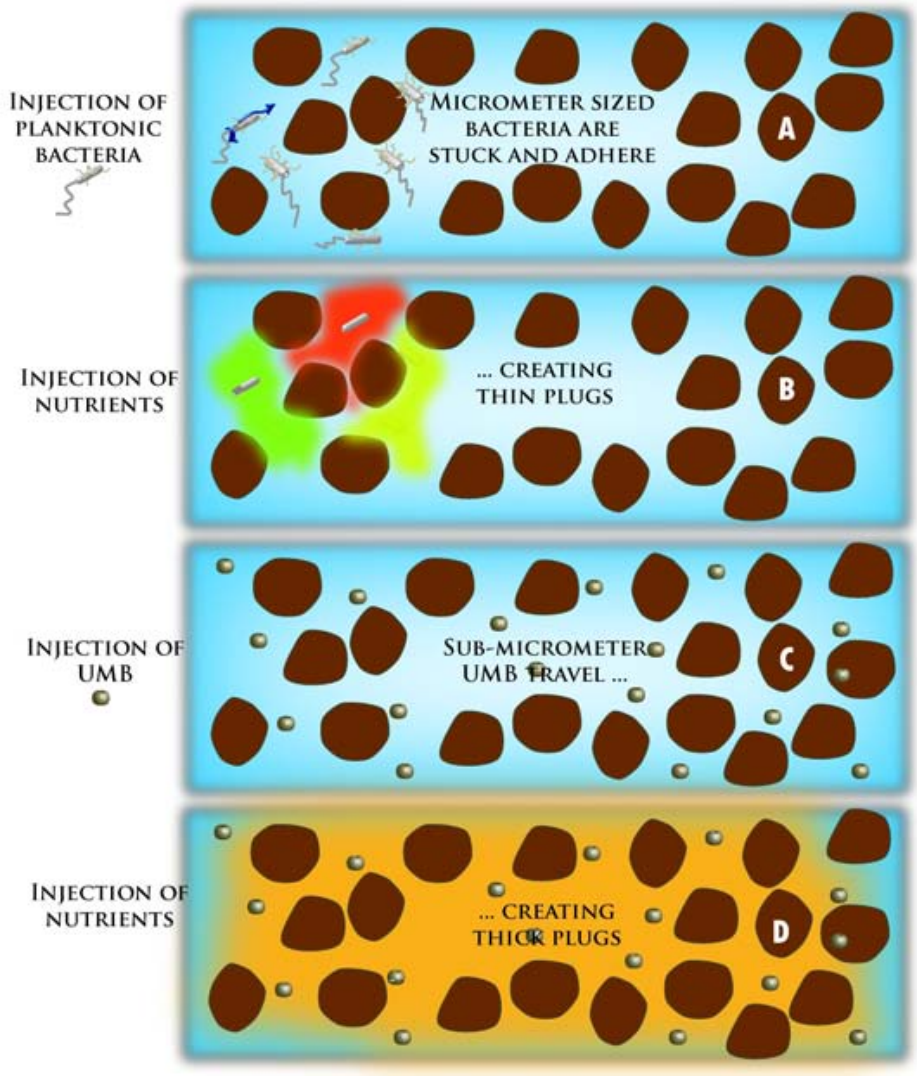

Figure 6: Biobarrier process.

Biofilm (lifestyle 4) is the predominant mode of growth of bacteria. Evidence that biofilm formation is an extremely ancient mechanism, that is, ~3.25 billions years ago, has been reported in [217, 272, 215]. One may have trouble finding a consensus

of how to define biofilms as our conception of them is changing on a daily basis. Here, we will adopt the definition given by Donlan and Costerton in [213], "the new definition of biofilm is a microbially derived sessile community characterized by cells that are irreversibly attached to a substratum or interface or to each other, are embedded in a matrix of extracellular polymeric substances that they have produced, and exhibit an altered phenotype with respect to growth rate and gene transcription". In addition to the "simple" definition, that is, microbes aggregated on a surface that live embedded within extracellular polymeric substances (EPS), Donlan and Costerton also consider the physiological and genetic modifications associated with the biofilm phenotype [108, 109]. The proteins produced (genes expressed) by cells within biofilms differ fundamentally from those produced by planktonic cells of the same strain [225, 226, 3]. A very important consequence, discussed in Section 2.5.3, of these profound modifications is that biofilms cells develop resistance to antibiotics and biocides [239].

2.4 DYNAMICS OF BIOFILM FORMATION

The formation of biofilms can be broken down into five different steps that are summarized in Figure 7. This section proposes to follow the path of a free-floating microorganism cell drifting within a fluid (e.g. water in a river) and to qualitatively describe the physical, chemical and biological processes that lead to the formation of a biofilm.

2.4.1 *Cell transport and initial attachment*

The journey of our minute organism can start within the water column of the Garonne, a French river crossing Toulouse near the Institut de Mécanique des Fluides. The cell will invariably exhibit a certain amount of movement that can look pretty chaotic, if the cell is small and the river is quiet, or will follow the flow, especially during spring when the flow rates are relatively large. Various processes are responsible for these transport phenomena; which can be broken down into

1. a passive component: effects of local hydrodynamics, Brownian movements and sedimentation [112].

2. an active component: motility of the cells. For example, microbes can get away from toxic solutes or head toward nutrients. These motile behaviors include chemotaxis, phototaxis and magnetotaxis [164, 101]. The mechanisms responsible for this movement are species-specific. Bacteria can use flagella for swimming through water; bacterial gliding and twitching for crossing surfaces; and buoyancy modifications for vertical motion [16].

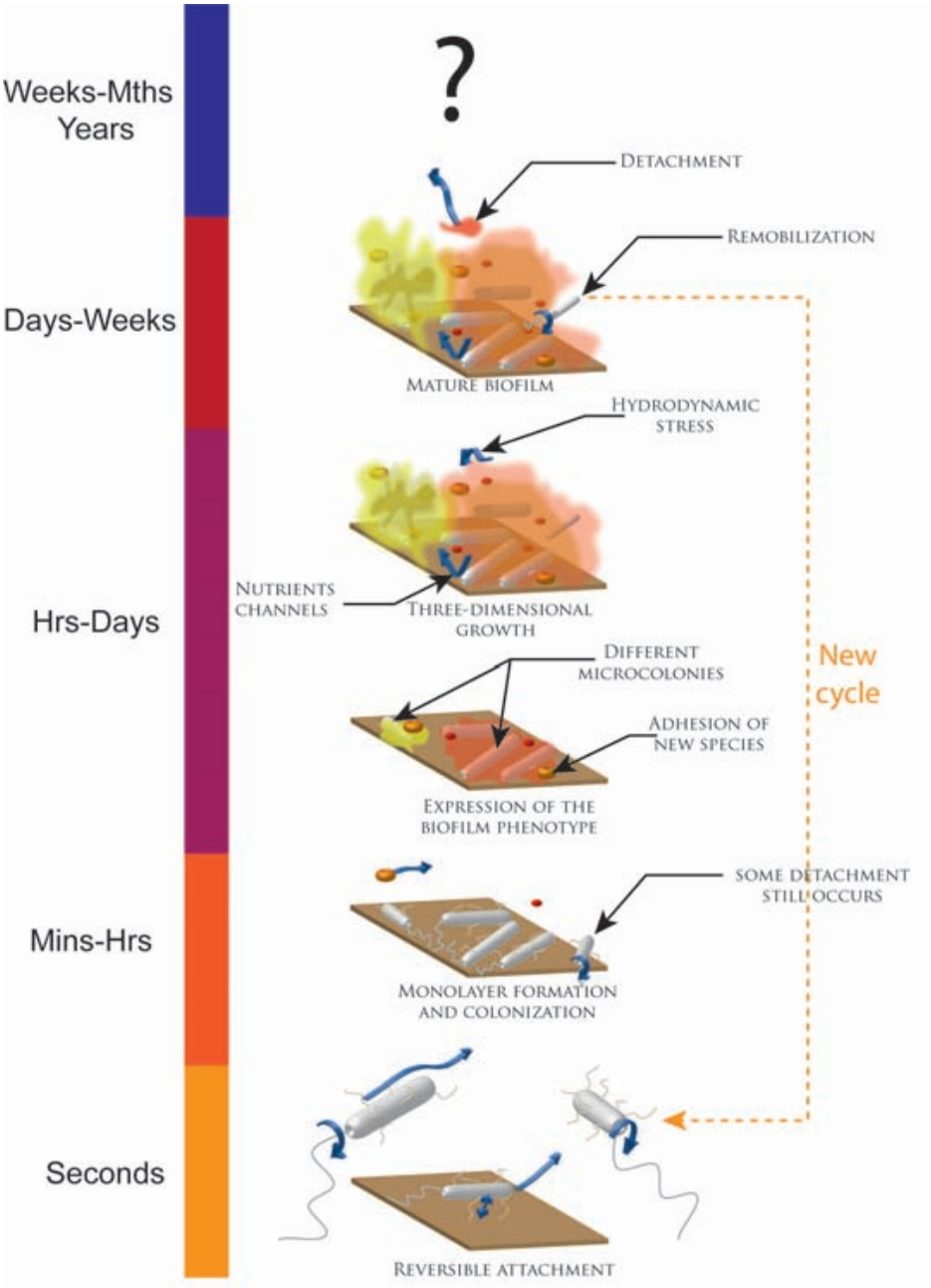

Figure 7: Schematics of biofilm formation.

At some point along its path, the cell will eventually reach the vicinities of the sediments bed that delineates the river channel. When it is close enough, the cell can undertake reversible adsorption, often described in terms of DLVO theory (*DLVO [Derjaguin-Landau-Verwey-Overbeek] theory describes surface interactions of charged colloidal particles (nanometer to micrometer sized) by taking into account van der Waals attraction and electrostatic, double layer, repulsion forces*), to a solid surface. Various physical and chemical factors play a role in bacterial adherence. For example,

surface microtopography, flow rates, local pressures, substrate hydrophobicity and electric charge, pH, salt concentration, type of organic compounds, time and temperature contact [135, 236, 297, 128, 61, 38, 261]. However, part of the process remains biological, that is, a "decision" of the cell is involved. For example, initial attachment can trigger specific membrane proteins [20, 32], especially for adherence to other living organisms, or direct planktonic production of "sticky" exopolysacharides.

Eventually, the second step of biofilms formation occurs. Some attached bacteria undergo physiological modifications (expression of the biofilm phenotype) that initiate the formation of microcolonies; the other cells can still exhibit detachment mechanisms (described in section 2.4.3). This expression of the biofilm is fundamental but yet, not fully understood. The stimuli involved in this decision making are barely tackled [60, 168]. Several fundamental questions have no definitive response:

1. How do bacteria sense the surface ? A current hypothesis is that signal molecules secreted by the microorganisms are in higher concentration in the vicinities of the solid surface (because, on the surface, the normal component of the flux is zero [204]).

2. How do other planktonic species interact with the microcolonies ? It is expected that other species will join the biofilm to form mixed bacterial consortia, specifically at this early stage of the biofilm formation. The first reason is that it is easier for the other cells to attach to the matrix than to the abiotic surface. In addition, a well established mature biofilm might not be inclined to accept new species, that is, mixing organisms after the initial stage is arguably more and more difficult [60].

3. Biological attachment and detachment are known to be closely related to quorum sensing phenomena (e.g. : [75, 291]) (*Quorum sensing designates a fundamental ability of microbes to communicate with each other by molecular signaling*) but what are the molecular mechanisms involved ?

2.4.2 *Growth and maturation*

This step corresponds to the cells' multiplication and biofilm expansion on the basis of the first microcolonies. Three-dimensional structures develop [267] and the matrix starts to interact strongly with the fluid. Then comes the maturation step. During this stage, variations of the biovolume and of the biomass are relatively small as compared to the growth step, but important structural modifications are triggered regarding interspecies relationships

Various parameters influence the kinetics of growth and maturation. These include biological (such as which species is involved or predation) or physico-chemical factors (such as local hydrodynamics [37], nutrient conditions [6], pH, presence of biocides). There is a continuing debate within the scientific community regarding

the relative importance of the biological and the physical factors. One must keep in mind that all aspects of the problem, even though they can seem very different, are closely connected. Biofilms are in fact dynamic systems that continuously modify the local physical, chemical and biological conditions surrounding them. These trigger dynamic retroaction processes between the biota and the environmental conditions. For example, Picioreanu (1998) [197] shows that local flux limitations can explain the biological and physical heterogeneities within biofilms. Metabolically active cells, initially chaotically distributed, consume and create various solutes and polymers, modifying the chemical speciation of the elements present in the medium as well as local hydrodynamics. Hence, gradients in concentrations and spatial heterogeneities of the shear stress appear, influencing the development of ecological niches favorable to different organisms [279, 289, 262, 94].

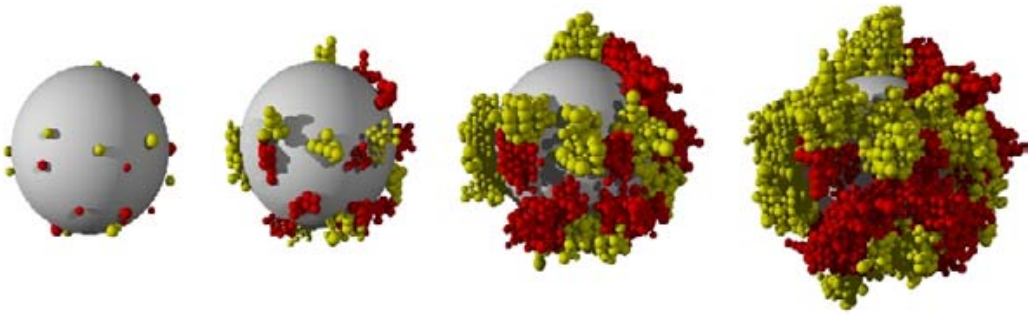

Figure 8: Modeling the formation of a two-species biofilm on a sphere in a mass transfer limited regime using cellular automata. Source C. Picioreanu [195, 196].

2.4.3 *Detachment*

Detachment refers to the liberation of flocs or individual organisms from the biofilm. There are various physical, biological and chemical processes responsible for these detachments. It can occur when forces applied to the matrix exceed its internal cohesion. This class of phenomena includes sloughing [213, 238], abrasion, predation (see in Figure 9) or reduction of the cohesion by chemical attacks or enzymes. Erosion refers to detachment induced by shear stress of the fluid on the matrix. Abrasion occurs when solid particles flowing within the bulk fluid collide with the biofilm, tearing off small flocs. An important feature of biofilms is that they display various layers corresponding to different degrees of cohesion [105, 189]. Internal layers are less exposed to hydrodynamics constraints, more dense and consequently more difficult to remove than external layers.

The second class of detachment phenomena deals with active remobilization of biofilms' cells to colonize new niches [226] by "swarming/seeding dispersal" strategies or "clumping dispersal" [122]. Seeding dispersal corresponds to the release of individual cells while clumping dispersal refers to the detachment of relatively large

Figure 9: Example of protozoan (stentor) grazing biofilm [193].

aggregations of cells and extracellular polymeric substances. Hence, detachment is a fundamental mechanism [262, 263] as (1) it partly controls the architecture of biofilms, (2) it modifies the shape of the fluid/biofilm interface inducing changes in mass and momentum transfer [238] and modifications of the adhesion properties, rugosity for example, that facilitate the recruitment of new species [251] and (3) it interferes with the proportions of the different species and their spatial distribution [49, 176, 95, 85].

Even though the dynamics of biofilms formation are usually classified as in Figure 7, there is actually no clear boundary between the different stages and this breakdown is only a schematic description. For example, detachment phenomena are concomitant to all other formation steps. For this reason, the artwork Figure 10 is outstanding as, in a less schematic manner, it captures simultaneously the complexity of the phenomena and the coexistence of all the processes.

2.5 BIOFILM STRUCTURE AND COMPOSITION

The architecture and the composition of biofilms are highly complex and diverse. For example:

- It has been shown that the marine organism *Serratia liquefaciens* forms biofilms in which the organism's cells are "arranged into vertical stalks that bear rosettes

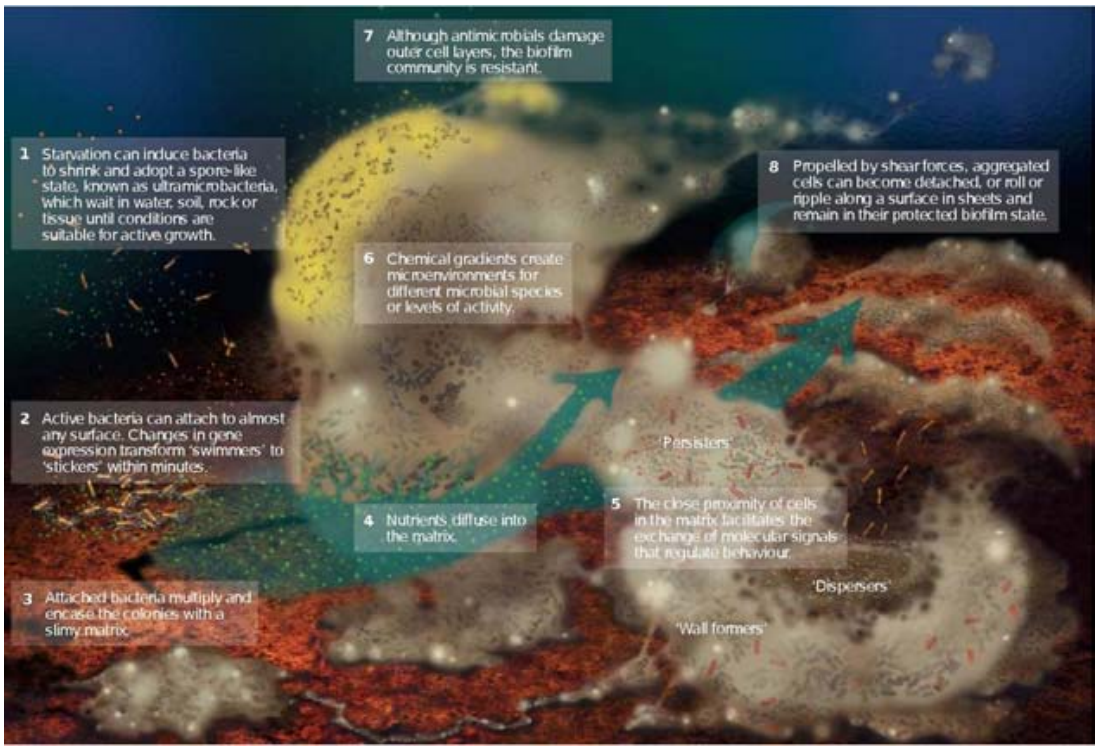

Figure 10: "Realistic" biofilm dynamics from [122].

of cells connected to other rosettes by long chains of cells and that each feature of this architectural marvel is controlled by specific genes [149]" (from [60]).

- One clone of *Pseudomonas aeruginosa (Pseudomonas aeruginosa is a Gram-negative, aerobic, rod-shaped bacterium and an opportunistic human pathogen)* forms "stumplike pedestals on colonized surfaces and that mobile cells of a second clone crawl up the pedestals and form the 'caps' of the mushrooms that are such a prominent feature of biofilms formed by this organism [258]" (from [60]).

The composition and the architecture of biofilms can significantly change from one biofilm to another. However, some aspects of their global composition and some patterns are specific to the biofilm phenotype. For example, well-fed biofilms are often flat and poorly structured whereas low nutrient concentrations lead to highly structured communities. The goal of this section of the thesis is to present the common composition and the key structural elements of biofilms.

2.5.1 *General composition*

Component	% (mass) of matrix
Water	up to 97%
Microbial cells	2-5%
Polysaccharides	1-2%
Proteins	<1-2%
DNA and RNA	<1-2%
Ions	?
Inorganic	?

Table 1: General composition of biofilms, adapted from [246].

Following Sutherland (2001) [246], the general composition of biofilms can be described as in Table 1. Most of the biofilm matrix (97% of the total mass) is actually water. The water can be bound within the capsules of microbial cells or can exist as a solvent whose physical properties such as viscosity are determined by the solutes dissolved in it [246]. Extracellular polysaccharides, proteins, DNA and RNA can be integrated into the notion of extracellular polymeric substance that is described in the next section. Inorganic compounds such as minerals or clay particles can get immobilized on the biofilm, depending on the environmental conditions.

2.5.2 *Extracellular polymeric substances (EPS)*

The EPS definition is in constant evolution, as new constituents, processes and functions are frequently discovered. Old definitions include: organic polymers that are often responsible for the cohesion of the cells within biofilms and for their adhesion to substrates [72]. One significant further step has come with the unification of the different concepts that are used to describe this matrix [154]. Nowadays, the EPS is known to be composed of a complex mixture of macromolecules including exopolysaccharides, proteins, DNA, RNA [245, 246] in addition to peptidoglycan, lipids, phospholipids and other cell components. They (1) are usually thought as the principal structuring component of the matrix, that is, the cement that holds the microorganisms together and to the surface and also (2) play other functional roles (Table 2). For example, alginate is a polyanion polysaccharide that is supposed to be involved in *Pseudomonas aeruginosa*'s resistance to antibiotics [122].

The extracellular DNA present in biofilms has been thought for many years to be only the result of cell lysis. However, it has been observed that DNA can be produced and sent outside the cell in small membranes [182, 137]. More recently, it has been shown that absence of this DNA can inhibit the biofilm growth [275] and that it can exhibit a very specific structural organization [27]. The intricacy and functionality of EPS remain to be fully understood, especially in natural environments. Most of the

EPS component	Role in biofilm
Neutral polysaccharides, amyloids	Structural components
Charged or hydrophobic polysaccharides	Ion exchange, sorption
Extracellular enzymes	Polymer degradation
Amphiphilic molecules Membrane vesicles	Interface interactions Export from cell Sorption
Lectins, nucleic acids	Specificity, recognition Genetic information Structure
Bacterial refractory polymers	Electron donor or acceptor?
Various polymers	Source of C, N, P

Table 2: The EPS defined, adapted from [100].

work has focused on *Pseudomonas aeruginosa*, or on other laboratory species, but natural biofilms seem particularly different [60, 100]. For instance, the production of EPS in natural biofilms is dynamic and can follow cyclic patterns as demonstrated in marine stromatolites [84] or can form honeycomb structures [89, 167, 252].

2.5.3 *Biofilm cells and their metabolism*

Bacterial metabolism englobes the ensemble of biochemical reactions that produce the energy and solutes that are necessary for the cell to function. There is an incredible diversity of cells belonging to various classes. Presenting all these metabolisms is far beyond the scope of this introduction. Here, we will focus on some important characteristics of bacteria and the modifications associated with the biofilm phenotype.

BACTERIAL METABOLISM Bacteria can be classified by their nutritional groups following the carbon source, the kind of energy source, the electron donor and the electron acceptor used for their development. Phototroph organisms take their energy from sunlight, by photosynthesis, while chemotrophs use chemical reactions that produce energy, mostly oxidation of electron donor at the expense of an electron acceptor such as dioxygen or nitrates. Among chemotrophs, there are lithotrophs that oxide inorganic compounds and organotrophs that use organic molecules. Eventually, during the catabolism, adenosine triphosphate (ATP) is synthesized as the energy source for the cell.

On the basis of the carbon source, bacteria are divided into heterotrophs, which use organic carbon and autotrophs, which feed on inorganic carbon sources, mostly on CO_2. Organisms can be further separated into aeroby if they use oxygen as the electron acceptor or anaeroby if they do not. This classification has its limitations but

is often utilized. For example, bacteria also need nitrogen, potassium, oxygen and minerals to form the amino-acids required to synthesized proteins; some bacteria can be heterotrophs with respect to the carbon source but autotrophs in relation to other basic compounds such as nitrogen.

SPECIFICITY OF BIOFILMS Cells exhibit fundamental phenotypic modifications associated with the biofilm lifestyle. The pattern of genes expression has been found to differ by between 20% and 70% as compared to the corresponding planktonic cell [22, 60]. A direct consequence of these modifications is that biofilm cells are more resilient and exhibit resistance to antibiotics and biocides. It was first suggested that biofilm acts as a barrier which prevents harmful components from reaching the cells. However, while it certainly slows down the diffusion, there has been a substantial amount of evidences that antibiotics can penetrate hundreds of micrometers into the matrix within seconds [183, 243]. Another hypothesis is that biofilms' cells lack the enzymes that are usually targeted by antibiotics [111, 240, 3, 225, 226].

In addition, within biofilms, the microbial cells, whether from the same species or from different species, are in close proximity to one another. This has various direct consequences:

- Metabolic symbiosis can appear. For example, some species can use solutes produced by other species [5, 96] or different cells can exchange genetic material [103, 124]; specialization through stratification can occur in response to various environmental conditions. For example, in aerobic conditions, aerobic bacteria develop in surface of the biofilms while anaerobic ones tend to form deeper within the biofilm, where oxygen has been already consumed by surface organisms [165].

- On the contrary, competition for available nutrients is intense; antimicrobial substances released by some cells, such as bacteriocins, microcins, antibiotics or phage, have a good chance of successfully attacking and possibly destroying neighboring heterologous cell types [133]; predator-prey dynamic relationships affect organisms within the matrix [180, 187].

Complex networks of relationships develop between the cells, that eventually end up forming evolutive microbial consortia, that continuously change.

2.5.4 *Water channels*

In many natural environments, biofilms form mushroom-like structures sprinkled with water channels [179] in which convective flows have been identified [160, 241]. The channels act as nutrient suppliers for the deepest microorganisms [158, 82]. To get a clear picture of these channels, one may imagine the way oxygen is carried out in the human body. For example, brain cells cannot live more than a few seconds

without oxygen, that is, the time for O_2 to diffuse through several millimeters of flesh. If the oxygen were to diffuse all the way from the lungs to our brain, it would take hours, and cells would die. Hence, in multicellular organisms larger than a few millimeters, veins convey the oxygen toward the cells until the critical millimeter length scale is reached. In the biofilms, the situation is similar. In thick biofilms, if the deepest cells were to wait for the nutrients to diffuse all the way through the biofilm, most of them would die. Nutrient channels are thus necessary. To what extent the formation of these channels is the result of an evolution of the microorganisms toward that end or a consequence of the transport processes on a shorter time-scale remains to be fully understood.

2.6 WHY DO BACTERIA FORM BIOFILMS ?

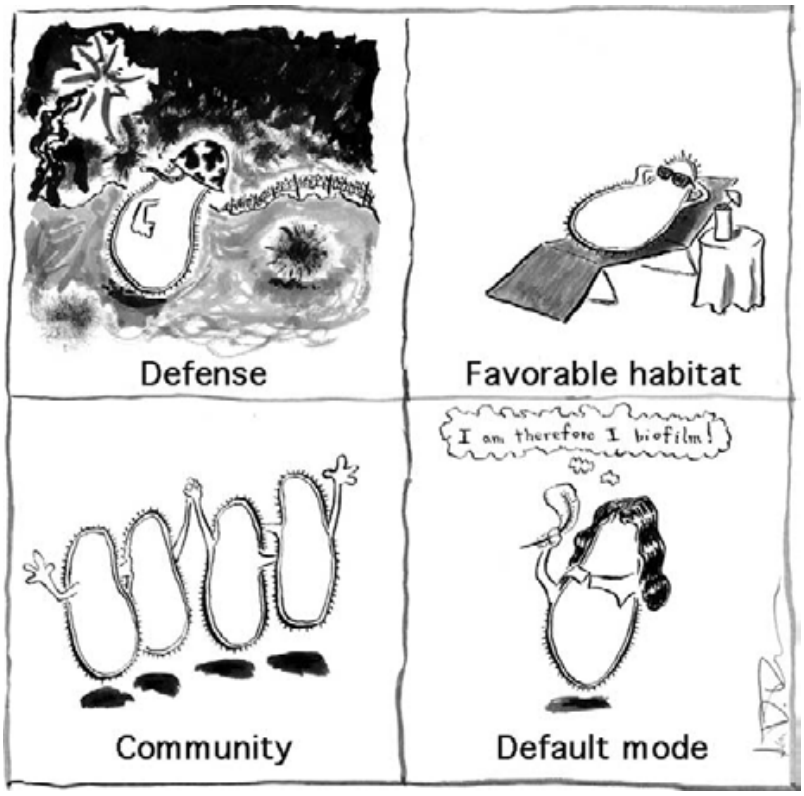

Figure 11: Artistic interpretation of the four driving forces behind bacterial biofilm formation [134].

The forces that drive bacteria to produce biofilms are closely connected to the theory of evolution. Bacteria tend to develop embedded within extracellular polymeric substances because this lifestyle promotes survival and growth of the population. That being said, the real question becomes: What are the physical, chemical and biological phenomena that make the biofilm mode better than the planktonic one?

Following Jefferson's work [134], these phenomena can be classified according to four different classes, as illustrated on Figure 11.

First of all, the biofilm form can develop as a defense mechanism in response to various environmental stresses such as mechanical stress (shear or osmotic), UV exposure, metal toxicity, acid exposure, dehydration and salinity, phagocytosis, iron deprivation and several antibiotics and antimicrobial agents [122]. EPS is thought to play a crucial role in the protection of the cells. For example, it might protect organisms from being crushed by important mechanical stresses, reduce the quantity of several toxic compounds that diffuse through the matrix and reach the deepest organisms or simply slow down the diffusion allowing the bacterial immune system to mount a specific attack. Evidence for such mechanisms includes the expression of specific proteins that trigger the expression of EPS in response to environmental stresses such as the upregulation of *proU* in *E. Coli* to adapt to transport or osmotic stresses [204]. Another example is the creation of starved, stationary dormant zones that seem to induce resistance in biofilm populations to antimicrobial agents. Arguably all biocides or antibiotics need at least some degree of metabolic activity in order to be efficient and, hence, might not kill dormant bacteria [122].

The second class of phenomena deals with fighting host immune systems in order to stay in a favorable habitat. For example, the human body, because of its adequate temperature and high concentrations of nutrients, represents an extremely appealing habitat for microorganisms. The counterpart is obviously that they will have to develop either in symbiosis with the host or to constantly struggle against its immune system. From this perspective, the biofilm mode of growth is an excellent strategy to remain fixed to the host. Specific microbial surface component recognizing adhesive matrix molecules (MSCRAMMs) are often expressed and play a key role in initial adherence of bacteria to host surfaces [194].

There are also various advantages associated with life in community

- A division of labor can develop. As previously discussed, some symbiotic relationships might occur. For example, myxobacteria can produce extra digestive enzymes as a community and, potentially, break down complex food substances. Communication is realized through the expression of auto-inducing molecular signals, that is, as previously discussed, quorum sensing.

- Because of their proximity, biofilms cells can perform genes transfer. These processes may directly benefit to the bacteria, for example by exchanging antibiotic resistance determinants [134].

- Some microorganisms might exhibit programmed cells death mechanisms, in order to reduce to metabolic activity in low nutrients conditions, that is, the biofilm might behave like a multicellular organism, although this is still a matter of debate [134].

- There are also evidences that the biofilm formation is the default mode of growth of microorganisms. When bacteria sense an adequate surface, that is, a free ecological niche, they develop the biofilm phenotype. For example, *algC*, a gene required for alginate synthesis, in *Pseudomonas aeruginosa* is upregulated within minutes of attachment [74]. Jefferson (2004) suggests that one may have to wonder more about what drives bacteria to develop the planktonic phenotype.

John Tyler Bonner would probably argue that size increase is the meaningful evolutionary concept that regroups all these advantages. In [28], he discusses the importance of size and scales on the evolution of Earth's organisms and states that "size is a prime mover in evolution". Bonner also says that "there has been a selection for larger organisms; under some circumstances size increase can confer advantages and promote reproductive success [...]. If there is an advantage to increased size, one of the simplest ways to achieve it is to become larger by becoming multicellular". The idea behind that is an ecological principle based on Darwinian evolution. There is a perpetual competition for survival in natural habitats. All size levels, except for the largest one, are occupied by some organisms. Biofilm could have developed originally as a result of cells aggregation (due to passive and maybe active phenomena) and have survived as the top-size free niche promotes survival and growth of the population.

2.7 MODELING BIOFILMS

Developing mathematical models has become a matter of utmost importance in scientific research in general. Direct observations are the cornerstone of scientific knowledge. Yet, quantifiable understanding regarding the processes at play as well as quantitative predictions cannot be achieved without mathematical analysis. This is particularly true within the context of biofilms where numerous extremely complex processes are at play simultaneously. B. E. Rittmann (2007) [221] states that mathematical modeling provides a quantitative relationship between the biofilm components and the processes. "The components include the various microbial types, extracellular polymeric substances (EPS), inert or dead biomass, the metabolic substrates for all the microbial species, metabolic products from the reactions they carry out, alkalinity, they hydrogen ion (for pH), and more. Processes include the metabolic reactions, transport of solutes and biomass, acid/base reaction, precipitation/dissolution, and physical deformations due to forces acting on the biofilm. Many of the processes, particularly the metabolic ones, are the services that the community provides human society". In a more general framework, mathematical modeling can help in identifying pertinent physical, biological and chemical parameters as well as discerning irrelevant ones. It also represents a unique predictive technique that can provide informations regarding future behaviors. Hence, models have become a key

component to provide responses to specific engineering applications or are used as a research tool.

Along with the realization of this modeling necessity, a substantial amount of theoretical works have been developed within the last decades. One critical aspect of the problem, which is particularly important in this work, is that biofilms are extremely heterogeneous. According to Bishop and Rittmann (1995), heterogeneity may be defined as "spatial differences in any parameters we think is important". An adapted list from Bishop and Rittmann (1995) [24], summarizes a few examples of possible biofilm heterogeneities:

1. Geometrical heterogeneity: biofilm thickness, biofilm surface roughness, biofilm porosity, substratum surface coverage with microbial biofilms.

2. Chemical heterogeneity: diversity of chemical solutes (nutrients, metabolic products, inhibitors), pH variations, diversity of reactions (aerobic/anaerobic, etc.).

3. Biological heterogeneity: microbial diversity of species and their spatial distribution, differences in activity (growing cells, EPS producing, dead cells, etc.).

4. Physical heterogeneity: biofilm density, biofilm permeability, biofilm viscoelasticity, viscosity, EPS properties, biofilm strength, solute concentration, solute diffusivity, presence of abiotic solids.

Length scales that are involved vary from nanometers (EPS polysaccharides) to millimeters or even centimeters (biofilm thickness) with an intermediate size of about several micrometers (cells) (Figure 12). All of these spatial scales are pertinent when working with biofilms. For example, let us consider the path of a nutrient molecule that originally is in the bulk fluid. It might be submitted to diffusion and convection within the water, then goes through the millimeters of EPS and eventually reaches the membrane of a cell. Once there, it has to cross the interface using specific transmembrane proteins such as porins.

These heterogeneities are extremely difficult to model because of the broad range of scales that are involved. One usually tries to avoid a purely multiscale description of the various processes. The primary reason for this is that our computational resources are limited and molecular modeling over centimeters is nearly impossible. Secondly, such models would contain an enormous amount of information that is mostly irrelevant at the macroscale. Various strategies have emerged to model the macroscopic behavior of biofilms, that is, to describe the phenomena in some averaged sense. Microscale modeling strategies as well as upscaling techniques and empirical formulations are presented and compared within the next sections.

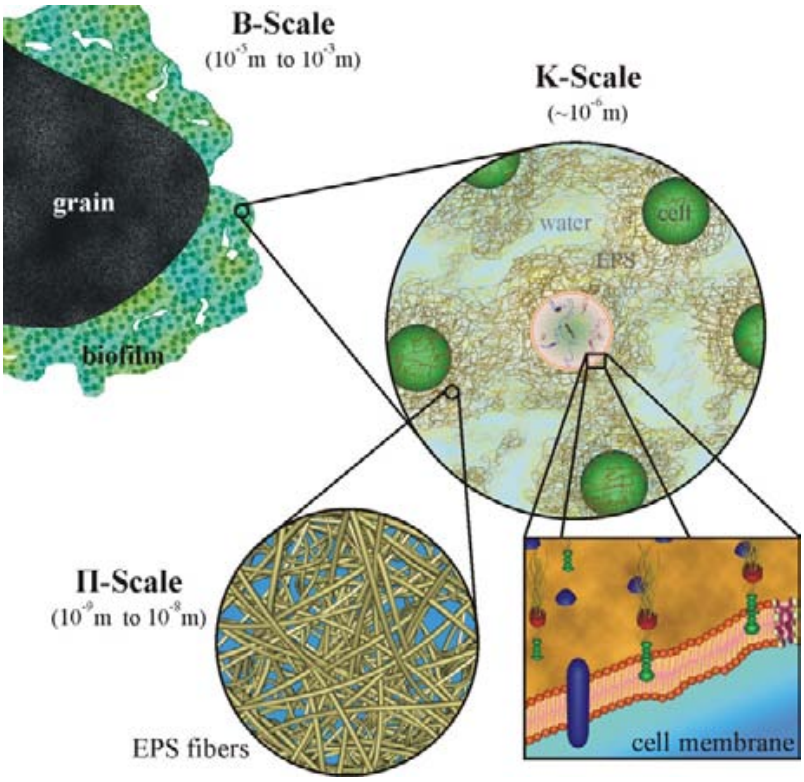

Figure 12: Multiscale representation of biofilms (adapted from [138]).

2.7.1 *Cellular-scale direct numerical simulations (DNS)*

CELLULAR AUTOMATA A cellular automaton (CA) model consists in an array of small compartments, each in one of a finite number of states. For each time step t+dt, a new generation is created as a function of the generation at time t, following a given set of rules. For example, the creation of a new microorganism cell requires that the set of rules specifies where to place it, as a function of the neighborhood of the mother cell. The rules typically take into account processes such as substrate uptake, metabolism, maintenance, cell division, transport and death. Although the main idea is the same, the set of rules that govern the spreading of the biomass differs from model to model [153]. Examples of early CA models include [104] and [280].

INDIVIDUAL-BASED MODELS Individual-based models simulate individual cells, rather than the behavior of a predefined grid (such as CA). All other aspects of the simulation, and the processes that are modeled, are very similar to those of the cellular automata. Advantages, disadvantages and problems that need to be tackled are thoroughly discussed in [153].

2.7.2 *Biofilm-scale empirical analysis*

Empirical analysis remains the most common technique. The macroscopic laws are guessed on the basis of the mathematical structure of the problem at the microscale, in conjunction with experimental data. As an example of one such technique, we will describe how cells transport is commonly described within the fluid phase. One usually cannot follow the Lagrangian trajectory of every single cell in the medium, but rather, assumes that these can be followed in terms of an homogenized concentration. In addition, cells transport within the bulk fluid is usually described in terms of a mass balanced equation in which it is assumed that fluxes are convective and diffusive. This is based on the assumption that the attachment mechanisms can be uncoupled from the transport processes, that is, that the characteristic times for attachment are much longer than those associated to diffusive and convective transport. If such an hypothesis is valid, then the mass-balance equation takes the form (e.g. [112])

$$\frac{\partial w_\gamma}{\partial t} + \boldsymbol{\nabla} \cdot \{(\mathbf{v}_\gamma + \zeta \mathbf{v}_s)\, w_\gamma\} = \boldsymbol{\nabla} \cdot \{k_\gamma \boldsymbol{\nabla} w_\gamma\} \tag{2.1}$$

which is an heuristic formulation of the Fokker-Planck equations for particles (see discussion in [212]). In Eq (2.1), w_γ refers to the concentration of cells within the water $\gamma - phase$, $\mathbf{v}_\gamma$ is the pointwise Eulerian velocity field (solution of the Navier-Stokes equation) within the $\gamma - phase$ and k_γ is the diffusion coefficient of the cells within the water. $\mathbf{v}_s$ is the maximum theoretical velocity for the sedimentation of a spherical particle in an infinite medium, that is,

$$\mathbf{v}_s = \frac{(\rho_p - \rho)\, \mathbf{g} d_p^2}{18\mu} \tag{2.2}$$

where ρ_p is the buoyant density of the particle and ρ the one of the bulk fluid. d_p is the diameter of the sphere, μ the viscosity of the bulk fluid and $\mathbf{g}$ is the gravitational acceleration. ζ is an empirical parameter such as $0 \leqslant \zeta \leqslant 1$, that takes into account, among others, the grain surface rugosity and the sphericity of the particles (see discussions in [123]).

2.7.3 *Upscaling from the cell-scale to the biofilm-scale*

The idea that biofilm models should be upscaled directly from the microscopic scale has been brought forth previously by Wanner and Gujer (1986) [271]. One can adopt the suggestions of Wanner et al. (1995) [269] by starting at the cellular level, where the biofilm is a discontinuous multiphase medium [285, 286]. B. D. Wood an co-workers performed such an analysis using the volume averaging with closure techniques [287, 284]. These include upscaling reactive solute transport within the

matrix, cellular growth and multispecies diffusion. In general, most of the work with volume averaging has focused on local mass equilibrium conditions, that is, when the gradients of concentrations within each phase are relatively small, the continuity conditions at the interfaces can be extended to the bulk phases. Hence, all intrinsic concentrations are equal and the mass transport can be described in terms of a single mass transport equation.

2.7.4 *Advantages and disadvantages*

	Advantages	Disadvantages
DNS	Realistic models Large amount of information	Time-consuming Limited to small sized volumes No microscale validation
Empirical analysis	Simple laws	No connection macro/micro No domain of validity
Upscaling	Connection macro/micro Domains of validity Description of large volumes	Non-equilibrium conditions Non-linearity Dynamic interfaces

Table 3: Advantages and disadvantages of the different models.

DNS (Direct Numerical Simulation) has been used to explore some physics of biofilm formation. In particular, cellular automata represent a very particular framework, that has recently met a great success. It can be used for different purposes, for example to study the influence of nutrient flux limitations within biofilms. It models biofilms starting at the cellular-scale, and hence, is quite realistic and captures a lot of information. On the other hand, these are often time-consuming simulations, that are limited to a relatively small total volume. In addition, each cell receives a set of basic rules that change from one model to another. The biofilm growth is obviously very sensible to these rules, and validation is not easy to perform.

Empirical development of macroscopic laws often ends up with relatively simple macroscopic equations that are convenient for data interpretation. However, upscaling techniques in general (for instance, homogenization, volume averaging, moments matching techniques), and volume averaging in particular, (1) relates the microscopic parameters to the observable macroscopic ones. As part of the process of volume averaging, the microscopic parameters that apply to these small scales can be explicitly linked to their macroscopic counterparts and (2) volume averaging indicates under what conditions the conservation equations are valid. The counterpart is the difficulty to treat non-equilibrium situations, non-linearity or dynamics of the interfaces

such as biofilm growth coupled with mass transfer. However, one must remember that these disadvantages are purely technical and can be overcome. If an averaged behavior exists, then upscaling techniques should be able to capture it. If it does not, then one needs to use DNS.

3

BIOFILMS IN POROUS MEDIA

3.1 THE SIGNIFICANCE OF BIOFILMS IN POROUS MEDIA

WHY DO BIOFILMS FORM WITHIN POROUS MEDIA ? In freshwater ecosystems, 99% of the microorganisms live within periphytic biofilms [60]. All of us have experienced the predominance of this slippery form of life, falling unexpectedly in the water. Yet, most of the bacteria remain hidden underneath the sediment surface. In fact, the riverine hyporheic compartment (*The hyporheic zone is the region beneath and lateral to the stream bed, where flow rates are sufficient to mix shallow water with surface water*) has been identified as particularly active in terms of bio-chemical processes. For example, this zone is known to play a key role in the self-purification properties of the rivers and in the biodegradation of toxic compounds. One may then wonder why microbes love living within these porous media so much and not just on the bottom of the river ? Porous media actually represent an extremely favorable habitat in terms of defensive capacity,

- Microorganisms are partly protected from shear stresses as the fluid velocity within the water column is much larger than within the pore throats.
- Steric hindrance might also limit predation, that is, relatively large predators are slowed down by the sediments. These have developed specific bioturbation techniques but the predator-prey equilibrium might be considerably modified.
- The surface available for attachment is particularly vast, favoring the biofilm lifestyle at the expense of the planktonic one.
- Within porous media, extensive heterogeneities of the physico-chemical properties develop. Pressure, nutrients concentrations, biocides concentrations, pH, electric charge, rugosity of surfaces vary extensively from one pore to another, providing a nearly infinite number of different environmental conditions. This does not favor the development of microorganisms in one specific area, but rather, provides ecological niches favorable to, virtually, every single species. For example, aerobic organisms are known to live nearby the surface, where concentrations of oxygen are relatively elevated whereas denytrifying bacteria can live deeper in the sediments.

REPRESENTATIONS OF BIOFILM GROWTH Historically, biofilms have been assumed to form continuous layers [277, 250, 63]. Other propositions suggest that biofilms arrange in patchy aggregates within pore throats [264]. Rittmann (1993) [219] emphasized that both representations can be correct, that is, the spatial distribution of attached microorganisms strongly depends on the physical, chemical and biological properties of the medium and even on its history [251, 266]. For example, hydrodynamics, nutrients conditions, microorganism species, predation and bioturbation are found to have a strong impact on the growth dynamics of biofilms [171, 250, 219] within porous media. Thullner et al. (2004) [256] also show that growth seems to happen predominantly within mixing zones for electron donor and acceptor. As the biofilm grows, these zones are progressively filled giving birth to new favorable areas. Hence, a strong coupling between the solute transport and the biofilm growth exists. Following the same line, Knutson et al. (2006) [142] argue that transverse dispersion (in opposition to longitudinal dispersion) is fundamental and must be taken into account for the determination of the biodegradation.

CONSEQUENCES OF BIOFILMS FORMATION As always with biofilms, retroaction processes occur between the matrix and the environment. One caveat within porous media is the multiscale aspect of the problem. Within subsurface soil or rocks, or the riverine hyporheic zone local biofilm growth within the pore space can induce substantial modifications to macroscopic mass and momentum transport dynamics [63, 264, 288, 242, 232, 250]. Evidence of this type of modification has been developed by observing variation, over time, of macroscopic parameters such as hydraulic conductivity and permeability as well as changes in porosity and dispersion, in conjunction with sampling indicating the presence of biofilm. For example, bioclogging induces significant charge loss and consequently, to a reduction of the permeability (readily ten times). This phenomenon has been the subject of many numerical and experimental studies [54, 44, 139, 88, 257, 256, 142, 138, 223] because it is involved in numerous applications such as biobarrier or biofouling.

3.2 MULTIPLE-SCALE ANALYSIS OF SOLUTE TRANSPORT IN POROUS MEDIA

The first pioneering experimental and theoretical works regarding the transport of non-reactive solutes have been undertaken in the 50s by Taylor [248], Aris [9], De Josselin de Jong [80] and Saffman [224]. Theoretical works focused mainly on the propagation of a pulse through a tube. Taylor and Aris showed that for relatively long times, when molecules of solute have had the time to visit the entire tube section, the transport can be described in terms of a one-equation advection-diffusion type equation, that is, by a Gaussian shaped signal. The spreading of the Gaussian is related to the diffusion coefficient in the diffusive regime but, interestingly, grows as

the square of the Péclet number, in the convective regime. The Péclet number can be defined by

$$\mathscr{P}e = \frac{\langle v_\gamma \rangle^\gamma \, \mathrm{d}}{\mathrm{D}_\gamma} \tag{3.1}$$

where $\langle v_\gamma \rangle^\gamma$ refers to the surface average of the norm of the pointwise velocity field, d is the diameter of the tube and D_γ is the diffusion coefficient of the solute within the fluid $\gamma - \mathrm{phase}$. The Péclet number is a dimensionless number comparing the characteristic times associated with diffusion $\frac{\mathrm{d}^2}{\mathrm{D}_\gamma}$ and convection $\frac{\mathrm{d}}{\langle v_\gamma \rangle^\gamma}$. The effective diffusivity, commonly termed dispersion at the homogenized scale, can be written

$$\mathrm{D}_{\mathrm{eff}} = \mathrm{D}_\gamma \left(1 + \frac{\mathscr{P}e^2}{192} \right) \tag{3.2}$$

The component of the effective diffusivity associated with the Péclet number arises from fluctuations of the local velocity field. A molecule initially positioned in the middle of the tube is submitted to larger velocities than the molecules nearby the wall. As a consequence, the signal tends to spread more in the convective regime than in the diffusive one. Later on, experiments focused on the determination of the dispersive properties of laboratory columns and in particular, on the behavior of dispersion in relation to the Péclet number. These early insights showed that diffusion and dispersion are very different mechanisms. Diffusion is related to the Brownian motion of the molecules within the bulk fluid, whereas dispersion is a complex mixture of chemical and hydrodynamic processes that take the form of an effective diffusion at the macroscale. The next step was to analyze data from experiments at the field-scale [107]. These showed that, because of the multiscale heterogeneities, (1) dispersion is not constant in relation to space and time and (2) that anomalous (non-Fickian) dispersion can occur, i.e., long tails in breakthrough curves are observed and the transport cannot be described in terms of a one-equation advection-diffusion type equation.

The mathematical description of Darcy-scale biodegradation in porous media was put forth in the 80s [247, 29, 30, 140]. Models were based on the assumption that the transport could be described in terms of the concentration in the water-phase, and did not take into account the biofilm as a different phase. Biofilm introduces a multiphase aspect in the transport processes, as well as additional heterogeneities and length scales. A single concentration can be used in some very specific conditions, for instance, in the local mass equilibrium situation. It corresponds to (1) biofilms thick enough to be treated as continua and (2) hydrodynamic and chemical conditions for which relatively small gradients of the pointwise pore-scale concentration appear. Other conditions are termed local mass non-equilibrium and can arise from chemical, physical or biological processes. For example, mass transfer limitation through [173] the biofilm-fluid interface can lead to non-equilibrium situations, especially if the

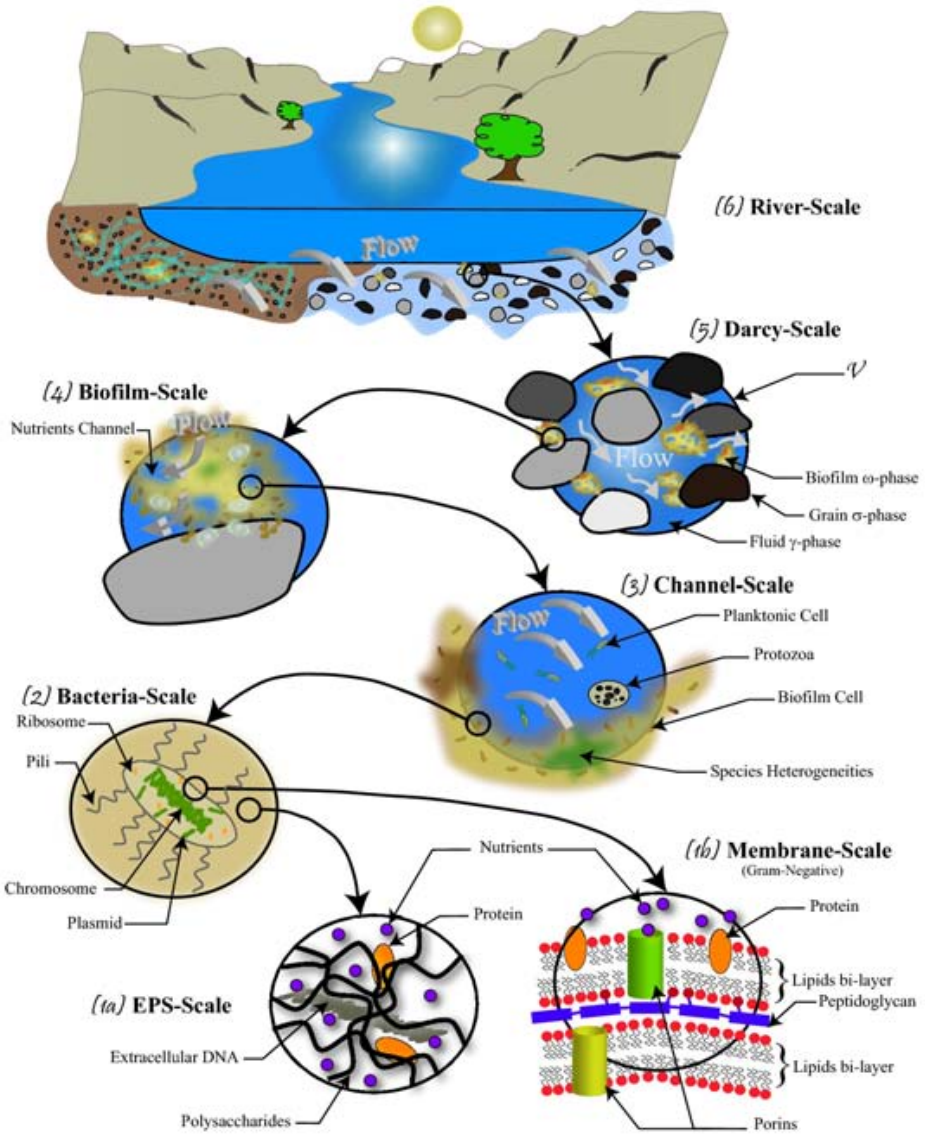

Figure 13: Hierarchy of the main scales involved in solute (nutrient) transport within porous media.

characteristic transport times within the fluid are shorter than within the biofilms. Similarly, mass consumption within the biofilm matrix can create strong concentration gradients and non-equilibrium conditions of mass between both phases (if the consumption is faster than the interfacial transfer [218, 4]). In the 90s and 2000s, a substantial amount of mathematical developments have been proposed to describe the transport of a solute undergoing biodegradation in porous media, the growth of biofilms and the momentum transport. These models have received a lot of attention in this thesis and are discussed in part IV.

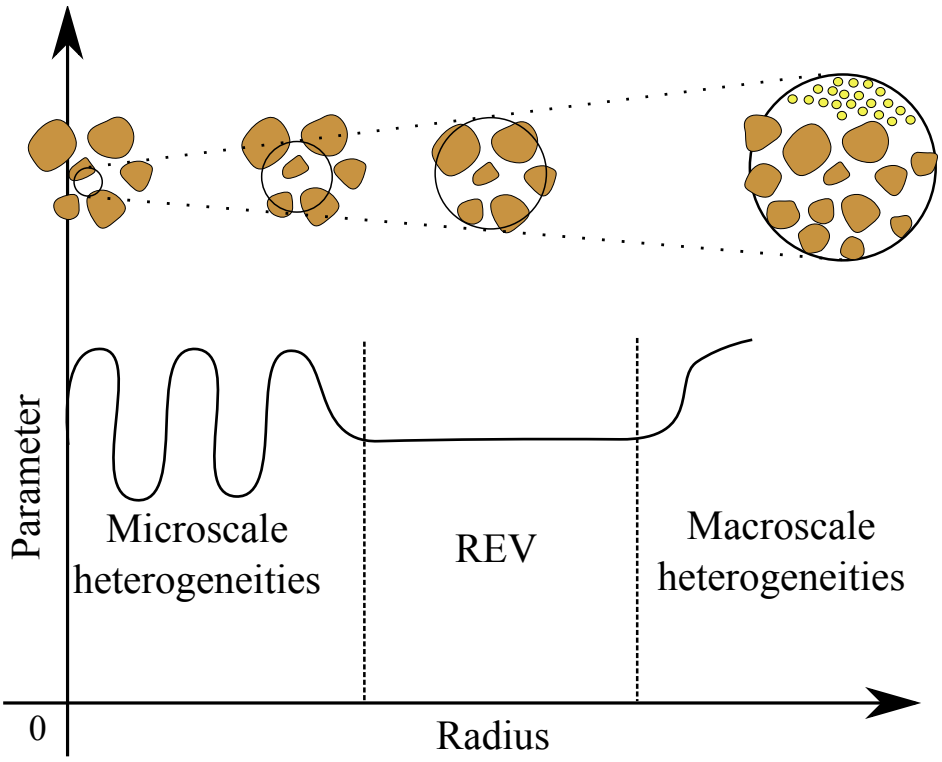

Figure 14: The REV concept.

Nowadays, the physics of transport in porous media is widely recognized as extremely complex as it deals with multiscale heterogeneities [67]. In the context of subsurface hydrology, processes within geological formations occur over multiple orders of magnitude in both space and time. Scales involved in pollutant/nutrient dispersion undertaking biodegradation in rivers subsurfaces colonized by microorganisms vary from sub-micrometer to hundreds of meters (see in Figure 13), involving heterogeneities of permeability, absorption, reaction, dispersive properties. In principle, the mass and momentum transport equations that apply to a porous medium could be solved at the sub-pore scale by computing numerical solutions with sufficient resolution over billions of pores. In the real world, however, this is impractical (albeit some strategies have been developed to approximate these simulations). Primarily, the reasons for this are (1) our computational resources are limited and (2) such detailed microscale solutions generally contain a substantial amount of information that is of low value to applications to the field. Information from the microscale generally has to be *filtered* in order to get rid of high frequency fluctuations; that is, perturbations in space or in time that represent deviations from some sort of averaged behavior. Once again two strategies have emerged. Models can either be derived using empirical analyses or upscaling techniques. Various upscaling procedures have been developed for this purpose, including both spatial and temporal averaging [274], ensemble averaging [69] and homogenization [23]. In performing the upscaling, it is

always necessary to invoke one or more *scaling laws [282]* that indicate the form of the redundancy in the microscale information. Usually, these scaling laws are specific statements regarding the amplitude of the fluctuations relative to the mean, and some notion of spatial and temporal stationarity in the processes of interest. For example, in the context of the deterministic volume averaging theory, a local description in space can be undertaken under the condition that the medium exhibits a hierarchy of length scales, that is, representative elementary volumes (REVs) can be defined and effective properties can be calculated locally on these REVs Figure 14.

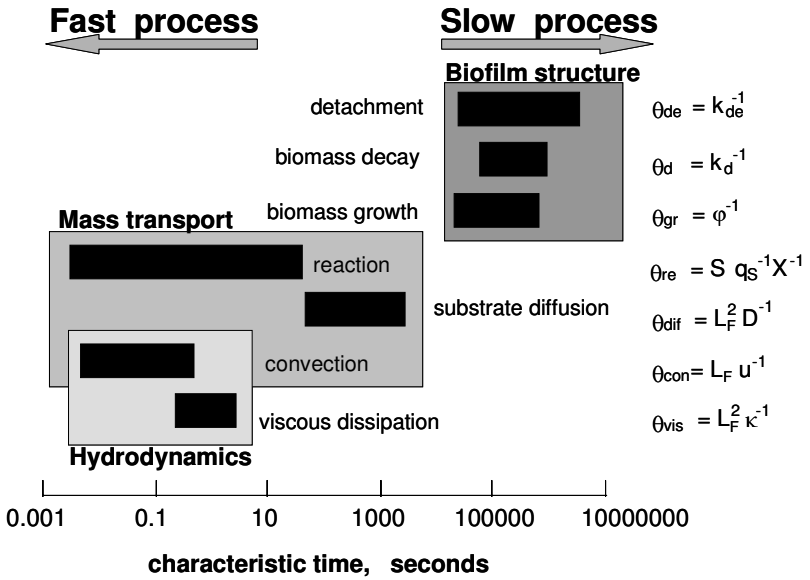

Figure 15: Temporal scales [270].

In addition to heterogeneities within the spatial continuum, processes associated with biofilms in porous media have the particularity to be heterogeneous in relation to the temporal continuum. Knowledge and understanding of the characteristic times corresponding to each process is fundamental. Processes that have similar characteristic times need to be treated simultaneously whereas processes that have very different characteristic times can be fully uncoupled. For example, let us consider the example of the nutrient given in the previous section. On the Figure 15, it is clear that mass transport phenomena and hydrodynamics need to be solved simultaneously whereas the modifications associated with the biofilm structure can be treated separately.

4

SCOPE AND STRUCTURE OF THE THESIS

IN BRIEF: WHERE ARE WE ? WHERE ARE WE GOING ?

The predominant methodology that has been adopted, so far, for the study of biofilm related problems in porous media (especially biodegradation) consists in (1) macroscopic observations, say breakthroughs curves (BTCs), and (2) interpretation of these in terms of either stochastic or mechanistic models. One issue, with the mechanistics models, is that accurate predictions require knowledge of the spatial distribution of the hydraulic, chemical, and biological properties. In other words, the formulation of the Darcy-scale models necessitates at least some information on the processes at the pore-scale and their spatial distribution. In most cases, however, the characterization of the subsurface is limited. Hence, modelers tend to use simplified heuristic transport equations involving effective parameters that are determined using inverse optimization techniques. The obvious counterpart is that most of the physics is lost. To overcome these difficulties, for field experiments, stochastic models represent an interesting alternative (e.g., discussion in [163]). In the stochastic framework, the BTCs are interpreted as probability density functions in multi-dimensional, heterogeneous domains [52, 53, 222].

However, advances in imaging techniques and modeling are allowing novel mechanistic strategies to emerge. An example of one such strategy, in the case of bioclogging, is suggested in [18]: "(1) focus efforts on the bioclogging mechanisms that are not well described yet in current mathematical models, (2) find the parameters and equations that describe these mechanisms at relevant scales, (3) incorporate these components in efficient pore-scale models based, e.g., on Lattice–Boltzmann formulations (e.g., [116]), and (4) upscale the resulting models to macroscopic scales, suitable for large-scale simulations". Although this methodology has been devised to study bioclogging, it is based on ideas that are much more general. We would rather propose the following approach (termed MVMV, for Micro-Validate-Macro-Validate, in the remainder of the thesis), that can be used to study a broad range of biofilms related problems in porous media, including mass transport and biodegradation:

1. image pore-scale biofilms growth within porous structures and formulate equations that describe the various pore-scale phenomena.

2. introduce these components in efficient pore-scale models based, for example, on Lattice–Boltzmann formulations (e.g., [116]) and validate the proposed mathematical descriptions.

3. upscale the set of differential equations (from the pore-scale to the Darcy-scale) in order to obtain different macroscale models and calculate effective parameters on the basis of 3-D realistic geometries.

4. develop the domains of validity of the various upscaled models, and validate the theoretical analysis against Darcy-scale experiments.

Steps 1 and 2 require a direct observation of the processes at the cell-scale and at the pore/biofilm-scale. This can be done using, for example, microfluidic devices in conjunction with microscopy techniques that are well known. However, the ability to directly observe biofilms within real porous structures would considerably limit experimental artefacts, that arise, for example, from dimensionality problems (2-D vs 3-D).

Steps 3 and 4 need some specific developments, that represent the core of this work. Darcy-scale models that are used to describe mass transport in such systems are not fully understood yet. In addition, effective parameters can be calculated in realistic situations, only if the spatial distribution of the different phases is known, that is, we would need to directly image biofilms within porous media.

Our goal, in this thesis, is to develop the elements that have been missing in order to implement such strategies. We address the development of the three-dimensional imaging technique and of the macrotransport theory. We study both the reactive and non-reactive situations. The reactive case obviously refers to biodegradation of chemicals or nutrients within porous media. The non-reactive problem refers to:

1. real situations, in which the pollutant is not degraded by the microorganisms.

2. a model situation, for which the physics of upscaling is easier to understand.

The macroscopic models are validated against Darcy-scale “numerical” experiments (direct numerical simulations at the pore-scale), under the assumption that steps 1 and 2 have already been performed, that is, we assume that we know the boundary-value-problem describing the mass transport problem at the pore-scale. We also illustrate the calculation of the effective parameters on real complex geometries.

STRUCTURE

The remainder of this thesis is organized as follows.

- First, we develop a technique for imaging biofilms in opaque porous media in three-dimensional configurations. The method uses X-ray microtomography to delineate between the biofilm-phase, the water-phase and the solid-phase. Part II is dedicated to the presentation of the method and discussions regarding

its scope of applications as well as its limitations. In particular, it is emphasized that direct observations of biofilms within porous media (1) would end some ancient debates regarding the spatial distribution of the microorganisms, (2) provides a tool for the validation of cellular automata models in porous media [116] and (3) captures a substantial amount of information regarding the pore-scale topology of the processes on a REV that can be used to develop mass transport models on a larger scale.

- Secondly, we develop Darcy-scale mass transport models that take the spatial distribution as an input parameters and that use this information to calculate effective properties that arise in the macroscale balanced equations. Following this line, the part III deals with the development of non-reactive Darcy-scale mass transport of a solute while part IV focuses on the biodegradation (reactive) transport processes on a similar scale. In both cases, the mathematical procedures are based on the deterministic upscaling technique termed volume averaging with closure. The models are validated against pore-scale direct numerical simulations and the physical as well as the mathematical significance of these models is thoroughly discussed.

- At last, in part V, we provide conclusive remarks and also discuss ongoing work and perspectives. In particular, we present the first numerical calculations of effective parameters (permeability) on the basis of the microtomography data.

WHAT'S NEW AND WHAT'S NOT ?

- The methodology (MVMV), presented in this part, to study and model biofilms related problems in porous media is new.

- The technique, presented in part II, for three-dimensional imaging of biofilms within porous media is new.

- The non-reactive models, presented in part III, are not new BUT the theoretical and numerical analyses that are used to determine their domains of validity and their relationships to one another are new. We present a comprehensive framework that did not exist and some insights to understand the physics of the upscaling process.

- The model, developed in part IV, is new. The idea to use such a perturbation decomposition is not new but it was never applied to any reactive case.

- The calculations of the permeabilities on the basis of realistic pore-scale geometries, as presented in part V, are new.

Part II

THREE-DIMENSIONAL IMAGING OF BIOFILMS IN POROUS MEDIA USING X-RAY COMPUTED MICROTOMOGRAPHY

1

INTRODUCTION - IMPORTANCE OF DIRECT OBSERVATIONS

Imaging biofilms within porous media represents an important challenge. The development of microscopy methods to directly observe the microorganisms at different scales is a *sine qua non* condition for understanding the mechanisms at play. The ability to image biofilm in three dimensions within porous media would also considerably aid in

1. providing the experimental data that has been lacking in order to validate the theoretical models that have been presented so far. For example, three-dimensional imaging of biofilms in porous media would provide the information that is necessary in order to delineate the domains of validity of both cellular automata and individual based approaches for the modeling of biofilms structures [153] and might trigger the development of new mathematical formulations.

2. developing new models and innovative modeling strategies. Two examples of such strategies (MVMV and Baveye's) are given and discussed in part I.

Various methods have been developed for imaging biofilms, including confocal laser scanning microscopy (CLSM) [155, 148] , light microscopy [14, 13], electron microscopy [203], atomic force microscopy [21], nuclear magnetic resonance imaging [161, 201] , infrared spectroscopy [184], optical coherence tomography [290], and high frequency ultrasound [234]. Unfortunately, many of the aforementioned techniques (1) are not applicable to porous media systems due to the inherent opacity of porous structures and (2) are also not well suited for imaging regions larger than several porous media grains. To circumvent problems (1) and (2), most of the work on pore-scale/biofilm-scale observations in porous media has focused on one-dimensional or two-dimensional networks [148, 254]. There has been some discussion of the differences induced by experimental dimensionality [254, 18, 255]. Baveye (2010) suggests that future work should focus on three-dimensional observations, using for example X-ray tomography, rather than on adapting pseudo one-dimensional or two-dimensional results to three-dimensional configurations.

As a noticeable exception, Seymour et al. [229, 231, 230] used non-invasive magnetic resonance microscopy to directly observe the three-dimensional velocity field

at the pore-scale and show that biofilm growth can induce anomalous transport. The issue with this technique is that it does not allow spatial resolution of the pore-scale geometry of the different phases within the porous matrix. Recent work presented by [131] focuses on the imaging of biofilm within porous media using monochromatic synchrotron based X-ray computed microtomography. Results from this work illustrate the ability of computed microtomography to provide experimental data for the validation of mathematical models of porous media associated with biofilm growth. However, the method is based so far on a cumbersome physical straining or on attachment of a contrast agent to the biofilm surface.

Here, we present a method for imaging non *a priori* labeled microbial biofilms in porous media using a benchtop X-ray computed tomography setup. The presented method allows for the three-dimensional reconstruction of the solid, aqueous and biofilm phases within a porous matrix with a voxel size of 9 μm (limitation only of the scanner at hand). A significant challenge, inherent to imaging biofilm within porous media using X-ray absorption tomography, lies in selecting proper contrast agents to aid in differentiating between materials with similar absorption coefficients, such as biofilm and water. Most conventional X-ray contrast agents diffuse readily into both the aqueous phase and biofilm [131]. The proposed method focuses on the use of a mixture of two different contrast agents that allow for differentiation of the solid, aqueous phase and biofilm regions within the experimental systems evaluated in this study. Herein, we will present only the final experimental procedure, that is, material and methods that proved the most successful. However, various preliminary tests were performed, including screening of various radiocontrast agents and of the corresponding concentrations.

The remainder of this part is organized as follows. First, we present the different protocols that are used in this experimental study. Then, we validate the use of the contrast agents by comparison of two-dimensional images obtained by (1) optical shadowscopy and (2) X-ray absorption radiography. Finally, the technique is applied to two different model porous media experimental systems containing polyamide or expanded polystyrene beads. Various reconstructed images are shown to illustrate the effectiveness of the method. The limitations of the technique are discussed as well as suggestions for future work.

2

MATERIAL AND METHODS

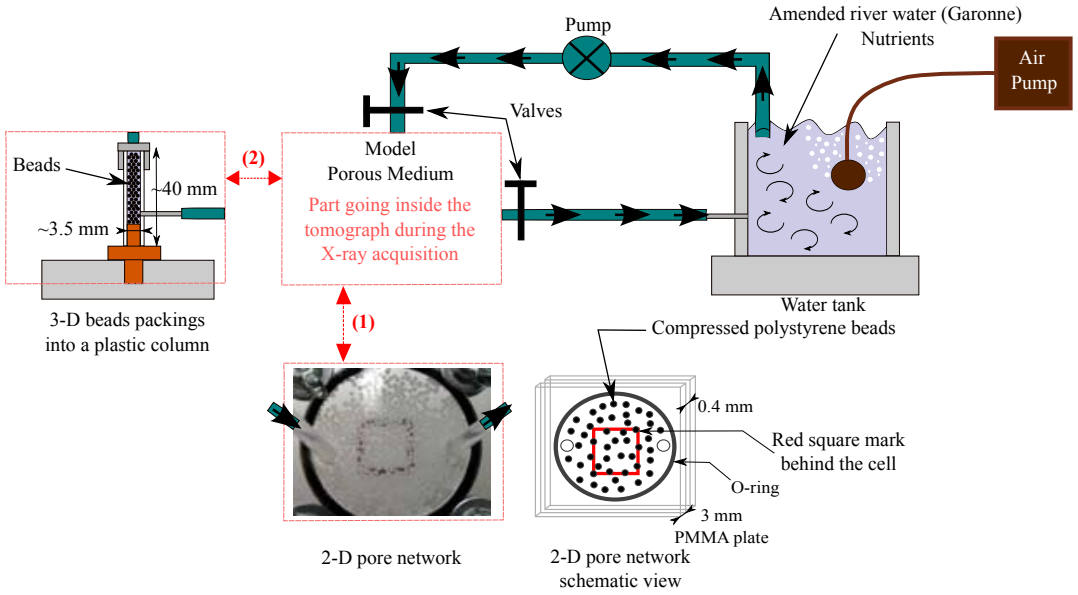

Figure 16: Flow system used for growing biofilm within (1) the two-dimensional pore network model and (2) the three-dimensional packed bead columns.

2.1 THE POROUS MODELS

Three types of porous media models were used for experimentation. Two-dimensional biofilm growth experiments were conducted using a porous medium network consisting of expanded polystyrene beads (500 to 1500 µm) compressed between two PMMA (Plexiglas®), 3 mm thick, transparent plates. Initial three-dimensional imaging was conducted using a polystyrene column (3.5 mm inner diameter) packed with 3 mm diameter polyamide beads. Additional three-dimensional biofilm imaging experiments were conducted using a polystyrene column (3.5 mm ID) packed with polystyrene beads (500 to 1500 µm). Expanded polystyrene has a lower X-ray absorption coefficient than polyamide, allowing an initial contrast between the biofilm and the beads. Schematics of the experimental devices can be found in Figure 16 and

Figure 17 for both the two-dimensional pore network and the three-dimensional column experiments.

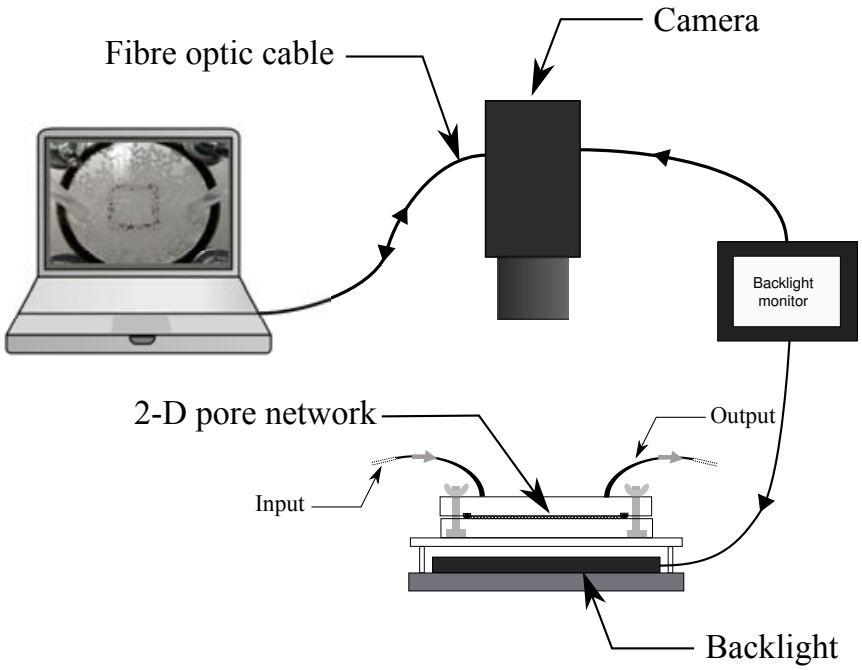

Figure 17: Optical visualization system for the two-dimensional pore network.

2.2 GROWING BIOFILMS

Raw water from the river Garonne (France) was collected, filtered using a 500 µm screen, clarified via sedimentation for approximately 24 hours. The river water was further amended with sodium acetate CH_3COONa; $3H_2O$ (carbon source) and potassium nitrate KNO_3 (electron acceptor) as indicated in Table 4. The prepared water was then placed in a 200 mL plastic feed tank used as the reservoir for experimentation. The feed tank was refilled with prepared river water daily for the duration of the experiments and constantly aerated using an air pump. The microbial flora naturally present in the prepared river water was experimentally determined to form sufficient biofilm with the porous medium for the purposes of this study. Flow within the experimental systems was induced using either a peristaltic or diaphragm pump (as detailed in Table 4). All experiments were conducted at $20°C \pm 1°C$ in the absence of light in order to control the growth of phototrophic organisms. Additional details are provided in Table 4.

	2-D pore network	3-D polyamide beads	3-D polystyrene beads
Beads diameters	500 to 1500 µm	3mm	500 to 1500 µm
Pump Type	Prominent Gamma/L diaphragm	Ismatec Mini-S 820 peristaltic	Watson Marlow 505 Du peristaltic
Nutrients			
Introduced at days	0, 3, 6 and 9	0, 4 and 7	0, 3, 6 and 9
CH_3COONa, $3H_2O$	0.66 g	0.16 g	0.66 g
KNO_3	0.33 g	0.06 g	0.33 g
Contrast agents			
C_{BaSO_4}	0.33 g/mL	0.66 g/mL	0.33 g/mL
C_{KI}	0.1 g/mL	0 g/mL	0.1 g/mL
Flow rates	3.5 mL/min	6 mL/min	0.07 and 0.5 mL/s

Table 4: Experimental parameters.

2.3 CONTRAST AGENT

As previously mentioned, both the biofilm and the aqueous phase have similar X-ray absorption properties. In addition, all the experimental systems evaluated in this study were designed using plastic materials in order to minimize the total X-ray exposure time of the microorganisms as well as to optimize the grey level scaling. Unfortunately, the plastic beads used as the experimental porous medium also have similar X-ray absorption properties to the biofilm and aqueous phase. Hence, obtaining contrast between the different phases requires the utilization of multiple contrast agents. Conventional contrast agents (e.g. potassium iodide) diffuse readily into biofilm when present in the aqueous phase. In this study, we use a medical suspension of micrometer sized barium sulfate (Micropaque, Guerbet, see in Figure 18), conceived to have a high density and low viscosity [62, 200], to enhance the absorption of the water-phase.

Although barium is usually highly toxic, it is commonly used as a medical radiocontrast agent for X-ray imaging of the gastrointestinal tract or angiography because of its insolubility in water and because it is known not to diffuse within the tissues. The idea behind the utilization of such a suspension is that particles are size excluded from the EPS matrix. If not totally immobilized, micrometer sized cells within biofilms are known to be greatly constrained in their motion. Hence, diffusion of similar sized barium sulfate particles through the polymeric matrix itself is likely to be negligible. To what extent the contrast agent can penetrate into the biofilm following the flow within nutrients channels and how this depends on the matrix architecture remains

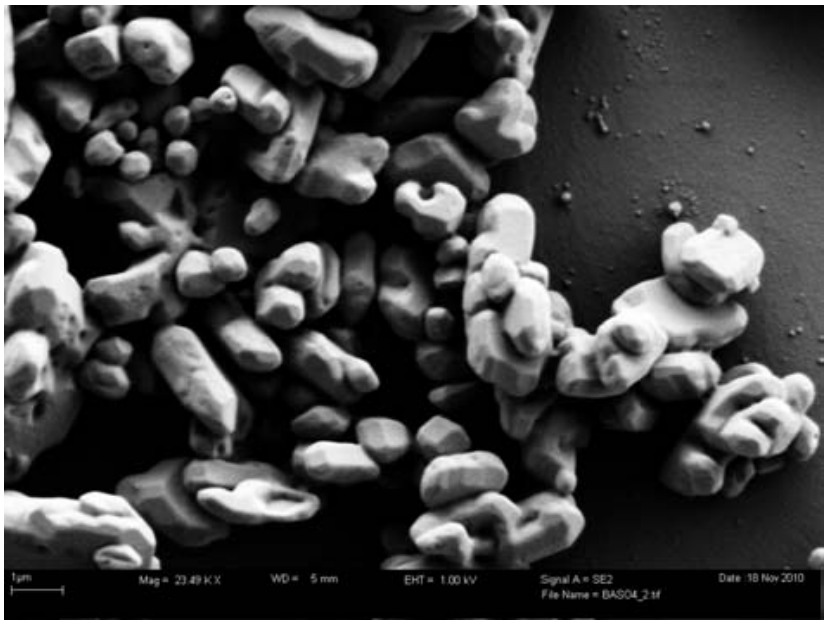

Figure 18: Scanning electron micrograph of the Micropaque barium sulfate particles. Courtesy of A. Phillips, J. Connolly and R. Guerlach (Montana state university).

to be fully characterized. It is interesting to emphasize that most studies concerned with convective flows within biofilms involve sub-micrometer sized particles [241] and that microbes grown with micrometer sized latex beads seem to be immobilized [87]. In addition, potassium iodide was added to the barium sulfate suspension in order to provide the required contrast between the polystyrene beads and the biofilm. Various ionic or non-ionic iodinated radiocontrast agents are used for medical purposes [10]. In our case, we only require that it readily diffuses within the polymeric matrix. In this context, iodide (whether NaI or KI) has proved to be adapted to X-ray microtomography for non-invasively imaging biological specimens [45].

For the polyamide beads, experiments focused on obtaining an important contrast between the biofilm and the water-phases, using only barium sulfate at higher concentrations. The details of the contrast agent mixtures used during experimentation are provided in Table 1. Preliminary scanning of the concentrations ratios were performed; herein, only the concentrations that proved to be the most successful are presented.

It is important to keep in mind that various strategies were formerly imagined, but only this one proved to be successful. In particular, a previous approach consisted in using barium sulfate to enhance the X-ray absorption of the biofilm-phase (in opposition to the water-phase). The barium sulfate was present within the water during the growth of the biofilm, and clean water was flushed in the column for the imaging. The idea was to trap the particles within the biofilm matrix, in order to provide a contrast between the biofilm-barium association and the water. Unfortunately, results showed

that it was pretty hard to delineate between the portion of the barium sulfate that was simply aggregating and the biofilm.

2.4 IMAGING PROTOCOLS

2.4.1 *Two-dimensional imaging*

The continuous flow of amended river water through the two-dimensional flow cells was induced and biofilm was allowed to develop for 10 days at which point optical imaging commenced using the system presented in Figure 17. A white LED backlight (PHLOX®) applied a uniform illumination of the pore network from beneath the stage and images were captured from above using a 12 bit (SensiCam) camera linked to a computer by a fiber optic cable (as illustrated in Fig (17)). Following optical imaging, 10 mL of the contrast agent solution consisting of 0.33 g/mL barium sulfate and 0.1 g/mL potassium iodide was injected into the flow cell. The system was then set to rest for approximately 1.5 hours in order to simulate the three-dimensional X-ray tomography image acquisition time frame (see Section 2.3.2). After this delay, a two-dimensional X-ray absorption radiograph was captured using a Skyscan 1174 tomograph with a pixel size of 12 μm.

2.4.2 *Three-dimensional imaging*

After 10 days of continuous flow the experimental flow cell was removed from the water flow circuit. 10 mL of the contrast mixture, containing a suspension of barium sulfate, potassium iodide, and water, was slowly injected through the porous model using a syringe. The concentrations of the contrast agent additives for the various experiments evaluated in this study are detailed in Table 1. The experimental flow cells then sat stagnant for approximately 15 minutes in order to allow for diffusion of the iodide into the biofilm. During these 15 minutes, a Skyscan 1174 tomograph was set to a tension voltage of approximately 50 kV and a current of 800 μA. All computed tomography imaging for this study was conducted at a resolution of 9 μm per pixel on a 360° rotation with a rotation step ranging from 0.5° to 0.7°. In each case, the total duration for tomographic imaging is approximately 1.5 hours. The major technical limitation we encountered during tomographic imaging was ring artifacts, regardless of the use of the ring artifact reduction option in the commercial software NRecon (SkyScan). Meanwhile, there is no limitation in the method itself which prevents the utilization of synchrotron based tomography (monochromatic) or new generations of scanners capable of producing higher quality images.

2.5 DATA ANALYSIS

2.5.1 *Two-dimensional image analysis*

Two-dimensional (radiographic) X-ray absorption images (12 bit TIFF images) and two-dimensional optical images (12 bit TIFF images) were post-processed using the open source software package ImageJ. For the X-ray images, we applied a FFT (Fast-Fourier Transform) bandpass filter to reduce extreme frequency noise. Then, the two data sets are compared using pseudocoloration based on a LookUp Table (LUT). This coloration was chosen on the basis of visualization purposes, as guides for the eyes. Quantitative measures, such as correlation ratios, strongly depend on the segmentation procedure. This is beyond the scope of this work to propose such methods; rather, we provide a qualitative analysis of the results. Representative images used for comparison of the two data sets are provided in Figure 19.

2.5.2 *Three-dimensional tomography*

The absorption projection images (12 bit TIFF images) were reconstructed using NRecon to obtain a set of cross-sectional slices (16 bit TIFF images) of the columns, using ring artifact and beam hardening correction. The various greyscale images presented in this article are encoded as 8 bit images for visualization purposes. For the polyamide beads, images were slightly smoothed and undergo global binarization using ImageJ Otsu's method. The surfaces are built in p3g, surface format, using the commercial software CTAn (Skyscan) and the three-dimensional geometry is observed using the software CTVol (Skyscan). The goal of this work is to provide an operational technique for imaging biofilm, i.e., to demonstrate that the use of a barium sulfate suspension as a contrast agent is feasible for imaging biofilm within a porous medium matrix.

3

RESULTS

3.1 TWO-DIMENSIONAL EXPERIMENTS

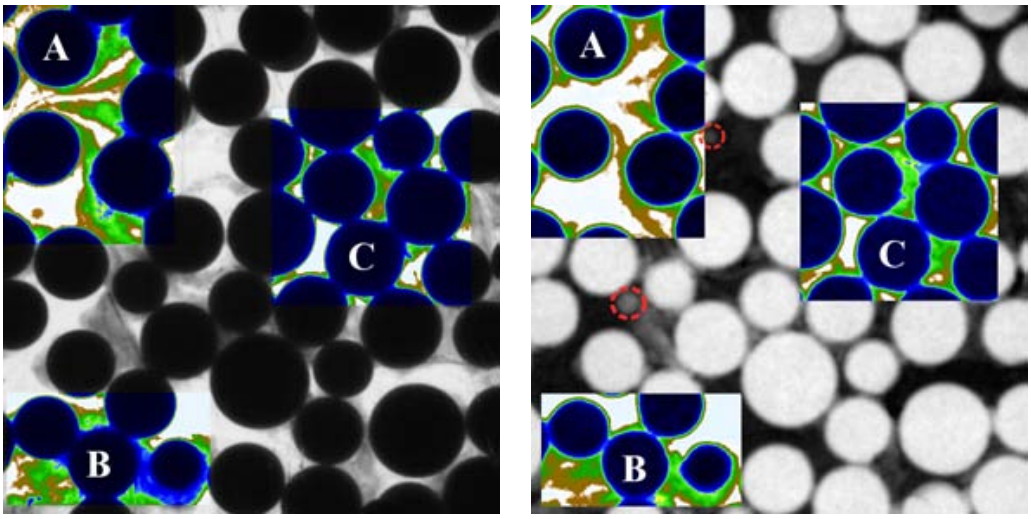

(1) Optical (2) Radiograph

Figure 19: Comparison of two-dimensional images after 10 days of growth obtained using (1) the visualization device detailed in Figure 17 and (2) Skyscan 1174 X-ray absorption radiograph captured approximately 1.5 hours after injection of the contrast agent mixture. Three zones A, B and C, assessing various pore-scale geometries, have undertaken pseudocoloration using ImageJ on the basis of a LookUp Table (LUT). The dark-blue parts correspond to the beads, the blue-green-brown parts to the biofilm and the white parts to the aqueous phase. The parts circled in red on the radiograph correspond to whether detached pieces of biofilm or gaz bubbles that are not present on the optical shadowscopy.

The purpose of the two-dimensional investigation was to evaluate the behavior of the contrast agent mixtures and to ensure that sufficient contrast between the various phases was achieved.

Potential issues identified include:

POTENTIAL ISSUE A Exclusion of the barium sulfate suspension from the biofilm EPS needs to be verified.

POTENTIAL ISSUE B The contrast agents need to be investigated to see whether interactions between the microorganisms and the contrast agents modify the EPS geometry, thereby preventing the acquisition of representative images.

POTENTIAL ISSUE C The injection of the contrast agent mixture needs to be examined to determine whether the induced shear stress associated with injection results in biofilm detachment from the porous media matrix or in modifications of the EPS geometry.

POTENTIAL ISSUE D It is necessary to determine whether prolonged (1.5 hour) X-ray exposure induces changes in the EPS geometry.

One caveat that must be taken into account when considering the presented X-ray computed tomography imaging method for biofilm investigations is that the technique is non-invasive, in that the biofilm growth can be imaged in situ, however X-ray exposure is expected to either severely retard microbial growth or kill the microorganisms all together. Thus the technique can be considered non-destructive to the porous media-biofilm matrix, however the imaging technique is still terminal. In order to investigate potential temporal changes to the biofilm matrix during imaging, a series of experiments were conducted to assess whether the issues previously identified as Problems A, B, C, and D negatively impact image accuracy and quality on the time-scale of a three-dimensional tomography acquisition (approximately 1.5 hours of exposure time using the Skyscan 1174 tomograph). Thus, images of a two-dimensional pore network colonized by biofilm obtained using both optical shadowscopy and X-ray computed tomography were compared. Results of the two-dimensional investigation are presented in Figure 19. Three zones, corresponding to different biofilm geometries, have been processed using a pseudocoloration to allow for comparison. Within Zone A, three biofilm filaments are clearly visible on both the optical image as well as the X-ray image. In Zones B and C, a clear correlation between the two geometries is apparent although discrepancies between the optical image and X-ray tomography image exist within these zones as well. Based upon the qualitative image comparison within these zones there appears to be good agreement between the two image capturing methods. Since the optical imaging method focuses, primarily, on a top-side view of the biofilm, the increased distribution of barium sulfate within the radiograph can be attributed to an increased flow channel volume within the biofilm that is not visible within the depth of field captured using optical microscopy. Thus the qualitative results presented in Figure 19 illustrate the utility of using X-rays (and the chosen contrast agents) to image biofilm, particularly when three-dimensional tomographs are captured as opposed to two-dimensional radiographs since the tomographs are capable of providing direct visualization of

the channeling suspected to be present within the biofilm present in Zones A, B, and C. The barium sulfate suspension used for imaging does not appear to significantly enter the EPS layer within these zones. Rather the barium sulfate appears to follow the aqueous phase flow channels. These conclusions are supported by the results, provided in the next section, concerning the successive use of barium sulfate and iodide. Hence, the issues previously detailed as A and B do not appear to significantly affect our imaging results. However, further investigations are required in order to elucidate the microscale behavior of the particles, especially in relation to the density of the EPS matrix and the physical properties of the contrast agent suspension. Nevertheless, the use of barium sulfate as a contrast agent for imaging biofilm within porous media is promising since the delineation of the topology of the flow channels and the associated impact on the transport processes at the pore-scale is definable within relatively large volumes.

While Problem D cannot be fully addressed using this two-dimensional experiment, we observed no substantial modifications to the EPS geometry after approximately 30 minutes of X-ray exposure. While biofilm associated microorganisms are expected to be severely inhibited or killed by exposure to X-rays, the biofilm matrix appears to be stable after exposure times of up to 1.5 hours from the benchtop tomography (Skyscan 1174) X-ray source used in this investigation. Three-dimensional results concerning this aspect of the problem are discussed in the next section.

3.2 RESULTS OF THE 3-D TOMOGRAPHY AND DISCUSSION

3.2.1 *Single polyamide bead*

The first set of 3-D experiments focuses on imaging of biofilm on 3 mm diameter polyamide beads. For this case, only the barium sulfate suspension was introduced as a contrast agent. Examples of projection data are presented in Figure 20 at time t = 0 without biofilm and at t = 10 days following the biofilm growth phase. Differences between these two raw images take the form of patchy white spots meaning, locally, lower X-ray absorption. These zones appear because biofilm has developed, constraining the local volume available for barium sulfate. This set of absorption data is used to reconstruct a set of cross-sectional slices on a single bead within the experimental column. Greyscale images as well as representative binary images are provided in Figure 21 at t = 0 and Figure 21 for t = 10 days. At t = 0, a cross-sectional circular shape, corresponding to the polyamide bead, is observed. After 10 days of biofilm growth, the boundary of the object that we imaged is tortuous and covers more surface. On the basis of the two-dimensional study presented in the preceding section, we interpret this additional area as biofilm. It is important to note that within Figure 21 there is no contrast between the plastic bead and the biofilm grown on the bead, further reinforcing the proposition that the barium sulfate suspension is excluded from the EPS layer of the biofilm. A solution of potassium iodide was then

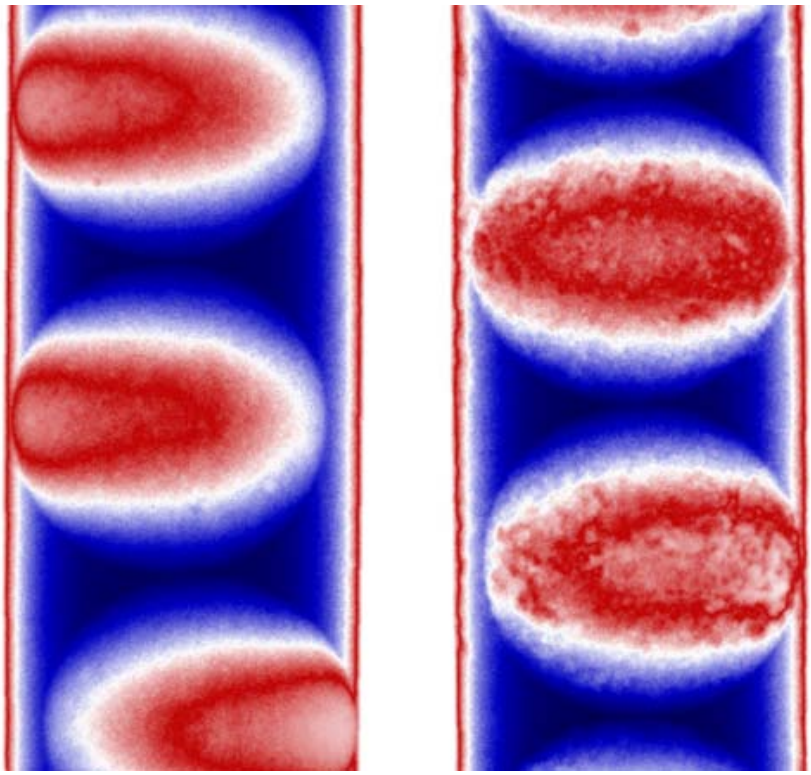

t=0 days t=10 days

Figure 20: Examples of projection images obtained with the SkyScan 1174 using BaSO4 as the contrast agent at time t = 0 days on the left and t = 10 days on the right. Both images have undertaken a pseudocoloration in ImageJ on the basis of the unionjack LUT (only for visualization purposes). Blue corresponds to the highest X-ray absorption, red to intermediate absorption and white to lowest absorption.

flushed through the system. A depiction of the polyamide bead after potassium iodide addition is provided as Figure 21. Iodide, when present in the aqueous phase, diffuses readily into biofilm present within the pore space. As a result, the contour of the polyamide bead is all that is visible in Figure 21, thereby confirming that the tortuous zone surrounding the bead in Figure 21 *is in fact biofilm.*

Surface reconstructions of the polyamide bead are provided in Figure 22. The surface reconstructions correspond to t = 0, prior to biofilm growth, and t = 10 days, after the biofilm growth phase. Contrast for both images is provided using the barium sulfate suspension. Within the imaged section, the biofilm appears to be highly heterogeneous and represents about 6% of the volume of the naked polyamide bead. Additional study is required in order to draw further conclusions on biofilm growth and development within our experimental system, however, the ability to image biofilm within porous media using the proposed technique has been established, which is the purpose of this study.

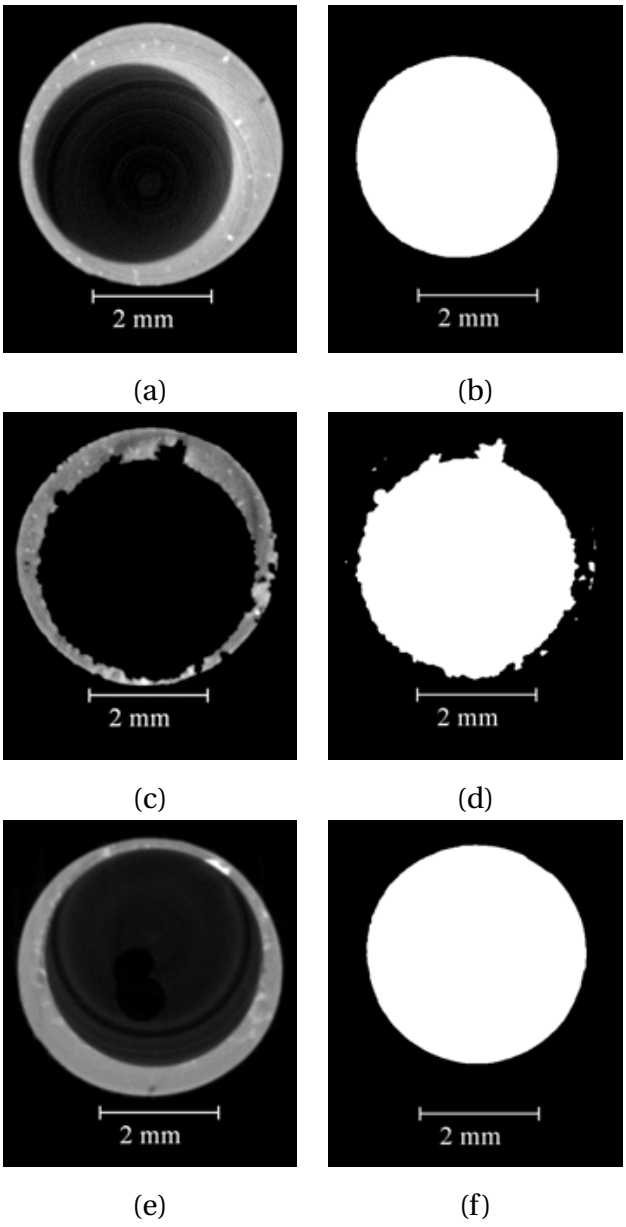

Figure 21: Cross-sectional reconstructed X-ray computed tomography data for a polyamide bead at t = 0 days with $BaSO_4$ (a) and (b); for a polyamide bead at t = 10 days, after biofilm growth, with $BaSO_4$ as the contrast agent (c) and (d); for a polyamide bead at t = 10 days using potassium iodide as the contrast agent (e) and (f). Images (a), (c) and (e) are grey scale initial images and (b), (d) and (e) their binarized counterpart (Otsu's algorithm with ImageJ).

3.2.2 *Results for the polydisperse expanded polystyrene beads*

For more complex porous structures, such as polydisperse polystyrene beads, the alignment of tomography data captured both prior to, as well as following biofilm

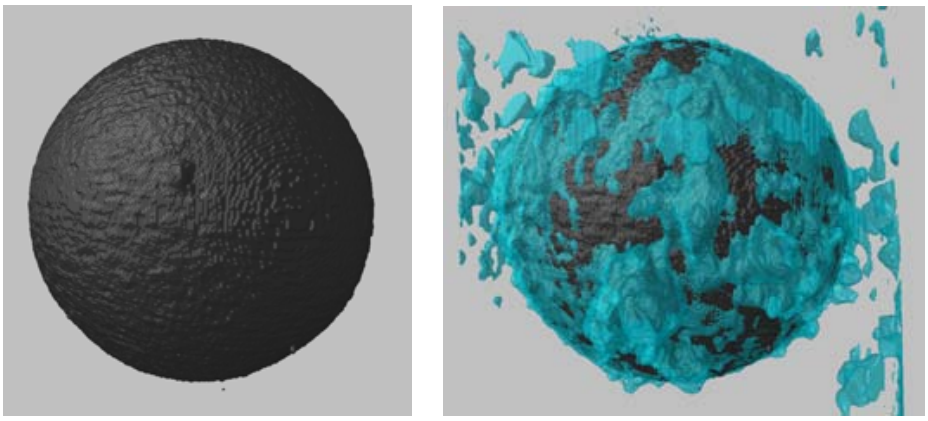

t=0 days t=10 days

Figure 22: Three-dimensional surface reconstructions of the polyamide bead at time t = 0 using $BaSO_4$ as the contrast agent and the biofilm (soft blue-green) and the polyamide bead (dark) at time t = 10 days.

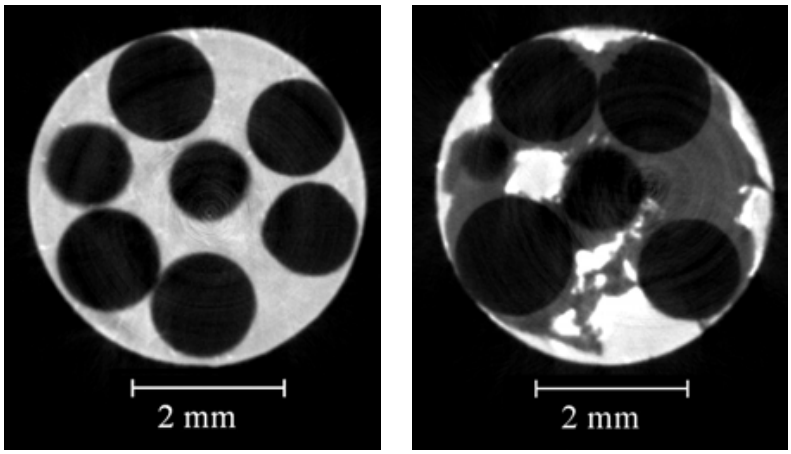

t=0 days t=10 days

Figure 23: Greyscale cross-sectional X-ray computed tomography for the experimental columns packed with polystyrene beads at t = 0 with the mixture of contrast agents and at time t = 10 days.

growth is not necessarily possible due to the potential for bead displacement due to fluid transport or biofilm growth. Thus image processing techniques such as image subtraction are not applicable. Image subtraction is not also desirable when working with natural media with heterogeneous solid phase X-ray absorption properties. Therefore, we developed a more direct technique. A mixture of the barium sulfate and potassium iodide contrast agents at two different concentrations was utilized to differentiate between the three materials present within the experimental system. Using this contrast mixture, tomographic imaging was performed. Preliminary imaging was carried out at time t = 0 after introducing the contrast agents mixture. Imaging

was also conducted at time t = 10 days, approximately 15 minutes after injecting the mixture of both contrast agents. Comparative results are provided in Figure 23 for the two data sets. Results for the t=0 data set indicate that the contrast agent solution delineates, clearly, the beads contained within the column. At t= 10 days the presence of three distinct phases is observed. The brightest phase corresponds to the barium sulfate (highest absorption coefficient). The dark regions correspond to beads and the intermediate greyscale values are interpreted as biofilm which the iodide has diffused into. Figure 24 illustrates the results of a comparative experiment examining biofilm growth within packed bead columns through which two different flow rates were applied. For this experiment two columns containing polystyrene beads and connected to the same water supply were exposed to flow rates of 0.07 mL/s and 0.5 mL/s. Within the two columns, biofilm growth is seen to decrease with increasing flow rate. While additional experiments are required in order to draw conclusions about biofilm growth within porous media, the presented results demonstrate that pore-scale information on biofilm growth within a porous medium is readily achievable using the proposed imaging method. Using the results generated using the presented method calculations of column or regional permeability can be performed numerically by solving Navier-Stokes equations. Darcy-scale dispersion tensors can also potentially be calculated using upscaling techniques.

Successive imaging of a single column was conducted in an effort to further evaluate the effect of X-ray exposure on biofilm structure (Problem D). The total exposure time was 3 hours and consisted of a sequence of 2 imaging cycles. At the conclusion of this experiment no change within the biofilm geometry were observable. This suggests that, for an acquisition time greater than 1.5 hours, X-rays at the energy emitted by the Skyscan 1174 tomograph (50 kV and 800 μA) do not modify the geometry of the biofilm EPS matrix.

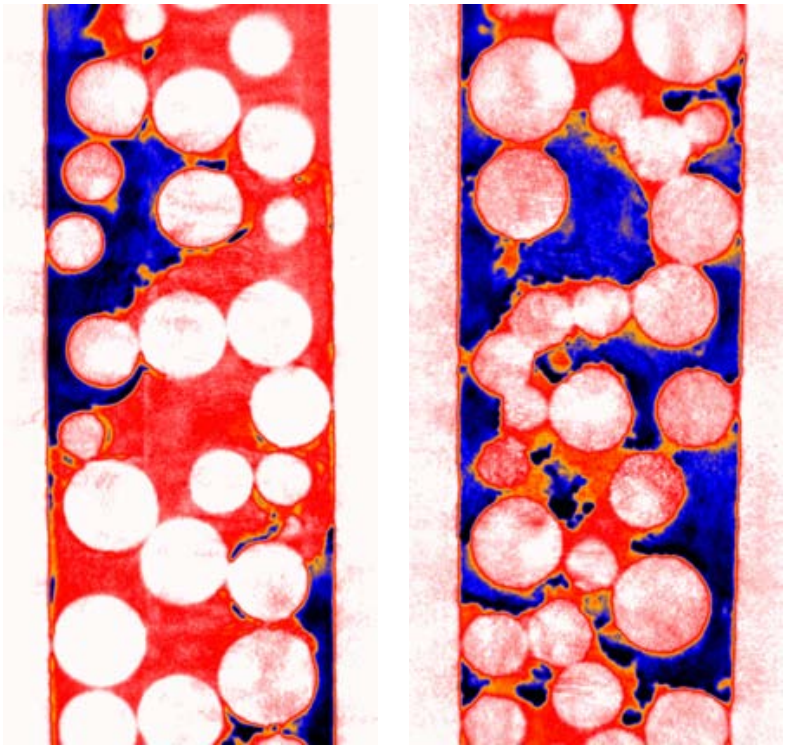

(a) Q=0.07 mL/s (b) Q=0.5 mL/s

Figure 24: Examples of reconstructed (X-ray Skyscan 1174 data) sectional slices for the entire length of the column obtained after 10 days at a flow rate of approximately (a) Q=0.07 mL/s and (b) Q=0.5 mL/s (a pseudocoloration has been applied to the images using ImageJ on the basis of the ceretec LUT and only for visualization purposes). The white-red parts correspond to the beads, the red parts to the biofilm and the blue-dark parts to the aqueous phase.

4

CONCLUSION AND DISCUSSION

CONCLUSION In this study, we present first results for a new method for imaging biofilm in porous media using X-ray computed tomography. We successfully used a mixture of two different contrast agents to obtain a three-phase contrasted three-dimensional representation of a model porous medium containing solids, water and biofilm. This approach, because of its simplicity, accessibility and applicability to complex porous structures, provides an interesting and versatile framework for studying biofilm within porous media systems. The method can potentially be used in the calculation of porous media effective parameters. In particular, the presented method opens possibilities for systematic studies of biofilm response, within porous media, to changes in physical, chemical and biological parameters. For example, modifications of local Reynolds and Péclet numbers, nutrient availability, temperature and pH stresses, and the impact of biofilm biodiversity on biofilm geometry within the three-dimensional porous media matrix can potentially be investigated. While the use of synchrotron X-ray sources hold the potential to provide higher quality imaging data and the imaging of biofilm in porous media has been investigated using synchrotron light and silver microspheres as a contrast agent [131], the method presented in this study is functional using both benchtop tomographs, such as the Skyscan 1174 as well as synchrotron X-ray sources, even though more sophisticated image processing procedures need to be developed. Thus the presented method is broadly applicable since imaging is not necessarily restricted by synchrotron accessibility and beam time constraints.

On the other hand, one significant limitation associated with the use of benchtop tomographs is that the required imaging time for porous media materials such as glass beads, soil or rock materials is significantly greater than the 1.5 hour image acquisition time reported in this study. As a result, investigations using these types of porous media are anticipated to require synchrotron light sources.

Future work will focus on (1) optimization of the image acquisition techniques such that images that can be easily (and impartially) segmented into their respective phases are obtained (whether it is using a different polychromatic or a monochromatic imaging system, optimizing the concentrations of the contrast agents, using separate imaging of the solid phase, etc.) (2) a comparison of this work with other three-dimensional planar imaging techniques such as confocal laser scanning microscopy,

for instance to provide further understanding of the interaction between the 1 μm $BaSO_4$ suspension and the architecture of the biofilm, (3) application to real porous samples with heterogeneities of absorption coefficients in the porous structures, and (4) an investigation of microbial retardation or mortality induced by X-ray exposure.

HOW CAN WE USE THIS INFORMATION ? In this thesis, we are particularly interested in using this information to model mass transport within porous media with biofilms. How can we use the 3-D images obtained using X-ray microtomography for this purpose ?

First, we need to define exactly what are the processes that we want to describe at the pore-scale level, that is, we need to derive a boundary value problem describing the mass balance within the system. For mass transport, it usually can include multiphasic descriptions of processes such as diffusion, convection, absorption or reaction. Generally, these involve complex non-linear mechanisms that are extremely difficult to upscale. Hence, this microscale problem needs to be defined carefully and often requires simplifications that must be clearly emphasized.

Once the small scale mathematical description of the problem is given, one can average the partial differential equations that are used to model the mass transport. Various upscaling techniques can be used toward that end, and are thoroughly discussed within the next part. These are aimed to determine the macroscale counterpart of the microscale boundary value problem. Under the assumption that a local (in space) description is desired, i.e., that a representative elementary volume can be defined, the effective parameters (for example dispersion or permeability) of the macroscale models can be calculated on the basis of this REV. In our case, we use the X-ray tomography technique in order to obtain the pore-scale topology of the processes on a REV, and use this as an input parameter for upscaled models. Deriving a macroscale theory that applies to solute transport is the goal of parts III (non-reactive) and IV (biologically mediated).

Part III

MODELING NON-REACTIVE NON-EQUILIBRIUM MASS TRANSPORT IN POROUS MEDIA

1

INTRODUCTION

In this part, we are interested in the Darcy-scale description of the transport of a conservative (non-reactive) solute tracer in porous media with biofilms. As previously emphasized, this case can refer to a physical situation in which the chemical species are not biodegraded. However, this is not the primary interest of this part. Here, we aim to understand the theory of volume averaging, and the different models that can be derived using this theory. The non-reactive problem is used as a simple case, in order to understand the upscaling process itself. We will focus on a biofilm-specific reactive situation in the next part, in which we use our knowledge of the upscaling process to develop a one-equation model that lends itself very well for the biofilm problem.

Following the same line, we also adopt a general formalism in this part, rather than a biofilm-specific one. For example, upscaling mass balanced equations from the pore-scale to the Darcy-scale in a dual-phase porous medium is, mathematically speaking, equivalent to upscaling from the Darcy-scale to a larger scale in a dual-region porous medium (Fig. 25). Hence, we consider a general framework defined by the mathematical structure of the boundary value problem at the small scale, rather than by the scale itself and the corresponding physical phenomena. Our goal is to develop a macroscale solute transport (via convection and diffusion) theory for discretely hierarchical and highly heterogeneous porous media containing two *different regions/phases* (Fig. 25). Depending on the value of the ratio of the characteristic times associated to the processes occurring in each region/phase and on the scale of application, these systems are usually referred to as mobile-immobile, mobile-mobile, dual-porosity, dual-permeability or, in a more general way, dual-continua [7, 43, 47, 48].

This part is organized as follows:

1. In this section, we briefly introduce the mathematical problem, discuss the various models and present the scientific scope for this part.

2. In section 2, we develop our macroscale transport theory and discuss the limitations associated to each model on the basis of theoretical analyses.

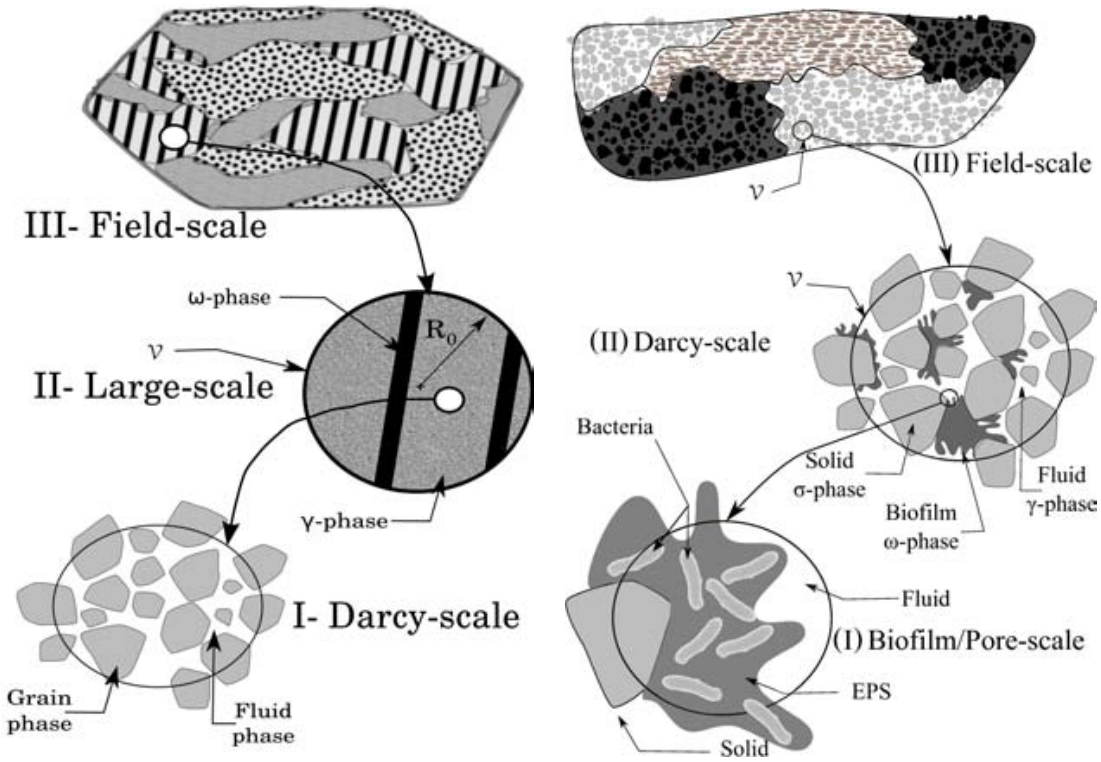

Figure 25: Hierarchy of the different scales for dual-region large-scale averaging (on the left) and dual-phase Darcy-scale averaging (on the right)

3. We advance a formal proof, section 3, for the equivalence between volume averaging and moments matching techniques regarding one-equation non-equilibrium models.

4. In section 4, we compare numerically on a simple two-dimensional example, the behavior of the models in response to a square input signal and delineate, on the basis of these computations and of the theoretical analysis carried out in the previous section, their domains of validity.

1.1 MICROSCOPIC DESCRIPTION OF THE PROBLEM

Herein, we present the boundary value problem that is used to describe the mass transport at the microscale (pore-scale/biofilm-scale for the biofilm problem, Darcy-scale for the larger scale problem). We consider two different phases/regions in which the solute undertakes diffusion/dispersion and convection. On the grains surface the flux is zero, that is, the solid σ is impermeable (this boundary condition BC4 exists only in the case of a pore-scale description and not for larger scales, unless when there are impervious nodules). We assume a continuity of the concentrations and of the flux at the boundary between the phases γ and ω. We consider only a diffusive flux on this boundary. This assumption is classically used for the biofilm transport problems, although an advective flux can be developed in the case of channeled biofilms if the matrix plus the channels are treated as a single continuum at the pore-scale [11]. For the sake of simplicity, we will consider that this (diffusive flux on the boundary) approximation is valid for both the biofilm and the larger scale problem. In essence, this means that the microscopic characteristic times associated with the advective terms in each phase/region are separated by several orders of magnitude, resulting essentially in a diffusive flux at the interface. In addition, we will not consider complex boundary conditions, such as jumps or conditions on chemical potentials. Although such boundary conditions would probably capture more physics of the problem, we aim to keep it simple in order to study the dual-continua upscaling process itself, more than the physics at the pore-scale.

The mass balanced equations take the form

$$\gamma-\mathrm{phase}: \frac{\partial c_\gamma}{\partial t} + \boldsymbol{\nabla}\cdot(c_\gamma \mathbf{v}_\gamma) = \boldsymbol{\nabla}\cdot(\mathbf{D}_\gamma\cdot\boldsymbol{\nabla} c_\gamma) \tag{1.1}$$

$$\begin{aligned}
&\mathrm{BC1}: && -\mathbf{n}_{\gamma\sigma}\cdot\mathbf{D}_\gamma\cdot\boldsymbol{\nabla}c_\gamma = 0 && \text{on } \mathscr{S}_{\gamma\sigma} && (1.2a)\\
&\mathrm{BC2}: && c_\omega = c_\gamma && \text{on } \mathscr{S}_{\gamma\omega} && (1.2b)\\
&\mathrm{BC3}: && -\mathbf{n}_{\gamma\omega}\cdot\mathbf{D}_\gamma\cdot\boldsymbol{\nabla}c_\gamma = -\mathbf{n}_{\gamma\omega}\cdot\mathbf{D}_\omega\cdot\boldsymbol{\nabla}c_\omega && \text{on } \mathscr{S}_{\gamma\omega} && (1.2c)\\
&\mathrm{BC4}: && -\mathbf{n}_{\omega\sigma}\cdot\mathbf{D}_\omega\cdot\boldsymbol{\nabla}c_\omega = 0 && \text{on } \mathscr{S}_{\omega\sigma} && (1.2d)
\end{aligned}$$

$$\omega - phase: \frac{\partial c_\omega}{\partial t} + \nabla \cdot (c_\omega \mathbf{v}_\omega) = \nabla \cdot (\mathbf{D}_\omega \cdot \nabla c_\omega) \tag{1.3}$$

In these equations, c_i is the concentration in the $i-phase$ supposed to be zero at $t = 0$. The velocity vector $\mathbf{v}_i$ is supposed to be known pointwise for the purposes of this study. $\mathbf{D}_i$ is the diffusion (pore-scale)/dispersion (Darcy-scale) tensor. $\mathscr{S}_{ij}$ is the interface between the $i-phase$ and the $j-phase$ and S_{ij} is the surface; $\mathbf{n}_{ij}$ is the corresponding normal vector pointing from i to j.

In the biofilm case, this representation is built on two assumptions: 1) the biofilm is thick enough to be treated as a continuum [287, 285], and 2) the microscale term $\nabla \cdot (c_\omega \mathbf{v}_\omega)$ describes the velocity induced by the nutrients channels that sometimes form within the biofilms. Such a description can be undertaken under the condition that there is a separation of the length scales corresponding to the diameter of the channels and to the width of the biofilm (the biofilm must be very large as compared to the size of the channels). These channels can also be treated, technically, as part of the fluid-phase in which case one can simply impose $\mathbf{v}_\omega = 0$ pointwise. The momentum transport can be modeled, at the pore-scale, using Navier-Stokes equations. For the purposes of this study, we will consider that the velocity field is known pointwise in the whole system. We will also assume that we are dealing with incompressible flows, which straightforwardly leads to an equation for the conservation of the mass that reduces to $\nabla \cdot \mathbf{v}_i = 0$.

For the dual-region problem, the microscale momentum transport equations already represent an homogenized problem that is often described in terms of a simple Darcy's law Equation (1.4).

$$\mathbf{v}_i = -\frac{\mathscr{K}_i}{\mu_i} (\nabla P_i - \rho_i \mathbf{g}) \tag{1.4}$$

Other formulations are possible such as Darcy-Forchheimer's or Brinkman's, depending on the physical situation at the pore-scale.

In addition, to simplify the ε_i from the equations, we assume $\nabla \varepsilon_i = 0$ and $\frac{\partial \varepsilon_i}{\partial t} = 0$. The conservation of the mass can also be written $\nabla \cdot \mathbf{v}_i = 0$ under the condition that the porous medium is homogeneous, that is, again, $\nabla \varepsilon_i = 0$.

1.2 FULLY NON-LOCAL MODELS

Upon averaging the microscopic boundary value problem, the macroscale transport process exhibits time and spatial non-locality under the most general conditions [144, 145, 68, 177, 43]. This behavior can be mathematically described via solutions or integro-differential equations that involve convolutions of a memory (kernel) function over space and time, i.e., the local solution depends on the solution everywhere in space and time, hence the word non-local. The non-locality is a rather complex

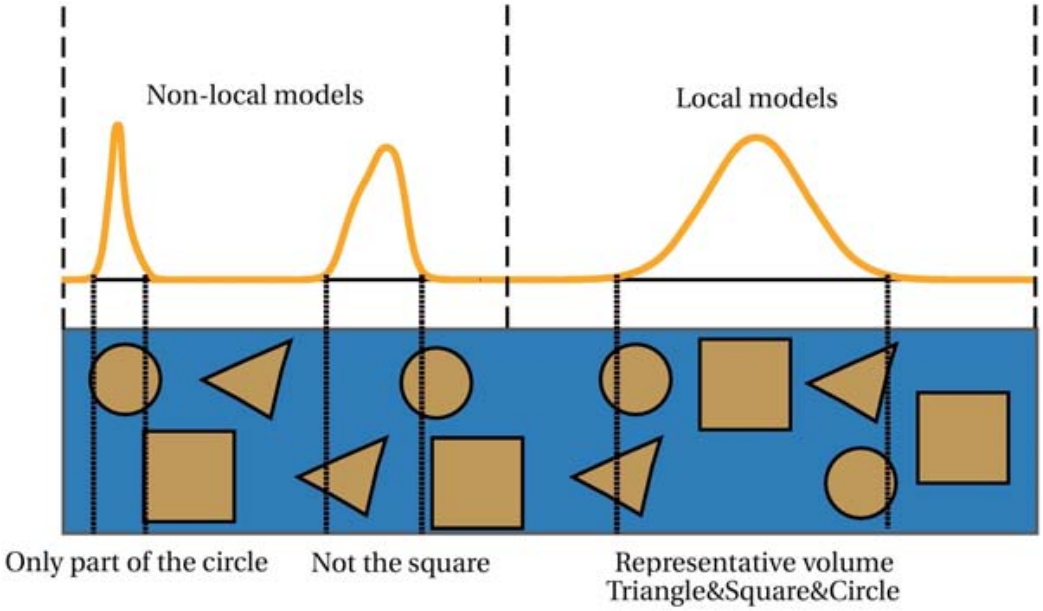

Figure 26: Simple illustration of the non-locality concept.

concept and, in addition to the formal definition, it is useful to give an example that can help in its comprehension. For instance, let us consider the propagation of a Dirac distribution, through a porous medium as represented on Fig (26). In the first stages of the propagation, the signal "sees" a very small portion of the porous structure that changes over space and time. The transport properties such as dispersion, permeability, volumic fraction of the phases can be defined only in relation to the signal itself and its history. The transport properties at one point of the medium change over space/time and depend on the shape of the signal, which is determined by what has happened before. In such situations, the transport is referred to as *non-local*. Going back to our example, the signal will spread until, eventually, it sees a *representative* portion of the porous medium. The medium that is seen by the signal will never be exactly the same but, if there is hierarchy of length scales, as presented on Fig (26), the transport properties will be identical in an averaged sense, and the transport becomes *local*.

One such example of a non-local model is given in [144] and can be written Equation (1.5)

$$\frac{\partial \langle\langle c \rangle\rangle}{\partial t} + \nabla \cdot \langle\langle \mathbf{q} \rangle\rangle = \langle\langle S \rangle\rangle \tag{1.5}$$

with

$$\mathbf{q} = \mathbf{v}c - \mathsf{D} \cdot \nabla c \tag{1.6}$$

where the ensemble average $\langle\langle\cdot\rangle\rangle$ refers to an average over an ensemble of velocity fields, often interpreted, for real field applications, in terms of its volume averaged counterpart under some ergodic conditions. If ergodicity does not apply [70, 71, 98], other volume averaged non-local theories have been formulated, for example in [282]. In both cases, non-local transport theories necessarily involve convolutions over space and time, and Eq (1.5) is only taken as an example. c is the pointwise microscale concentration, $\mathbf{v}$ is the microscale velocity field, D is the microscale diffusion tensor and S is the microscale source term. The macroscopic flux can be written Equation (1.7)

$$\langle\langle\mathbf{q}\rangle\rangle = \mathbf{V}\langle\langle c\rangle\rangle - \int dx_1 \int_{-\infty}^{t} dt_1 \left[\mathsf{D}(\mathbf{x}-\mathbf{x}_1, t-t_1)\cdot\boldsymbol{\nabla}\langle\langle c(\mathbf{x}_1,t_1)\rangle\rangle\right. \tag{1.7}$$
$$\left. +\mathbf{w}(\mathbf{x}-\mathbf{x}_1, t-t_1)\left(\frac{\partial\langle\langle c(\mathbf{x}_1,t_1)\rangle\rangle}{\partial t_1} + \mathbf{V}\cdot\boldsymbol{\nabla}_1\langle\langle c(\mathbf{x}_1,t_1)\rangle\rangle\right) - \boldsymbol{\sigma}(\mathbf{x}_1,t_1)\langle\langle S(\mathbf{x}_1,t_1)\rangle\rangle\right]$$

in which $\mathbf{V}$ is a weighted averaged velocity; D, $\mathbf{w}$ and $\boldsymbol{\sigma}$ are averaged quantities that depend mostly on a Green's function that can be calculated through the resolution of a microscale boundary value problem. The difficulty with such fully non-local theories is that the resulting macroscale problem Equation (1.5) exhibits, under most circumstances, almost as many degrees of freedom as the original microscale problem. These representations are extremely important from a fundamental perspective, but they may not always significantly reduce the information content of the underlying microscale model.

Other solutions to get an accurate response include direct numerical simulations, but it is not often tractable for most of porous systems because of the complexity involved. Degraded models, but still rather accurate if one is concerned with the estimate of the flux exchanged between the different phases/regions, can be derived under the form of mixed models for mobile/immobile systems, i.e., systems with high diffusivity contrast and no advection in the low diffusivity phase/region [8, 159, 83].

Anyways, these formulations are often overly complex and, hence, it is of utmost importance to develop local models that approximate the convolutions under some asymptotic limitations, whenever it is possible. Toward this goal, various degrees of approximations have been proposed for non-local models (e.g., [43, 121]), usually based on various conjectures about the time and space scales of the transport phenomena involved. Developing these space local models and understanding their limitations is the goal of this part. Various techniques are available to perform such operations. Herein, we use the filtering process that consists in (1) volume averaging over a locally periodic representative elementary volume (REV) and (2) closing the problem by imposing a relationship between the fluctuations at the small scale and the macroscopic variables. We also provide a theoretical analysis in terms of the spatial moments matching technique.

1.3 VOLUME AVERAGE DEFINITIONS FOR THIS WORK

To obtain a macroscopic equation for the mass transport, we average each microscopic equation over a representative region (REV), for example at the Darcy-scale, $\mathcal{V}$ Fig (25). $\mathcal{V}_\gamma$ and $\mathcal{V}_\omega$ are the Euclidean spaces representing the γ- and ω-phases within the REV. V_γ and V_ω are the Lebesgue measures of $\mathcal{V}_\gamma$ and $\mathcal{V}_\omega$, that is, the volumes of the respective phases. The Darcy-scale *superficial* average of c_i (where i represents γ or ω) is defined the following way

$$\langle c_\gamma \rangle = \frac{1}{V}\int_{\mathcal{V}_\gamma} c_\gamma \, dV, \ \langle c_\omega \rangle = \frac{1}{V}\int_{\mathcal{V}_\omega} c_\omega \, dV \tag{1.8}$$

Then, we define *intrinsic* averaged quantities

$$\langle c_\gamma \rangle^\gamma = \frac{1}{V_\gamma}\int_{\mathcal{V}_\gamma} c_\gamma \, dV, \ \langle c_\omega \rangle^\omega = \frac{1}{V_\omega}\int_{\mathcal{V}_\omega} c_\omega \, dV \tag{1.9}$$

Volumes V_γ and V_ω are related to the volume V by

$$\varepsilon_\gamma = \frac{V_\gamma}{V}, \ \varepsilon_\omega = \frac{V_\omega}{V} \tag{1.10}$$

with ε_γ and ε_ω called volume fractions of the relevant phases/regions.

To simplify the developments, we assume that both volume fractions are constant through time and space (we have already discussed and justified this quasi-steady assumption in the case of growing biofilms). In addition, we have

$$\langle c_\gamma \rangle = \varepsilon_\gamma \langle c_\gamma \rangle^\gamma, \ \langle c_\omega \rangle = \varepsilon_\omega \langle c_\omega \rangle^\omega \tag{1.11}$$

During the averaging process, there arise terms involving the point values for c_γ, c_ω, $\mathbf{v}_\gamma$ and $\mathbf{v}_\omega$. To treat these term conventionally, one defines perturbation decompositions as follows

$$c_\gamma = \langle c_\gamma \rangle^\gamma + \tilde{c}_\gamma \tag{1.12}$$
$$c_\omega = \langle c_\omega \rangle^\omega + \tilde{c}_\omega \tag{1.13}$$
$$\mathbf{v}_\gamma = \langle \mathbf{v}_\gamma \rangle^\gamma + \tilde{\mathbf{v}}_\gamma \tag{1.14}$$
$$\mathbf{v}_\omega = \langle \mathbf{v}_\omega \rangle^\omega + \tilde{\mathbf{v}}_\omega \tag{1.15}$$

Under the assumption that the transport is local, we have the following properties for the perturbations

$$\langle \tilde{c}_\gamma \rangle^\gamma = 0$$
$$\langle \tilde{c}_\omega \rangle^\omega = 0$$

In addition, we define a volume-fraction weighted averaged concentration [285, 188]

$$\langle c \rangle^{\gamma\omega} = \frac{\varepsilon_\gamma}{\varepsilon_\gamma + \varepsilon_\omega} \langle c_\gamma \rangle^\gamma + \frac{\varepsilon_\omega}{\varepsilon_\gamma + \varepsilon_\omega} \langle c_\omega \rangle^\omega \tag{1.16}$$

Perturbation decompositions associated with this weighted averaged concentration are

$$c_\gamma = \langle c \rangle^{\gamma\omega} + \hat{c}_\gamma \tag{1.17a}$$
$$c_\omega = \langle c \rangle^{\gamma\omega} + \hat{c}_\omega \tag{1.17b}$$

With this latter definition, we do not generally have the condition that the intrinsic average of the deviation is zero, i.e., $\langle \tilde{c}_\gamma \rangle^\gamma, \langle \tilde{c}_\omega \rangle^\omega = 0$. However, we do have a generalization of this idea in the form

$$\varepsilon_\omega \langle \hat{c}_\omega \rangle^\omega + \varepsilon_\gamma \langle \hat{c}_\gamma \rangle^\gamma = 0 \tag{1.18}$$

1.4 TWO-EQUATION MODELS

TWO-EQUATION QUASI-STEADY MODEL One set of approximations of the convolutions Eq (1.5) leads to the description of the transport as a system of two equations coupled by a linear exchange operator Eqs (1.19)-(1.20) [2, 48, 47].

$$\begin{aligned} \varepsilon_\gamma \frac{\partial \langle c_\gamma \rangle^\gamma}{\partial t} + \varepsilon_\gamma \mathbf{V}_{\gamma\gamma}(\infty) \cdot \nabla \langle c_\gamma \rangle^\gamma + \varepsilon_\gamma \mathbf{V}_{\gamma\omega}(\infty) \cdot \nabla \langle c_\omega \rangle^\omega &= \varepsilon_\gamma \nabla \cdot (\mathbf{D}_{\gamma\gamma}(\infty) \cdot \nabla \langle c_\gamma \rangle^\gamma) \\ &+ \varepsilon_\gamma \nabla \cdot (\mathbf{D}_{\gamma\omega}(\infty) \cdot \nabla \langle c_\omega \rangle^\omega) \\ &- h(\infty)(\langle c_\gamma \rangle^\gamma - \langle c_\omega \rangle^\omega) \\ &+ \varepsilon_\gamma Q^\gamma(\mathbf{x}, t) \end{aligned} \tag{1.19}$$

$$\begin{aligned} \varepsilon_\omega \frac{\partial \langle c_\omega \rangle^\omega}{\partial t} + \varepsilon_\omega \mathbf{V}_{\omega\gamma}(\infty) \cdot \nabla \langle c_\gamma \rangle^\gamma + \varepsilon_\omega \mathbf{V}_{\omega\omega}(\infty) \cdot \nabla \langle c_\omega \rangle^\omega &= \varepsilon_\omega \nabla \cdot (\mathbf{D}_{\omega\gamma}(\infty) \cdot \nabla \langle c_\gamma \rangle^\gamma) \\ &+ \varepsilon_\omega \nabla \cdot (\mathbf{D}_{\omega\omega}(\infty) \cdot \nabla \langle c_\omega \rangle^\omega) \\ &- h(\infty)(\langle c_\omega \rangle^\omega - \langle c_\gamma \rangle^\gamma) \\ &+ \varepsilon_\omega Q^\omega(\mathbf{x}, t) \end{aligned} \tag{1.20}$$

In these equations, the macroscale parameters $\mathbf{V}_{ij}(\infty)$ and $\mathbf{D}_{ij}(\infty)$ are effective velocity and dispersion tensors of the two-equation model; and the parameter $h(\infty)$ is a macroscale mass exchange coefficient. The term Q^i is a source term that accounts for particular boundary and initial conditions.

Even though the model Eqs (1.19)-(1.20) captures a lot of the characteristic times scales (or, equivalently, the eigenvalues of the temporal portion of the problem) associated with the transport processes, such a formulation still loses important features. The main assumptions underlying the two-equation model are that (1) the hypothesis of separation of length scales is valid, and (2) the time scale associated with the macroscale concentrations, $\langle c_i \rangle^i$, are very large as compared to the characteristic time for the relaxation of the fluctuations, $\tilde{c}_i$ (defined by $\tilde{c}_i = c_i - \langle c_i \rangle^i$). In particular, it has been pointed out that the first-order constant mass exchange coefficient is applicable under certain limitations [192]. It must be emphasized that the macroscale mass transfer coefficient, h, depends on both the medium properties and the boundary/initial conditions, and that this parameter is generally a dynamic one that changes in time as the solution evolves. As an effort to account for this transient behavior, various models, aiming to filter less information from the microscale and to capture more characteristic times associated with interphases transfers have been developed. These models can be grouped together, and are known generally as multi-rate mass transfer models [120].

TWO-EQUATION TRANSIENT CLOSURE

One other interesting idea that deserves additional consideration is one that aims to estimate one or the other convolution at a time. Traditionally, these two hypotheses have been used together, that is, both the convolutions in space and in time are approximated in the same model. However, fully eliminating spatial non-local parameters while keeping the time convolutions can lead to very interesting formulations. In particular, we are interested in the time non-local model Eqs (1.21)-(1.22) proposed in [177, 237]. In this model, the hypothesis of quasi-stationarity of the closure problems is not required. The result is that the macroscopic equations contain time convolutions.

$$\begin{aligned}
\varepsilon_\gamma \frac{\partial \langle c_\gamma \rangle^\gamma}{\partial t} + \varepsilon_\gamma \mathbf{V}_{\gamma\gamma}(t) \cdot * \frac{\partial}{\partial t} \nabla \langle c_\gamma \rangle^\gamma + \varepsilon_\gamma \mathbf{V}_{\gamma\omega}(t) \cdot * \frac{\partial}{\partial t} \nabla \langle c_\omega \rangle^\omega &= \varepsilon_\gamma \nabla \cdot \left(\mathbf{D}_{\gamma\gamma}(t) \cdot * \frac{\partial}{\partial t} \nabla \langle c_\gamma \rangle^\gamma \right) \\
&+ \varepsilon_\gamma \nabla \cdot \left(\mathbf{D}_{\gamma\omega}(t) \cdot * \frac{\partial}{\partial t} \nabla \langle c_\omega \rangle^\omega \right) \\
&- h(t) * \frac{\partial}{\partial t} \left(\langle c_\gamma \rangle^\gamma - \langle c_\omega \rangle^\omega \right) \\
&+ \varepsilon_\gamma Q^\gamma(\mathbf{x}, t) \qquad (1.21)
\end{aligned}$$

$$\begin{aligned}\varepsilon_\omega \frac{\partial \langle c_\omega \rangle^\omega}{\partial t} + \varepsilon_\omega \mathbf{V}_{\omega\gamma}(t) \cdot * \frac{\partial}{\partial t} \boldsymbol{\nabla} \langle c_\gamma \rangle^\gamma + \varepsilon_\omega \mathbf{V}_{\omega\omega}(t) \cdot * \frac{\partial}{\partial t} \boldsymbol{\nabla} \langle c_\omega \rangle^\omega &= \varepsilon_\omega \boldsymbol{\nabla} \cdot \left(\mathbf{D}_{\omega\gamma}(t) \cdot * \frac{\partial}{\partial t} \boldsymbol{\nabla} \langle c_\gamma \rangle^\gamma \right) \\ &+ \varepsilon_\omega \boldsymbol{\nabla} \cdot \left(\mathbf{D}_{\omega\omega}(t) \cdot * \frac{\partial}{\partial t} \boldsymbol{\nabla} \langle c_\omega \rangle^\omega \right) \\ &- h(t) * \frac{\partial}{\partial t} \left(\langle c_\omega \rangle^\omega - \langle c_\gamma \rangle^\gamma \right) \\ &+ \varepsilon_\omega Q^\omega(\mathbf{x}, t) \end{aligned} \tag{1.22}$$

Here the operator $*$ indicates the convolutions in time. When the characteristic time for the relaxation of the effective parameters, in particular of the mass transfer function, $h(t)$, is very small as compared to the characteristic time for temporal variations of $\langle c_i \rangle^i$, the convolutions tend toward a simple integration leading back to Eqs (1.19)-(1.20) (cf. Section 4.1 and 4.2 in [43]). Notice that we will use a global notation $\mathbf{D}_{ij}$ to indicate either $\mathbf{D}_{ij}(t)$ or $\mathbf{D}_{ij}(\infty)$ when there is no ambiguity as to which one we are referring to.

An important limitation with this approach is the postulate that the non-locality in time is weakly coupled with the non-locality in space. Significant coupling can arise from particular choices of boundary and initial conditions; as an example, coupling would be expected for a delta pulse. As the signal propagates through the medium, the mass spreads in space and in time and the influence of the non-locality is often reduced. Hence, the convolution formulation given by Eqs (1.21)-(1.22) refers to situations in which the perturbations are well captured by the first-order spatial closure associated with a two-equation model but in which a fully transient closure is necessary.

Another problem with Eqs (1.21)-(1.22) or even with Eqs (1.19)-(1.20) is that the system of coupled equations that needs to be solved is rather complex. Discretization of the convolutions can be performed, but a computational solution would be quite time-consuming. As a consequence, Eqs (1.21)-(1.22) are generally avoided, albeit they have been used to interpret some experimental data [147]. Even Eqs (1.19)-(1.20) are often being replaced by a simple advection-dispersion equation.

1.5 ONE-EQUATION MODELS

These two-equation models showed good agreement in numerous works with both numerical computations and experimental data [55, 81, 115, 35, 57] and can be confidently used to explore some physical aspects of the problem. In particular, two very different situations leading to simple Fickian dispersion have been identified [150, 205, 48].

ONE-EQUATION LOCAL MASS EQUILIBRIUM MODEL

On the one hand, when the macroscopic concentration in one phase/region can be expressed as a thermodynamic function of the concentration in the other phase/re-

gion, the situation is called local mass equilibrium [205] and a one-equation model Eq (1.23) represents a reasonable approximation of the mass transport problem.

$$(\varepsilon_\gamma + \varepsilon_\omega)\frac{\partial \langle c\rangle^{\gamma\omega}}{\partial t} + \mathbf{V}\cdot\boldsymbol{\nabla}\langle c\rangle^{\gamma\omega} = \boldsymbol{\nabla}\cdot\{\mathbf{D}^{equ}\cdot\boldsymbol{\nabla}\langle c\rangle^{\gamma\omega}\} \tag{1.23}$$

where

$$\langle c\rangle^{\gamma\omega} = \frac{\varepsilon_\gamma}{\varepsilon_\gamma+\varepsilon_\omega}\langle c_\gamma\rangle^{\gamma} + \frac{\varepsilon_\omega}{\varepsilon_\gamma+\varepsilon_\omega}\langle c_\omega\rangle^{\omega} \tag{1.24}$$

ONE-EQUATION TIME-ASYMPTOTIC NON-EQUILIBRIUM MODEL

On the other hand, the time-infinite comportment of the first two spatial centered moments reveals that two-equation models have a time-asymptotic behavior which can be described in terms of a classical advection/dispersion one-equation model Eq (1.25) [295, 2]. It corresponds to a particular time constrained local non-equilibrium situation for which the tracer does not exhibit anomalous dispersion.

$$(\varepsilon_\gamma + \varepsilon_\omega)\frac{\partial \langle c\rangle^{\gamma\omega}}{\partial t} + \mathbf{V}\cdot\boldsymbol{\nabla}\langle c\rangle^{\gamma\omega} = \boldsymbol{\nabla}\cdot\{\mathbf{D}^{\infty}\cdot\boldsymbol{\nabla}\langle c\rangle^{\gamma\omega}\} \tag{1.25}$$

However, the conditions under which this one-equation approximation is valid remain unclear. This kind of simplification has not received a lot of attention. It has been examined previously for the case of a stratified medium and an asymptotic behavior Eq (1.26) was proved directly from the lower-scale mass balance equations for stratified systems [166], and used extensively in [150] which introduced the word Taylor's dispersion. More generally, it has been suggested in [295] that some time constraints can be formulated allowing this one-equation description of the transport processes. They considered the time-infinite behavior of the first two centered spatial moments to determine an expression for the effective velocity and the dispersion tensor. The work by [65] in a reactive case suggests that this behavior is quite general, that is, it seems that a multidomain decomposition of the medium is necessary only to describe short time phenomena (at least when the spatial operators are linear). Such simplifications in the modelization, as well as a minimalist description of the dimensionality of the problem Eq (1.26), are extremely appealing from an experimental point of view and are often used without extensive discussions.

$$(\varepsilon_\gamma + \varepsilon_\omega)\frac{\partial \langle c\rangle^{\gamma\omega}}{\partial t} + V^{\infty}\frac{\partial \langle c\rangle^{\gamma\omega}}{\partial x} = D^{\infty}\frac{\partial^2 \langle c\rangle^{\gamma\omega}}{\partial x^2} \tag{1.26}$$

In this equation, we use V^{∞} for the velocity in the one-dimensional situation (as compared to $\mathbf{V}$ for the tensor) to avoid any confusion with future notations.

ONE-EQUATION SPECIAL DECOMPOSITION NON-EQUILIBRIUM MODEL

Apart from this two-equation model and its two particular behaviors, a one-equation non-equilibrium theory Eq (1.27), based on a very distinct background, is also available in [205] for mass transport and in [178] for heat transfer. The method used for the development of this model differs from the volume averaging with closure theory and finds its essence in a peculiar perturbation decomposition. This one-equation non-equilibrium model can also be obtained using the homogenization theory and this has been devised in [178]. Numerical simulations in [205] suggest that both one-equation local non-equilibrium models Eq (1.25) and Eq (1.27) might be one and the same. However, it is not straightforward from the expression of the dispersion tensors $\mathbf{D}^{\infty}$ and $\mathbf{D}^{*}$ and their connection needs to be clarified.

$$(\varepsilon_\gamma + \varepsilon_\omega)\frac{\partial \langle c\rangle^{\gamma\omega}}{\partial t} + \mathbf{V}\cdot\boldsymbol{\nabla}\langle c\rangle^{\gamma\omega} = \boldsymbol{\nabla}\cdot\{\mathbf{D}^{*}\cdot\boldsymbol{\nabla}\langle c\rangle^{\gamma\omega}\} \tag{1.27}$$

DISCUSSION

The counterpart of all these one-equation models is that they capture less physics of the transport processes than two-equation models and, hence, there are some stronger assumptions associated with Eqs (1.25), (1.26) and (1.27). For example, consider the mass transport within two tubes flowing at two very different mean velocities. Following the work in [248] and later in [9], the description of this system can be undertaken at long times using two independent advection-dispersion equations and not by a single one. Hence, it is important to develop an intelligible domain of validity that can be used in applications. Unfortunately, the works aforementioned do not provide explicit representations of these assumptions, except for some elements in [249], that can be used by experimenters. In most developments of this type, it is unclear when it is possible to neglect the influence of higher order moments and what are the temporal constraints associated with the time-infinite limits considered. In the volume averaging developments, constraints focus on the characteristic times of the fluctuations, and it is not always clear how this should be used to specify constraints for experimental studies.

1.6 SCOPE OF THIS PART

To summarize, we have the following models, classified decreasingly in relation to the quantitity of information they capture from the microscale problem, and their complexity thereof.

- A fully non-local formulation (*Model A*) Eq (1.5) which is an exact solution (in terms of ensemble average not necessarily equivalent to volume average) but often impractical.

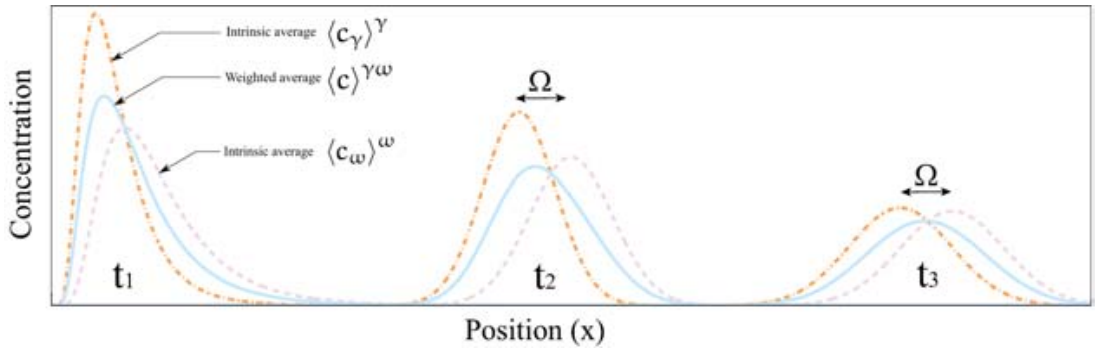

Figure 27: Schematic representation of the transient behavior of a pulse evolving in a two-phase/region porous medium.

- A two-equation transient closure model (*Model B*) Eqs (1.21-1.22) involving time convolutions that account for time non-locally but approximates the spatial convolutions, using effective parameters calculated on a REV.
- A two-equation quasi-stationary model (*Model C*) Eqs (1.19-1.20) that approximates the spatial convolutions similarly to *Model B* but also approximates the time convolutions.
- A one-equation non-equilibrium model (*Model* D) Eqs (1.25) and (1.26) that approximates both convolutions, under stronger temporal hypothesis than *Model C*.
- A one-equation non-equilibrium model (*Model* E) Eq (1.27), obtained using a special perturbation decomposition.
- A one-equation local mass equilibrium model (*Model* F) Eq (1.23) that imposes strong physical limitations regarding the pointwise concentration within the different phases.

The main contributions of this study are to

1. develop a comprehensive framework, based on the volume averaging with closure theory, for the development of the *Models B to F*.
2. study the limitations associated to *Model C* in relation to *Model B*. This connection has already been discussed in [177, 237] using some rather intuitive arguments. Herein, we study the analytical response of both models to sinusoidal excitations on a very simple stratified geometry. We show that the *Model C* is valid if and only if the characteristic time for the relaxation of the effective parameters is significantly smaller than the period of the input signal.
3. express the constraints that allow one to use *Model D* instead of *Model C*. For the expression of these constraints, we will only consider the case of an infinite

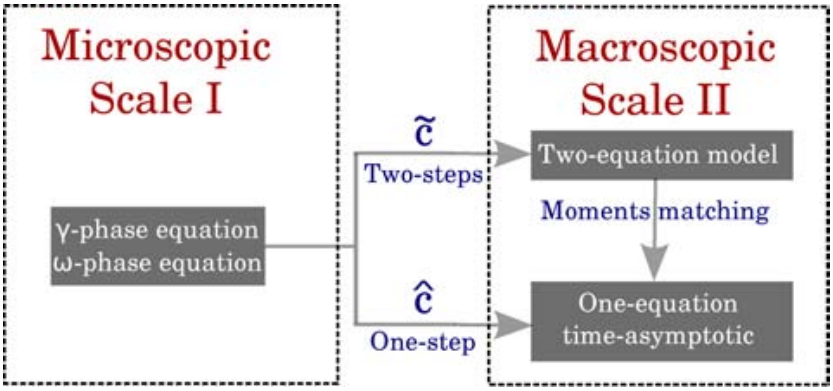

Figure 28: Schematic representation of the two methods that can be used for the development of a one-equation non-equilibrium model.

one-dimensional porous medium in which the boundary/initial condition is a Dirac distribution. There has been some discussion concerning the influence of the boundary conditions on the time-asymptotic regime [73] but we will not consider such situations. This is particularly interesting to express the inequalities that are used to describe the time restrictions only in terms of the effective parameters of the two-equation quasi-stationary model. The reason for this is that these are quite intuitive, that is, with some experience one may apprehend these limitations really well. The situation is reminiscent to the problem of defining a measure of Gaussian-like distribution in probabilistic analysis. Hence, our work is based on the expression of higher order moments and especially of the standardized moments of order 3 and 4, that is, respectively skewness and kurtosis. Physical interpretations of the constraints are thoroughly discussed. The main idea is that, at long times, the spreading dominates all other types of deformation of the signal, as illustrated on Fig (27).

4. study the convergence of the *Model C* toward the *Model D* in terms of spatial moments.

5. advance a formal proof for the equivalence (Fig. 28) between *Models D and E*. As an aside, it is interesting to emphasize that very few effort has been dedicated to establishing connections between the various upscaling techniques. Noticeable exceptions are a comparison of ensemble averaging and volume averaging [283], a comparison of the moment matching technique and the homogenization theory [12], a comparison of the homogenization theory and the volume averaging theory [31] and an equivalence between the continuous time random walk technique and the volume averaging theory [186].

6. group these information on a domain of validity illustration. Establishing the domains of validity of macroscopic models represents a critical issue for both theoreticians and experimenters. The procedure of upscaling aims to reduce the

number of degrees of freedom of a problem by eliminating redundancy in the information at the microscopic scale (see in [282]). It must be understood that the quantity of information that must be eliminated depends on the problem itself but also on the tolerance that one has toward the solutions. Hence, constraints are usually expressed in terms of orders of magnitude of dimensionless numbers such as the Péclet number for example. For the dual-region situation, the reader is referred to the discussion in [113] and more specifically to the Fig. 2 which provides a very good description of the domains of validity of the different models in terms of two Péclet numbers and the ratio between the two. Herein, we show that a temporal axis must also be considered and we discuss the effect of the boundary conditions on these domains. It is shown that for the modelization of a pulse through a porous medium, one may first consider a fully non-local model at small times, then the transient two-equation model, the two-equation quasi-stationary formulation and at last the one-equation form.

2

MATHEMATICAL DEVELOPMENTS FOR THE MACROTRANSPORT THEORY

2.1 TWO-EQUATION (MODELS B AND C)

2.1.1 *Volume averaging*

To start, the averaging operators and decompositions defined above are applied to Eqs (1.1)-(1.3); the details of this process are provided in Appendix A. The result is

$\gamma-phase$

$$\begin{aligned}\frac{\partial \varepsilon_\gamma \langle c_\gamma\rangle^\gamma}{\partial t} &= \boldsymbol{\nabla}\cdot\left[\mathbf{D}_\gamma\cdot\left(\boldsymbol{\nabla}\left(\varepsilon_\gamma\langle c_\gamma\rangle^\gamma\right)+\frac{1}{V}\int_{\mathscr{S}_{\gamma\omega}}\mathbf{n}_{\gamma\omega}c_\gamma dS+\frac{1}{V}\int_{\mathscr{S}_{\gamma\sigma}}\mathbf{n}_{\gamma\sigma}c_\gamma dS\right)\right]\\ &+ \frac{1}{V}\int_{\mathscr{S}_{\gamma\omega}}\mathbf{n}_{\gamma\omega}\cdot\mathbf{D}_\gamma\cdot\boldsymbol{\nabla}c_\gamma dS+\frac{1}{V}\int_{\mathscr{S}_{\gamma\sigma}}\mathbf{n}_{\gamma\sigma}\cdot\mathbf{D}_\gamma\cdot\boldsymbol{\nabla}c_\gamma dS\\ &- \boldsymbol{\nabla}\cdot\left(\varepsilon_\gamma\langle\mathbf{v}_\gamma c_\gamma\rangle^\gamma\right)\end{aligned} \tag{2.1}$$

$\omega-phase$

$$\begin{aligned}\frac{\partial \varepsilon_\omega \langle c_\omega\rangle^\omega}{\partial t} &= \boldsymbol{\nabla}\cdot\left[\mathbf{D}_\omega\cdot\left(\boldsymbol{\nabla}\left(\varepsilon_\omega\langle c_\omega\rangle^\omega\right)+\frac{1}{V}\int_{\mathscr{S}_{\omega\gamma}}\mathbf{n}_{\omega\gamma}c_\omega dS+\frac{1}{V}\int_{\mathscr{S}_{\omega\sigma}}\mathbf{n}_{\omega\sigma}c_\omega dS\right)\right]\\ &+ \frac{1}{V}\int_{\mathscr{S}_{\omega\gamma}}\mathbf{n}_{\omega\gamma}\cdot\mathbf{D}_\omega\cdot\boldsymbol{\nabla}c_\omega dS+\frac{1}{V}\int_{\mathscr{S}_{\omega\sigma}}\mathbf{n}_{\omega\sigma}\cdot\mathbf{D}_\omega\cdot\boldsymbol{\nabla}c_\omega dS\\ &- \boldsymbol{\nabla}\cdot\left(\varepsilon_\omega\langle\mathbf{v}_\omega c_\omega\rangle^\omega\right)\end{aligned} \tag{2.2}$$

To make further progress, we decompose the concentrations as an average plus a fluctuation Eqs (1.12)-(1.13) and assume that the hypothesis of spatial locality (separation of length scales) is valid (see in Appendix A). We show that the macroscopic equation takes the form

$\gamma-phase$

$$\begin{aligned}\frac{\partial \varepsilon_\gamma \langle c_\gamma\rangle^\gamma}{\partial t} + &= \nabla\cdot\left[\varepsilon_\gamma \mathbf{D}_\gamma\cdot\left(\nabla\langle c_\gamma\rangle^\gamma + \frac{1}{V_\gamma}\int_{\mathscr{S}_{\gamma\omega}} \mathbf{n}_{\gamma\omega}\tilde{c}_\gamma\, dS + \frac{1}{V_\gamma}\int_{\mathscr{S}_{\gamma\sigma}} \mathbf{n}_{\gamma\sigma}\tilde{c}_\gamma\, dS\right)\right]\\ &+ \frac{1}{V}\int_{\mathscr{S}_{\gamma\omega}} \mathbf{n}_{\gamma\omega}\cdot\mathbf{D}_\gamma\cdot\nabla\tilde{c}_\gamma\, dS + \frac{1}{V}\int_{\mathscr{S}_{\gamma\sigma}} \mathbf{n}_{\gamma\sigma}\cdot\mathbf{D}_\gamma\cdot\nabla\tilde{c}_\gamma\, dS - \nabla\cdot(\varepsilon_\gamma\langle\tilde{c}_\gamma\tilde{\mathbf{v}}_\gamma\rangle)\\ &- \nabla\cdot(\varepsilon_\gamma\langle c_\gamma\rangle^\gamma\langle\mathbf{v}_\gamma\rangle^\gamma) \qquad (2.3)\end{aligned}$$

$\omega-$phase

$$\begin{aligned}\frac{\partial \varepsilon_\omega \langle c_\omega\rangle^\omega}{\partial t} &= \nabla\cdot\left[\varepsilon_\omega \mathbf{D}_\omega\cdot\left(\nabla\langle c_\omega\rangle^\omega + \frac{1}{V_\omega}\int_{\mathscr{S}_{\omega\gamma}} \mathbf{n}_{\omega\gamma}\tilde{c}_\omega\, dS + \frac{1}{V_\omega}\int_{\mathscr{S}_{\omega\sigma}} \mathbf{n}_{\omega\sigma}\tilde{c}_\omega\, dS\right)\right]\\ &+ \frac{1}{V}\int_{\mathscr{S}_{\omega\gamma}} \mathbf{n}_{\omega\gamma}\cdot\mathbf{D}_\omega\cdot\nabla\tilde{c}_\omega\, dS + \frac{1}{V}\int_{\mathscr{S}_{\omega\sigma}} \mathbf{n}_{\omega\sigma}\cdot\mathbf{D}_\omega\cdot\nabla\tilde{c}_\omega\, dS - \nabla\cdot(\varepsilon_\omega\langle\tilde{c}_\omega\tilde{\mathbf{v}}_\omega\rangle)\\ &- \nabla\cdot(\varepsilon_\omega\langle c_\omega\rangle^\omega\langle\mathbf{v}_\omega\rangle^\omega) \qquad (2.4)\end{aligned}$$

Equations (2.3)-(2.4) represent a macroscopic description of the transport processes. However, the problem is not under a closed form, that is, in addition to terms involving $\langle c_i\rangle^i$ there are terms involving $\tilde{c}_i$. In order to close the problem, we need (1) to determinate the boundary value problems that the perturbations satisfy and (2) to uncouple, in these problems, the contributions varying at the macroscale (source terms) from those varying at the microscale.

2.1.2 *Fluctuations equations*

Going back to their definition $\tilde{c}_i = c_i - \langle c_i\rangle^i$ suggests that the set of equations governing the behavior of these perturbations can be obtained by subtracting Eqs (2.1)-(2.2) to, respectively, Eqs (1.1)-(1.3). This operation, in conjunction with the previous averaging process, leads to two different set of equations. One governs the macroscopic concentrations Eqs (2.1)-(2.2) or Eqs (2.3)-(2.4). The other, the results of the operations (1.1 minus 2.1) and (1.3 minus 2.2), describes the perturbations. *A priori*, these are coupled and must be solved simultaneously, that is, we end up with a non-local description of the transport. Under the assumption that a local solution is desired, the coupling can be broken down by assuming a separation of length scales. Hence, we use (1.1 minus 2.3) and (1.3 minus 2.4) instead of (1.1 minus 2.1) and (1.3 minus 2.2) to describe the behavior of the perturbations. For the same reason, we assume that derivatives of macroscopic concentrations can be neglected in comparison to derivatives of fluctuations. For a more detailed discussion, the reader is referred to the work of Quintard and Whitaker in [207, 208, 209, 210, 211]. This operation leads to

$$\frac{\partial \tilde{c}_\gamma}{\partial t} + \nabla \cdot (\tilde{c}_\gamma \mathbf{v}_\gamma) - \langle \nabla \cdot (\tilde{c}_\gamma \mathbf{v}_\gamma) \rangle^\gamma + \tilde{\mathbf{v}}_\gamma . \nabla \langle c_\gamma \rangle^\gamma = \nabla \cdot \{ \mathbf{D}_\gamma \cdot \nabla \tilde{c}_\gamma \} - \langle \nabla \cdot \{ \mathbf{D}_\gamma \nabla \tilde{c}_\gamma \} \rangle^\gamma \tag{2.5}$$

$$\begin{aligned}
&\text{BC1}: && -\mathbf{n}_{\gamma\sigma} \cdot (\mathbf{D}_\gamma \cdot \nabla \tilde{c}_\gamma) = \mathbf{n}_{\gamma\sigma} \cdot (\mathbf{D}_\gamma \cdot \nabla \langle c_\gamma \rangle^\gamma) && \text{on } \mathscr{S}_{\gamma\sigma} && (2.6a)\\
&\text{BC2}: && \tilde{c}_\gamma - \tilde{c}_\omega = -(\langle c_\gamma \rangle^\gamma - \langle c_\omega \rangle^\omega) && \text{on } \mathscr{S}_{\gamma\omega} && (2.6b)\\
&\text{BC3}: && \mathbf{n}_{\gamma\omega} \cdot (\mathbf{j}_{\tilde{c}_\gamma} - \mathbf{j}_{\tilde{c}_\omega}) = -\mathbf{n}_{\gamma\omega} \cdot (\mathbf{j}_{\langle c_\gamma \rangle^\gamma} - \mathbf{j}_{\langle c_\omega \rangle^\omega}) && \text{on } \mathscr{S}_{\gamma\omega} && (2.6c)\\
&\text{BC4}: && -\mathbf{n}_{\omega\sigma} \cdot (\mathbf{D}_\omega \cdot \nabla \tilde{c}_\omega) = \mathbf{n}_{\omega\sigma} \cdot (\mathbf{D}_\omega \cdot \nabla \langle c_\omega \rangle^\omega) && \text{on } \mathscr{S}_{\omega\sigma} && (2.6d)
\end{aligned}$$

$$\frac{\partial \tilde{c}_\omega}{\partial t} + \nabla \cdot (\tilde{c}_\omega \mathbf{v}_\omega) - \langle \nabla \cdot (\tilde{c}_\omega \mathbf{v}_\omega) \rangle^\omega + \tilde{\mathbf{v}}_\omega . \nabla \langle c_\omega \rangle^\omega = \nabla \cdot \{ \mathbf{D}_\omega \cdot \nabla \tilde{c}_\omega \} - \langle \nabla \cdot \{ \mathbf{D}_\omega \nabla \tilde{c}_\omega \} \rangle^\omega \tag{2.7}$$

where $\mathbf{j}_{\Phi_i} = -\mathbf{D}_i \cdot \nabla \Phi_i$. At this point, the problem on the perturbations is still coupled with the macroscopic concentrations but in a weaker sense. Using the superposition principle for linear operators, in conjunction with the separation of the length scales, one can perform the following change in variables, without any additional assumption [178, 237].

$$\tilde{c}_\gamma = \mathbf{b}_{\gamma\gamma} \cdot * \frac{\partial}{\partial t} \nabla \langle c_\gamma \rangle^\gamma + \mathbf{b}_{\gamma\omega} \cdot * \frac{\partial}{\partial t} \nabla \langle c_\omega \rangle^\omega - r_\gamma * \frac{\partial}{\partial t} (\langle c_\gamma \rangle^\gamma - \langle c_\omega \rangle^\omega) \tag{2.8}$$

$$\tilde{c}_\omega = \mathbf{b}_{\omega\gamma} \cdot * \frac{\partial}{\partial t} \nabla \langle c_\gamma \rangle^\gamma + \mathbf{b}_{\omega\omega} \cdot * \frac{\partial}{\partial t} \nabla \langle c_\omega \rangle^\omega - r_\omega * \frac{\partial}{\partial t} (\langle c_\gamma \rangle^\gamma - \langle c_\omega \rangle^\omega) \tag{2.9}$$

The $*$ operator refers to convolutions in time defined by

$$e(t) * f(t) = \int_0^t e(\tau) f(t-\tau) d\tau \tag{2.10}$$

The $\mathbf{b}$ and r fields can be interpreted as integrals of the corresponding Green's functions when the spatial locality is assumed (see discussions in [282]). The goal of this expression is to find variables that can be calculated locally on a REV.

In addition, we will assume that the medium can be represented locally by a periodic boundary condition. This concept concerning the notion of representative elementary volume (REV) is widely misunderstood. In hierarchical porous media, under the assumption that a REV can be defined, the information that is necessary to calculate the effective parameters of the models is contained in a relatively small

representative portion of the medium. For this representative volume, there are two type of boundary conditions. The first one concerns the different regions/phases inside the REV ans is determined by the physics of the processes at the microscale. The second type refers to the external boundary condition between the REV and the rest of the porous medium. This condition is not determined by the physics at the small scale but rather represents a closure of the problem. At first, it is unclear how this choice should be made and it results in a significant amount of confusion in the literature. From a theoretical point of view, if the REV is large enough, it has been shown [274] that effective parameters do not depend on this boundary condition.

In real situations, this constraint is never exactly satisfied, that is, this boundary condition has an impact on the fields. However, in the macroscopic equations, the perturbations appear only under integrated quantities. Because of this, the dependence of effective parameters upon the solution of the closure problem is essentially mathematically of a weak form [190]. Hence, one could choose, say, Dirichlet, Neuman, mixed or periodic boundary conditions to obtain a local solution which produces acceptable values for the associated averaged quantities. The periodic boundary condition lends itself very well for this application as it induces very little perturbation in the local fields, in opposition to, say, Dirichlet boundary conditions (this is particularly useful for non-isotropic unit cell characteristics). It must be understood that this does not mean that the medium is interpreted as being physically periodic. For the remainder of this work, we will assume that the medium can be represented locally by a periodic cell and that the effective parameters can be calculated over this representative part of the medium.

2.1.3 *Closure problems*

Upon substituting these expressions for the fluctuations in Eqs (2.5) to (2.7), we can collect separately terms involving $\boldsymbol{\nabla}\langle c_\gamma\rangle^\gamma$, $\boldsymbol{\nabla}\langle c_\omega\rangle^\omega$ and $\langle c_\gamma\rangle^\gamma - \langle c_\omega\rangle^\omega$. This is based on the assumption that the fluctuations can be decomposed on the basis of $\{\langle c_\gamma\rangle^\gamma, \langle c_\omega\rangle^\omega, \boldsymbol{\nabla}\langle c_\gamma\rangle^\gamma, \boldsymbol{\nabla}\langle c_\omega\rangle^\omega\}$, that is, higher order derivatives can be neglected.

Collecting terms involving $\langle c_\gamma\rangle^\gamma - \langle c_\omega\rangle^\omega$ leads to Eqs (2.11) to (2.13)

$$\frac{\partial r_\gamma}{\partial t} + \mathbf{v}_\gamma \cdot \boldsymbol{\nabla} r_\gamma = \boldsymbol{\nabla} \cdot \{\mathbf{D}_\gamma \cdot \boldsymbol{\nabla} r_\gamma\} - \varepsilon_\gamma^{-1} h(t) \tag{2.11}$$

$$\begin{aligned}
&\text{BC1}: && -\mathbf{n}_{\gamma\sigma} \cdot (\mathbf{D}_\gamma \cdot \boldsymbol{\nabla} r_\gamma) = 0 && \text{on } \mathscr{S}_{\gamma\sigma} && (2.12a)\\
&\text{BC2}: && r_\gamma - r_\omega = 1 && \text{on } \mathscr{S}_{\gamma\omega} && (2.12b)\\
&\text{BC3}: && \mathbf{n}_{\gamma\omega} \cdot (\mathbf{D}_\gamma \cdot \boldsymbol{\nabla} r_\gamma - \mathbf{D}_\omega \cdot \boldsymbol{\nabla} r_\omega) = 0 && \text{on } \mathscr{S}_{\gamma\omega} && (2.12c)\\
&\text{BC4}: && -\mathbf{n}_{\omega\sigma} \cdot (\mathbf{D}_\omega \cdot \boldsymbol{\nabla} r_\omega) = 0 && \text{on } \mathscr{S}_{\omega\sigma} && (2.12d)\\
& && \text{Periodicity}: r_i(\mathbf{x} + \mathbf{p}_k) = r_i(\mathbf{x}) && k = 1,2,3 && (2.12e)
\end{aligned}$$

$$\frac{\partial r_\omega}{\partial t} + \mathbf{v}_{\gamma\omega} \cdot \nabla r_\omega = \nabla \cdot \{\mathsf{D}_\omega \cdot \nabla r_\omega\} + \varepsilon_\omega^{-1} h(t) \tag{2.13}$$

where, using previous assumptions, we can write

$$\begin{aligned} h(t) = & \quad \varepsilon_\gamma \langle \nabla \cdot \{\mathsf{D}_\gamma \nabla r_\gamma\} \rangle^\gamma = -\varepsilon_\omega \langle \nabla \cdot \{\mathsf{D}_\omega \nabla r_\omega\} \rangle^\omega \\ = & \quad \frac{1}{V} \int_{\mathscr{S}_{\gamma\omega}} \mathbf{n}_{\gamma\omega} \cdot \mathsf{D}_\gamma \cdot \nabla r_\gamma \, dS = -\frac{1}{V} \int_{\mathscr{S}_{\gamma\omega}} \mathbf{n}_{\omega\gamma} \cdot \mathsf{D}_\omega \cdot \nabla r_\omega \, dS \end{aligned} \tag{2.14}$$

We have used $\mathbf{p}_k$ to represent the three lattice vectors that are needed to describe the 3-D spatial periodicity.

Collecting terms involving $\nabla \langle c_\gamma \rangle^\gamma$ leads to Eqs (2.15) to (2.17)

$$\frac{\partial \mathbf{b}_{\gamma\gamma}}{\partial t} + \mathbf{v}_\gamma \cdot (\nabla \mathbf{b}_{\gamma\gamma} - r_\gamma \mathbf{I}) + \tilde{\mathbf{v}}_\gamma = \nabla \cdot \{\mathsf{D}_\gamma \cdot (\nabla \mathbf{b}_{\gamma\gamma} - r_\gamma \mathbf{I})\} - \langle \tilde{\mathbf{v}}_\gamma r_\gamma \rangle^\gamma - \varepsilon_\gamma^{-1} \boldsymbol{\beta}_1^* \tag{2.15}$$

$$\text{BC1}: \quad -\mathbf{n}_{\gamma\sigma} \cdot (\mathsf{D}_\gamma \cdot \nabla \mathbf{b}_{\gamma\gamma}) = \mathbf{n}_{\gamma\sigma} \cdot \mathsf{D}_\gamma \quad \text{on } \mathscr{S}_{\gamma\sigma} \tag{2.16a}$$

$$\text{BC2}: \quad \mathbf{b}_{\gamma\gamma} - \mathbf{b}_{\omega\gamma} = 0 \quad \text{on } \mathscr{S}_{\gamma\omega} \tag{2.16b}$$

$$\text{BC3}: \quad -\mathbf{n}_{\gamma\omega} \cdot \mathsf{D}_\gamma \cdot (\nabla \mathbf{b}_{\gamma\gamma} - r_\gamma \mathbf{I}) = \mathbf{n}_{\gamma\omega} \cdot \mathsf{D}_\gamma - \mathbf{n}_{\gamma\omega} \cdot \mathsf{D}_\omega \cdot (\nabla \mathbf{b}_{\omega\gamma} - r_\omega \mathbf{I}) \quad \text{on } \mathscr{S}_{\gamma\omega} \tag{2.16c}$$

$$\text{BC4}: \quad -\mathbf{n}_{\omega\sigma} \cdot (\mathsf{D}_\omega \cdot \nabla \mathbf{b}_{\omega\gamma}) = 0 \quad \text{on } \mathscr{S}_{\omega\sigma} \tag{2.16d}$$

$$\text{Periodicity}: \ \mathbf{b}_{ij}(\mathbf{x} + \mathbf{p}_k) = \mathbf{b}_{ij}(\mathbf{x}) \quad k = 1,2,3 \tag{2.16e}$$

$$\frac{\partial \mathbf{b}_{\omega\gamma}}{\partial t} + \mathbf{v}_\gamma \cdot (\nabla \mathbf{b}_{\omega\gamma} - r_\omega \mathbf{I}) = \nabla \cdot \{\mathsf{D}_\omega \cdot (\nabla \mathbf{b}_{\omega\gamma} - r_\omega \mathbf{I})\} - \langle \tilde{\mathbf{v}}_\omega r_\omega \rangle^\omega + \varepsilon_\omega^{-1} \boldsymbol{\beta}_1^* \tag{2.17}$$

where

$$\boldsymbol{\beta}_1^* = \langle \nabla \cdot \{\mathsf{D}_\gamma \cdot (\nabla \mathbf{b}_{\gamma\gamma} - r_\gamma \mathbf{I})\} \rangle = -\langle \nabla \cdot \{\mathsf{D}_\omega \cdot (\nabla \mathbf{b}_{\omega\gamma} - r_\omega \mathbf{I})\} \rangle \tag{2.18}$$

$$= \frac{1}{V} \int_{\mathscr{S}_{\gamma\omega}} \mathbf{n}_{\gamma\omega} \cdot \mathsf{D}_\gamma \cdot (\nabla \mathbf{b}_{\gamma\gamma} - r_\gamma \mathbf{I}) \, dS = -\frac{1}{V} \int_{\mathscr{S}_{\gamma\omega}} \mathbf{n}_{\omega\gamma} \cdot \mathsf{D}_\omega \cdot (\nabla \mathbf{b}_{\omega\gamma} - r_\omega \mathbf{I}) \, dS \tag{2.19}$$

Collecting terms involving $\nabla \langle c_\omega \rangle^\omega$ leads to Eqs (2.20) to (2.22)

$$\frac{\partial \mathbf{b}_{\gamma\omega}}{\partial t} + \mathbf{v}_\gamma \cdot (\boldsymbol{\nabla}\mathbf{b}_{\gamma\omega} + r_\gamma \mathbf{I}) = \boldsymbol{\nabla} \cdot \{\mathbf{D}_\gamma \cdot (\boldsymbol{\nabla}\mathbf{b}_{\gamma\omega} + r_\gamma \mathbf{I})\} + \langle \tilde{\mathbf{v}}_\gamma r_\gamma \rangle^\gamma - \varepsilon_\gamma^{-1} \boldsymbol{\beta}_2^* \tag{2.20}$$

$$\text{BC1}: \quad -\mathbf{n}_{\gamma\sigma} \cdot (\mathbf{D}_\gamma \cdot \boldsymbol{\nabla}\mathbf{b}_{\gamma\omega}) = 0 \quad \text{on } \mathscr{S}_{\gamma\sigma} \tag{2.21a}$$

$$\text{BC2}: \quad \mathbf{b}_{\gamma\omega} - \mathbf{b}_{\omega\omega} = 0 \quad \text{on } \mathscr{S}_{\gamma\omega} \tag{2.21b}$$

$$\text{BC3}: \quad \mathbf{n}_{\gamma\omega} \cdot \mathbf{D}_\gamma \cdot (\boldsymbol{\nabla}\mathbf{b}_{\gamma\omega} + r_\gamma \mathbf{I}) = \mathbf{n}_{\gamma\omega} \cdot \mathbf{D}_\omega + \mathbf{n}_{\gamma\omega} \cdot \mathbf{D}_\omega \cdot (\boldsymbol{\nabla}\mathbf{b}_{\omega\omega} + r_\omega \mathbf{I}) \quad \text{on } \mathscr{S}_{\gamma\omega} \tag{2.21c}$$

$$\text{BC4}: \quad -\mathbf{n}_{\omega\sigma} \cdot (\mathbf{D}_\omega \cdot \boldsymbol{\nabla}\mathbf{b}_{\omega\gamma}) = \mathbf{n}_{\omega\sigma} \cdot \mathbf{D}_\omega \quad \text{on } \mathscr{S}_{\omega\sigma} \tag{2.21d}$$

$$\text{Periodicity}: \quad \mathbf{b}_{ij}(\mathbf{x} + p_k) = \mathbf{b}_{ij}(\mathbf{x}) \quad k = 1,2,3 \tag{2.21e}$$

$$\frac{\partial \mathbf{b}_{\omega\omega}}{\partial t} + \mathbf{v}_\omega \cdot (\boldsymbol{\nabla}\mathbf{b}_{\omega\omega} + r_\omega \mathbf{I}) + \tilde{\mathbf{v}}_\omega = \boldsymbol{\nabla} \cdot \{\mathbf{D}_\omega \cdot (\boldsymbol{\nabla}\mathbf{b}_{\omega\omega} + r_\omega \mathbf{I})\} + \langle \tilde{\mathbf{v}}_\omega r_\omega \rangle^\omega + \varepsilon_\omega^{-1} \boldsymbol{\beta}_2^* \tag{2.22}$$

where

$$\boldsymbol{\beta}_2^* = \langle \boldsymbol{\nabla} \cdot \{\mathbf{D}_\gamma \cdot (\boldsymbol{\nabla}\mathbf{b}_{\gamma\omega} + r_\gamma \mathbf{I})\} \rangle = -\langle \boldsymbol{\nabla} \cdot \{\mathbf{D}_\omega \cdot (\boldsymbol{\nabla}\mathbf{b}_{\omega\omega} + r_\omega \mathbf{I})\} \rangle \tag{2.23}$$

$$= \frac{1}{V} \int_{\mathscr{S}_{\gamma\omega}} \mathbf{n}_{\gamma\omega} \cdot \mathbf{D}_\gamma \cdot (\boldsymbol{\nabla}\mathbf{b}_{\gamma\omega} + r_\gamma \mathbf{I})\, dS = -\frac{1}{V} \int_{\mathscr{S}_{\gamma\omega}} \mathbf{n}_{\omega\gamma} \cdot \mathbf{D}_\omega \cdot (\boldsymbol{\nabla}\mathbf{b}_{\omega\omega} + r_\omega \mathbf{I})\, dS \tag{2.24}$$

The unicity of the fields is provided by

$$\langle r_\gamma \rangle^\gamma = 0,\ \langle r_\omega \rangle^\omega = 0,\ \langle \mathbf{b}_{\gamma\gamma} \rangle^\gamma = 0,\ \langle \mathbf{b}_{\gamma\gamma} \rangle^\gamma = 0,\ \langle \mathbf{b}_{\gamma\omega} \rangle^\gamma = 0,\ \langle \mathbf{b}_{\omega\gamma} \rangle^\omega = 0,\ \langle \mathbf{b}_{\omega\omega} \rangle^\omega = 0 \tag{2.25}$$

$$r_\gamma(t=0) = r_\omega(t=0) = 0,\ \mathbf{b}_{\gamma\gamma}(t=0) = \mathbf{b}_{\gamma\omega}(t=0) = \mathbf{b}_{\omega\gamma}(t=0) = \mathbf{b}_{\omega\omega}(t=0) = 0 \tag{2.26}$$

Both problems are coupled together but uncoupled from the macroscopic problems Eqs (2.3)-(2.4). Hence, these fields can be calculated locally on a REV. However, fluctuations still remain in Eqs (2.3)-(2.4) and it is now necessary to uncouple the macroscopic equations from the perturbations.

2.1.4 *Macroscopic equations Model B*

In order to get rid of these perturbations, we inject Eqs (2.8)-(2.9) in Eqs (2.3)-(2.4). The result can be expressed by Eqs (2.27)-(2.28) [178, 237]

$$\begin{aligned}\varepsilon_\gamma \frac{\partial \langle c_\gamma\rangle^\gamma}{\partial t} + \varepsilon_\gamma \mathbf{V}_{\gamma\gamma}.*\frac{\partial}{\partial t}\boldsymbol{\nabla}\langle c_\gamma\rangle^\gamma + \varepsilon_\gamma \mathbf{V}_{\gamma\omega}.*\frac{\partial}{\partial t}\boldsymbol{\nabla}\langle c_\omega\rangle^\omega = \;& \varepsilon_\gamma \boldsymbol{\nabla}.\{\mathbf{D}_{\gamma\gamma}.*\frac{\partial}{\partial t}\boldsymbol{\nabla}\langle c_\gamma\rangle^\gamma\}\\ &+\varepsilon_\gamma \boldsymbol{\nabla}.\{\mathbf{D}_{\gamma\omega}.*\frac{\partial}{\partial t}\boldsymbol{\nabla}\langle c_\omega\rangle^\omega\}\\ &-h*\frac{\partial}{\partial t}(\langle c_\gamma\rangle^\gamma - \langle c_\omega\rangle^\omega)\\ &+\varepsilon_\gamma Q^\gamma(x,y,z,t) \qquad (2.27)\end{aligned}$$

$$\begin{aligned}\varepsilon_\omega \frac{\partial \langle c_\omega\rangle^\omega}{\partial t} + \varepsilon_\omega \mathbf{V}_{\omega\gamma}.*\frac{\partial}{\partial t}\boldsymbol{\nabla}\langle c_\gamma\rangle^\gamma + \varepsilon_\omega \mathbf{V}_{\omega\omega}.*\frac{\partial}{\partial t}\boldsymbol{\nabla}\langle c_\omega\rangle^\omega = \;& \varepsilon_\omega \boldsymbol{\nabla}.\{\mathbf{D}_{\omega\gamma}.*\frac{\partial}{\partial t}\boldsymbol{\nabla}\langle c_\gamma\rangle^\gamma\}\\ &+\varepsilon_\omega \boldsymbol{\nabla}.\{\mathbf{D}_{\omega\omega}.*\frac{\partial}{\partial t}\boldsymbol{\nabla}\langle c_\omega\rangle^\omega\}\\ &-h*\frac{\partial}{\partial t}(\langle c_\omega\rangle^\omega - \langle c_\gamma\rangle^\gamma)\\ &+\varepsilon_\omega Q^\omega(x,y,z,t) \qquad (2.28)\end{aligned}$$

Herein, the macroscopic boundary conditions are described by the source terms distributions $\varepsilon_\gamma Q^\gamma(x,y,z,t)$ and $\varepsilon_\omega Q^\omega(x,y,z,t)$. Effective velocities, containing intrinsic averages of the microscale velocities, are

$$\mathbf{V}_{\gamma\gamma} = \langle \mathbf{v}_\gamma\rangle^\gamma - \varepsilon_\gamma^{-1}\boldsymbol{\beta}_1^* - \langle \tilde{\mathbf{v}}_\gamma r_\gamma\rangle^\gamma \qquad (2.29)$$

$$\mathbf{V}_{\omega\omega} = \langle \mathbf{v}_\omega\rangle^\omega + \varepsilon_\omega^{-1}\boldsymbol{\beta}_2^* + \langle \tilde{\mathbf{v}}_\omega r_\omega\rangle^\omega \qquad (2.30)$$

Interphase coupling arising from the interfacial flux as well as from fluctuations of the velocities can be written

$$\mathbf{V}_{\gamma\omega} = -\varepsilon_\omega^{-1}\boldsymbol{\beta}_2^* + \langle \tilde{\mathbf{v}}_\gamma r_\gamma\rangle^\gamma \qquad (2.31)$$

$$\mathbf{V}_{\omega\gamma} = \varepsilon_\gamma^{-1}\boldsymbol{\beta}_1^* - \langle \tilde{\mathbf{v}}_\omega r_\omega\rangle^\omega \qquad (2.32)$$

For dispersion effects, dominant terms are

$$\mathbf{D}_{\gamma\gamma} = \mathbf{D}_\gamma\left(\mathbf{I} + \frac{1}{V_\gamma}\int_{\mathscr{S}_{\gamma\omega}} \mathbf{n}_{\gamma\omega}\mathbf{b}_{\gamma\gamma}\,dS\right) - \langle \tilde{\mathbf{v}}_\gamma \mathbf{b}_{\gamma\gamma}\rangle^\gamma \qquad (2.33)$$

$$\mathbf{D}_{\omega\omega} = \mathbf{D}_\omega\left(\mathbf{I} + \frac{1}{V_\omega}\int_{\mathscr{S}_{\gamma\omega}} \mathbf{n}_{\omega\gamma}\mathbf{b}_{\omega\omega}\,dS\right) - \langle \tilde{\mathbf{v}}_\omega \mathbf{b}_{\omega\omega}\rangle^\omega \qquad (2.34)$$

Interphase dispersion couplings are

$$\mathbf{D}_{\gamma\omega} = \mathbf{D}_\gamma\left(\frac{1}{V_\gamma}\int_{\mathscr{S}_{\gamma\omega}}\mathbf{n}_{\gamma\omega}\mathbf{b}_{\gamma\omega}\,dS\right)-\langle\tilde{\mathbf{v}}_\gamma\mathbf{b}_{\gamma\omega}\rangle^\gamma \tag{2.35}$$

$$\mathbf{D}_{\omega\gamma} = \mathbf{D}_\omega\left(\frac{1}{V_\omega}\int_{\mathscr{S}_{\gamma\omega}}\mathbf{n}_{\omega\gamma}\mathbf{b}_{\omega\gamma}\,dS\right)-\langle\tilde{\mathbf{v}}_\omega\mathbf{b}_{\omega\gamma}\rangle^\omega \tag{2.36}$$

and the first-order exchange coefficient

$$h=\frac{1}{V}\int_{\mathscr{S}_{\gamma\omega}}\mathbf{n}_{\gamma\omega}\cdot\mathbf{D}_\gamma\cdot\boldsymbol{\nabla}r_\gamma\,dS=-\frac{1}{V}\int_{\mathscr{S}_{\gamma\omega}}\mathbf{n}_{\omega\gamma}\cdot\mathbf{D}_\omega\cdot\boldsymbol{\nabla}r_\omega\,dS \tag{2.37}$$

With these definitions, it must be understood that all the effective parameters exhibit a time-dependence, even though we have used $\mathbf{D}_{ij}$, $\mathbf{V}_{ij}$ and h instead of $\mathbf{D}_{ij}(t)$, $\mathbf{V}_{ij}(t)$ and $h(t)$, to simplify the notations.

2.1.5 *Local Model C and conditions for time-locality*

$$\begin{aligned}\varepsilon_\gamma\frac{\partial\langle c_\gamma\rangle^\gamma}{\partial t}+\varepsilon_\gamma\mathbf{V}_{\gamma\gamma}(\infty).\boldsymbol{\nabla}\langle c_\gamma\rangle^\gamma+\varepsilon_\gamma\mathbf{V}_{\gamma\omega}(\infty).\boldsymbol{\nabla}\langle c_\omega\rangle^\omega &= \varepsilon_\gamma\boldsymbol{\nabla}.\{\mathbf{D}_{\gamma\gamma}(\infty).\boldsymbol{\nabla}\langle c_\gamma\rangle^\gamma\}\\ &+\varepsilon_\gamma\boldsymbol{\nabla}.\{\mathbf{D}_{\gamma\omega}(\infty).\boldsymbol{\nabla}\langle c_\omega\rangle^\omega\}\\ &-h(\infty)\left(\langle c_\gamma\rangle^\gamma-\langle c_\omega\rangle^\omega\right)\\ &+\varepsilon_\gamma Q^\gamma(x,y,z,t)\end{aligned} \tag{2.38}$$

$$\begin{aligned}\varepsilon_\omega\frac{\partial\langle c_\omega\rangle^\omega}{\partial t}+\varepsilon_\omega\mathbf{V}_{\omega\gamma}(\infty).\boldsymbol{\nabla}\langle c_\gamma\rangle^\gamma+\varepsilon_\omega\mathbf{V}_{\omega\omega}(\infty).\boldsymbol{\nabla}\langle c_\omega\rangle^\omega &= \varepsilon_\omega\boldsymbol{\nabla}.\{\mathbf{D}_{\omega\gamma}(\infty).\boldsymbol{\nabla}\langle c_\gamma\rangle^\gamma\}\\ &+\varepsilon_\omega\boldsymbol{\nabla}.\{\mathbf{D}_{\omega\omega}(\infty).\boldsymbol{\nabla}\langle c_\omega\rangle^\omega\}\\ &-h(\infty)\left(\langle c_\omega\rangle^\omega-\langle c_\gamma\rangle^\gamma\right)\\ &+\varepsilon_\omega Q^\omega(x,y,z,t)\end{aligned} \tag{2.39}$$

Effective parameters, such as $h(t)$, undertake a transient regime and then reach a stationary state, that is, after a given relaxation time τ_1, $h(t)$ tends toward a constant $h(\infty)$. To understand when the local two-equation model Eqs (2.38)-(2.39) represents a good approximation of Eqs (2.27)-(2.28) boils down to understanding when

$$\boldsymbol{\nabla}\cdot\{\mathbf{D}_{ij}(t)\cdot*\frac{\partial}{\partial t}\boldsymbol{\nabla}\langle c_j\rangle^j(t)\}\text{ can be approximated by }\boldsymbol{\nabla}\cdot\{\mathbf{D}_{ij}(\infty)\cdot\boldsymbol{\nabla}\langle c_j\rangle^j(t)\}$$

$$\mathbf{V}_{ij}(t)\cdot*\frac{\partial}{\partial t}\boldsymbol{\nabla}\langle c_j\rangle^j(t)\text{ by }\mathbf{V}_{ij}(\infty)\cdot\boldsymbol{\nabla}\langle c_j\rangle^j(t)$$

$$h(t) * \frac{\partial}{\partial t}\left(\langle c_\gamma\rangle^\gamma(t) - \langle c_\omega\rangle^\omega(t)\right) \text{ by } h(\infty)\left(\langle c_\gamma\rangle^\gamma(t) - \langle c_\omega\rangle^\omega(t)\right)$$

It is understood that the convolutions converge toward the local formulation Eqs (2.38)-(2.39) when the effective parameters relax quickly in comparison to characteristic times for macroscopic variations. Under this condition, for any effective parameter κ and any function f, the convolution can be approximated the following way [237, 177]

$$\kappa(t) * \frac{\partial}{\partial t} f(t) \approx \kappa(\infty) * \frac{\partial}{\partial t} f(t) = \int_0^t \kappa(\infty)\frac{\partial}{\partial \tau} f(\tau)\, d\tau = \kappa(\infty) f(t) \tag{2.40}$$

To illustrate this asymptotic behavior, we consider a simplified configuration for which an analytical solution is available. Explicitly, we are interested in the following microscale diffusion problem

$$\frac{\partial c_\gamma^{micro}}{\partial t} = D_\gamma \frac{\partial^2 c_\gamma^{micro}}{\partial x^2} \tag{2.41}$$

with $-l \leqslant x \leqslant +l$, zero initial concentration and the boundary conditions $x = \pm l$ maintained at concentration $\sin(\omega t)$ for $t \geqslant 0$ (such a physical situation is purely theoretical for mass transport but could be realizable for heat transfer problems). The idea behind the use of a sinusoidal input is that the macroscopic signal is characterized by a single time, say $T = \frac{1}{\omega}$. We define the macroscopic averaged quantities as

$$\langle \phi_\gamma\rangle^\gamma = \frac{1}{2l}\int_{-l}^{+l} \phi_\gamma dx \tag{2.42}$$

The averaged mass balanced equations can be written

$$\varepsilon_\gamma \frac{d\langle c_\gamma^*\rangle^\gamma}{dt} + h(t) * \frac{d\langle c_\gamma^*\rangle^\gamma}{dt} = h * \frac{d}{dt}\sin(\omega t) \tag{2.43}$$

and

$$\varepsilon_\gamma \frac{d\langle c_\gamma\rangle^\gamma}{dt} + h(\infty)\langle c_\gamma\rangle^\gamma = h\sin(\omega t) \tag{2.44}$$

in which we have added the $*$ superscript to differentiate between the non-local and the local formulations. It is fundamental to notice that, in this very particular configuration, the constraints associated with Eq (2.43) are exactly satisfied, that is,

$\langle c_\gamma^* \rangle^\gamma = \langle c_\gamma^{micro} \rangle^\gamma$. In our case, for obvious symmetry reasons, $\langle c_\gamma^{micro} \rangle^\gamma$ does not vary along the z axis. Hence, the spatial locality is exactly verified and the closure on the perturbations is an exact solution.

Therefore, we only need to compare $\langle c_\gamma \rangle^\gamma$ with $\langle c_\gamma^* \rangle^\gamma$, in order to understand the behavior of the local model in relation to the non-local formulation. Toward this goal, we first determine the microscale solution of Eq (2.41), and calculate $\langle c_\gamma^* \rangle^\gamma = \langle c_\gamma^{micro} \rangle^\gamma$. As a second step, we solve Eq (2.44) to determine $\langle c_\gamma \rangle^\gamma$. At last, we develop a characteristic time τ_1 for the relaxation of h and compare the long-time macroscopic results for various ratio $\frac{\tau_1}{T}$.

Expression of the pointwise microscopic solution and $\langle c_\gamma^* \rangle^\gamma = \langle c_\gamma^{micro} \rangle^\gamma$

The analytical microscopic solution of the problem can be written [39] page (105)

$$\begin{aligned} c_\gamma^{micro} &= A\sin(\omega t + \Phi) \\ &+ 16 l^2 \omega \pi D_\gamma \sum_{n=0}^{\infty} \frac{(-1)^n (2n+1)}{16 l^4 \omega^2 + D_\gamma^2 \pi^4 (2n+1)^4} \cos\left(\frac{(2n+1)\pi x}{2l}\right) e^{-D_\gamma (2n+1)^2 \pi^2 t / 4l^2} \end{aligned} \tag{2.45}$$

with

$$\Phi = \arg\left\{\frac{\cosh kx\,(1+i)}{\cosh kl\,(1+i)}\right\} \tag{2.46}$$

$$A = \sqrt{\frac{\cosh 2kx + \cos 2kx}{\cosh 2kl + \cos 2kl}} \tag{2.47}$$

$$k = \sqrt{\frac{\omega}{2D_\gamma}} \tag{2.48}$$

Hence, at long times, we have

$$\boxed{\langle c_\gamma^* \rangle^\gamma = \langle c_\gamma^{micro} \rangle^\gamma \underset{t\to\infty}{=} \langle A\sin(\omega t + \Phi) \rangle^\gamma} \tag{2.49}$$

Local solution $\langle c_\gamma \rangle^\gamma$

Using Laplace transforms on Eq (2.44), we obtain

$$\langle c_\gamma \rangle^\gamma = \frac{\frac{h}{\varepsilon_\gamma}}{\sqrt{\left(\frac{h}{\varepsilon_\gamma}\right)^2 + \omega^2}} \sin\left(\omega t - \arctan\left(\frac{\varepsilon_\gamma \omega}{h}\right)\right) + \frac{\frac{h}{\varepsilon_\gamma}}{\left(\frac{h}{\varepsilon_\gamma}\right)^2 + \omega^2} e^{-\frac{h}{\varepsilon_\gamma} t} \tag{2.50}$$

and at long times

$$\boxed{\langle c_\gamma\rangle^\gamma \underset{t\to\infty}{=} \frac{\frac{h}{\varepsilon_\gamma}}{\sqrt{\left(\frac{h}{\varepsilon_\gamma}\right)^2+\omega^2}}\sin\left(\omega t-\arctan\left(\frac{\varepsilon_\gamma\omega}{h}\right)\right)} \tag{2.51}$$

Relaxation of h

The determination of a characteristic time τ_1 for the relaxation of h is actually the most difficult part. Going back to its definition, Eq (2.37), we have

$$h=\frac{1}{2l}\int_{-l}^{+l} D_\gamma\frac{\partial r_\gamma}{\partial x}dx \tag{2.52}$$

with r_γ solution of the following boundary value problem

$$\frac{\partial r_\gamma}{\partial t}=D_\gamma\frac{\partial^2 r_\gamma}{\partial x^2}-\varepsilon_\gamma^{-1}h \tag{2.53}$$

$$\text{BC}: \qquad r_\gamma=1 \qquad \text{on } \mathscr{S}_{\gamma\omega} \tag{2.54}$$

We also have

$$\langle r_\gamma\rangle^\gamma=0 \tag{2.55}$$

One way around the calculation of h is to decompose r_γ using

$$r_\gamma=1-R_\gamma*\frac{\partial}{\partial t}h$$

Hence, we have R_γ solution of (straightforward in Laplace space)

$$\frac{\partial R_\gamma}{\partial t}=D_\gamma\frac{\partial^2 R_\gamma}{\partial x^2}+\varepsilon_\gamma^{-1} \tag{2.56}$$

$$\text{BC}: \qquad R_\gamma=0 \qquad \text{on } \mathscr{S}_{\gamma\omega} \tag{2.57}$$

The solution of Equation (2.56) is [39] p. 130

$$R_\gamma = \frac{l^2}{2\varepsilon_\gamma D_\gamma}\{1 - \frac{x^2}{l^2} - \frac{32}{\pi^3}\sum_{n=0}^{\infty}\frac{(-1)^n}{(2n+1)^3}\cos\frac{(2n+1)\pi x}{2l}e^{-D_\gamma(2n+1)^2\pi^2 t/4l^2}\} \quad (2.58)$$

and the expression of h is derived from Equation (2.55)

$$\langle R_\gamma\rangle^\gamma(t) * \frac{\partial}{\partial t}h(t) = 1 \quad (2.59)$$

A characteristic time for the asymptotic relaxation of h corresponds to the long-time relaxation of $\langle R_\gamma\rangle^\gamma$, that is, $\tau_1 = \frac{4l^2}{\pi^2 D_\gamma}$. By definition, the $h(\infty)$ appearing in Equation (2.44) corresponds to the stationary part of Equation (2.59), that is,

$$h(\infty) = \frac{3\varepsilon_\gamma D_\gamma}{l^2} \quad (2.60)$$

Comparison of $\langle c_\gamma^{micro}\rangle^\gamma$ *and* $\langle c_\gamma\rangle^\gamma$ *in the long-time limit for various ratio* $\frac{\tau_1}{T}$

We fix $l = 0.5$, $\varepsilon_\gamma = 0.6$ and the time t is normalized in relation to a characteristic time for the oscillations, that is, $t' = \frac{t}{T} = \omega t$. We compare the results for different ratio $\frac{\tau_1}{T} = \frac{4l^2}{\pi^2 D_\gamma}\omega$ in the long time regime, that is, all the exponentially decaying terms are not considered. We integrate and plot Equation (2.61) using MAPLE^{TM} (Micro on Figure 29)

$$\langle c_\gamma^*\rangle^\gamma = \langle c_\gamma^{micro}\rangle^\gamma \approx \langle A\sin(\omega t + \Phi)\rangle^\gamma \quad (2.61)$$

and we compare it to (Local on Figure 29)

$$\langle c_\gamma\rangle^\gamma = \frac{\frac{h}{\varepsilon_\gamma}}{\sqrt{\left(\frac{h}{\varepsilon_\gamma}\right)^2 + \omega^2}}\sin\left(\omega t - \arctan\left(\frac{\varepsilon_\gamma\omega}{h}\right)\right) \quad (2.62)$$

It is clear from Fig (29) that we require $\tau_1 \ll T$ in order for the Eq (2.43) to converge toward Eq (2.44), that is, the characteristic time of the macroscopic signal needs to be much larger than the characteristic time for the relaxation of the exchange coefficient h. In a more general context, this suggests that the Eqs (2.38)-(2.39) represent a good approximation of Eqs (2.27)-(2.28) under the condition that $T \gg \tau_1$, in which τ_1 can be estimated using

$$\tau_1 = \mathcal{O}\left(\max\{\frac{l_\gamma}{\langle v_\gamma\rangle^\gamma}, \frac{l_\omega}{\langle v_\omega\rangle^\omega}, \frac{l_\gamma^2}{D_\gamma}, \frac{l_\omega^2}{D_\omega}\}\right) \quad (2.63)$$

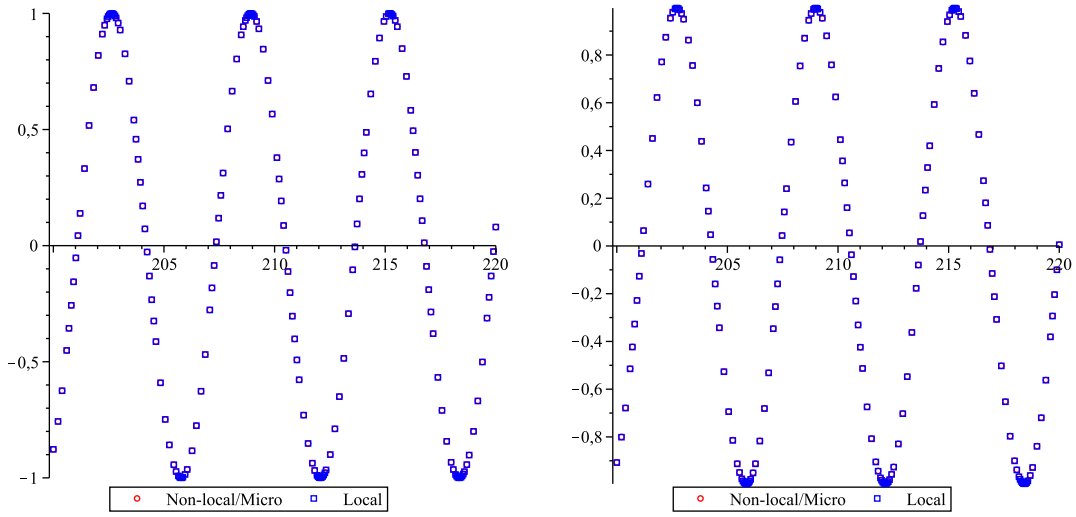

a) $\frac{\tau_1}{T} = 0.01$ b) $\frac{\tau_1}{T} = 0.1$

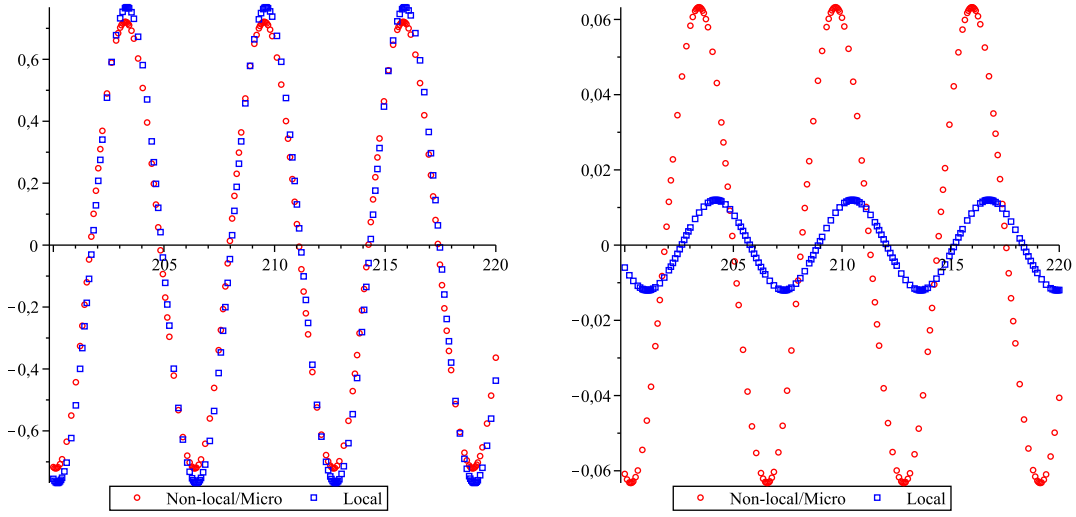

c) $\frac{\tau_1}{T} = 1$ d) $\frac{\tau_1}{T} = 100$

Figure 29: Comparison of the responses $\langle c_\gamma^{micro} \rangle^\gamma = \langle c_\gamma^* \rangle^\gamma$ (Non-local/Micro) and $\langle c_\gamma \rangle^\gamma$ (Local), plotted as functions of $\frac{t}{T}$, for various ratio $\frac{\tau_1}{T}$ ($\varepsilon_\gamma = 0.6$, $l = 0.5$).

and

$$T = \mathcal{O}\left(\min\{T_{\langle c_\gamma\rangle^\gamma}, T_{\langle c_\omega\rangle^\omega}, T_{\nabla\langle c_\gamma\rangle^\gamma}, T_{\nabla\langle c_\omega\rangle^\omega}, T_{\nabla^2\langle c_\gamma\rangle^\gamma}, T_{\nabla^2\langle c_\omega\rangle^\omega}\}\right) \tag{2.64}$$

where T_ϕ is the characteristic time associated with time variations of ϕ. These are related to (1) the macroscopic processes but also to (2) the boundary condition, as illustrated in the previous sinusoidal example.

Can we make a "better" two-equation model ?

There is an interesting idea that would consist in adapting the exchange coefficient h to the oscillations, that is, developing h as a function of ω. The purpose of this section is to investigate the pertinence of such a method.

As a reminder, we have

$$\boxed{\langle c_\gamma^*\rangle^\gamma = \langle c_\gamma^{micro}\rangle^\gamma \underset{t\to\infty}{=} \langle A\sin(\omega t + \Phi)\rangle^\gamma} \tag{2.65}$$

with

$$\Phi = \arg\{\frac{\cosh kx\,(1+i)}{\cosh kl\,(1+i)}\} \tag{2.66}$$

$$A = \sqrt{\frac{\cosh 2kx + \cos 2kx}{\cosh 2kl + \cos 2kl}} \tag{2.67}$$

$$k = \sqrt{\frac{\omega}{2D_\gamma}} \tag{2.68}$$

and

$$\boxed{\langle c_\gamma\rangle^\gamma \underset{t\to\infty}{=} \frac{\frac{h(\omega)}{\varepsilon_\gamma}}{\sqrt{\left(\frac{h(\omega)}{\varepsilon_\gamma}\right)^2+\omega^2}}\sin\left(\omega t - \arctan\left(\frac{\varepsilon_\gamma\omega}{h(\omega)}\right)\right)} \tag{2.69}$$

There is a decomposition of $\langle c_\gamma^*\rangle^\gamma$ Eq. (2.70) that considerably helps in the comparison of both signals.

$$\langle c_\gamma^*\rangle^\gamma = \langle c_\gamma^{micro}\rangle^\gamma \underset{t\to\infty}{=} \langle A\sin(\omega t + \Phi)\rangle^\gamma = C\sin(\omega t + D) \tag{2.70}$$

where

$$C = \sqrt{(\langle A\sin(\Phi)\rangle^{\gamma})^2 + (\langle A\cos(\Phi)\rangle^{\gamma})^2} \tag{2.71}$$

and

$$D = \arctan\left(\frac{\langle A\sin(\Phi)\rangle^{\gamma}}{\langle A\cos(\Phi)\rangle^{\gamma}}\right) \tag{2.72}$$

Hence, we would need both amplitudes and phases to be equal, that is,

$$\frac{\frac{h_{amplitude}(\omega)}{\varepsilon_{\gamma}}}{\sqrt{\left(\frac{h_{amplitude}(\omega)}{\varepsilon_{\gamma}}\right)^2 + \omega^2}} = \sqrt{(\langle A\sin(\Phi)\rangle^{\gamma})^2 + (\langle A\cos(\Phi)\rangle^{\gamma})^2} \tag{2.73}$$

and

$$-\arctan\left(\frac{\varepsilon_{\gamma}\omega}{h_{phase}(\omega)}\right) \equiv \arctan\left(\frac{\langle A\sin(\Phi)\rangle^{\gamma}}{\langle A\cos(\Phi)\rangle^{\gamma}}\right) \tag{2.74}$$

This can be expressed by

$$\boxed{h_{amplitude}(\omega) = \frac{\varepsilon_{\gamma}\omega\sqrt{(\langle A\sin(\Phi)\rangle^{\gamma})^2 + (\langle A\cos(\Phi)\rangle^{\gamma})^2}}{\sqrt{1 - (\langle A\sin(\Phi)\rangle^{\gamma})^2 - (\langle A\cos(\Phi)\rangle^{\gamma})^2}}} \tag{2.75}$$

and

$$\boxed{h_{phase}(\omega) \equiv -\frac{\varepsilon_{\gamma}\omega\langle A\cos(\Phi)\rangle^{\gamma}}{\langle A\sin(\Phi)\rangle^{\gamma}}} \tag{2.76}$$

Therefore, it seems that h is overdetermined by this system. Using a formulation with an exchange coefficient $h(\omega)$ that depends on the frequency of the input, it looks like it is not possible to recover the phase and the amplitude simultaneously. On Fig (30), we plotted both $h_{amplitude}$ and h_{phase} and showed that these two expressions only overlap in the low frequency limit.

2.2 ONE-EQUATION LONG-TIME BEHAVIOR (MODEL D)

We are now interested in a long time simplification of this two-equation local model. It has been shown in [295] that the system Eqs (2.38)-(2.39) has a time-asymptotic

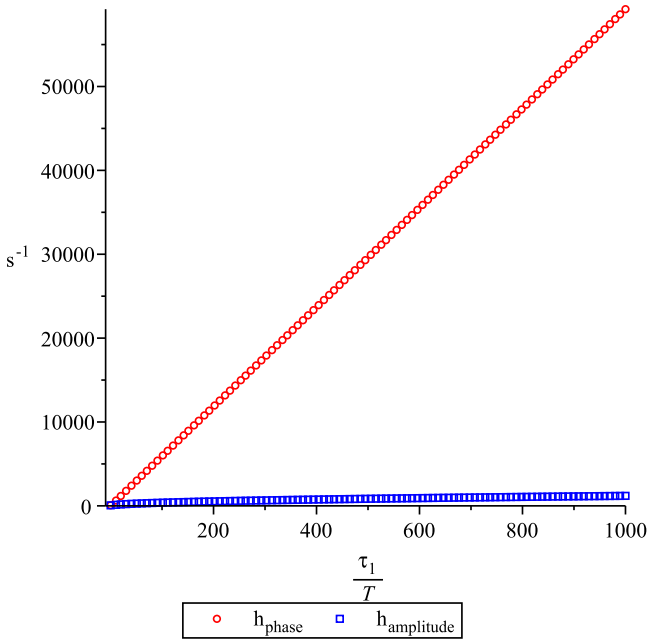

Figure 30: Representations of h_{phase} and $h_{amplitude}$ as functions of $\frac{\tau_1}{T} = \omega \frac{4l^2}{\pi^2 D_\gamma}$.

behavior for semi-infinite or infinite systems which can be described in terms of a one equation advection-diffusion type model Eq (2.77).

$$(\varepsilon_\gamma + \varepsilon_\omega) \frac{\partial \langle c \rangle^{\gamma\omega}}{\partial t} + \mathbf{v} \cdot \boldsymbol{\nabla} \langle c \rangle^{\gamma\omega} = \boldsymbol{\nabla} \cdot \{ \mathbf{D}^\infty \cdot \boldsymbol{\nabla} \langle c \rangle^{\gamma\omega} \} \tag{2.77}$$

The analysis is based on the study of the long time behavior of the first two centered spatial moments. There is an interesting discussion concerning higher order moments which has not been tackled yet. One usually assumes that the behavior of centered spatial moments of order superior to three can be neglected. From the analysis conducted in [295], it is emphasized that, in a dual-phase situation, the distance between the signals in each phase tends toward a constant Ω at long times Fig (27). Thus, the signal $\langle c \rangle^{\gamma\omega}$ can not be exactly Gaussian shaped at long times, that is, there is no convergence in terms of centered moments. However, we show that we have a convergence in terms of these moments standardized to the second order centered moment. In essence, it means that in the time-asymptotic regime, the spreading dominates all other forms of deformation of the spatial signal. This idea is reminiscent to the Taylor-Aris dispersion in a tube. Herein, we provide a rigorous analysis in which (1) we develop constraints for neglecting of higher order moments and (2) we study the convergence toward the asymptotic regime. We show that the concentration fields asymptotically tend toward a Gaussian shape signal in space described by Eq (2.78)

$$\frac{\partial \langle c \rangle^{\gamma\omega}}{\partial t} + V^{\infty} \frac{\partial \langle c \rangle^{\gamma\omega}}{\partial x} = D^{\infty} \frac{\partial^2 \langle c \rangle^{\gamma\omega}}{\partial x^2} + Q^{\gamma\omega} \tag{2.78}$$

with Eq (2.79)

$$\langle c \rangle^{\gamma\omega} = \frac{\varepsilon_\gamma}{\varepsilon_\gamma + \varepsilon_\omega} \langle c_\gamma \rangle^{\gamma} + \frac{\varepsilon_\omega}{\varepsilon_\gamma + \varepsilon_\omega} \langle c_\omega \rangle^{\omega} \tag{2.79}$$

and Eq (2.80)

$$Q^{\gamma\omega} = \frac{\varepsilon_\gamma}{\varepsilon_\gamma + \varepsilon_\omega} Q^{\gamma} + \frac{\varepsilon_\omega}{\varepsilon_\gamma + \varepsilon_\omega} Q^{\omega} \tag{2.80}$$

The following are our main hypotheses, and are thoroughly discussed along the demonstration:

HYPOTHESIS 1 Our work is limited to a 1-D infinite medium in which we assume that there is no mass in the system at $t = 0$ and the input is a Dirac signal.

HYPOTHESIS 2 We will only consider the case $Q^{\gamma}(t) = Q^{\omega}(t) = Q^{\gamma\omega}\delta(t)$.

HYPOTHESIS 3 We make the following approximations $V_{\gamma\omega} - V_{\omega\gamma} \ll V_{\gamma\gamma} - V_{\omega\omega}$ and $D_{\gamma\omega} - D_{\omega\gamma} \ll D_{\gamma\gamma} - D_{\omega\omega}$.

Our strategy consists in using various mathematical objects, known as spatial moments, that measure some fundamental aspects of the spatial distribution of the concentration. We start with the study of the simple raw spatial moments and show that, using Laplace space formulations and mathematical analyses of the boundary value problem, the dominant term at long times captures an information regarding the asymptotic velocity of propagation of the signal. To recover information regarding the spreading of the signals, we define centered moments and formulate an expression of the n^{th} order centered moments based on an extrapolation from the first centered moments. The goal is to compare these to the centered moments of the one-equation model Eq. (2.78) that are explicitly presented in section 2.2.3. We prove that there is not an asymptotic convergence of the two-equation model toward a one-equation model in terms of central moments. However, we show that there is a weaker convergence in terms of standardized moments and this is discussed in section 2.2.4. Eventually, we propose a measure defined in terms of a relative difference of the standardized moments between the two-equation and the one-equation models. We also thoroughly discuss sufficient conditions for the convergence in section 2.2.5.

2.2.1 *Raw moments analysis*

To start our mathematical analysis, we define the raw spatial moments in the $i-phase$ by Eq (2.81)

$$\mu_n^i(t) = \int_{-\infty}^{+\infty} x^n \langle c_i \rangle^i dx \tag{2.81}$$

First, our goal is to study the temporal behavior of these raw moments. Toward that end, we derive the moments generating differential equations Eqs (2.82)-(2.83). There are, at least, two ways to develop these equations. The first one is based on the Fourier transform moments generating function and the second consists in a direct integration by part of the equations (2.38)-(2.39), for $n \geqslant 2$

$$\begin{aligned}\frac{\partial \mu_n^\gamma}{\partial t} &= n(n-1) D_{\gamma\gamma} \mu_{n-2}^\gamma + n(n-1) D_{\gamma\omega} \mu_{n-2}^\omega + n V_{\gamma\gamma} \mu_{n-1}^\gamma + n V_{\gamma\omega} \mu_{n-1}^\omega \\ &\quad - \tfrac{h}{\varepsilon_\gamma} (\mu_n^\gamma - \mu_n^\omega)\end{aligned} \tag{2.82}$$

$$\begin{aligned}\frac{\partial \mu_n^\omega}{\partial t} &= n(n-1) D_{\omega\gamma} \mu_{n-2}^\gamma + n(n-1) D_{\omega\omega} \mu_{n-2}^\omega + n V_{\omega\gamma} \mu_{n-1}^\gamma + n V_{\omega\omega} \mu_{n-1}^\omega \\ &\quad - \tfrac{h}{\varepsilon_\omega} (\mu_n^\omega - \mu_n^\gamma)\end{aligned} \tag{2.83}$$

with

$$\frac{\partial \mu_0^\gamma}{\partial t} = -\frac{h}{\varepsilon_\gamma} \left(\mu_0^\gamma - \mu_0^\omega\right) \tag{2.84}$$

$$\frac{\partial \mu_0^\omega}{\partial t} = -\frac{h}{\varepsilon_\omega} \left(\mu_0^\omega - \mu_0^\gamma\right) \tag{2.85}$$

and

$$\frac{\partial \mu_1^\gamma}{\partial t} = V_{\gamma\gamma} \mu_0^\gamma + V_{\gamma\omega} \mu_0^\omega - \frac{h}{\varepsilon_\gamma} \left(\mu_1^\gamma - \mu_1^\omega\right) \tag{2.86}$$

$$\frac{\partial \mu_1^\omega}{\partial t} = V_{\omega\gamma} \mu_0^\gamma + V_{\omega\omega} \mu_0^\omega - \frac{h}{\varepsilon_\omega} \left(\mu_1^\omega - \mu_1^\gamma\right) \tag{2.87}$$

It is straightforward to show that

$$\mu_0 = \frac{(Q^\gamma(t) - Q^\omega(t)) * e^{-\alpha t}}{(\varepsilon_\gamma + \varepsilon_\omega)} \begin{bmatrix} \varepsilon_\omega \\ -\varepsilon_\gamma \end{bmatrix} + Q^{\gamma\omega} \begin{bmatrix} 1 \\ 1 \end{bmatrix} \tag{2.88}$$

where $\alpha = h\left(\frac{1}{\varepsilon_\gamma} + \frac{1}{\varepsilon_\omega}\right)$. For the sake of simplicity, we will only consider the case $Q^\gamma(t) = Q^\omega(t) = Q^{\gamma\omega}\delta(t)$, which leads to $\mu_0 = Q^{\gamma\omega} \begin{bmatrix} 1 \\ 1 \end{bmatrix}$. This assumption is not fundamental but leads to substantial simplifications.

LAPLACE SPACE FORMULATION To make further progress, we consider the Laplace transforms of the moments defined by Eq (2.89)

$$\bar{\mu}_n^i = \int_{-\infty}^{+\infty} e^{-pt} \mu_n^i(t)\, dt \tag{2.89}$$

The Laplace transform of the equations (2.82)-(2.83) leads to Eqs (2.90) and (2.91)

$$\begin{aligned} p\bar{\mu}_n^\gamma \quad &= n(n-1) D_{\gamma\gamma} \bar{\mu}_{n-2}^\gamma + n(n-1) D_{\gamma\omega} \bar{\mu}_{n-2}^\omega + n V_{\gamma\gamma} \bar{\mu}_{n-1}^\gamma + n V_{\gamma\omega} \bar{\mu}_{n-1}^\omega \\ &\quad - \tfrac{h}{\varepsilon_\gamma} (\bar{\mu}_n^\gamma - \bar{\mu}_n^\omega) \end{aligned} \tag{2.90}$$

$$\begin{aligned} p\bar{\mu}_n^\omega \quad &= n(n-1) D_{\omega\gamma} \bar{\mu}_{n-2}^\gamma + n(n-1) D_{\omega\omega} \bar{\mu}_{n-2}^\omega + n V_{\omega\gamma} \bar{\mu}_{n-1}^\gamma + n V_{\omega\omega} \bar{\mu}_{n-1}^\omega \\ &\quad - \tfrac{h}{\varepsilon_\omega} (\bar{\mu}_n^\omega - \bar{\mu}_n^\gamma) \end{aligned} \tag{2.91}$$

which can be set under a matricial form Eq (2.92)

$$\begin{aligned} \begin{bmatrix} p + \frac{h}{\varepsilon_\gamma} & -\frac{h}{\varepsilon_\gamma} \\ -\frac{h}{\varepsilon_\omega} & p + \frac{h}{\varepsilon_\omega} \end{bmatrix} \begin{bmatrix} \bar{\mu}_n^\gamma \\ \bar{\mu}_n^\omega \end{bmatrix} \quad &= \quad n(n-1) \begin{bmatrix} D_{\gamma\gamma} & D_{\gamma\omega} \\ D_{\omega\gamma} & D_{\omega\omega} \end{bmatrix} \begin{bmatrix} \bar{\mu}_{n-2}^\gamma \\ \bar{\mu}_{n-2}^\omega \end{bmatrix} \\ &\quad + n \begin{bmatrix} V_{\gamma\gamma} & V_{\gamma\omega} \\ V_{\omega\gamma} & V_{\omega\omega} \end{bmatrix} \begin{bmatrix} \bar{\mu}_{n-1}^\gamma \\ \bar{\mu}_{n-1}^\omega \end{bmatrix} \end{aligned} \tag{2.92}$$

We have for $n \geqslant 2$, Eq (2.93)

$$\bar{\mu}_n = n(n-1) \mathbf{A}^{-1} \mathbf{D} \bar{\mu}_{n-2} + n \mathbf{A}^{-1} \mathbf{V} \bar{\mu}_{n-1} \tag{2.93}$$

and Eqs (2.94)-(2.95) to complete the sequence

$$\bar{\mu}_0 = \frac{1}{p}\begin{bmatrix} Q^{\gamma\omega} \\ Q^{\gamma\omega} \end{bmatrix} \tag{2.94}$$

$$\bar{\mu}_1 = \mathbf{A}^{-1}\mathbf{V}\bar{\mu}_0 \tag{2.95}$$

with Eq (2.96)

$$\mathbf{A} = \begin{bmatrix} p + \frac{h}{\varepsilon_\gamma} & -\frac{h}{\varepsilon_\gamma} \\ -\frac{h}{\varepsilon_\omega} & p + \frac{h}{\varepsilon_\omega} \end{bmatrix} \tag{2.96}$$

with Eq (2.97)

$$\begin{aligned} \mathbf{A}^{-1} &= \frac{1}{p^2 + ph\left(\frac{1}{\varepsilon_\gamma} + \frac{1}{\varepsilon_\omega}\right)} \begin{bmatrix} p + \frac{h}{\varepsilon_\omega} & \frac{h}{\varepsilon_\gamma} \\ \frac{h}{\varepsilon_\omega} & p + \frac{h}{\varepsilon_\gamma} \end{bmatrix} \\ &= \frac{1}{p+\alpha}\mathbf{I} + \frac{\alpha}{p\,(p+\alpha)}\mathbf{\Lambda}^{\varepsilon} \\ &= \frac{1}{p+\alpha}\,(\mathbf{I} - \mathbf{\Lambda}^{\varepsilon}) + \frac{1}{p}\mathbf{\Lambda}^{\varepsilon} \end{aligned} \tag{2.97}$$

and with $\alpha = h\left(\frac{1}{\varepsilon_\gamma} + \frac{1}{\varepsilon_\omega}\right)$, $\mathbf{\Lambda}^{\varepsilon} = \begin{bmatrix} \varepsilon_\gamma & \varepsilon_\omega \\ \varepsilon_\gamma & \varepsilon_\omega \end{bmatrix}$, $\bar{\mu}_n = \begin{bmatrix} \bar{\mu}_n^{\gamma} \\ \bar{\mu}_n^{\omega} \end{bmatrix}$, $\mathbf{D} = \begin{bmatrix} D_{\gamma\gamma} & D_{\gamma\omega} \\ D_{\omega\gamma} & D_{\omega\omega} \end{bmatrix}$ and $\mathbf{V} = \begin{bmatrix} V_{\gamma\gamma} & V_{\gamma\omega} \\ V_{\omega\gamma} & V_{\omega\omega} \end{bmatrix}$.

GENERAL EXPRESSION IN LAPLACE SPACE AND LONG TIME LIMIT OF THE RAW SPATIAL MOMENTS

It is straightforward to show that, for $n \geqslant 1$,

$$\begin{bmatrix} \bar{\mu}_n \\ \bar{\mu}_{n-1} \end{bmatrix} = n \begin{bmatrix} \mathbf{A}^{-1}\mathbf{V} & (n-1)\mathbf{A}^{-1}\mathbf{D} \\ \frac{1}{n}\mathbf{I}_2 & \mathbf{0}_2 \end{bmatrix} \begin{bmatrix} \bar{\mu}_{n-1} \\ \bar{\mu}_{n-2} \end{bmatrix} \tag{2.98}$$

and that we have Eq (2.99)

$$p\begin{bmatrix}\bar{\mu}_n\\ \bar{\mu}_{n-1}\end{bmatrix} = n!\left(\prod_{k=n-1}^{k=0}\begin{bmatrix}\mathbf{A}^{-1}\mathbf{V} & k\mathbf{A}^{-1}\mathbf{D}\\ \frac{1}{k+1}\mathbf{I}_2 & \mathbf{0}_2\end{bmatrix}\right)\begin{bmatrix}\mathbf{A}^{-1} & \mathbf{0}_2\\ \mathbf{0}_2 & \mathbf{0}_2\end{bmatrix}\begin{bmatrix}\mathbf{Q}\\ 0\end{bmatrix} \tag{2.99}$$

We adopt a block matrix notation with Eqs (2.100), (2.101), (2.102), (2.103) and (2.104)

$$\mathbf{A}^{-1}\mathbf{V} = \frac{1}{p+\alpha}(\mathbf{V}-\mathbf{\Lambda}^{\varepsilon}\mathbf{V})+\frac{1}{p}\mathbf{\Lambda}^{\varepsilon}\mathbf{V} \tag{2.100}$$

$$\mathbf{A}^{-1}\mathbf{D} = \frac{1}{p+\alpha}(\mathbf{D}-\mathbf{\Lambda}^{\varepsilon}\mathbf{D})+\frac{1}{p}\mathbf{\Lambda}^{\varepsilon}\mathbf{D} \tag{2.101}$$

$$\mathbf{0}_2 = \begin{bmatrix}0 & 0\\ 0 & 0\end{bmatrix} \tag{2.102}$$

$$\mathbf{I}_2 = \begin{bmatrix}1 & 0\\ 0 & 1\end{bmatrix} \tag{2.103}$$

$$\mathbf{Q} = \begin{bmatrix}Q^{\gamma\omega}\\ Q^{\gamma\omega}\end{bmatrix} \tag{2.104}$$

Although Eq (2.99) represents a convenient formulation of the moments generating differential equations, it is still quite complex. The dominant term at long times can be extracted using the following final value theorem Eq (2.105)

$$\lim_{t\to\infty} f(t) = \lim_{p\to 0} p\bar{f}(p) \tag{2.105}$$

Multiplying Eq (2.99) by $p^n$and taking the limit when $p\to 0$ leads to Eq (2.106), for $n\geqslant 1$.

$$\lim_{p\to 0}(p\bar{\mu}_n^{\gamma}) = \lim_{p\to 0}(p\bar{\mu}_n^{\omega}) = \lim_{t\to\infty}(\mu_n^{\gamma}) = \lim_{t\to\infty}(\mu_n^{\omega}) = n!\,(V^{\infty}t)^n\,Q^{\gamma\omega}+\mathcal{O}\left(t^{n-1}\right) \tag{2.106}$$

where we have Eq (2.107)

$$V^{\infty} = \frac{\varepsilon_{\gamma}\left(V_{\gamma\gamma} + V_{\gamma\omega}\right) + \varepsilon_{\omega}\left(V_{\omega\gamma} + V_{\omega\omega}\right)}{\varepsilon_{\gamma} + \varepsilon_{\omega}} = \frac{\varepsilon_{\gamma}\langle v_{\gamma}\rangle^{\gamma} + \varepsilon_{\omega}\langle v_{\omega}\rangle^{\omega}}{\varepsilon_{\gamma} + \varepsilon_{\omega}} \tag{2.107}$$

The dominant term corresponds in fact to the moments of the following transport equations

$$\frac{\partial\langle c_{\gamma}\rangle^{\gamma}}{\partial t} + V^{\infty}\nabla\langle c_{\gamma}\rangle^{\gamma} = Q^{\gamma\omega} \tag{2.108}$$

$$\frac{\partial\langle c_{\omega}\rangle^{\omega}}{\partial t} + V^{\infty}\nabla\langle c_{\omega}\rangle^{\omega} = Q^{\gamma\omega} \tag{2.109}$$

This term contains the information about the asymptotic velocity of propagation of the signal within the 1-D infinite medium, but looses information concerning the spreading. In this context, it is more interesting to consider the centered spatial moments, that is we follow the signal on a frame moving at the velocity V^{∞}. The centered moments are defined by Eq (2.110).

$$m_n^i = \int_{-\infty}^{+\infty} \left(x - \mu_1^i\right)^n \langle c_i\rangle^i dx \tag{2.110}$$

2.2.2 *First centered moments and convergence*

Herein, we used Maple^{TM} to solve analytically the differential equations Eqs (2.82) and (2.83). We adopt a general notation *exp* for all the exponentially decaying terms. Results for the first order moments normalized to the total mass can be found in Eqs (2.111) and (2.112)

$$\frac{m_1^{\gamma}}{Q^{\gamma\omega}} = \underbrace{\frac{\varepsilon_{\omega}}{\varepsilon_{\gamma} + \varepsilon_{\omega}} \frac{1}{\alpha}\left(\Delta V + V_{\gamma\omega} - V_{\omega\gamma}\right)}_{C_1^{\gamma} = \frac{\varepsilon_{\omega}}{\varepsilon_{\gamma} + \varepsilon_{\omega}}\Omega} + V^{\infty} t + exp \tag{2.111}$$

$$\frac{m_1^{\omega}}{Q^{\gamma\omega}} = -\underbrace{\frac{\varepsilon_{\gamma}}{\varepsilon_{\gamma} + \varepsilon_{\omega}} \frac{1}{\alpha}\left(\Delta V + V_{\gamma\omega} - V_{\omega\gamma}\right)}_{C_1^{\omega} = \frac{\varepsilon_{\gamma}}{\varepsilon_{\gamma} + \varepsilon_{\omega}}\Omega} + V^{\infty} t + exp \tag{2.112}$$

with

$$\Omega = \frac{1}{\alpha}\left(\Delta V + V_{\gamma\omega} - V_{\omega\gamma}\right) \tag{2.113}$$

and

$$\Delta V = V_{\gamma\gamma} - V_{\omega\omega} \tag{2.114}$$

.

The constant Ω appearing in the first order moments represents the shift Fig (27) between the two signals.

For the second order moments, we have Eqs (2.115) and (2.116).

$$\frac{1}{2}\frac{m_2^\gamma}{Q^{\gamma\omega}} = C_2^\gamma + D^\infty t + exp \tag{2.115}$$

$$\frac{1}{2}\frac{m_2^\omega}{Q^{\gamma\omega}} = C_2^\omega + D^\infty t + exp \tag{2.116}$$

with Eq (2.117)

$$\begin{aligned} D^\infty &= \frac{\varepsilon_\gamma\left(D_{\gamma\gamma} + D_{\gamma\omega}\right) + \varepsilon_\omega\left(D_{\omega\gamma} + D_{\omega\omega}\right)}{\varepsilon_\gamma + \varepsilon_\omega} \\ &\quad + \frac{1}{\alpha\left(\varepsilon_\gamma + \varepsilon_\omega\right)^2}\left(\Delta V + V_{\gamma\omega} - V_{\omega\gamma}\right)\left(\varepsilon_\gamma\varepsilon_\omega\Delta V - \varepsilon_\gamma^2 V_{\gamma\omega} + \varepsilon_\omega^2 V_{\omega\gamma}\right) \end{aligned} \tag{2.117}$$

Exponentially decaying terms have all a similar form which is a sum of $t^n e^{-k\alpha t}$where n and k are integers. Hence, the time for the relaxation of the centered moments tends toward infinity when α tends toward zero. This represents our first constraint, we need $t \gg \frac{1}{\alpha}$, that is, in terms of orders of magnitude, under the condition that the volume fractions are rather similar (same order of magnitude)

$$t \gg \frac{1}{h} \tag{2.118}$$

Going back to the discussion about the two separated tubes, we now see why such a system can not be described by a single equation since $h = 0$ in this case and the relaxation time tends toward infinity. In addition, it is important to notice that, at this point, we have reached the same conclusions that in [295] and found a similar expression for D^∞, without proving it from the study of the higher order moments.

2.2.3 *Centered moments for the weighted average*

To make further progress, considering our interest in the weighted concentration defined by Eq. 1.16, we study the weighted central moments defined by Eq (2.119)

$$m_n^{\gamma\omega} = \frac{\varepsilon_\gamma}{\varepsilon_\gamma + \varepsilon_\omega} m_n^\gamma + \frac{\varepsilon_\omega}{\varepsilon_\gamma + \varepsilon_\omega} m_n^\omega \tag{2.119}$$

The different values for these moments are presented below. It is important to keep in mind that the centered moments, in the long time limit, for the one-equation models are those of a normal distribution, that is,

$$\frac{m_n^{\gamma\omega}}{Q^{\gamma\omega}} = (n-1)!!\,(2D^\infty t)^{\frac{n}{2}} \text{ for } n \textit{ even}$$
$$\frac{m_n^{\gamma\omega}}{Q^{\gamma\omega}} = 0 \text{ for } n \text{ odd}$$

FIRST ORDER

$$\frac{m_1^{\gamma\omega}}{Q^{\gamma\omega}} = V^\infty t + exp \tag{2.120}$$

There are two important conclusions that can be formulated from Eq (2.120).

- In this expression, it is apparent that the first order weighted centered moments is propagating at V^∞ at long times and that the relaxation is purely driven by the exponential terms. However, even though the constant shift disappears when considering the weighted concentration, it is still unclear why the signal can be described by a Gaussian as, *a priori*, the constant shift still induces a strong effect on the higher order moments.

- It also shows that the relaxation toward a one-equation model is faster for the weighted average concentration than for the intrinsic concentrations. There has been some discussions about what should be used as a macroscopic concentration for a one-equation model in a multiphase configuration [77]. For example, in a porous medium colonized by biofilms, experimenters tend to use the concentration only in the water-phase whereas the results herein suggest that the weighted concentration should be considered, and this would bring some simplified behavior.

At this point, we make the following approximations $V_{\gamma\omega} - V_{\omega\gamma} \ll \Delta V$ and $D_{\gamma\omega} - D_{\omega\gamma} \ll \Delta D$. These are not necessary but (1) they lead to interesting simplifications and (2) they are verified in most cases, as, $V_{\gamma\gamma}$ and $V_{\omega\omega}$ contain the dominant terms $\langle v_\gamma \rangle^\gamma$ and $\langle v_\omega \rangle^\omega$, unlike $V_{\gamma\omega}$ and $V_{\omega\gamma}$. Hence, ΔV and ΔD can be interpreted as the velocity and dispersion contrasts between both phases.

SECOND ORDER Solving the differential equations leads to Eq (2.121)

$$\frac{1}{2}\frac{m_2^{\gamma\omega}}{Q^{\gamma\omega}} = -\frac{3}{2}\frac{\varepsilon_\gamma\varepsilon_\omega}{(\varepsilon_\gamma+\varepsilon_\omega)^2}\Omega^2 + D^\infty t + exp \tag{2.121}$$

This expression shows that a constant is still involved. Hence, an obvious constraint for the asymptotic regime to be reached is Eq (2.122).

$$t \gg \frac{\frac{3}{2}\frac{\varepsilon_\gamma\varepsilon_\omega}{(\varepsilon_\gamma+\varepsilon_\omega)^2}\Omega^2}{D^\infty} \tag{2.122}$$

This represents a sufficient constraint for the convergence of the second order centered moment but it is still unclear what is happening for higher orders moments.

THIRD ORDER Considering the third order moment leads to Eq (2.123)

$$\begin{aligned}\frac{1}{2}\frac{m_3^{\gamma\omega}}{Q^{\gamma\omega}} &= 9\frac{\varepsilon_\gamma\varepsilon_\omega}{\alpha^2(\varepsilon_\gamma+\varepsilon_\omega)^2}\Delta V\Delta D + 8\frac{\varepsilon_\gamma\varepsilon_\omega(\varepsilon_\gamma-\varepsilon_\omega)}{\alpha^3(\varepsilon_\gamma+\varepsilon_\omega)^3}\Delta V^3 \\ &+ \left(6\frac{\varepsilon_\gamma\varepsilon_\omega}{\alpha(\varepsilon_\gamma+\varepsilon_\omega)^2}\Delta V\Delta D + 3\frac{\varepsilon_\gamma\varepsilon_\omega(\varepsilon_\gamma-\varepsilon_\omega)}{\alpha^2(\varepsilon_\gamma+\varepsilon_\omega)^3}\Delta V^3\right)t + exp\end{aligned} \tag{2.123}$$

For a Gaussian shaped signal, the third order centered moment is zero, like other odd order moments. In our case, it tends toward infinity as a $\mathcal{O}(t)$. At first, this is quite disheartening and we clearly do not have a convergence in terms of the centered moments. Thus, it is legitimate to wonder how the description of this signal can be undertaken using a one-equation model. In the next section, we show that the $\mathcal{O}(t)$ behavior can be neglected as compared to the weighted spreading of the signal, measured by $m_2^{\gamma\omega}$.

FOURTH ORDER

$$\frac{1}{3}\frac{m_4^{\gamma\omega}}{Q^{\gamma\omega}} = c_4 + C_4 t + 4(D^\infty t)^2 + exp \tag{2.124}$$

We see that the dominant term at long time in Eq (2.124) is $(D^\infty t)^2$ which is the fourth order moments corresponding to Eq (2.78).

N-TH ORDER We were unable to formally prove a general expression for the n-th order centered moment. However, the calculation of these, up to the sixth order, leads to the following conclusions

- We have $\frac{m_n^{\gamma\omega}}{Q^{\gamma\omega}} = (n-1)!!(2D^\infty t)^{\frac{n}{2}} + \mathcal{O}\left(t^{\frac{n}{2}}\right)$ for n even, with the double factorial given by $(n-1)!! = \prod_{i;0\leqslant 2i n-1}(n-1-2i)$.

- We have $\frac{m_{n-1}^{\gamma\omega}}{Q^{\gamma\omega}} = \mathcal{O}\left(t^{\frac{n}{2}-1}\right)$ for $n-1$ odd.

2.2.4 *Standardized moments, skewness and kurtosis*

The goal of this section is to understand the time-asymptotic behavior of the standardized moments defined by, for $n \geqslant 2$,

$$M_n^{\gamma\omega} = \frac{m_n^{\gamma\omega}}{\left(m_2^{\gamma\omega}\right)^{\frac{n}{2}}} \tag{2.125}$$

For the one-equation model, with a Dirac input, we have, at long times

$$M_n^{\gamma\omega} = (n-1)!! = \prod_{i;0\leqslant 2i\leqslant n-1} (n-1-2i) \text{ for } n \textit{ even}$$
$$M_n^{\gamma\omega} = 0 \text{ for } n \text{ odd}$$

In our case, we can calculate the time-infinite limit of the standardized moments on the basis of the equations given in section 2.2.3. For the orders 3 and 4, this leads to:

SKEWNESS

$$\lim_{t\to\infty} M_3^{\gamma\omega} = 0 \tag{2.126}$$

KURTOSIS

$$\lim_{t\to\infty} M_4^{\gamma\omega} = 3 \tag{2.127}$$

In the context of statistical physics, the skewness and the kurtosis are often used to test for the normality of a set of data, that is, these are considered sufficient measures for the normality of a distribution. In our case, it seems that the signal tends toward a Gaussian in the sense of the skewness and kurtosis. In a more rigorous perspective, it is necessary to consider the general formulation of the leading terms of all the higher order centered moments. From the results extrapolated in section 2.2.3, we have

$$\frac{m_n^{\gamma\omega}}{Q^{\gamma\omega}} = (n-1)!!\,(2D^{\infty}t)^{\frac{n}{2}} + o\left(t^{\frac{n}{2}}\right),\ n \text{ even and } \frac{m_{n-1}^{\gamma\omega}}{Q^{\gamma\omega}} = \mathcal{O}\left(t^{\frac{n}{2}-1}\right),\ n \text{ odd}$$

It is straightforward that for n even,

$$\lim_{t\to\infty} M_n^{\gamma\omega} = (n-1)!!$$

and for n odd,

$$\lim_{t\to\infty} M_n^{\gamma\omega} = 0$$

that is, there is a convergence of the two-equation model toward a one-equation model in terms of standardized moments. In other words, it means that we never rigorously, i.e., for finite t, have a normal distribution of the concentrations but that the spreading, i.e., the second order centered moment, is dominating all other kind of deformation of the signal at long times.

2.2.5 *Constraints and convergence*

In this section, we develop the constraints that indicate when the one-equation model can be used instead of the two-equation one. First of all, as previously discussed, we need

$$\textbf{Constraint A: } t \gg \frac{1}{h} \tag{2.128}$$

In addition, for the second order, we need constraints such as Eq (2.129).

$$\frac{3}{2}\frac{\varepsilon_\gamma \varepsilon_\omega}{(\varepsilon_\gamma+\varepsilon_\omega)^2}\Omega^2 \ll D^\infty t \tag{2.129}$$

To develop clear constraints that apply to any order, we define a measure of this difference in terms of standardized moments. We say that the one-equation formulation represents a good approximation of the transport processes if and only if

1. **Constraint A:** $t \gg \frac{1}{h}$ is satisfied
2. **Constraint B:** For $n \geqslant 2$, we have $\delta_n = |\frac{m_n^{\gamma\omega} - m_n^\infty}{(m_2^\infty)^{\frac{n}{2}}}| \ll 1$ where m_n^∞ is the nth-order moment of the Gaussian asymptotic one-equation model.

SECOND ORDER With this definition, we still have the same constraint associated with the second order Eq (2.130).

$$\frac{3}{2}\frac{\varepsilon_\gamma \varepsilon_\omega}{(\varepsilon_\gamma+\varepsilon_\omega)^2}\frac{\Omega^2}{D^\infty} \ll t \tag{2.130}$$

There is an interesting physical interpretation for this constraint. Going back to Fig (27), we see that it means that the distance between the peaks of the signals in each phase must be small as compared to the spreading of the signals.

In addition, the definition of D^∞ is

$$D^\infty = \frac{\varepsilon_\gamma (D_{\gamma\gamma} + D_{\gamma\omega}) + \varepsilon_\omega (D_{\omega\gamma} + D_{\omega\omega})}{\varepsilon_\gamma + \varepsilon_\omega} + \frac{\varepsilon_\gamma \varepsilon_\omega}{\alpha (\varepsilon_\gamma + \varepsilon_\omega)^2} \Delta V^2 \tag{2.131}$$

and obviously

$$D^\infty \geqslant \frac{\varepsilon_\gamma \varepsilon_\omega}{\alpha (\varepsilon_\gamma + \varepsilon_\omega)^2} \Delta V^2 \tag{2.132}$$

because

$$\frac{\varepsilon_\gamma (D_{\gamma\gamma} + D_{\gamma\omega}) + \varepsilon_\omega (D_{\omega\gamma} + D_{\omega\omega})}{\varepsilon_\gamma + \varepsilon_\omega} \geqslant 0 \tag{2.133}$$

Going back to the definition of Ω, we have

$$\Omega = \frac{1}{\alpha} \Delta V \tag{2.134}$$

Hence, a sufficient condition for the expression of this constraint on the second order term is also

$$t \gg \frac{1}{\alpha} \tag{2.135}$$

Obviously, if the volumic fraction occupied by one of the phases is negligible, then the two-equation model can be replaced by a one-equation description. This is an important result, but we will not consider such simple cases. We assume that the volumic fractions of each phase are rather similar (not separated by several orders of magnitudes), so that the sufficient condition boils down to

$$t \gg \frac{1}{h} \tag{2.136}$$

with a convergence in $\mathcal{O}\left(\frac{1}{t}\right)$.

THIRD ORDER For the third order moment, **Constraint B** can be expressed by Eq (2.137)

$$9 \frac{\varepsilon_\gamma \varepsilon_\omega}{h^2 (\varepsilon_\gamma + \varepsilon_\omega)^2} \Delta V \Delta D + 8 \frac{\varepsilon_\gamma \varepsilon_\omega (\varepsilon_\gamma - \varepsilon_\omega)}{h^3 (\varepsilon_\gamma + \varepsilon_\omega)^3} \Delta V^3 + 2 \left(6 \frac{\varepsilon_\gamma \varepsilon_\omega}{h (\varepsilon_\gamma + \varepsilon_\omega)^2} \Delta V \Delta D + 3 \frac{\varepsilon_\gamma \varepsilon_\omega (\varepsilon_\gamma - \varepsilon_\omega)}{h^2 (\varepsilon_\gamma + \varepsilon_\omega)^3} \Delta V^3 \right) t \ll (2 D^\infty t)^{\frac{3}{2}} \tag{2.137}$$

As a first step toward the derivation of a sufficient condition associated with Eq (2.137), we impose the inequality Eq (2.138):

$$\frac{1}{h}\left(9\frac{\varepsilon_\gamma\varepsilon_\omega}{h(\varepsilon_\gamma+\varepsilon_\omega)^2}\Delta V\Delta D+8\frac{\varepsilon_\gamma\varepsilon_\omega(\varepsilon_\gamma-\varepsilon_\omega)}{h^2(\varepsilon_\gamma+\varepsilon_\omega)^3}\Delta V^3\right)\ll 2\left(6\frac{\varepsilon_\gamma\varepsilon_\omega}{h(\varepsilon_\gamma+\varepsilon_\omega)^2}\Delta V\Delta D+3\frac{\varepsilon_\gamma\varepsilon_\omega(\varepsilon_\gamma-\varepsilon_\omega)}{h^2(\varepsilon_\gamma+\varepsilon_\omega)^3}\Delta V^3\right)t \tag{2.138}$$

In terms of orders of magnitude, a sufficient condition for Eq (2.138) to be true is

Constraint A: $t \gg \frac{1}{h}$

As a consequence of imposing Eq (2.138), the inequality described by Eq (2.137) now reduces to Eq (2.139)

$$2\left(6\frac{\varepsilon_\gamma\varepsilon_\omega}{h(\varepsilon_\gamma+\varepsilon_\omega)^2}\Delta V\Delta D+3\frac{\varepsilon_\gamma\varepsilon_\omega(\varepsilon_\gamma-\varepsilon_\omega)}{h^2(\varepsilon_\gamma+\varepsilon_\omega)^3}\Delta V^3\right)t\ll(2D^\infty t)^{\frac{3}{2}} \tag{2.139}$$

This can be simplified, and leads to an equivalent inequality Eq (2.140)

$$\frac{1}{2}\left(6\frac{\varepsilon_\gamma\varepsilon_\omega}{h(\varepsilon_\gamma+\varepsilon_\omega)^2}\frac{\Delta V\Delta D}{(D^\infty)^{\frac{3}{2}}}+3\frac{\varepsilon_\gamma\varepsilon_\omega(\varepsilon_\gamma-\varepsilon_\omega)}{h^2(\varepsilon_\gamma+\varepsilon_\omega)^3}\frac{\Delta V^3}{(D^\infty)^{\frac{3}{2}}}\right)^2\ll t \tag{2.140}$$

A sufficient condition, in terms of orders of magnitude, is Eq (2.141) in conjunction with Eq (2.142)

$$\frac{1}{h^2}\frac{\Delta V^2\Delta D^2}{(D^\infty)^3}\ll t \tag{2.141}$$

$$\frac{1}{h^4}\frac{\Delta V^6}{(D^\infty)^3}\ll t \tag{2.142}$$

Using the definition of D^∞ Eq (2.131), it is straightforward to show that

$$\frac{1}{h}\frac{\Delta V^2\Delta D^2}{(D^\infty)^3}\leqslant 1 \tag{2.143}$$

and

$$\frac{1}{h^3}\frac{\Delta V^6}{(D^\infty)^3}\leqslant 1 \tag{2.144}$$

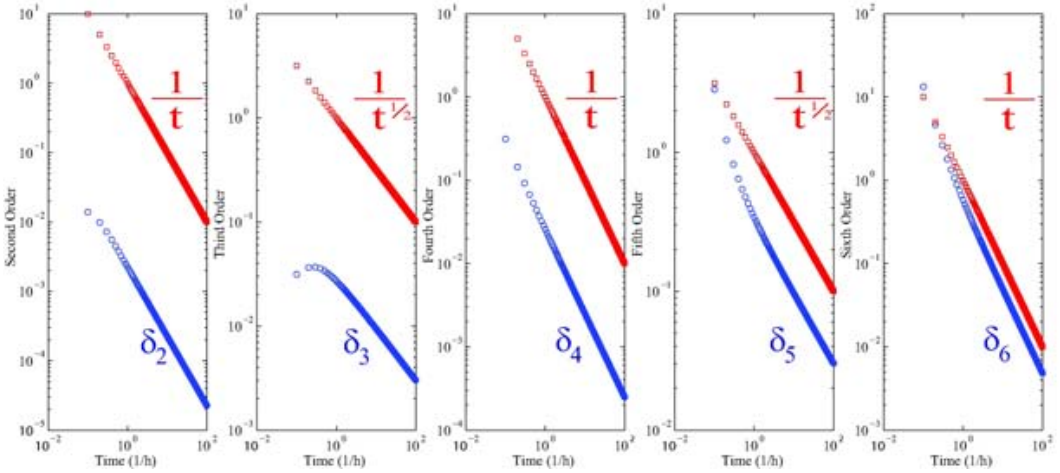

Figure 31: Convergence of the two-equation quasi-stationary model toward the one-equation asymptotic model in terms of standardized moments measure δ_n for $V_{\omega\gamma} = V_{\gamma\omega} = D_{\omega\gamma} = D_{\gamma\omega} = 0$, $V_{\gamma\gamma} = 5$, $V_{\omega\omega} = 1$, $D_{\gamma\gamma} = 10$, $D_{\omega\omega} = 5$ and $h = 1$.

and hence,

$$\textbf{Constraint A: } t \gg \frac{1}{h}$$

is a sufficient condition, for a convergence in $\mathcal{O}\left(\frac{1}{\sqrt{t}}\right)$.

The convergence is polynomial in terms of standardized moments, in opposition to the classical view of the single-continuum problem which is an exponential convergence in terms of centered moments [33]. For the skewness, the expression of the error given by **Constraint B** tends toward zero as a $\mathcal{O}\left(\frac{1}{\sqrt{t}}\right)$ whereas, for the kurtosis, it tends toward zero as a $\mathcal{O}\left(\frac{1}{t}\right)$. This difference in the convergence means that the signal recovers quicker the "peakedness" of the normal distribution than the symmetry. Notice that δ_n can also be expressed as series such as $\sum_n a_n \frac{1}{t^{\frac{n}{2}}}$, leading to similar conclusions regarding the long-time convergence.

2.2.6 *Numerical simulations*

In this section, we are interested in solving Eqs (2.82) and (2.83) numerically and then calculating the expression of the δ_n. Our goal is to sudy numerically the behavior of the moments, up to the order six. We used the MATLAB^{TM} solver ode15s with a relative tolerance of $2.22045\,10^{-14}$ to provide some direct evidences for the **Constraint:** $t \gg \frac{1}{h}$. A convergence study concerning the tolerance parameter was performed showing that, for the chosen one, no significant discretization error was apparent. Results are presented Fig (31) up to the sixth order for δ_n. The results are given on a log-log graph, highlighting two different regimes. For small times, the dominant term is the

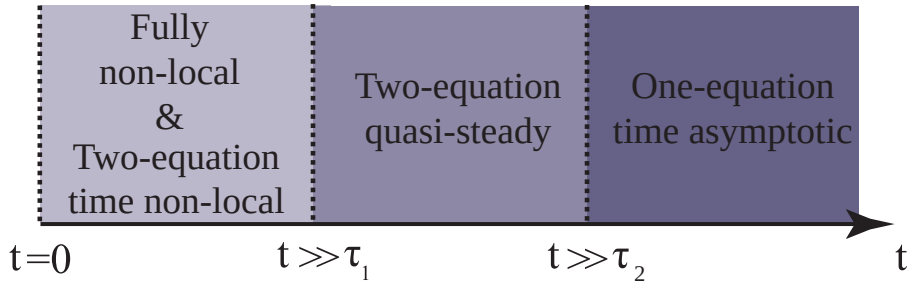

Figure 32: Schematic summary of the domains of validity of the different models for a pulse in a dual-phase/region infinite porous medium. τ_1 is a characteristic time for the relaxation of the effective parameters and τ_2 is a characteristic time associated with the mass exchange coefficient in the two-equation model.

exponential part. For longer times, the various errors tend linearly toward zero with a $-\frac{1}{2}$ or -1 slopes, that is, the convergence is driven by a $\mathcal{O}\left(\frac{1}{\sqrt{t}}\right)$ or $\mathcal{O}\left(\frac{1}{t}\right)$ and this is coherent with the theoretical analysis. Direct numerical resolutions of the closure problems for the different macroscopic models, comparisons with Direct Numerical Simulations (DNS) and associated breakthrough curves can be found in [78] on a simple 2-D geometry.

2.2.7 *Discussion*

In essence, this part is an extension of [295] and [177, 178, 237, 205] in that we (1) provide a comprehensive framework that can be used by experimenters for the choice of the dual-continua models that are used at the Darcy-scale to describe mass transport, (2) solve the issue of higher order moments in the one-equation situation and (3) study the convergence of the two-equation model toward the one-equation formulation. Assuming that the spatial non-locality can be separated from the temporal non-locality and that the hypothesis of separation of length scales is valid can lead to various Darcy-scale models. These correspond to specific statements that are made concerning the characteristic times of the problem. For the case of a pulse propagating through an infinite dual-phase/region porous medium, the different constraints are summarized Fig (32), in terms of orders of magnitudes. Experimenters should consider carefully these different limitations and mathematical models should be chosen on the basis of solid physical reasons.

2.3 PECULIAR PERTURBATION DECOMPOSITION (MODEL E)

A different way to obtain one-equation local non-equilibrium models consists in decomposing concentrations as follows

$$c_i = \langle c \rangle^{\gamma\omega} + \hat{c}_i \tag{2.145}$$

In this case, the fluctuation is defined in relation to the weighted average on both phases/regions. The problem is closed using [205] Eq (52) (in which η is used instead of γ), [178] Eqs (42) and (43), for heat transfer. It has been proposed in [205] for the large-scale averaging problem and applied in [77] for a reactive case (linear kinetics). The closure can be written

$$\hat{c}_i = \mathbf{b}_i \cdot \boldsymbol{\nabla} \langle c \rangle^{\gamma\omega} \tag{2.146}$$

This decomposition may be very efficient since it allows to directly develop a macroscopic one-equation model, to reduce the number of closure parameters and it is also useful for upscaling various class of problems such as reactive ones. The counterpart is that the assumptions behind the first order closure and the quasi-stationarity of the fluctuations problems are stronger in this case because (1) the closure recovers less characteristic times than the $\tilde{c}$ decomposition and (2) the norm of the $\hat{c}_i$ perturbation is larger than the norm of $\tilde{c}_i$. The macroscopic mass balanced equation takes the form [205]Eq (56) (in which η is used instead of γ)

$$(\varepsilon_\gamma + \varepsilon_\omega)\, \partial_t \langle c \rangle^{\gamma\omega} + \mathbf{V} \cdot \boldsymbol{\nabla} \langle c \rangle^{\gamma\omega} = \boldsymbol{\nabla} \cdot \{\mathbf{D}^* \cdot \boldsymbol{\nabla} \langle c \rangle^{\gamma\omega}\} \tag{2.147}$$

The $\hat{c}_i$ perturbation decomposition leads to the following expression of dispersion, see in [205]Eq (57) (in which η is used instead of γ) and [78].

$$\mathbf{D}^* = \sum_{i=\gamma,\omega} \varepsilon_i \left[\mathbf{D}_i \cdot \left(\mathbf{I} + \langle \boldsymbol{\nabla} \mathbf{b}_i \rangle^i \right) - \langle \mathbf{v}_i \mathbf{b}_i \rangle^i \right] \tag{2.148}$$

CLOSURE PROBLEM The determination of effective parameters requires the calculation of a single problem which can be found in [205] Eqs (53) to (55) (in which η is used instead of γ) and in [78].

$$\mathbf{v}_\gamma \cdot \boldsymbol{\nabla} \mathbf{b}_\gamma = \boldsymbol{\nabla} \cdot \{\mathbf{D}_\gamma \cdot \boldsymbol{\nabla} \mathbf{b}_\gamma\} - \tilde{\mathbf{v}}_\gamma - \varepsilon_\gamma^{-1} \mathbf{U}^* \tag{2.149}$$

$$\begin{aligned}
\text{B.C.1}: &\quad -\mathbf{n}_{\gamma\sigma}\cdot(\mathsf{D}_\gamma\cdot\boldsymbol{\nabla}\mathbf{b}_\gamma)=\mathbf{n}_{\gamma\sigma}\cdot\mathsf{D}_\gamma && \text{on } \mathscr{S}_{\gamma\sigma} && (2.150a)\\
\text{B.C.1}: &\quad \mathbf{b}_\gamma=\mathbf{b}_\omega && \text{on } \mathscr{S}_{\gamma\omega} && (2.150b)\\
\text{B.C.2}: &\quad -\mathbf{n}_{\gamma\omega}\cdot\left(\mathbf{j}_{\mathbf{b}_\gamma}-\mathbf{j}_{\mathbf{b}_\omega}\right)=-\mathbf{n}_{\gamma\omega}\cdot(\mathbf{D}_\omega-\mathbf{D}_\gamma) && \text{on } \mathscr{S}_{\gamma\omega} && (2.150c)\\
\text{B.C.4}: &\quad -\mathbf{n}_{\omega\sigma}\cdot(\mathsf{D}_\omega\cdot\boldsymbol{\nabla}\mathbf{b}_\omega)=\mathbf{n}_{\omega\sigma}\cdot\mathsf{D}_\omega && \text{on } \mathscr{S}_{\omega\sigma} && (2.150d)\\
\text{Periodicity}: &\quad \mathbf{b}_i(\mathbf{x}+p_k)=\mathbf{b}_i(\mathbf{x}) && k=1,2,3 && (2.150e)\\
\text{Unicity}: &\quad \langle\mathbf{b}_i\rangle^i=0 && && (2.150f)
\end{aligned}$$

$$\mathbf{v}_\omega\cdot\boldsymbol{\nabla}\mathbf{b}_\omega=\boldsymbol{\nabla}\cdot\{\mathbf{D}_\omega\cdot\boldsymbol{\nabla}\mathbf{b}_\omega\}-\tilde{\mathbf{v}}_\omega+\varepsilon_\omega^{-1}\mathbf{U}^* \tag{2.151}$$

with

$$\mathbf{U}^* = \varepsilon_\gamma\varepsilon_\omega\frac{\langle\mathbf{v}_\gamma\rangle^\gamma-\langle\mathbf{v}_\omega\rangle^\omega}{\varepsilon_\gamma+\varepsilon_\omega} \tag{2.152}$$

2.4 LOCAL MASS EQUILIBRIUM (MODEL F)

The local mass equilibrium situation corresponds to

$$\langle c_\gamma\rangle^\gamma\cong\langle c_\omega\rangle^\omega\cong\langle c\rangle^{\gamma\omega} \tag{2.153}$$

In other words, this means that the concentration gradients within the phases/regions are sufficiently small to extend the thermodynamic equilibrium at the interface to the bulk phases/regions. This represents a very particular physical situation for which the total mass within the medium can be described by a single weighted concentration $\langle c\rangle^{\gamma\omega}$, that is, by a one-equation model such as Eq (2.154). The associated constraints have been extensively discussed and can be found in [274, 114, 287, 260]. These are usually expressed in terms of orders of magnitude of dimensionless numbers. In this situation, a reasonable approximation [274] of the two-equation model is [205] Eq (20) (in which η is used instead of γ)

$$(\varepsilon_\gamma+\varepsilon_\omega)\,\partial_t\langle c\rangle^{\gamma\omega}+\mathbf{V}\cdot\boldsymbol{\nabla}\langle c\rangle^{\gamma\omega}=\boldsymbol{\nabla}\cdot\{\mathbf{D}^{equ}\cdot\boldsymbol{\nabla}\langle c\rangle^{\gamma\omega}\} \tag{2.154}$$

It can be obtained by summing Eqs (2.38) and (2.39) and, therefore, the local mass equilibrium dispersion tensor can be written [205] Eq (22) (in which η is used instead of γ)

$$\mathbf{D}^{equ}=\sum_{i,j=\gamma\text{ or }\omega}\mathbf{D}_{ij}=\sum_{i=\gamma,\omega}\varepsilon_i\langle\mathbf{D}_i\cdot(\mathbf{I}+\boldsymbol{\nabla}\mathbf{B}_i)-\tilde{\mathbf{v}}_i\mathbf{B}_i\rangle^i \tag{2.155}$$

with a closure on the perturbations that takes the form

$$\tilde{c}_i = \mathbf{B}_i \cdot \boldsymbol{\nabla} \langle c \rangle^{\gamma\omega}$$

The effective velocity takes the very simple form [205]Eq (23) (in which η is used instead of γ)

$$\mathbf{V} = \varepsilon_\gamma \langle \mathbf{v}_\gamma \rangle^\gamma + \varepsilon_\omega \langle \mathbf{v}_\omega \rangle^\omega \tag{2.156}$$

The closure parameters $\mathbf{B}_i$ are simply related to those of the two-equation model by

$$\mathbf{B}_\gamma = \mathbf{b}_{\gamma\gamma} + \mathbf{b}_{\gamma\omega} \tag{2.157a}$$
$$\mathbf{B}_\omega = \mathbf{b}_{\omega\gamma} + \mathbf{b}_{\omega\omega} \tag{2.157b}$$

or they can be calculated solving directly the following boundary value problem at the microscale

$$\mathbf{v}_\gamma \cdot \boldsymbol{\nabla}\mathbf{B}_\gamma = \boldsymbol{\nabla} \cdot \{\mathbf{D}_\gamma \cdot \boldsymbol{\nabla}\mathbf{B}_\gamma\} - \tilde{\mathbf{v}}_\gamma - \varepsilon_\gamma^{-1}\boldsymbol{\beta}^* \tag{2.158}$$

$$\text{B.C.1}: \quad -\mathbf{n}_{\gamma\sigma} \cdot (\mathbf{D}_\gamma \cdot \boldsymbol{\nabla}\mathbf{B}_\gamma) = \mathbf{n}_{\gamma\sigma} \cdot \mathbf{D}_\gamma \quad \text{on } \mathscr{S}_{\gamma\sigma} \tag{2.159a}$$
$$\text{B.C.1}: \quad \mathbf{B}_\gamma = \mathbf{B}_\omega \quad \text{on } \mathscr{S}_{\gamma\omega} \tag{2.159b}$$
$$\text{B.C.2}: \quad -\mathbf{n}_{\gamma\omega} \cdot \left(\mathbf{j}_{\mathbf{B}_\gamma} - \mathbf{j}_{\mathbf{B}_\omega}\right) = -\mathbf{n}_{\gamma\omega} \cdot (\mathbf{D}_\omega - \mathbf{D}_\gamma) \quad \text{on } \mathscr{S}_{\gamma\omega} \tag{2.159c}$$
$$\text{B.C.4}: \quad -\mathbf{n}_{\omega\sigma} \cdot (\mathbf{D}_\omega \cdot \boldsymbol{\nabla}\mathbf{B}_\omega) = \mathbf{n}_{\omega\sigma} \cdot \mathbf{D}_\omega \quad \text{on } \mathscr{S}_{\omega\sigma} \tag{2.159d}$$
$$\text{Periodicity}: \quad \mathbf{B}_i(\mathbf{x} + p_k) = \mathbf{B}_i(\mathbf{x}) \quad k = 1,2,3 \tag{2.159e}$$
$$\text{Unicity}: \quad \langle \mathbf{B}_i \rangle^i = 0 \tag{2.159f}$$

$$\mathbf{v}_\omega \cdot \boldsymbol{\nabla}\mathbf{B}_\omega = \boldsymbol{\nabla} \cdot \{\mathbf{D}_\omega \cdot \boldsymbol{\nabla}\mathbf{B}_\omega\} - \tilde{\mathbf{v}}_\omega + \varepsilon_\omega^{-1}\boldsymbol{\beta}^* \tag{2.160}$$

with

$$\boldsymbol{\beta}^* = -\frac{1}{V}\int_{A_{\gamma\omega}} \mathbf{n}_{\gamma\omega} \cdot \mathbf{j}_{\mathbf{B}_\gamma} \, dA \tag{2.161}$$

3

FORMAL EQUIVALENCE BETWEEN *MODEL D AND E*

The goal of this part is to obtain a formal proof of the equivalence between Eqs (2.77) and (2.147), that is, to prove $\mathbf{D}^* = \mathbf{D}^\infty$.

3.1 REMINDER OF THE EXPRESSIONS FOR THE DISPERSION TENSORS

3.1.1 *One-equation time-asymptotic non-equilibrium model*

The dispersion tensor Eq (1.25) can be written [295] Eqs (97) to (99)

$$\begin{aligned}\mathbf{D}^\infty &= \sum_{i,j=\gamma \text{ or } \omega} \mathbf{D}_{ij} + \frac{1}{h}\left(\mathbf{U}^* + \mathbf{d}_\omega - \mathbf{d}_\gamma\right)\left(\mathbf{U}^* - \boldsymbol{\beta}^*\right) \\ &= \mathbf{D}^{equ} + \frac{1}{h}\left(\mathbf{U}^* + \mathbf{d}_\omega - \mathbf{d}_\gamma\right)\left(\mathbf{U}^* - \boldsymbol{\beta}^*\right) \end{aligned} \tag{3.1}$$

Both parts of this expression have very distinct physical meaning. $\sum_{i,j=\gamma \text{ or } \omega} \mathbf{D}_{ij}^{**}$ represents the sum of the dispersion terms, which strictly speaking, corresponds to local mass equilibrium dispersion, and is rather similar to the single phase situation. However, the second part stands for the multiphase aspects. It expresses the contrast effect between the $\gamma-phase$ and the $\omega-phase$. It tends toward 0 when the exchange coefficient α^{**} tends toward infinity and is mainly driven by the square of

$$\mathbf{U}^* = \varepsilon_\gamma \varepsilon_\omega \frac{\langle \mathbf{v}_\gamma \rangle^\gamma - \langle \mathbf{v}_\omega \rangle^\omega}{\varepsilon_\gamma + \varepsilon_\omega} \tag{3.2}$$

It also contains

$$\boldsymbol{\beta}^* = -\frac{1}{V}\int_{A_{\gamma\omega}} \mathbf{n}_{\gamma\omega} \cdot \mathbf{j}_{\mathbf{B}_\gamma} \, dA \tag{3.3a}$$

$$\mathbf{d}_\omega - \mathbf{d}_\gamma = \sum_{i=\gamma,\omega} \varepsilon_i \left\langle \mathbf{D}_i \cdot \boldsymbol{\nabla} r_i - \tilde{\mathbf{v}}_i r_i \right\rangle^k \tag{3.3b}$$

This asymptotic behavior was proved directly from the lower-scale equation in [166] for stratified systems, and used extensively in [150] which introduced the word

Taylor's dispersion, for that particular case, because of the square dependence of the dispersion coefficient with the velocity difference.

Notice that there are usually six closure (or mapping) variables associated to the two-equation model, that is $\mathbf{b}_{\gamma\gamma}, \mathbf{b}_{\gamma\omega}, \mathbf{b}_{\omega\gamma}, \mathbf{b}_{\omega\omega}, r_\gamma, r_\omega$. In the expression of the dispersion Eq (3.1) only four closure variables remain, namely r_γ, r_ω and $\mathbf{B}_\gamma, \mathbf{B}_\omega$. They are simply related to those of the two-equation model by

$$\mathbf{B}_\gamma = \mathbf{b}_{\gamma\gamma} + \mathbf{b}_{\gamma\omega} \tag{3.4a}$$
$$\mathbf{B}_\omega = \mathbf{b}_{\omega\gamma} + \mathbf{b}_{\omega\omega} \tag{3.4b}$$

CLOSURE PROBLEMS The set of effective parameters previously introduced can be computed through the resolution of the two following closure problems. They can be straightforwardly derived from [2] Eqs (49) to (56) (in which η is used instead of γ).

$$\mathbf{v}_\gamma \cdot \boldsymbol{\nabla} r_\gamma = \boldsymbol{\nabla} \cdot \{\mathbf{D}_\gamma \cdot \boldsymbol{\nabla} r_\gamma\} - \varepsilon_\gamma^{-1} h \tag{3.5}$$

$$\text{B.C.1}: \quad -\mathbf{n}_{\gamma\sigma} \cdot (\mathbf{D}_\gamma \cdot \boldsymbol{\nabla} r_\gamma) = 0 \quad \text{on } \mathscr{S}_{\gamma\sigma} \tag{3.6a}$$
$$\text{B.C.1}: \quad r_\gamma = r_\omega \quad \text{on } \mathscr{S}_{\gamma\omega} \tag{3.6b}$$
$$\text{B.C.2}: \quad -\mathbf{n}_{\gamma\omega} \cdot \left(\mathbf{j}_{r_\gamma} - \mathbf{j}_{r_\omega}\right) = 0 \quad \text{on } \mathscr{S}_{\gamma\omega} \tag{3.6c}$$
$$\text{B.C.4}: \quad -\mathbf{n}_{\omega\sigma} \cdot (\mathbf{D}_\omega \cdot \boldsymbol{\nabla} r_\omega) = 0 \quad \text{on } \mathscr{S}_{\omega\sigma} \tag{3.6d}$$
$$\text{Periodicity}: \quad r_i(\mathbf{x} + p_k) = r_i(\mathbf{x}) \quad k = 1,2,3 \tag{3.6e}$$
$$\text{Unicity}: \quad \langle r_i \rangle^i = 0 \tag{3.6f}$$

$$\mathbf{v}_\omega \cdot \boldsymbol{\nabla} r_\omega = \boldsymbol{\nabla} \cdot \{\mathbf{D}_\omega \cdot \boldsymbol{\nabla} r_\omega\} + \varepsilon_\omega^{-1} h \tag{3.7}$$

$$\mathbf{v}_\gamma \cdot \boldsymbol{\nabla} \mathbf{B}_\gamma = \boldsymbol{\nabla} \cdot \{\mathbf{D}_\gamma \cdot \boldsymbol{\nabla} \mathbf{B}_\gamma\} - \tilde{\mathbf{v}}_\gamma - \varepsilon_\gamma^{-1} \boldsymbol{\beta}^* \tag{3.8}$$

$$\begin{aligned}
&\text{B.C.1}: && -\mathbf{n}_{\gamma\sigma}\cdot(\mathsf{D}_\gamma\cdot\boldsymbol{\nabla}\mathbf{B}_\gamma)=\mathbf{n}_{\gamma\sigma}\cdot\mathsf{D}_\gamma && \text{on } \mathscr{S}_{\gamma\sigma} && (3.9a)\\
&\text{B.C.1}: && \mathbf{B}_\gamma=\mathbf{B}_\omega && \text{on } \mathscr{S}_{\gamma\omega} && (3.9b)\\
&\text{B.C.2}: && -\mathbf{n}_{\gamma\omega}\cdot\left(\mathbf{j}_{\mathbf{B}_\gamma}-\mathbf{j}_{\mathbf{B}_\omega}\right)=-\mathbf{n}_{\gamma\omega}\cdot(\mathbf{D}_\omega-\mathbf{D}_\gamma) && \text{on } \mathscr{S}_{\gamma\omega} && (3.9c)\\
&\text{B.C.4}: && -\mathbf{n}_{\omega\sigma}\cdot(\mathsf{D}_\omega\cdot\boldsymbol{\nabla}\mathbf{B}_\omega)=\mathbf{n}_{\omega\sigma}\cdot\mathsf{D}_\omega && \text{on } \mathscr{S}_{\omega\sigma} && (3.9d)\\
&\text{Periodicity}: && \mathbf{B}_i(\mathbf{x}+p_k)=\mathbf{B}_i(\mathbf{x}) && k=1,2,3 && (3.9e)\\
&\text{Unicity}: && \langle\mathbf{B}_i\rangle^i=0 && && (3.9f)
\end{aligned}$$

$$\mathbf{v}_\omega\cdot\boldsymbol{\nabla}\mathbf{B}_\omega=\boldsymbol{\nabla}\cdot\{\mathbf{D}_\omega\cdot\boldsymbol{\nabla}\mathbf{B}_\omega\}-\tilde{\mathbf{v}}_\omega+\varepsilon_\omega^{-1}\boldsymbol{\beta}^* \tag{3.10}$$

3.1.2 *One-equation special perturbation decomposition*

The dispersion tensor takes the form Eq (3.11)

$$\mathbf{D}^*=\sum_{i=\gamma,\omega}\varepsilon_i\left[\mathbf{D}_i\cdot\left(\mathbf{I}+\langle\boldsymbol{\nabla}\mathbf{b}_i\rangle^i\right)-\langle\mathbf{v}_i\mathbf{b}_i\rangle^i\right] \tag{3.11}$$

CLOSURE PROBLEM The determination of effective parameters requires the calculation of a single problem which can be found in [205] Eqs (53) to (55) (in which η is used instead of γ) and in [78].

$$\mathbf{v}_\gamma\cdot\boldsymbol{\nabla}\mathbf{b}_\gamma=\boldsymbol{\nabla}\cdot\{\mathbf{D}_\gamma\cdot\boldsymbol{\nabla}\mathbf{b}_\gamma\}-\tilde{\mathbf{v}}_\gamma-\varepsilon_\gamma^{-1}\mathbf{U}^* \tag{3.12}$$

$$\begin{aligned}
&\text{B.C.1}: && -\mathbf{n}_{\gamma\sigma}\cdot(\mathsf{D}_\gamma\cdot\boldsymbol{\nabla}\mathbf{b}_\gamma)=\mathbf{n}_{\gamma\sigma}\cdot\mathsf{D}_\gamma && \text{on } \mathscr{S}_{\gamma\sigma} && (3.13a)\\
&\text{B.C.1}: && \mathbf{b}_\gamma=\mathbf{b}_\omega && \text{on } \mathscr{S}_{\gamma\omega} && (3.13b)\\
&\text{B.C.2}: && -\mathbf{n}_{\gamma\omega}\cdot\left(\mathbf{j}_{\mathbf{b}_\gamma}-\mathbf{j}_{\mathbf{b}_\omega}\right)=-\mathbf{n}_{\gamma\omega}\cdot(\mathbf{D}_\omega-\mathbf{D}_\gamma) && \text{on } \mathscr{S}_{\gamma\omega} && (3.13c)\\
&\text{B.C.4}: && -\mathbf{n}_{\omega\sigma}\cdot(\mathsf{D}_\omega\cdot\boldsymbol{\nabla}\mathbf{b}_\omega)=\mathbf{n}_{\omega\sigma}\cdot\mathsf{D}_\omega && \text{on } \mathscr{S}_{\omega\sigma} && (3.13d)\\
&\text{Periodicity}: && \mathbf{b}_i(\mathbf{x}+p_k)=\mathbf{b}_i(\mathbf{x}) && k=1,2,3 && (3.13e)\\
&\text{Unicity}: && \langle\mathbf{b}_i\rangle^i=0 && && (3.13f)
\end{aligned}$$

$$\mathbf{v}_\omega\cdot\boldsymbol{\nabla}\mathbf{b}_\omega=\boldsymbol{\nabla}\cdot\{\mathbf{D}_\omega\cdot\boldsymbol{\nabla}\mathbf{b}_\omega\}-\tilde{\mathbf{v}}_\omega+\varepsilon_\omega^{-1}\mathbf{U}^* \tag{3.14}$$

3.2 MATHEMATICAL DEVELOPMENT

At this point, the mapping variables $r_\gamma, r_\omega, \mathbf{B}_\gamma, \mathbf{B}_\omega$ and $\mathbf{b}_\gamma, \mathbf{b}_\omega$ are solutions of different boundary value problems Eqs (3.5) to (3.7), Eqs (3.8) to (3.10) and Eqs (3.12) to (3.14). In order to find a relationship between these closure variables, we introduce the following source terms decomposition based on the superposition principle for linear operators

$$\mathbf{B}_i = \mathbf{B}_{Ii} + B_{IIi}\boldsymbol{\beta}^* \tag{3.15a}$$
$$\mathbf{b}_i = \mathbf{b}_{Ii} + b_{IIi}\mathbf{U}^* \tag{3.15b}$$
$$r_i = r_{IIi}\alpha^{**} \tag{3.15c}$$

As a consequence of the previous decomposition, Eqs (3.5) to (3.7), Eqs (3.8) to (3.10) and Eqs (3.12) to (3.14) reduce to only two boundary value problems. $\mathbf{B}_{Ii}$ and $\mathbf{b}_{Ii}$ are solutions of the following closure problem Type I

$$\mathbf{v}_\gamma \cdot \boldsymbol{\nabla}\boldsymbol{\Phi}_{I\gamma} = \boldsymbol{\nabla}\cdot\{\mathbf{D}_\gamma \cdot \boldsymbol{\nabla}\boldsymbol{\Phi}_{I\gamma}\} - \tilde{\mathbf{v}}_\gamma \tag{3.16}$$

$$\text{B.C.1}: \quad -\mathbf{n}_{\gamma\sigma}\cdot(\mathbf{D}_\gamma\cdot\boldsymbol{\nabla}\boldsymbol{\Phi}_{I\gamma}) = \mathbf{n}_{\gamma\sigma}\cdot\mathbf{D}_\gamma \quad \text{on } \mathscr{S}_{\gamma\sigma} \tag{3.17a}$$
$$\text{B.C.1}: \quad \boldsymbol{\Phi}_{I\gamma} = \boldsymbol{\Phi}_{I\omega} \quad \text{on } \mathscr{S}_{\gamma\omega} \tag{3.17b}$$
$$\text{B.C.2}: \quad -\mathbf{n}_{\gamma\omega}\cdot\left(\mathbf{j}_{\boldsymbol{\Phi}_{I\gamma}} - \mathbf{j}_{\boldsymbol{\Phi}_{I\omega}}\right) = -\mathbf{n}_{\gamma\omega}\cdot(\mathbf{D}_\omega - \mathbf{D}_\gamma) \quad \text{on } \mathscr{S}_{\gamma\omega} \tag{3.17c}$$
$$\text{B.C.4}: \quad -\mathbf{n}_{\omega\sigma}\cdot(\mathbf{D}_\omega\cdot\boldsymbol{\nabla}\boldsymbol{\Phi}_{I\omega}) = \mathbf{n}_{\omega\sigma}\cdot\mathbf{D}_\omega \quad \text{on } \mathscr{S}_{\omega\sigma} \tag{3.17d}$$
$$\text{Periodicity}: \quad \boldsymbol{\Phi}_{Ii}(\mathbf{x}+p_k) = \boldsymbol{\Phi}_{Ii}(\mathbf{x}) \quad k=1,2,3 \tag{3.17e}$$

$$\mathbf{v}_\omega \cdot \boldsymbol{\nabla}\boldsymbol{\Phi}_{I\omega} = \boldsymbol{\nabla}\cdot\{\mathbf{D}_\omega \cdot \boldsymbol{\nabla}\boldsymbol{\Phi}_{I\omega}\} - \tilde{\mathbf{v}}_\omega \tag{3.18}$$

Unicity of the solutions is provided by the following conditions

$$\varepsilon_\gamma \langle \mathbf{B}_{I\gamma}\rangle^\gamma + \varepsilon_\omega \langle \mathbf{B}_{I\omega}\rangle^\omega = \mathbf{0} \tag{3.19a}$$
$$\varepsilon_\gamma \langle \mathbf{b}_{I\gamma}\rangle^\gamma + \varepsilon_\omega \langle \mathbf{b}_{I\omega}\rangle^\omega = \mathbf{0} \tag{3.19b}$$

B_{IIi}, b_{IIi} and r_{IIi} are solutions of the following closure problem Type II

$$\mathbf{v}_\gamma \cdot \boldsymbol{\nabla}\Phi_{II\gamma} = \boldsymbol{\nabla}\cdot\{\mathbf{D}_\gamma \cdot \boldsymbol{\nabla}\Phi_{II\gamma}\} - \varepsilon_\gamma^{-1} \tag{3.20}$$

$$\begin{aligned}
\text{B.C.1}: \quad & -\mathbf{n}_{\gamma\sigma}\cdot(\mathbf{D}_\gamma\cdot\boldsymbol{\nabla}\Phi_{\text{II}\gamma})=0 && \text{on } \mathscr{S}_{\gamma\sigma} && (3.21a)\\
\text{B.C.1}: \quad & \Phi_{\text{II}\gamma}=\Phi_{\text{II}\omega} && \text{on } \mathscr{S}_{\gamma\omega} && (3.21b)\\
\text{B.C.2}: \quad & -\mathbf{n}_{\gamma\omega}\cdot\left(\mathbf{j}_{\Phi_{\text{II}\gamma}}-\mathbf{j}_{\Phi_{\text{II}\omega}}\right)=0 && \text{on } \mathscr{S}_{\gamma\omega} && (3.21c)\\
\text{B.C.4}: \quad & -\mathbf{n}_{\omega\sigma}\cdot(\mathbf{D}_\omega\cdot\boldsymbol{\nabla}\Phi_{\text{II}\omega})=0 && \text{on } \mathscr{S}_{\omega\sigma} && (3.21d)\\
\text{Periodicity}: \quad & \Phi_{\text{II}i}(\mathbf{x}+p_k)=\Phi_{\text{II}i}(\mathbf{x}) && k=1,2,3 && (3.21e)
\end{aligned}$$

$$\mathbf{v}_\omega\cdot\boldsymbol{\nabla}\Phi_{\text{II}\omega}=\boldsymbol{\nabla}\cdot\{\mathbf{D}_\omega\cdot\boldsymbol{\nabla}\Phi_{\text{II}\omega}\}+\varepsilon_\omega^{-1} \tag{3.22}$$

Unicity of the solutions is provided by the following conditions

$$\begin{aligned}
\varepsilon_\gamma\langle B_{\text{II}\gamma}\rangle^\gamma+\varepsilon_\omega\langle B_{\text{II}\omega}\rangle^\omega &= 0 && (3.23a)\\
\varepsilon_\gamma\langle b_{\text{II}\gamma}\rangle^\gamma+\varepsilon_\omega\langle b_{\text{II}\omega}\rangle^\omega &= 0 && (3.23b)\\
\langle r_{\text{II}\omega}\rangle^\omega=\frac{1}{h}\,;\ \langle r_{\text{II}\gamma}\rangle^\gamma &= 0 && (3.23c)
\end{aligned}$$

$\mathbf{b}_{Ii}$ and $\mathbf{B}_{Ii}$ are solutions of the same problem and satisfy the same unicity equation. Hence, we have

$$\mathbf{b}_{Ii}=\mathbf{B}_{Ii} \tag{3.24}$$

which implies

$$\mathbf{b}_i=\mathbf{B}_i-B_{\text{II}i}\boldsymbol{\beta}^*+b_{\text{II}i}\mathbf{U}^* \tag{3.25}$$

It is also important to notice that $b_{\text{II}i}$ and $B_{\text{II}i}$ are solution of the same problem Type II and satisfy the same unicity equations so that we have

$$\mathbf{b}_i=\mathbf{B}_i+b_{\text{II}i}(\mathbf{U}^*-\boldsymbol{\beta}^*) \tag{3.26}$$

Finally $b_{\text{II}i}$ and $r_{\text{II}i}$ are solution of the same problem but do not satisfy the same unicity equations so that they only differ by a constant. After some simple algebra, we obtain

$$\mathbf{b}_i=\mathbf{B}_i+\frac{1}{\alpha^{**}}\left(r_i-\frac{\varepsilon_\omega}{(\varepsilon_\gamma+\varepsilon_\omega)}\right)(\mathbf{U}^*-\boldsymbol{\beta}^*) \tag{3.27}$$

Table 5: Equivalence of the approximations associated to the volume averaging theory and to the moments matching technique.

Approximation of	Moments matching technique	Volume averaging theory
Convolutions in space	Spatial moments matching up to the second order	First order closure
Convolutions in time	Time-infinite behavior of the spatial moments	Quasi-stationarity of the closure problems

3.3 DISCUSSION

Injecting this expression of $\mathbf{b}_i$, i.e. Eq (3.27), in Eq (3.11) straightforwardly leads to

$$\mathbf{D}^* = \mathbf{D}^\infty \tag{3.28}$$

One may realize that the physics underlying the time-asymptotic hypothesis in one-phase or two-phase systems have very different backgrounds. In the single-phase configuration, the equality of the dispersion tensors between the volume averaging theory as devised in [274] and the moments matching technique as devised in [33] is straightforward. In this single-phase case, the problem is not homogenizable at very short times, that is, one needs to consider only long times to avoid the convolutions. This limitation corresponds to the time needed for a particle to visit the entire microscopic domain. In a dual-phase situation, this assumption of the single-phase case is reminiscent to the quasi-stationary hypothesis on the standard perturbations, although not exactly similar because of the contrast of properties and of the exchange between both phases. The time-asymptotic behavior of the two-equation model corresponds to a macroscopic relaxation of the two-equation boundary-value-problem, that is, a relaxation of the first two spatial moments or of the nonstandard perturbation. This represents a very different approximation.

The result expressed by Eq (3.28) provides a direct equivalence between the moments matching method and a special volume averaging theory based on a different decomposition technique. This conclusion has various consequences

- Two-equation models provide a solid basis for exploring physical aspects of the dispersion problem.
- Going back to the discussion about the choice of the proper mass transfer coefficient (see [151, 186]) the results obtained in this paper show that the other proposed values would lead to an incorrect asymptotic dispersion equation, even if they can work better at some limited stages of the transient evolution.

- We use the moments matching technique on an already homogenized set of equations, that is, we do not start at the microscopic scale as proposed in [33]. Although it has not been devised yet, we believe that the two-equation model can be obtained using the method in [33] and the equivalence developed in this article strongly reinforces the relationship between the volume averaging theory and the moments matching techniques.

- This equality Eq (3.28) also allows to see a similar problem from two different viewpoints Table 5. The long time limit is traduced, in the $\hat{c}$ decomposition, as a quasi-stationary closure problem and this is a new interesting way of seeing the time-asymptotic hypothesis in the multiphase configuration. Moreover, Eq (3.28) shows that a very strong relationship exists between the closure on $\hat{c}$ and the moments matching method limited to the second order, as applied in [295, 2].

4

NUMERICAL SIMULATIONS ON A SIMPLE EXAMPLE AND DOMAINS OF VALIDITY

In this part, we are interested in computing some of the previous models on a simple 2D geometry (Fig. 33) in order to catch the main characteristics of the problem and to delineate their domain of validity. In particular, we study the response of models local in times because (1) these are the most suited, because of their inherent simplicity, for experimental studies and (2) developing a computational method for the resolution of the complex integro-differential equations (with the convolutions) is beyond the scope of this thesis. We show that even for an input signal introducing many characteristic times, the time-asymptotic model may give a rather good approximation at short times and gains in precision as the time tends toward infinity.

The $\gamma-\mathrm{phase}$ is convective and diffusive whereas the $\omega-\mathrm{phase}$ is only diffusive (called Mobile-Immobile situation). One example of such a system could be the study of a tracer transport between two plates colonized by biofilms (aggregations of micro-organisms coated in protective extra-cellular substances). The closure problems Type I and Type II (Fig. 34) presented in the next section are solved using the Comsol^{TM} multiphysics package. Notice that because of the very particular geometry and because we impose periodic boundary conditions, the closure field is 1D. We also fully solve the balanced momentum equations so that we do not consider any upscaling

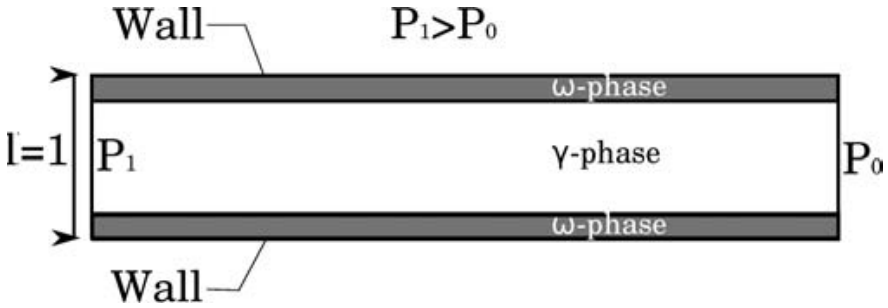

Figure 33: Schematic description of the 2D system

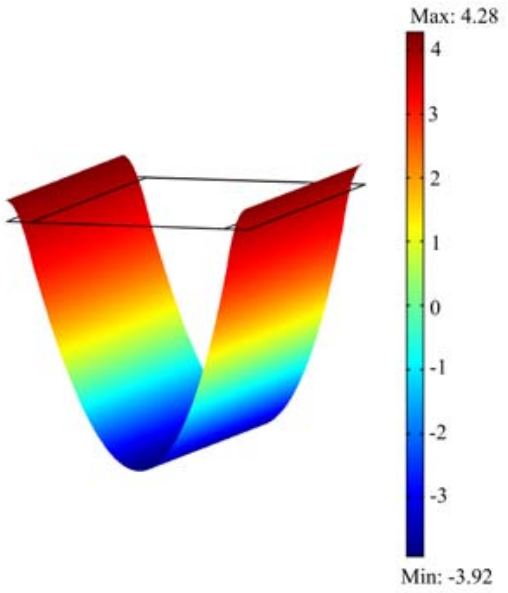

Figure 34: Norm of the b_i field for $\mathscr{P}e = 200$

of momentum equations. The closure problems only depends upon a Péclet number defined as

$$\mathscr{P}e = \frac{\langle v_\gamma \rangle^\gamma L}{D_\gamma} \tag{4.1}$$

where we choose

$$L = 1 \tag{4.2a}$$
$$\frac{D_\omega}{D\gamma} = 0.8 \tag{4.2b}$$
$$\varepsilon_\omega = 0.2 \tag{4.2c}$$

The dimensionless time is defined by

$$t' = \frac{\langle v_\gamma \rangle t}{L} \tag{4.3}$$

and the concentration is normalized to the amplitude of the input concentration.

On the one hand, we solve the entire 2D microscopic problem on a total length of 60L (called DNS for Direct Numerical Simulation) for a square input for different Péclet numbers. On the other hand, we solve the 1D upscaled local equilibrium, non-equilibrium and two-equation models on a total length of 60L (Fig. 35). Then, we observe breakthrough curves at 10L and 50L for Péclet numbers of 2, 20 and 200.

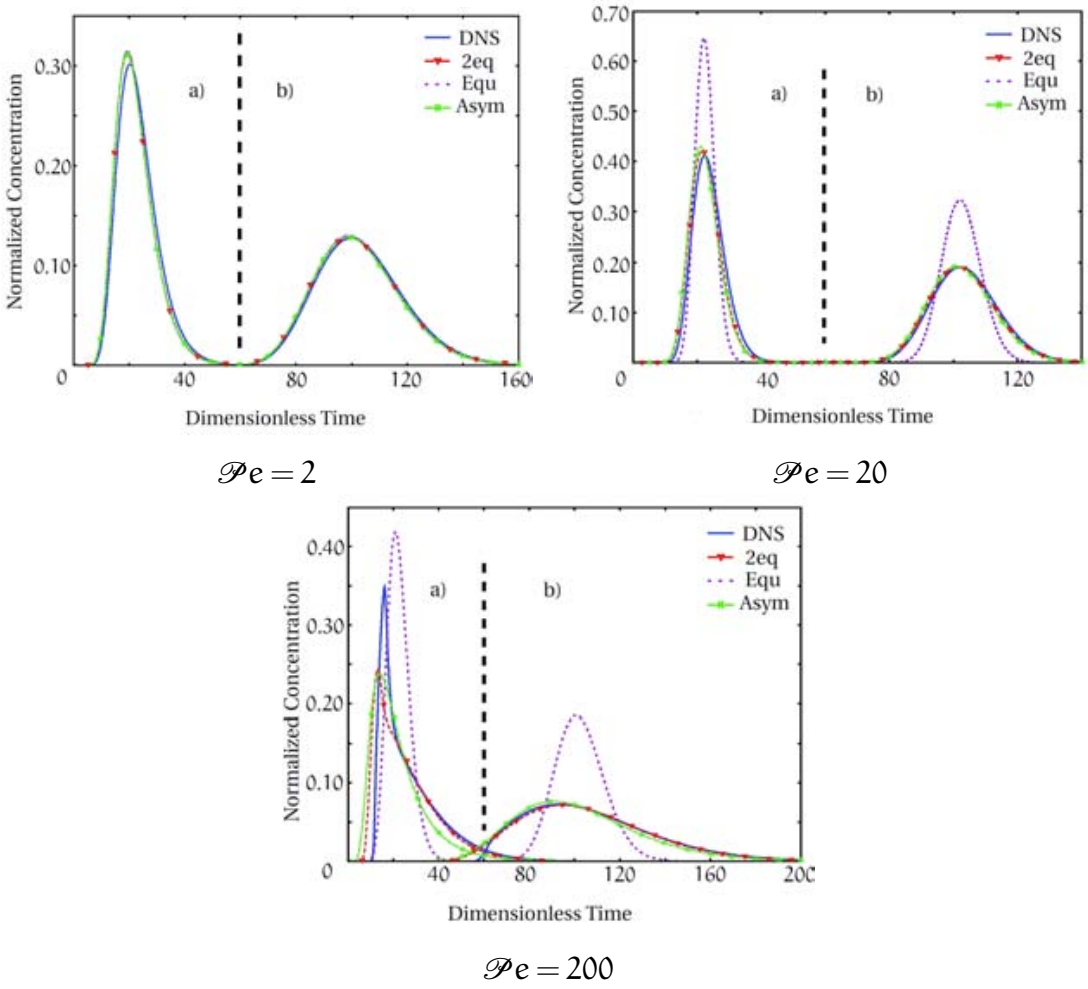

Figure 35: Breakthrough curves for various $\mathscr{P}e$ after a) 10L and b) 50L for a square input of width $\delta t' = 5$ starting at $t' = 0$. The solid line corresponds to the DNS, the dotted line to the local mass equilibrium model, the dashed line with triangles to the two-equation model and the dashed-dotted line with stars to the time-asymptotic model.

On Fig. 35, we see that the three homogenized models provide a very good approximation of the transport problem. At low Péclet, time and space non-locality tend to disappear because time and length scales are separated by several orders of magnitude. Meanwhile, some very little discrepancy still remains at the peak of the signal at 10L. At the very beginning of the system, the time-width of the signal propagating is of the same order of magnitude as the characteristic time for the relaxation of the effective parameters. When the signal spreads, the non-locality disappears and at 50L all the signals are in good agreement. The propagation is even slow enough for the local mass equilibrium assumption to be well-founded, that is, the exchange coefficient is big enough for the multiphase contrast term in the expression of the time-asymptotic dispersion Eq (3.1) to be insignificant.

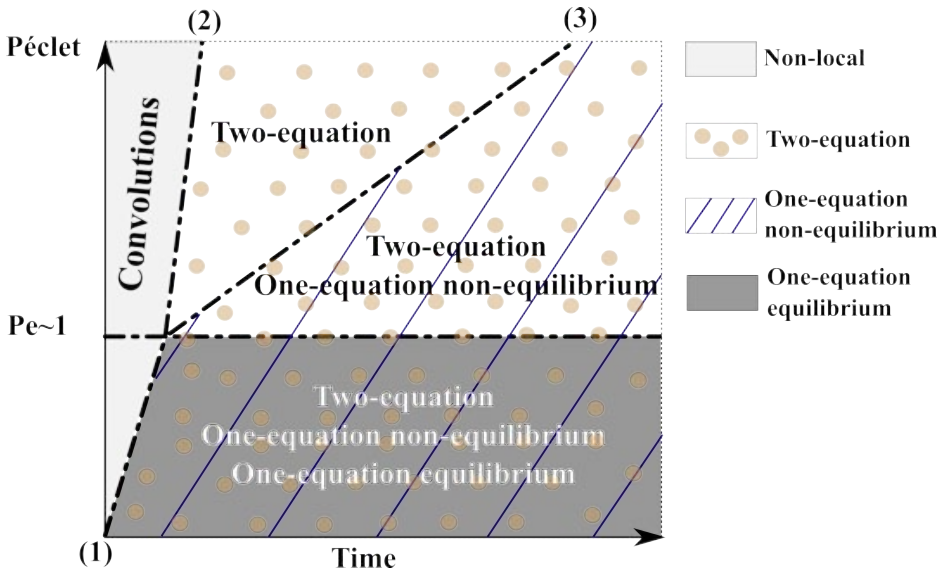

Figure 36: Domains of validity of the different models as a function of the Péclet number and of the time for a square input signal.

When the Péclet number reaches values around 20, the local mass equilibrium assumption starts to become inappropriate. Fig. 35 shows that the local mass equilibrium model gives a poor approximation of the signal whereas both non-equilibrium models are still in good agreement. The fact that the peaks for these two models arise earlier than the one of the DNS is again characteristic of non-locality. Memory functions or fully non-local theories (such as n-equations models) should be considered in this case.

For Péclet numbers around 200, Fig. 35, the local mass equilibrium model is completely inaccurate. The two-equation model provides the best approximation because it captures more characteristic times than the time-asymptotic one. Except for non-locality (especially at 10L), it recovers the shape of the signal. However, even for a square input signal and high Péclet numbers, the time-asymptotic model is still rather accurate. As the signal spreads, all the non-equilibrium models tend toward the correct solution and this means that domains of validity need a time dimension. Results suggest that the one-equation local non-equilibrium model might represent, in cases such as intermediate Péclet numbers, macroscopic stationarity or asymptotic regimes, a good compromise, in terms of computational demand, between the two-equation and the local mass equilibrium models. The importance of non-locality is also emphasized and becomes particularly obvious in the high Péclet number situation.

On the basis of these results, domains of validity can be determined for a square input signal identical in both phases Fig. 36. When the Péclet number is below or approximately unity, the local mass equilibrium condition is verified except at very short times where fully non-local theories or n-equation models should be considered.

Above unity, the situation is more complex as three different regimes are identified. At very short times, the situation can not be described even by the quasi-stationary two-equation model and non-local theories are necessary. At intermediate times, the two-equation model represents the only alternative to convolutions. As the time tends toward infinity and the signal spreads, the one-equation non-equilibrium model can be used to describe the mass transport. The boundaries between these different regimes depend, among others, on the input boundary condition, on the microscopic topology and on the processes. The constraints associated to the boundary (1) and (2), Fig. 36, between the non-local and local zone have been extensively discussed [1, 2, 48, 113, 43]. However, little is known on the limitations associated with (3), Fig. 36, and it requires further investigation.

Concerning the influence of the boundary conditions on the domains of validity, it is important to emphasize that two-equation models allow to modify separately the conditions for each phase unlike one-equation models. As a consequence, in situations where the boundary conditions in one phase are very different from the conditions in the other phase, two-equation models must be considered at the expense of one-equation models. Additionally, two-equation models are likely to provide a better approximation of the transport processes when many modes are excited, that is, for a Dirac input for example.

5

CONCLUSION

This part presents a comprehensive macrostransport theory in dual-phase and dual-region porous media. In particular, we show the following fundamental points

- The method of volume averaging represents an adapted framework for this purpose and allows to develop various deterministic models, capturing more or less information from the microscale processes, that can be used to describe the Darcy-scale transport with biofilms, or larger scale heterogeneities. The domains of validity are well defined on the basis of theoretical analyses (in particular spatial moments matching) and numerical simulations.

- The fundamental analysis carried out in section 3 leads to $\mathbf{D}^{\infty} = \mathbf{D}^{*}$. It has broad practical implications since these one-equation models, because of their intrinsic simplicity, are widely used by experimenters. In addition, these models were obtained using very distinct techniques, that is, moments matching for the time-asymptotic model and a closure on a peculiar perturbation for the model. From a theoretical point of view, equivalence between these two methods shows that (1) two-equation quasi-steady models provide a reliable basis for the study of the dispersion problem, (2) the idea of matching moments up to the second order is similar to the closure on the spatial perturbations and (3) the time-asymptotic limit of the moments corresponds to the quasi-stationarity of the perturbation problem.

- The numerical results obtained for a Mobile-Immobile problem with different Péclet numbers show that (1) the local mass equilibrium model has a restricted area of validity and must be used very carefully (see discussion in [73]), (2) the one-equation non-equilibrium model produces a reasonable approximation of the transport at long times, even for a square input signal and high Péclet numbers, (3) the two-equation model gives, in all cases, better results and (4) domains of validity representations need a time dimension.

Part IV

MODELING BIOLOGICALLY REACTIVE NON-EQUILIBRIUM MASS TRANSPORT IN POROUS MEDIA WITH BIOFILMS

1

INTRODUCTION

1.1 ABSTRACT

In this part, we develop a one-equation non-equilibrium model to describe the Darcy-scale transport of a solute undergoing biodegradation in porous media. Our approach is based on the development of a macrotransport theory reminiscent to the dual-phase situation studied in the previous part, but in a reactive case. Most of the mathematical models that describe the macroscale transport in such systems have been developed intuitively on the basis of simple conceptual schemes. There are two problems with such an heuristic analysis. First, it is unclear how much information these models are able to capture; that is, it is not clear what the model's domain of validity is. Second, there is no obvious connection between the macroscale effective parameters and the microscopic processes and parameters. As an alternative, a number of upscaling techniques have been developed to derive the appropriate macroscale equations that are used to describe mass transport and reactions in multiphase media. These approaches have been adapted to the problem of biodegradation in porous media with biofilms, but most of the work has focused on systems that are restricted to small concentration gradients at the microscale. This assumption, referred to as the *local mass equilibrium* approximation, generally has constraints that are overly restrictive. In this work, we devise a model that does not require the assumption of local mass equilibrium to be valid. In this approach, one instead requires only that, at sufficiently long times, anomalous behaviors of the third and higher spatial moments can be neglected; this, in turn, implies that the macroscopic model is well represented by a convection-dispersion-reaction type equation. This strategy is very much in the spirit of the developments for Taylor dispersion presented by Aris (1956). On the basis of our numerical results, we carefully describe the domain of validity of the model and show that the *time-asymptotic constraint* may be adhered to even for systems that are not at local mass equilibrium.

1.2 CONTEXT

Biodegradation in porous media has been the subject of extensive studies from the environmental engineering point of view [172, 220, 277, 278, 294]. Reactions are mediated by microorganisms (primarily bacteria, fungi, archaea, and protists, although others may be present) aggregated and coated within an extracellular polymeric matrix; together, these which form are generically called biofilms. There has been significant interest for their role in bioremedation of soils and subsurfaces [235, 227, 276, 97, 46, 29, 30] and, more recently, for their application to supercritical CO_2 storage [174, 64]. Numerous models for describing the transport of solutes, such as organic contaminants or injected nutrients, through geological formations as illustrated in Fig (37), have been developed. Reviews of these mathematical and physical representations of biofilms processes can be found in [79] and [181].

1.2.1 *One-equation local mass equilibrium model*

In many applications, the macroscopic balance laws for mass transport in such hierarchical porous media with biofilms have been elaborated by inspection. For example, the advection-dispersion-reaction type equation (1.1) is commonly considered to describe the Darcy-scale transport of a contaminant/nutrient represented by a concentration $\langle c_\gamma \rangle^\gamma$ in the water $\gamma - phase$. Brackets notations are here as a reminder that this concentration must be defined in some averaged sense.

$$\frac{\partial \langle c_\gamma \rangle^\gamma}{\partial t} + \langle \mathbf{v}_\gamma \rangle^\gamma \cdot \boldsymbol{\nabla} \langle c_\gamma \rangle^\gamma = \boldsymbol{\nabla} \cdot (\mathbf{D} \cdot \boldsymbol{\nabla} \langle c_\gamma \rangle^\gamma) + \mathscr{R}_\gamma \tag{1.1}$$

In this expression, $\langle \mathbf{v}_\gamma \rangle^\gamma$ is the groundwater velocity and $\mathbf{D}$ is a dispersion tensor. The reaction rate is usually assumed to have a Monod form $\mathscr{R}_\gamma = -\alpha \frac{\langle c_\gamma \rangle^\gamma}{\langle c_\gamma \rangle^\gamma + \mathscr{K}}$, where α and $\mathscr{K}$ are parameters (discussed in §2.5). It is common to assume that the solute transport can be uncoupled from the growth process [285, 198], that is, to consider that the characteristic times for these two processes are separated by several orders of magnitude. This Monod expression can be extended to include both electron acceptor and electron donor concentrations or simplified to a linear reaction rate in the limit $\langle c_\gamma \rangle^\gamma \ll \mathscr{K}$.

If one started using Eq (1.1) as an empirical representation of the mass transport and reaction process, it would not be immediately obvious how the microscale processes influence each of the macroscale parameters that appear in the balance. To understand how information is passed through the scales of observation, it is necessary to start by considering the microscale physics of the phenomena. At the pore-scale, biofilms in porous media are usually represented by convective-diffusive processes within the fluid $\gamma - phase$, and diffusive-reactive processes within the

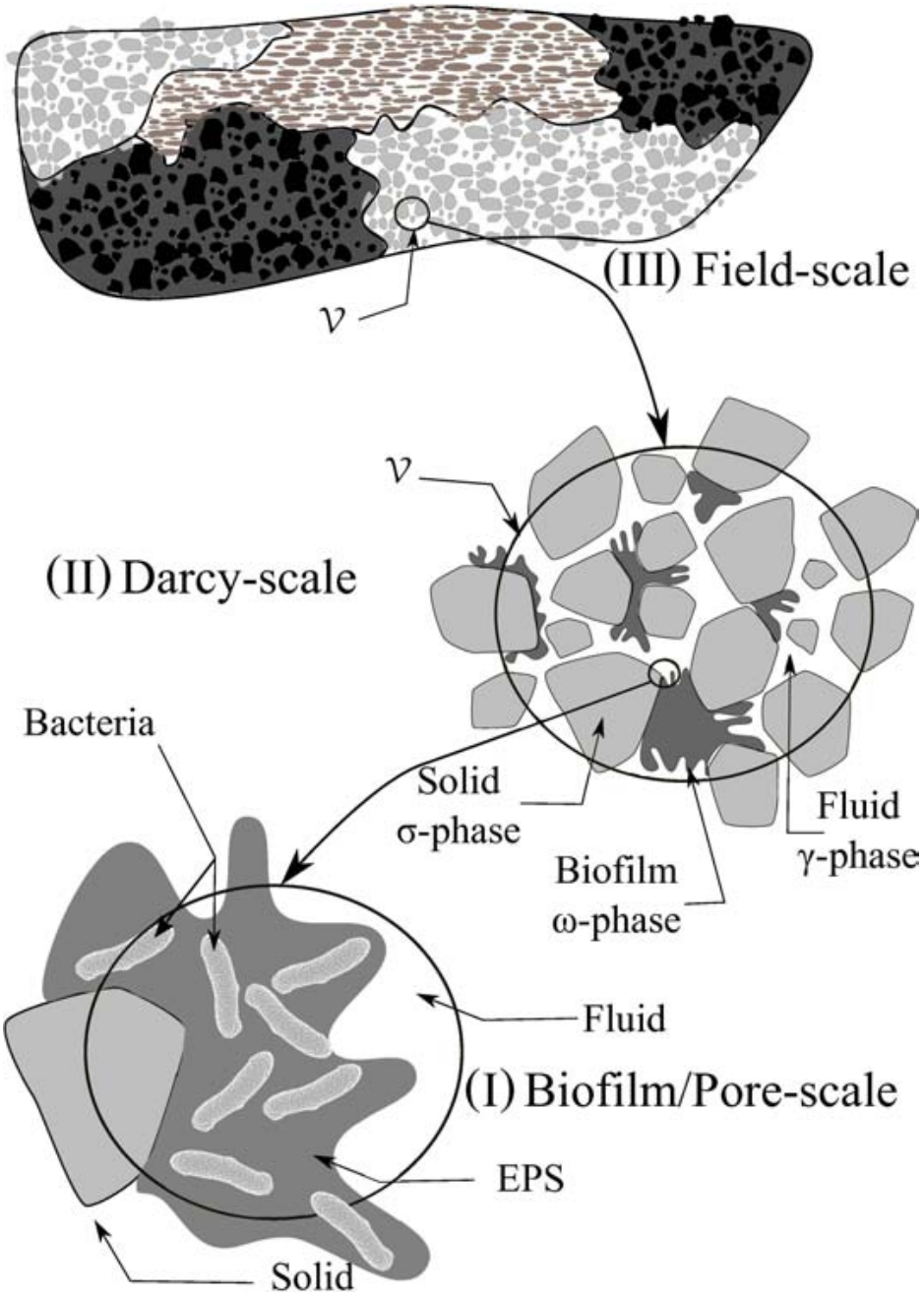

Figure 37: Hierarchy of the main scales

biofilm $\omega - phase$. This representation is built on three assumptions: 1) the biofilm is thick enough to be treated as a continuum [287, 285], 2) the rate of reaction of planktonic cells (suspended in the water-phase) can be neglected compared to biofilms species (fixed on a surface and embedded within extracellular polymeric substances), and 3) the microscale channels that sometimes form within the biofilms are treated as part of the continuous fluid-phase. The mass exchange process between the fluid and biofilm phases is described by a continuity of the flux and of the concentrations

at the interface, and a zero-flux condition is applied to the solid boundaries. Equation (1.1) represents a one-equation approximation of all these processes at the Darcy-scale, and such an approach is frequently used in the literature. Nevertheless, merely one physical situation, referred to as the local mass equilibrium, has been clearly identified to be properly described by only $\langle c_\gamma \rangle^\gamma$. In this case, the averaged concentrations in both phases are equal (strictly speaking, linked by a thermodynamical constant often close to unity). In other words, when the gradients of the pointwise concentrations within each phase can be neglected, the continuity at the interface between the biofilms and the water-phases can be extended to the bulk phases and the modelization can be undertaken using a one-equation model.

1.2.2 *Multiple-continua models*

Along with the identification of these limitations, some studies have worked out models that capture more physics of the reactive transport. The fluid-biofilm system has some obvious similarities to mobile-immobile configurations, and one might consider a multiple-continua description for biofilms in porous media under some circumstances. Several models have been developed with an explicit representation of the multiple-region aspects of the reactive transport. These include the *microcolony* [175] and *idealized biofilm* [65, 221, 219, 19] models in which the porous medium is decomposed into a solid impermeable grain, a diffusive-reactive biofilm, a diffusive boundary layer and an advective-diffusive bulk water-phase. This representation leads to two-equation models where each equation describes the behavior of the averaged concentration on one single phase, and there is exchange between phases sharing common boundaries. Such models are able to capture more complex dynamics than one-equation local mass equilibrium models. Unfortunately, there are still two difficulties with such an representations

PROBLEM 1 There is only an intuitive (rather than formal) relationship between the problem at the microscale and the one at the Darcy-scale. Hence, (1) it is still unclear when this model should be applied instead of the one-equation local mass equilibrium model for example, and (2) the dependence of the effective parameters (dispersion, effective velocities, mass exchange coefficients and effective reaction rate) on the microscale processes and geometry remains unknown.

PROBLEM 2 The system of differential equations that need to be solved is more complex, and, thus, is more difficult to use in applications.

As a solution to the *Problem 1*, one can find a more precise connection between the macroscopic model and the associated microscale boundary value problem through upscaling methods. The physics of non-reactive transport has been widely addressed by deterministic techniques such as homogenization, moments matching and volume averaging with closure. Such approaches have been adapted to the problem of reactive

transport with biofilms in porous media. These include the work of Wood et al. [284] and Golfier et al. [114] who used the volume averaging with closure theory [274] to compute effective parameters of the medium. However, except for two limit cases that have been studied by Orgogozo et al. [191], most of the work with volume averaging has focused on the local mass equilibrium assumption which is often excessively restrictive. To address the non-equilibrium situation in this two-phase configuration, one could consider two-equation models Eqs (1.2)

$$\varepsilon_\gamma \frac{\partial \langle c_\gamma \rangle^\gamma}{\partial t} + \mathbf{V}^{**}_{\gamma\gamma} \cdot \boldsymbol{\nabla} \langle c_\gamma \rangle^\gamma + \mathbf{V}^{**}_{\gamma\omega} \cdot \boldsymbol{\nabla} \langle c_\omega \rangle^\omega = \boldsymbol{\nabla} \cdot \left(\mathbf{D}^{**}_{\gamma\gamma} \cdot \boldsymbol{\nabla} \langle c_\gamma \rangle^\gamma \right) + \boldsymbol{\nabla} \cdot \left(\mathbf{D}^{**}_{\gamma\omega} \cdot \boldsymbol{\nabla} \langle c_\omega \rangle^\omega \right) - h^{**} \left(\langle c_\gamma \rangle^\gamma - \langle c_\omega \rangle^\omega \right) \tag{1.2a}$$

$$\varepsilon_\omega \frac{\partial \langle c_\omega \rangle^\omega}{\partial t} + \mathbf{V}^{**}_{\omega\gamma} \cdot \boldsymbol{\nabla} \langle c_\gamma \rangle^\gamma + \mathbf{V}^{**}_{\omega\omega} \cdot \boldsymbol{\nabla} \langle c_\omega \rangle^\omega = \boldsymbol{\nabla} \cdot \left(\mathbf{D}^{**}_{\omega\gamma} \cdot \boldsymbol{\nabla} \langle c_\gamma \rangle^\gamma \right) + \boldsymbol{\nabla} \cdot \left(\mathbf{D}^{**}_{\omega\omega} \cdot \boldsymbol{\nabla} \langle c_\omega \rangle^\omega \right) - h^{**} \left(\langle c_\omega \rangle^\omega - \langle c_\gamma \rangle^\gamma \right) + \mathscr{R}_\omega \tag{1.2b}$$

Here, $\langle c_i \rangle^i$ is the concentration of the solute in the $i-phase$. $\mathbf{V}^{**}_{ij}$ and $\mathbf{D}^{**}_{ij}$ (i and j are dummy indexes for γ, water-phase, or ω, biofilm-phase) are the macroscopic velocities and dispersion tensors of the two-equation model and h^{**} is the mass exchange coefficient. Eqs (1.2) can be seen as a general compact way to write dual continua models [58, 48, 47, 2, 115, 7, 81]. The previous denominations refer to the scale of application and the physical processes involved whereas the two-equation models definition refers to the mathematical structure of the problem. These have been extensively used in hydrology and chemical engineering to describe the non-reactive mass transport in matrix-fracture media [8], in two-region large-scale systems [83] as well as for the heat transfer [91] in two-phase/region porous media. However, the complexity of the problem is quite intimidating. Hence, the dilemma of reconciling *Problem 1* and *Problem 2* in a non-equilibrium situation appears fundamental.

1.2.3 *A one-equation, non-equilibrium model*

There has been some interesting work suggesting that it is possible to develop a one-equation model that applies to non-equilibrium conditions under some time-constraints. Cunningham and Mendoza-Sanchez in [65] compared the behaviors of the one-equation model Eq (1.1) ("the simple model") and the "idealized biofilm" model. They show that these are equivalent under steady state conditions and "effectively indistinguishable when the rate-controlling process is either external mass transfer or internal mass transfer" under transient conditions. From a more fundamental perspective, Zanotti and Carbonell showed in [295] that, for the non-reactive case, two-equation models have a time-asymptotic behavior which can be described in terms of a one-equation model. The demonstration is based on the moments matching principle at long times and does not assume local mass equilibrium. They considered the time-infinite behavior of the first two centered moments of a two-

equation model developed using the volume averaging with closure theory. The essential idea here is that the time-asymptotic behavior of a multidomain formulation can be undertaken using a one-equation model even in a non-equilibrium (i.e., where the concentrations in the two regions are not at equilibrium relative to one another) situation.

One could follow the approach of Zanotti and Carbonell to develop an upscaled theory for the reactive case, but their approach is not straightforward. For example, in the reactive case it is not possible to adopt a time-infinite limit of the zeroth order moment. This is primarily because the chemical species is consumed by the microorganisms and, consequently, its mass tends toward zero. One resolution is to determine only the long-time rate of consumption, by considering eigenvalue problems or Laplace transformations. However, this approach leads to a very complex two-step analysis.

The development of the one-equation time-asymptotic model in one-step would be a useful development. Dykaar and Kitanidis developed such a technique in [92] starting directly from the microscale boundary value problem and using a Taylor-Aris-Brenner moment analysis; in their analysis they computed the dispersion tensor, the effective reaction rate and the effective solute velocity. However, there are two areas in this previous work that could be improved; these are as follows

1. They considered a macroscopic average of the solute concentration only on the fluid-phase and, while the model does not assume local mass equilibrium, it is ambiguous as to what the specific model limitations are.

2. The moments matching technique in their analysis [92] makes the assumption that the behavior of the third and higher spatial moments can be neglected and that only the smallest eigenvalue of the spatial operator can be considered to describe the reaction rate. These hypothesis have different meanings in the single phase configuration and in the multiphase situation. In the work by Dykaar and Kitanidis, it is unclear how the phase configuration applies to the analysis.

In the non-reactive case, it has been proven [78] that the the two-step method proposed by Zanotti and Carbonell is strictly equivalent to a one-step technique based on a particular volume averaging theory presented in that work. The essential feature of that theory, presented in the previous part for a non-reactive situation, is the definition of a useful but unusual perturbation decomposition. This decomposition is usually undertaken using fluctuations, conventionally defined in applications to subsurface hydrology by Gray [118]. For that kind of description, the pointwise concentration is expressed as an intrinsic averaged on the phase plus a perturbation. In a $n-phase$ system, this decomposition leads to an n-equation macroscopic system and in our case would lead to the two-equation model previously discussed. Rather than using an intrinsic averaged on each phase, the perturbation concept can be

extended to a weighted volume averaging $\langle c\rangle^{\gamma\omega}$ of the pointwise concentration on all the different phases Eq (1.3), leading to a one-equation model. It is defined as

$$\langle c\rangle^{\gamma\omega} = \frac{\varepsilon_\gamma}{\varepsilon_\gamma+\varepsilon_\omega}\langle c_\gamma\rangle^{\gamma} + \frac{\varepsilon_\omega}{\varepsilon_\gamma+\varepsilon_\omega}\langle c_\omega\rangle^{\omega} \tag{1.3}$$

where ε_i is the volumic fraction occupied by the $i-phase$.

In this study, we use this variant of the technique of volume averaging with closure in the reactive case to develop a one-equation model. This model is different from those based on the local mass equilibrium assumption in that it does not impose specific conditions regarding the concentration in the two phases. Rather, it requires only that at long times the resulting balance equation is fully described by an advection-dispersion-reaction type equation, that is, by its first two spatial moments. This assumption means that the transport process is dispersive, and that the reactions do not themselves lead to spatial asymmetries for an initially symmetric solute distribution. This is very much in the spirit of the work by Dykaar and Kitanidis except that our model Eq (1.4) describes the total mass present in the system and, hence, exhibits different effective velocity $\mathbf{v}^*$, dispersion tensor $\mathbf{D}^*$ and reaction rate α^*. The constraints associated with the theoretical development are also extensively discussed.

$$\frac{\partial\langle c\rangle^{\gamma\omega}}{\partial t} + \mathbf{v}^*\cdot\boldsymbol{\nabla}\langle c\rangle^{\gamma\omega} = \boldsymbol{\nabla}\cdot(\mathbf{D}^*\cdot\boldsymbol{\nabla}\langle c\rangle^{\gamma\omega}) - \alpha^*\langle c\rangle^{\gamma\omega} \tag{1.4}$$

The remainder of the part is organized as follows. First, we derive the one-equation non-equilibrium reactive model. The microscopic equations describing the system at the pore scale are written and we use the volume averaging upscaling process; we define a unique fluctuation that is subsequently used to obtain a macroscopic (but unclosed) one-equation model. Then, we establish a link between the two scales through a closure problems. Finally, we show that a closed form of the macroscopic equation can be obtained where effective parameters depend explicitly upon closure variables solved over a representative cell. We explore numerically some solutions to the closure problem, and compare the non-equilibrium model to (1) the local equilibrium model and (2) pore-scale simulations.

2

UPSCALING

2.1 MICROSCOPIC EQUATIONS

Our study starts with the pore-scale description of the transport of a contaminant/nutrient in the porous medium. In the fluid (γ) phase, convective and diffusive transport are considered, and it is assumed that there is no reaction. In the biofilm (ω) phase, only diffusive transport and a reaction are considered. For the purposes of this paper, the velocity field is assumed to be known pointwise as a vector field. Mass balanced equations for the biofilm-fluid-solid system takes the following form

$$\gamma-\mathrm{phase}: \qquad \frac{\partial c_\gamma}{\partial t}+\nabla\cdot(c_\gamma \mathbf{v}_\gamma)=\nabla\cdot(\mathbf{D}_\gamma\cdot\nabla c_\gamma) \tag{2.1}$$

$$\begin{aligned}
&\text{BC1}: && -(\mathbf{n}_{\gamma\sigma}\cdot\mathbf{D}_\gamma)\cdot\nabla c_\gamma=0 && \text{on } \mathscr{S}_{\gamma\sigma} && (2.2a)\\
&\text{BC2}: && c_\omega=c_\gamma && \text{on } \mathscr{S}_{\gamma\omega} && (2.2b)\\
&\text{BC3}: && -(\mathbf{n}_{\gamma\omega}\cdot\mathbf{D}_\gamma)\cdot\nabla c_\gamma=-(\mathbf{n}_{\gamma\omega}\cdot\mathbf{D}_\omega)\cdot\nabla c_\omega && \text{on } \mathscr{S}_{\gamma\omega} && (2.2c)\\
&\text{BC4}: && -(\mathbf{n}_{\omega\sigma}\cdot\mathbf{D}_\omega)\cdot\nabla c_\omega=0 && \text{on } \mathscr{S}_{\omega\sigma} && (2.2d)
\end{aligned}$$

$$\omega-\mathrm{phase}: \qquad \frac{\partial c_\omega}{\partial t}=\nabla\cdot(\mathbf{D}_\omega\cdot\nabla c_\omega)+\mathscr{R}_\omega \tag{2.3}$$

Here, c_γ is the chemical species concentration in the $\gamma-\mathrm{phase}$, and c_ω is the concentration in the $\omega-\mathrm{phase}$ (which can be interpreted as the volume average concentration in the extracellular space [284, 287]). The symbols $\mathbf{D}_\gamma$ and $\mathbf{D}_\omega$ represent the diffusion tensors in the γ and ω-phases, respectively; $\mathscr{R}_\omega$ is the reaction rate in the ω-phase, the formulation of this term is detailed in section 2.5; $\mathbf{n}_{\gamma\omega}$ is the unit normal pointing from the γ-phase to the ω-phase; $\mathbf{n}_{\gamma\sigma}$ is the unit normal pointing from the γ-phase to the σ-phase; $\mathbf{n}_{\omega\sigma}$ is the unit normal pointing from the ω-phase to the σ-phase; $\mathscr{S}_{\gamma\omega}$ is the Euclidean space representing the interface between the γ-phase and the ω-phase; $\mathscr{S}_{\gamma\sigma}$ is the interface between the γ-phase and the σ-phase; and $\mathscr{S}_{\omega\sigma}$ is the interface between the ω-phase and the ω-phase.

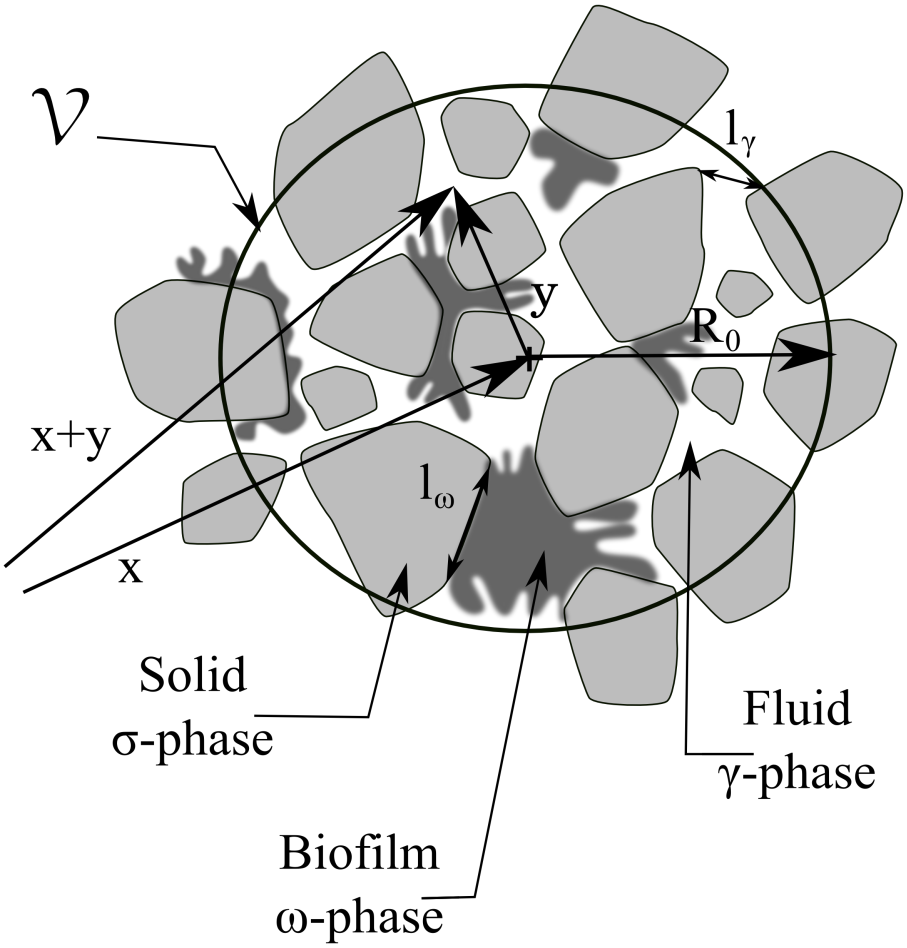

Figure 38: Pore-scale description of a Darcy-scale averaging volume

2.2 AVERAGES DEFINITIONS

To obtain a macroscopic equation for the mass transport at the Darcy-scale, we average each microscopic equation at the pore-scale over a representative region (REV), $\mathcal{V}$ Figs (37) and (38). $\mathcal{V}_\gamma$ and $\mathcal{V}_\omega$ are the Euclidean spaces representing the γ- and ω-phases in the REV. V_γ and V_ω are the Lebesgue measures of $\mathcal{V}_\gamma$ and $\mathcal{V}_\omega$, that is,

the volumes of the respective phases. The Darcy-scale *superficial* average of c_i (where i represents γ or ω) is defined the following way

$$\langle c_\gamma \rangle = \frac{1}{V} \int_{\mathcal{V}_\gamma(\mathbf{x},t)} c_\gamma \, dV, \ \langle c_\omega \rangle = \frac{1}{V} \int_{\mathcal{V}_\omega(\mathbf{x},t)} c_\omega \, dV \tag{2.4}$$

Then, we define *intrinsic* averaged quantities

$$\langle c_\gamma \rangle^\gamma = \frac{1}{V_\gamma(\mathbf{x},t)} \int_{\mathcal{V}_\gamma(\mathbf{x},t)} c_\gamma \, dV, \ \langle c_\omega \rangle^\omega = \frac{1}{V_\omega(\mathbf{x},t)} \int_{\mathcal{V}_\omega(\mathbf{x},t)} c_\omega \, dV \tag{2.5}$$

Volumes $V_\gamma(\mathbf{x},t)$ and $V_\omega(\mathbf{x},t)$ are related to the volume V by

$$\varepsilon_\gamma(\mathbf{x},t) = \frac{V_\gamma(\mathbf{x},t)}{V}, \ \varepsilon_\omega(\mathbf{x},t) = \frac{V_\omega(\mathbf{x},t)}{V} \tag{2.6}$$

Hence, we have

$$\langle c_\gamma \rangle = \varepsilon_\gamma(\mathbf{x},t) \langle c_\gamma \rangle^\gamma, \ \langle c_\omega \rangle = \varepsilon_\omega(\mathbf{x},t) \langle c_\omega \rangle^\omega \tag{2.7}$$

Due to the growth process, the geometry associated with the biofilm-phase can evolve in time. However, we will assume that changes in the V_γ and V_ω volumes are decoupled from the transport problem. There is substantial support for this approximation because the characteristic time for growth is much larger than the characteristic time for transport processes [285, 198]. Moreover, porosities ε_γ and ε_ω are also supposed constant in space so that we consider a homogeneous porous medium.

As stated above, the goal of this part is to devise a one-equation model that describes the evolution of the solute mass in the two phases by a single equation at the Darcy-scale. Toward that end, we define two additional macroscopic concentrations. The first is the spatial average concentration, defined by

$$\langle c \rangle = \varepsilon_\gamma \langle c_\gamma \rangle^\gamma + \varepsilon_\omega \langle c_\omega \rangle^\omega \tag{2.8}$$

The second is a volume-fraction weighted averaged concentration [285, 188]

$$\langle c \rangle^{\gamma\omega} = \frac{\varepsilon_\gamma}{\varepsilon_\gamma + \varepsilon_\omega} \langle c_\gamma \rangle^\gamma + \frac{\varepsilon_\omega}{\varepsilon_\gamma + \varepsilon_\omega} \langle c_\omega \rangle^\omega \tag{2.9}$$

During the averaging process, there arise terms involving the point values for c_γ, c_ω, and $\mathbf{v}_\gamma$. To treat these term conventionally, one defines perturbation decompositions as follows

$$c_\gamma = \langle c_\gamma \rangle^\gamma + \tilde{c}_\gamma \tag{2.10}$$

$$c_\omega = \langle c_\omega \rangle^\omega + \tilde{c}_\omega \tag{2.11}$$

$$\mathbf{v}_\gamma = \langle \mathbf{v}_\gamma \rangle^\gamma + \tilde{\mathbf{v}}_\gamma \tag{2.12}$$

With these conventional decompositions, the averaging process would lead to the formulation of a two-equation model, where a separate upscaled equation would be developed for each phase.

We will adopt a fundamentally different concentration decomposition which allows the development of a one-equation model that is different from the one-equation model that assumes local mass equilibrium. To do so, we define the weighted averaged concentration, $\langle c \rangle^{\gamma\omega}$ by the decompositions

$$c_\gamma = \langle c \rangle^{\gamma\omega} + \hat{c}_\gamma \tag{2.13a}$$
$$c_\omega = \langle c \rangle^{\gamma\omega} + \hat{c}_\omega \tag{2.13b}$$

Notice that with this definition, we do not generally have the condition that the intrinsic average of the deviation is zero, i.e., $\langle \tilde{c}_\gamma \rangle^\gamma, \langle \tilde{c}_\omega \rangle^\omega = 0$. However, we do have a generalization of this idea in the form

$$\varepsilon_\omega \langle \hat{c}_\omega \rangle^\omega + \varepsilon_\gamma \langle \hat{c}_\gamma \rangle^\gamma = 0 \tag{2.14}$$

2.3 AVERAGING EQUATIONS

To start, the averaging operators and decompositions defined above are applied to Eqs (2.1) and (2.3); the details of this process are provided in Appendix A. The result is

$\gamma - phase$

$$\begin{aligned} \tfrac{\partial \varepsilon_\gamma \langle c_\gamma \rangle^\gamma}{\partial t} \quad &+ \nabla \cdot (\varepsilon_\gamma \langle c_\gamma \rangle^\gamma \langle \mathbf{v}_\gamma \rangle^\gamma) = \nabla \cdot \left[\varepsilon_\gamma \mathbf{D}_\gamma \cdot \left(\nabla \langle c_\gamma \rangle^\gamma + \frac{1}{V_\gamma} \int_{\mathscr{S}_{\gamma\omega}} \mathbf{n}_{\gamma\omega} \tilde{c}_\gamma \, dS + \frac{1}{V_\gamma} \int_{\mathscr{S}_{\gamma\sigma}} \mathbf{n}_{\gamma\sigma} \tilde{c}_\gamma \, dS \right) \right] \\ &+ \frac{1}{V} \int_{\mathscr{S}_{\gamma\omega}} (\mathbf{n}_{\gamma\omega} \cdot \mathbf{D}_\gamma) \cdot \nabla c_\gamma \, dS + \frac{1}{V} \int_{\mathscr{S}_{\gamma\sigma}} (\mathbf{n}_{\gamma\sigma} \cdot \mathbf{D}_\gamma) \cdot \nabla c_\gamma \, dS - \nabla \cdot \langle \tilde{c}_\gamma \tilde{\mathbf{v}}_\gamma \rangle \end{aligned} \tag{2.15}$$

$\omega-phase$

$$\begin{aligned}\frac{\partial \varepsilon_\omega \langle c_\omega\rangle^\omega}{\partial t} &= \boldsymbol{\nabla}\cdot\left[\varepsilon_\omega \mathbf{D}_\omega\cdot\left(\boldsymbol{\nabla}\langle c_\omega\rangle^\omega + \frac{1}{V_\omega}\int_{\mathscr{S}_{\omega\gamma}} \mathbf{n}_{\omega\gamma}\tilde{c}_\omega\, dS + \frac{1}{V_\omega}\int_{\mathscr{S}_{\omega\sigma}} \mathbf{n}_{\omega\sigma}\tilde{c}_\omega\, dS\right)\right]\\ &+\frac{1}{V}\int_{\mathscr{S}_{\omega\gamma}} (\mathbf{n}_{\omega\gamma}\cdot\mathbf{D}_\omega)\cdot\boldsymbol{\nabla}c_\omega\, dS + \frac{1}{V}\int_{\mathscr{S}_{\omega\sigma}} (\mathbf{n}_{\omega\sigma}\cdot\mathbf{D}_\omega)\cdot\boldsymbol{\nabla}c_\omega\, dS\\ &+\varepsilon_\omega\langle\mathscr{R}_\omega\rangle^\omega \end{aligned} \tag{2.16}$$

2.4 THE MACROSCOPIC CONCENTRATION IN A MULTIPHASE SYSTEM

At this point, one clearly needs two macroscale equations to describe the system (one-equation for each phase) and it is unclear how the mass transport should be represented using a single macroscopic concentration. To understand this point, it is necessary to embrace a more general view of the problem. Experimentally, biofilms are often studied in laboratory devices such as columns. One may then ask the questions (1) "What concentration are we measuring at the output of a column colonized by biofilm ?" and (2) "How do we establish a relationship between this experimental measure and the concentration in our model ?".

Let us start with the question (1). The concentration measured at the output depends on the design of the column, the physical and chemical properties of the porous medium and of the flow as well as on the experimental device used for the measure. For example, let us assume that we are trying to obtain the elution curve of a tracer (concentration c_i in the $i-phase$) at the output of the column by sampling the water on relatively small time intervals ΔT (say, a hundred samples for one elution curve) and then measuring the concentration within each volume. For high microscopic Péclet numbers, one may measure a quantity close to $\langle c_\gamma\rangle^\gamma$ as the transport is driven by the convection in the water-phase. For microscopic Péclet numbers lower than unity, that is, a transport driven by diffusion, one may measure something closer to $\langle c\rangle^{\gamma\omega}$. In this context, a general definition of the concentration would be

$$\langle C\rangle = \int_0^t\int_{\mathscr{V}} G(\mathbf{x}-\mathbf{y}, t-\tau)c(\mathbf{y},\tau)\, dV(\mathbf{y})\, d\tau \tag{2.17}$$

where G is a spatio-temporal kernel corresponding to a weighting function accounting for the measurement device, the column device and the physics of the transport, and c is the concentration distribution defined by

$$c = \begin{pmatrix} c_\gamma & \text{in the } \gamma-phase\\ c_\omega & \text{in the } \omega-phase\\ 0 & \text{in the } \sigma-phase \end{pmatrix} \tag{2.18}$$

Then, it is necessary to address question (2), that is, we must find a relationship between $\langle C \rangle$ and the concentrations appearing in our models. There are two different ways to proceed. First, it is possible to formulate a generalized volume averaging theory to directly describe the transport of $\langle C \rangle$. This has been proposed in [208]. Second, it is feasible to describe the transport of a relatively simple averaged concentration and to apply the correct kernel *a posteriori*. In this case, the concentration to be used in the model can be chosen on the basis of its relevance from a theoretical point of view.

In this part, we use $\langle c \rangle^{\gamma\omega}$ as a macroscopic concentration, that is, we are interested in following the spatio-temporal macroscopic evolution of the total component mass in the porous medium. One significant advantage of this definition is that, in a non-reactive medium, the concentration $\langle c \rangle^{\gamma\omega}$ is conservative; unlike the individual phase averages, which are not conservative due to interphase mass transfer. For example, $\langle c_\gamma \rangle^\gamma$ is often used as a macroscopic concentration but looses many features of the transport processes. Then, to go back to $\langle C \rangle$, one needs to determine the kernel F defined by

$$\langle C \rangle = \int_0^t \int_{\mathcal{V}} F(\mathbf{x}-\mathbf{y}, t-\tau) \langle c \rangle^{\gamma\omega}(\mathbf{y}, \tau) \, dV(\mathbf{y}) \, d\tau \tag{2.19}$$

The precise determination of the kernel G or F represents an extremely difficult task so that, in real problems, one can usually only approximately apprehend the correct concentration to use for a specific problem. Such descriptions are inevitable but one must keep in mind that these are approximations.

Going back to the macroscopic equations (2.15) and (2.16), it is then necessary to make all intrinsic concentrations $\langle c_i \rangle^i$ disappear. This kind of description can be developed using the nonconventional decompositions defined by $\langle c \rangle^{\gamma\omega}$ [205] which naturally arises when summing Eqs (2.15) and (2.16). We have applied this kind of analysis to the two macroscale equations developed above; the detailed derivation can be found in Appendix B. The following non-closed equation results from this analysis

$$\begin{aligned} \frac{\partial \langle c \rangle^{\gamma\omega}}{\partial t} + \boldsymbol{\nabla} \cdot \left(\frac{\varepsilon_\gamma}{\varepsilon_\gamma + \varepsilon_\omega} \langle c \rangle^{\gamma\omega} \langle \mathbf{v}_\gamma \rangle^\gamma \right) = \; & \boldsymbol{\nabla} \cdot \left\{ \left(\frac{\varepsilon_\omega}{\varepsilon_\gamma + \varepsilon_\omega} \mathbf{D}_\omega + \frac{\varepsilon_\gamma}{\varepsilon_\gamma + \varepsilon_\omega} \mathbf{D}_\gamma \right) \cdot \boldsymbol{\nabla} \langle c \rangle^{\gamma\omega} \right\} \\ & + \boldsymbol{\nabla} \cdot \left(\frac{\varepsilon_\omega}{\varepsilon_\gamma + \varepsilon_\omega} \mathbf{D}_\omega \cdot \langle \boldsymbol{\nabla} \hat{c}_\omega \rangle^\omega + \frac{\varepsilon_\gamma}{\varepsilon_\gamma + \varepsilon_\omega} \mathbf{D}_\gamma \cdot \langle \boldsymbol{\nabla} \hat{c}_\gamma \rangle^\gamma \right) \\ & + \frac{\varepsilon_\omega}{\varepsilon_\gamma + \varepsilon_\omega} \langle \mathscr{R}_\omega \rangle^\omega - \frac{1}{\varepsilon_\gamma + \varepsilon_\omega} \boldsymbol{\nabla} \cdot \langle \hat{c}_\gamma \mathbf{v}_\gamma \rangle \end{aligned} \tag{2.20}$$

2.5 REACTION TERM

The form of the reaction rate has not yet been detailed but, at this point, it is important to make further progress. The classical dual-Monod [170] reaction rate for electron donor A and acceptor B, is widely adopted to describe biofilm substrate uptake and growth in systems with a single substrate and a single terminal electron acceptor. In this case, the reaction rate is given by a hyperbolic kinetic expression of the form

$$\mathscr{R}_\omega = -\alpha \frac{c_{A\omega}}{c_{A\omega}+\mathscr{K}_A}\frac{c_{B\omega}}{c_{B\omega}+\mathscr{K}_B} \tag{2.21}$$

Here, the α is the substrate uptake rate parameter (often expanded as $\alpha = k\langle\rho_b\rangle$, where k is the specific substrate uptake rate parameter, and $\langle\rho_b\rangle$ is the microbial concentration; cf. [286]). One often consider the case where the electron acceptor is not limiting $c_{B\omega} \ \mathscr{K}_B$, in which case the kinetics take the classical Monod form

$$\mathscr{R}_\omega = -\alpha \frac{c_{A\omega}}{c_{A\omega}+\mathscr{K}_A} \tag{2.22}$$

which can be written

$$\mathscr{R}_\omega = -\alpha \frac{c_\omega}{c_\omega+\mathscr{K}} \tag{2.23}$$

This is beyond the scope of this paper to propose a technique to upscale such non-linear kinetics and we will only consider the linear case.

$$\mathscr{R}_\omega = -\frac{\alpha}{\mathscr{K}} c_\omega \tag{2.24}$$

These linear kinetics can be seen as a particular case of the classical Monod for which $c_\omega \ll \mathscr{K}$, that is, a highly reactive biofilm or relatively low concentrations. This approximation has been undertaken incalculable times [244, 41, 36] and is discussed in [65, 92].

2.6 NON-CLOSED MACROSCOPIC FORMULATION

Introducing linear kinetics in Eq (2.20) leads to

$$\begin{aligned}
\frac{\partial\langle c\rangle^{\gamma\omega}}{\partial t} + \boldsymbol{\nabla}\cdot\left(\frac{\varepsilon_\gamma}{\varepsilon_\gamma+\varepsilon_\omega}\langle c\rangle^{\gamma\omega}\langle \mathbf{v}_\gamma\rangle^{\gamma}\right) = \quad & \boldsymbol{\nabla} \cdot\{\left(\frac{\varepsilon_\omega}{\varepsilon_\gamma+\varepsilon_\omega}\mathbf{D}_\omega + \frac{\varepsilon_\gamma}{\varepsilon_\gamma+\varepsilon_\omega}\mathbf{D}_\gamma\right)\cdot\boldsymbol{\nabla}\langle c\rangle^{\gamma\omega}\} \\
+ \quad & \boldsymbol{\nabla}\cdot\left(\frac{\varepsilon_\omega}{\varepsilon_\gamma+\varepsilon_\omega}\mathbf{D}_\omega\cdot\langle\boldsymbol{\nabla}\hat{c}_\omega\rangle^{\omega} + \frac{\varepsilon_\gamma}{\varepsilon_\gamma+\varepsilon_\omega}\mathbf{D}_\gamma\cdot\langle\boldsymbol{\nabla}\hat{c}_\gamma\rangle^{\gamma}\right) \\
- \quad & \frac{1}{\varepsilon_\gamma+\varepsilon_\omega}\boldsymbol{\nabla}\cdot\langle\hat{c}_\gamma\tilde{\mathbf{v}}_\gamma\rangle - \frac{1}{\varepsilon_\gamma+\varepsilon_\omega}\boldsymbol{\nabla}\cdot(\langle\hat{c}_\gamma\rangle\langle\mathbf{v}_\gamma\rangle^{\gamma}) \\
- \quad & \frac{\varepsilon_\omega}{\varepsilon_\gamma+\varepsilon_\omega}\frac{\alpha}{\mathscr{K}}(\langle c\rangle^{\gamma\omega} + \langle\hat{c}_\omega\rangle^{\omega})
\end{aligned} \tag{2.25}$$

Although Eq (2.25) represents a macroscale mass transport equation, it is not yet under a conventional form because deviation concentrations still remain. Eliminating these deviation concentrations, and hence uncoupling the physics at the microscale from the physics at the macroscale, is referred to as the closure problem.

3

CLOSURE

3.1 DEVIATION EQUATIONS

To close Eq (2.25), we first need to develop balance equations for the concentration deviations, $\hat{c}_\gamma$ and $\hat{c}_\omega$. Going back to their definitions Eqs (2.13) suggests that these equations can be obtained by subtracting the averaged equation Eq (2.20) to the microscopic mass balanced equations Eqs (2.1) and (2.3). To make further progress, it is necessary to make some simplifications. We will assume that all the terms containing only second order derivatives of surface integrated or volume averaged quantities are negligible compared to spatial derivatives of fluctuation quantities over the REV. As an aside, terms containing derivatives of averaged quantities are often referred to as non-local terms. This means that these can not be calculated locally on a REV; rather, they act as source terms and, if they can not be neglected, that is, if the hypothesis of separation of length scales is not valid, they impose a coupling between the microscale and the macroscale problems.

Eq (2.1) minus Eq (2.20)

$$\begin{aligned}\frac{\partial \hat{c}_\gamma}{\partial t} + \boldsymbol{\nabla}\cdot(\mathbf{v}_\gamma \hat{c}_\gamma) =& \boldsymbol{\nabla}\cdot(\mathbf{D}_\gamma\cdot\boldsymbol{\nabla}\hat{c}_\gamma) - \boldsymbol{\nabla}\cdot(\tilde{\mathbf{v}}_\gamma\langle c\rangle^{\gamma\omega}) - \frac{\varepsilon_\omega}{\varepsilon_\omega+\varepsilon_\gamma}\boldsymbol{\nabla}\cdot(\langle\mathbf{v}_\gamma\rangle^\gamma\langle c\rangle^{\gamma\omega}) \\ &- \boldsymbol{\nabla}\cdot\left(\frac{\varepsilon_\omega}{\varepsilon_\gamma+\varepsilon_\omega}\mathbf{D}_\omega\cdot\langle\boldsymbol{\nabla}\hat{c}_\omega\rangle^\omega + \frac{\varepsilon_\gamma}{\varepsilon_\gamma+\varepsilon_\omega}\mathbf{D}_\gamma\cdot\langle\boldsymbol{\nabla}\hat{c}_\gamma\rangle^\gamma\right) \\ &+ \frac{\alpha}{\mathcal{K}}\frac{\varepsilon_\omega}{\varepsilon_\omega+\varepsilon_\gamma}(\langle c\rangle^{\gamma\omega} + \langle\hat{c}_\omega\rangle^\omega) + \frac{1}{\varepsilon_\gamma+\varepsilon_\omega}\boldsymbol{\nabla}\cdot\langle\hat{c}_\gamma\mathbf{v}_\gamma\rangle \end{aligned} \tag{3.1}$$

Eq (2.3) minus Eq (2.20)

$$\begin{aligned}\frac{\partial \hat{c}_\omega}{\partial t} =& \boldsymbol{\nabla}\cdot(\mathbf{D}_\omega\cdot\boldsymbol{\nabla}\hat{c}_\omega) + \frac{\varepsilon_\gamma}{\varepsilon_\gamma+\varepsilon_\omega}\boldsymbol{\nabla}\cdot(\langle\mathbf{v}_\gamma\rangle^\gamma\langle c\rangle^{\gamma\omega}) \\ &- \boldsymbol{\nabla}\cdot\left(\frac{\varepsilon_\omega}{\varepsilon_\gamma+\varepsilon_\omega}\mathbf{D}_\omega\cdot\langle\boldsymbol{\nabla}\hat{c}_\omega\rangle^\omega + \frac{\varepsilon_\gamma}{\varepsilon_\gamma+\varepsilon_\omega}\mathbf{D}_\gamma\cdot\langle\boldsymbol{\nabla}\hat{c}_\gamma\rangle^\gamma\right) \\ &- \frac{\alpha}{\mathcal{K}}\frac{\varepsilon_\gamma}{\varepsilon_\omega+\varepsilon_\gamma}\langle c\rangle^{\gamma\omega} + \frac{\alpha}{\mathcal{K}}\frac{\varepsilon_\omega}{\varepsilon_\omega+\varepsilon_\gamma}\langle\hat{c}_\omega\rangle^\omega - \frac{\alpha}{\mathcal{K}}\hat{c}_\omega + \frac{1}{\varepsilon_\gamma+\varepsilon_\omega}\boldsymbol{\nabla}\cdot\langle\hat{c}_\gamma\mathbf{v}_\gamma\rangle \end{aligned} \tag{3.2}$$

We will impose the condition that we are interested in primarily the asymptotic behavior of the system; thus, we can adopt a quasi-steady hypothesis. In essence, this constraint indicates that there is a separation of time scales for the relaxation of $\hat{c}_\gamma$ and $\hat{c}_\omega$ as compared to the time scale for changes in the average concentration, $\langle c \rangle^{\gamma\omega}$. Such constraints can be put in the form

$$\begin{aligned} T^*_\gamma &\gg \frac{l^2_\gamma}{\|\mathbf{D}_\gamma\|}, \frac{l_\gamma}{\langle v_\gamma \rangle^\gamma} \\ T^*_\omega &\gg \frac{l^2_\omega}{\|\mathbf{D}_\omega\|}, \frac{\mathcal{K}}{\alpha} \end{aligned} \tag{3.3}$$

where T^*_γ (respectively T^*_ω) is a characteristic time associated to $\frac{\partial \hat{c}_\gamma}{\partial t}$ (respectively $\frac{\partial \hat{c}_\omega}{\partial t}$); $\|.\|$ is the tensorial norm given by

$$\|\mathbf{T}\| = \tfrac{1}{2}\sqrt{\mathbf{T} : \mathbf{T}} = \tfrac{1}{2}\sqrt{T_{ij}T_{ji}} \tag{3.4}$$

The vector norm is given by

$$\langle v_\gamma \rangle^\gamma = (\langle \mathbf{v}_\gamma \rangle^\gamma \cdot \langle \mathbf{v}_\gamma \rangle^\gamma)^{\frac{1}{2}} \tag{3.5}$$

This hypothesis is the key to understanding the time-asymptotic behavior of the model developed herein. It has been shown in [78, 205], in the non-reactive case, that this quasi-stationarity assumption is equivalent to time-asymptotic models derived through moments analysis [295] from two-equation models. In other words, the assumption of quasi-stationarity on the $\hat{c}$ perturbations is much more restrictive than the one on $\tilde{c}$ which leads to the two-equation model. One other way of seeing it is to express $\hat{c}$ as

$$\hat{c}_i = \langle \hat{c}_i \rangle^i + \tilde{c}_i \tag{3.6}$$

so that

$$\frac{\partial \hat{c}_i}{\partial t} = \frac{\partial \langle \hat{c}_i \rangle^i}{\partial t} + \frac{\partial \tilde{c}_i}{\partial t} \tag{3.7}$$

Hence, imposing constraints on $\frac{\partial \hat{c}_i}{\partial t}$ results in constraints on $\frac{\partial \tilde{c}_i}{\partial t}$ but also on $\frac{\partial \langle \hat{c}_i \rangle^i}{\partial t}$; in opposition to constraints only on $\frac{\partial \tilde{c}_i}{\partial t}$ in the two-equation models. With these approximations, the closure problems can be rewritten as follows

$$\begin{aligned}\boldsymbol{\nabla}\cdot(\mathbf{v}_\gamma\hat{c}_\gamma) = \quad & \boldsymbol{\nabla} \cdot(\mathbf{D}_\gamma\cdot\boldsymbol{\nabla}\hat{c}_\gamma) - \boldsymbol{\nabla}\cdot(\tilde{\mathbf{v}}_,\langle c\rangle^{\gamma\omega}) - \frac{\varepsilon_\omega}{\varepsilon_\omega+\varepsilon_\gamma}\boldsymbol{\nabla}\cdot(\langle\mathbf{v}_\gamma\rangle^\gamma\langle c\rangle^{\gamma\omega}) \\ & - \boldsymbol{\nabla}\cdot\left(\frac{\varepsilon_\omega}{\varepsilon_\gamma+\varepsilon_\omega}\mathbf{D}_\omega\cdot\langle\boldsymbol{\nabla}\hat{c}_\omega\rangle^\omega + \frac{\varepsilon_\gamma}{\varepsilon_\gamma+\varepsilon_\omega}\mathbf{D}_\gamma\cdot\langle\boldsymbol{\nabla}\hat{c}_\gamma\rangle^\gamma\right) \\ & + \frac{\varepsilon_\gamma}{\varepsilon_\gamma+\varepsilon_\omega}(\boldsymbol{\nabla}\cdot\langle\hat{c}_\gamma\tilde{\mathbf{v}}_\gamma\rangle^\gamma + \langle\mathbf{v}_\gamma\rangle^\gamma\boldsymbol{\nabla}\langle\hat{c}_\gamma\rangle^\gamma) \\ & + \frac{\alpha}{\mathcal{K}}\frac{\varepsilon_\omega}{\varepsilon_\omega+\varepsilon_\gamma}(\langle c\rangle^{\gamma\omega} + \langle\hat{c}_\omega\rangle^\omega) \end{aligned} \tag{3.8}$$

$$\text{BC1}: \quad -(\mathbf{n}_{\gamma\sigma}\cdot\mathbf{D}_\gamma)\cdot\boldsymbol{\nabla}\hat{c}_\gamma = (\mathbf{n}_{\gamma\sigma}\cdot\mathbf{D}_\gamma)\cdot\boldsymbol{\nabla}\langle c\rangle^{\gamma\omega}\text{ on }\mathscr{S}_{\gamma\sigma} \tag{3.9a}$$

$$\text{BC2}: \quad \hat{c}_\omega = \hat{c}_\gamma\text{ on }\mathscr{S}_{\gamma\omega} \tag{3.9b}$$

$$\text{BC3}: \quad -(\mathbf{n}_{\gamma\omega}\cdot\mathbf{D}_\gamma)\cdot\boldsymbol{\nabla}\hat{c}_\gamma = -(\mathbf{n}_{\gamma\omega}\cdot\mathbf{D}_\omega)\cdot\boldsymbol{\nabla}\hat{c}_\omega - \{\mathbf{n}_{\gamma\omega}\cdot(\mathbf{D}_\omega-\mathbf{D}_\gamma)\}\cdot\boldsymbol{\nabla}\langle c\rangle^{\gamma\omega}\text{ on }\mathscr{S}_{\gamma\omega} \tag{3.9c}$$

$$\text{BC4}: \quad -(\mathbf{n}_{\omega\sigma}\cdot\mathbf{D}_\omega)\cdot\boldsymbol{\nabla}\hat{c}_\omega = (\mathbf{n}_{\omega\sigma}\cdot\mathbf{D}_\omega)\cdot\boldsymbol{\nabla}\langle c\rangle^{\gamma\omega}\text{ on }\mathscr{S}_{\omega\sigma} \tag{3.9d}$$

$$\begin{aligned} 0 = \quad & \boldsymbol{\nabla} \cdot(\mathbf{D}_\omega\cdot\boldsymbol{\nabla}\hat{c}_\omega) + \frac{\varepsilon_\gamma}{\varepsilon_\gamma+\varepsilon_\omega}\boldsymbol{\nabla}\cdot(\langle\mathbf{v}_\gamma\rangle^\gamma\langle c\rangle^{\gamma\omega}) \\ & - \boldsymbol{\nabla}\cdot\left(\frac{\varepsilon_\omega}{\varepsilon_\gamma+\varepsilon_\omega}\mathbf{D}_\omega\cdot\langle\boldsymbol{\nabla}\hat{c}_\omega\rangle^\omega + \frac{\varepsilon_\gamma}{\varepsilon_\gamma+\varepsilon_\omega}\mathbf{D}_\gamma\cdot\langle\boldsymbol{\nabla}\hat{c}_\gamma\rangle^\gamma\right) \\ & + \frac{\varepsilon_\gamma}{\varepsilon_\gamma+\varepsilon_\omega}(\boldsymbol{\nabla}\cdot\langle\hat{c}_\gamma\tilde{\mathbf{v}}_,\rangle^\gamma + \langle\mathbf{v}_\gamma\rangle^\gamma\boldsymbol{\nabla}\langle\hat{c}_\gamma\rangle^\gamma) \\ & - \frac{\alpha}{\mathcal{K}}\frac{\varepsilon_\gamma}{\varepsilon_\omega+\varepsilon_\gamma}\langle c\rangle^{\gamma\omega} + \frac{\alpha}{\mathcal{K}}\frac{\varepsilon_\omega}{\varepsilon_\omega+\varepsilon_\gamma}\langle\hat{c}_\omega\rangle^\omega - \frac{\alpha}{\mathcal{K}}\hat{c}_\omega \end{aligned} \tag{3.10}$$

3.2 REPRESENTATION OF THE CLOSURE SOLUTION

The mathematical structure of this problem indicates that there are a number of nonhomogeneous quantities involving $\langle c\rangle^{\gamma\omega}$ that act as forcing terms. Under the conditions that a *local* macroscopic equation is desired, it can be shown (c.f., [282]) that the general solution to this problem takes the form

$$\hat{c}_\gamma = \mathbf{b}_\gamma\cdot\boldsymbol{\nabla}\langle c\rangle^{\gamma\omega} - s_\gamma\langle c\rangle^{\gamma\omega} \tag{3.11}$$

$$\hat{c}_\omega = \mathbf{b}_\omega\cdot\boldsymbol{\nabla}\langle c\rangle^{\gamma\omega} - s_\omega\langle c\rangle^{\gamma\omega} \tag{3.12}$$

Here, the variables $\mathbf{b}_\gamma$, $\mathbf{b}_\omega$, s_γ, and s_ω can be interpreted as integrals of the associated Greens functions for the closure problem. This closure fails to capture any characteristic time associated to the exchange between both phases in opposition to the closure used for two-equation models which describes one characteristic time associated with the exchange. Only non-local theories or direct pore-scale simulations would be able to recover all the characteristic times involved in this process.

Upon substituting this general form into the closure problem, we can collect terms involving $\nabla\langle c\rangle^{\gamma\omega}$ and $\langle c\rangle^{\gamma\omega}$. The result is the following set of coupled closure problems in which derivatives of averaged quantities are neglected

Problem I (s-problem)

$$\nabla\cdot(\mathbf{v}_\gamma s_\gamma)=\nabla\cdot(\mathbf{D}_\gamma\cdot\nabla s_\gamma)-\frac{\alpha}{\mathcal{K}}\frac{\varepsilon_\omega}{\varepsilon_\omega+\varepsilon_\gamma}-\frac{\alpha}{\mathcal{K}}\frac{\varepsilon_\gamma}{\varepsilon_\omega+\varepsilon_\gamma}\langle s_\gamma\rangle^\gamma \tag{3.13}$$

$$\begin{aligned}
&\text{BC1}: && -(\mathbf{n}_{\gamma\sigma}\cdot\mathbf{D}_\gamma)\cdot\nabla s_\gamma &&= && 0 && \text{on } \mathscr{S}_{\gamma\sigma} && (3.14a)\\
&\text{BC2}: && s_\omega &&= && s_\gamma && \text{on } \mathscr{S}_{\gamma\omega} && (3.14b)\\
&\text{BC3}: && -(\mathbf{n}_{\gamma\omega}\cdot\mathbf{D}_\gamma)\cdot\nabla s_\gamma &&= && -(\mathbf{n}_{\gamma\omega}\cdot\mathbf{D}_\omega)\cdot\nabla s_\omega && \text{on } \mathscr{S}_{\gamma\omega} && (3.14c)\\
&\text{BC4}: && -(\mathbf{n}_{\omega\sigma}\cdot\mathbf{D}_\omega)\cdot\nabla s_\omega &&= && 0 && \text{on } \mathscr{S}_{\omega\sigma} && (3.14d)
\end{aligned}$$

$$0=\nabla\cdot(\mathbf{D}_\omega\cdot\nabla s_\omega)+\frac{\alpha}{\mathcal{K}}\frac{\varepsilon_\gamma}{\varepsilon_\omega+\varepsilon_\gamma}+\frac{\alpha}{\mathcal{K}}\frac{\varepsilon_\omega}{\varepsilon_\omega+\varepsilon_\gamma}\langle s_\omega\rangle^\omega-\frac{\alpha}{\mathcal{K}}s_\omega \tag{3.15}$$

Problem II (b-problem)

$$\begin{aligned}
\mathbf{v}_\gamma\cdot\nabla\mathbf{b}_\gamma=&\nabla\cdot(\mathbf{D}_\gamma\cdot\nabla\mathbf{b}_\gamma)-\tilde{\mathbf{v}}_\gamma-\frac{\varepsilon_\omega}{\varepsilon_\omega+\varepsilon_\gamma}\langle\mathbf{v}_\gamma\rangle^\gamma-\frac{\alpha}{\mathcal{K}}\frac{\varepsilon_\gamma}{\varepsilon_\omega+\varepsilon_\gamma}\langle\mathbf{b}_\gamma\rangle^\gamma\\
&+\frac{\varepsilon_\omega}{\varepsilon_\gamma+\varepsilon_\omega}\mathbf{D}_\omega\cdot\langle\nabla s_\omega\rangle^\omega+\frac{\varepsilon_\gamma}{\varepsilon_\gamma+\varepsilon_\omega}\mathbf{D}_\gamma\cdot\langle\nabla s_\gamma\rangle^\gamma\\
&-2\mathbf{D}_\gamma\cdot\nabla s_\gamma+\mathbf{v}_\gamma s_\gamma-\frac{\varepsilon_\gamma}{\varepsilon_\omega+\varepsilon_\gamma}\langle s_\gamma\mathbf{v}_\gamma\rangle^\gamma
\end{aligned} \tag{3.16}$$

$$\begin{aligned}
&\text{BC1}: && -(\mathbf{n}_{\gamma\sigma}\cdot\mathbf{D}_\gamma)\cdot\nabla\mathbf{b}_\gamma &&= && (\mathbf{n}_{\gamma\sigma}\cdot\mathbf{D}_\gamma)(1-s_\gamma) && \text{on } \mathscr{S}_{\gamma\sigma} && (3.17a)\\
&\text{BC2}: && \mathbf{b}_\omega &&= && \mathbf{b}_\gamma && \text{on } \mathscr{S}_{\gamma\omega} && (3.17b)\\
&\text{BC3}: && -\mathbf{n}_{\gamma\omega}\cdot(\mathbf{D}_\gamma\cdot\nabla\mathbf{b}_\gamma-\mathbf{D}_\omega\cdot\nabla\mathbf{b}_\omega) &&= && -\mathbf{n}_{\gamma\omega}\cdot(\mathbf{D}_\omega-\mathbf{D}_\gamma)(1-s_\gamma) && \text{on } \mathscr{S}_{\gamma\omega} && (3.17c)\\
&\text{BC4}: && -(\mathbf{n}_{\omega\sigma}\cdot\mathbf{D}_\omega)\cdot\nabla\mathbf{b}_\omega &&= && (\mathbf{n}_{\omega\sigma}\cdot\mathbf{D}_\omega)(1-s_\omega) && \text{on } \mathscr{S}_{\omega\sigma} && (3.17d)
\end{aligned}$$

$$\begin{aligned}
0=&\nabla\cdot(\mathbf{D}_\omega\cdot\nabla\mathbf{b}_\omega)+\frac{\varepsilon_\gamma}{\varepsilon_\gamma+\varepsilon_\omega}\langle\mathbf{v}_\gamma\rangle^\gamma+\frac{\alpha}{\mathcal{K}}\frac{\varepsilon_\omega}{\varepsilon_\omega+\varepsilon_\gamma}\langle\mathbf{b}_\omega\rangle^\omega-\frac{\alpha}{\mathcal{K}}\mathbf{b}_\omega\\
&+\frac{\varepsilon_\omega}{\varepsilon_\gamma+\varepsilon_\omega}\mathbf{D}_\omega\cdot\langle\nabla s_\omega\rangle^\omega+\frac{\varepsilon_\gamma}{\varepsilon_\gamma+\varepsilon_\omega}\mathbf{D}_\gamma\cdot\langle\nabla s_\gamma\rangle^\gamma-2\mathbf{D}_\omega\cdot\nabla s_\omega-\frac{\varepsilon_\gamma}{\varepsilon_\omega+\varepsilon_\gamma}\langle s_\gamma\mathbf{v}_\gamma\rangle^\gamma
\end{aligned} \tag{3.18}$$

There is an interesting discussion concerning the concept of representative elementary volume (REV) which is often misunderstood. Within hierarchical porous media, there is substantial redundancy in the spatial structure of the transport processes at the microscale, that is, the information needed to calculate the effective parameters is contained in a relatively small representative portion of the medium. Within this REV, internal boundary conditions Eqs (3.17) between the different phases are determined by the physics at the pore-scale. However, in order to ensure unicity of the s and $\mathbf{b}$ fields, it is also mandatory to adopt a representation for the external boundary condition between the REV and the rest of the porous medium. This condition is not

determined by the physics at the pore-scale but rather represents a way of closing the problem. At first, it is unclear how this choice should be made and it results in a significant amount of confusion in the literature. From a theoretical point of view, if the REV is large enough (read if the hypothesis of separation of length scales is verified), it has been shown [274] that effective parameters do not depend on this boundary condition.

In the real world, this constraint is never exactly satisfied, that is, the boundary condition can substantially influence the microscopic fields. However, it is important to notice that in the macroscopic Eq (2.25), $\hat{c}$ appear only under integrated quantities. Because of this, the dependence of effective parameters upon the solution of the closure problem is essentially mathematically of a weak form [190]. Hence, one could choose, say, Dirichlet, Neumann, mixed or periodic boundary conditions to obtain a local solution which produces acceptable values for the associated averaged quantities. As previously discussed in the literature [268, 93, 216, 199, 51], the periodic boundary condition lends itself very well for this application as it induces very little perturbation in the local fields, in opposition to, say, Dirichlet boundary conditions. It must be understood that this does not mean that the medium is interpreted as being physically periodic. For the remainder of this work, we will assume that the medium can be represented locally by a periodic cell Eq (3.19) and that the effective parameters can be calculated over this representative part of the medium.

$$\text{Periodicity}: \qquad \hat{c}_i(\mathbf{x}+l_k) = \hat{c}_i(\mathbf{x}) \qquad k = x,y,z \tag{3.19}$$

We also have Eqs (3.20) and (3.21)

$$\text{Periodicity}: \qquad \mathbf{b}_i(\mathbf{x}+l_k) = \mathbf{b}_i(\mathbf{x}) \qquad k = x,y,z \tag{3.20}$$

$$\text{Periodicity}: \qquad s_i(\mathbf{x}+l_k) = s_i(\mathbf{x}) \qquad k = x,y,z \tag{3.21}$$

In these equations Eqs (3.19), (3.20) and (3.21), we have used l_k to represent the three lattice vectors that are needed to describe the 3-D spatial periodicity.

In addition to these periodic boundary conditions, one usually needs to impose constraints on the intrinsic averaged of the closure fields in order to ensure unicity of the solutions. To find out these additional equations, we use $\langle \tilde{c}_\gamma \rangle^\gamma, \langle \tilde{c}_\omega \rangle^\omega = 0$. In our case, this is not necessary to constrain the fields because the reactive part of the spatial operator ensures, mathematically, unicity of the solutions. However, numerical computations, in situations where the reaction has little importance in comparison to other processes, can lead to some discrepancies. To avoid this problem, it is important to impose $\varepsilon_\omega \langle \hat{c}_\omega \rangle^\omega + \varepsilon_\gamma \langle \hat{c}_\gamma \rangle^\gamma = 0$, that is, $\varepsilon_\omega \langle \mathbf{b}_\omega \rangle^\omega + \varepsilon_\gamma \langle \mathbf{b}_\gamma \rangle^\gamma = 0$ and $\varepsilon_\omega \langle s_\omega \rangle^\omega + \varepsilon_\gamma \langle s_\gamma \rangle^\gamma = 0$.

3.3 CLOSED MACROSCOPIC EQUATION

Substituting Eqs (3.11) and (3.12) into Eq (2.25) leads to

$$\frac{\partial \langle c\rangle^{\gamma\omega}}{\partial t} + \mathbf{v}^* \cdot \boldsymbol{\nabla} \langle c\rangle^{\gamma\omega} = \boldsymbol{\nabla} \cdot (\mathbf{D}^* \cdot \boldsymbol{\nabla} \langle c\rangle^{\gamma\omega}) - \alpha^* \langle c\rangle^{\gamma\omega} \tag{3.22}$$

where the effective parameters are given by

$$\mathbf{v}^* = \frac{\varepsilon_\gamma}{\varepsilon_\gamma + \varepsilon_\omega} (\langle \mathbf{v}_\gamma\rangle^\gamma + \mathbf{D}_\gamma \cdot \langle \boldsymbol{\nabla} s_\gamma\rangle^\gamma - \langle s_\gamma \mathbf{v}_\gamma\rangle^\gamma) + \frac{\varepsilon_\omega}{\varepsilon_\gamma + \varepsilon_\omega} \left(\mathbf{D}_\omega \cdot \langle \boldsymbol{\nabla} s_\omega\rangle^\omega + \frac{\alpha}{\mathscr{K}} \langle \mathbf{b}_\omega\rangle^\omega \right) \tag{3.23}$$

$$\mathbf{D}^* = \frac{\varepsilon_\gamma}{\varepsilon_\gamma + \varepsilon_\omega} [\mathbf{D}_\gamma \cdot (\mathbf{I} - \mathbf{I}\langle s_\gamma\rangle^\gamma + \langle \boldsymbol{\nabla} \mathbf{b}_\gamma\rangle^\gamma) - \langle \mathbf{v}_\gamma \mathbf{b}_\gamma\rangle^\gamma] + \frac{\varepsilon_\omega}{\varepsilon_\gamma + \varepsilon_\omega} [\mathbf{D}_\omega \cdot (\mathbf{I} - \mathbf{I}\langle s_\omega\rangle^\omega + \langle \boldsymbol{\nabla} \mathbf{b}_\omega\rangle^\omega)] \tag{3.24}$$

$$\alpha^* = \frac{\alpha}{\mathscr{K}} \frac{\varepsilon_\omega}{\varepsilon_\gamma + \varepsilon_\omega} (1 - \langle s_\omega\rangle^\omega) \tag{3.25}$$

For simplicity, the porosities are taken to be constants. If the model is applied to media with non constant porosities, one should take care to consider gradients of ε (c.f., Appendixes). Moreover, the macroscopic equation is written under a non-conservative form so that it exhibits only effective velocity, dispersion and effective reaction rate. It is convenient to write it this way for the purpose of comparing the asymptotic model with other models.

However, notice that a more general conservative expression would be

$$\frac{\partial \langle c\rangle^{\gamma\omega}}{\partial t} + \boldsymbol{\nabla} \cdot \left(\frac{\varepsilon_\gamma}{\varepsilon_\gamma + \varepsilon_\omega} \langle c\rangle^{\gamma\omega} \langle \mathbf{v}_\gamma\rangle^\gamma \right) = \boldsymbol{\nabla} \cdot (\mathbf{D}_c^* \cdot \boldsymbol{\nabla} \langle c\rangle^{\gamma\omega}) - \boldsymbol{\nabla} \cdot (\mathbf{d}_c^* \langle c\rangle^{\gamma\omega}) - \mathbf{v}_c^* \cdot \boldsymbol{\nabla} \langle c\rangle^{\gamma\omega} - \alpha_c^* \langle c\rangle^{\gamma\omega} \tag{3.26}$$

where the effective parameters are given by

$$\mathbf{d}_c^* = \frac{\varepsilon_\gamma}{\varepsilon_\gamma + \varepsilon_\omega} (\mathbf{D}_\gamma \cdot \langle \boldsymbol{\nabla} s_\gamma\rangle^\gamma - \langle s_\gamma \mathbf{v}_\gamma\rangle^\gamma) + \frac{\varepsilon_\omega}{\varepsilon_\gamma + \varepsilon_\omega} (\mathbf{D}_\omega \cdot \langle \boldsymbol{\nabla} s_\omega\rangle^\omega) \tag{3.27}$$

$$\mathbf{v}_c^* = \frac{\varepsilon_\omega}{\varepsilon_\gamma + \varepsilon_\omega} \frac{\alpha}{\mathscr{K}} \langle \mathbf{b}_\omega\rangle^\omega \tag{3.28}$$

$$\mathbf{D}_c^* = \frac{\varepsilon_\gamma}{\varepsilon_\gamma + \varepsilon_\omega} [\mathbf{D}_\gamma \cdot (\mathbf{I} - \mathbf{I}\langle s_\gamma\rangle^\gamma + \langle \boldsymbol{\nabla} \mathbf{b}_\gamma\rangle^\gamma) - \langle \mathbf{v}_\gamma \mathbf{b}_\gamma\rangle^\gamma] + \frac{\varepsilon_\omega}{\varepsilon_\gamma + \varepsilon_\omega} [\mathbf{D}_\omega \cdot (\mathbf{I} - \mathbf{I}\langle s_\omega\rangle^\omega + \langle \boldsymbol{\nabla} \mathbf{b}_\omega\rangle^\omega)] \tag{3.29}$$

$$\alpha_c^* = \frac{\alpha}{\mathscr{K}} \frac{\varepsilon_\omega}{\varepsilon_\gamma + \varepsilon_\omega} (1 - \langle s_\omega\rangle^\omega) \tag{3.30}$$

Notice that, at this point, if $\mathbf{v}_c^*$ plays mathematically the role of a velocity, it is directly linked to the chemical reaction and should not be discarded if one considers non-convective flows.

4

NUMERICAL RESULTS

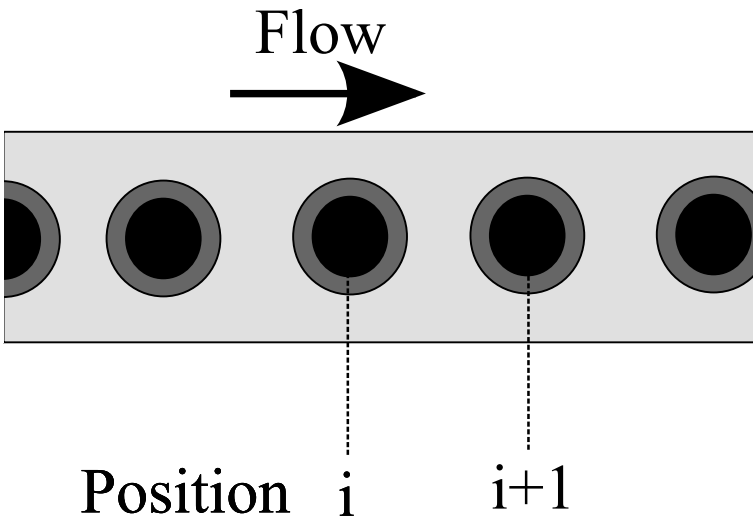

Figure 39: Total geometry

Ideally, one could compare the theory developed above with the results of direct experimental measurements conducted at both the microscale and at the macroscale. Theoretically, it is possible to obtain a three dimensional image of the three phases biofilm-liquid-solid. This is an area of active research [229], and workers are continuing to develop methods such that the microscale structure of a biofilm within a porous medium can be measured [130, 76]. Currently, however, the results from such multi-scale experimental measurements are not available.

The goal of this section, then, is to provide some characteristic features of the model previously devised on a simplified 2D medium Figs (39) and (40) using numerical methods. We adopt a conceptual construction which captures the main physics of the problem. In Fig (40), $\sigma-phase$ is represented by solid black, the $\gamma-phase$ is given by light grey, and the grey lies for the $\omega-phase$. One should notice that at the macroscale only a 1D model is needed for this particular geometry. For both the 2D and 1D models, the output boundary condition is set to free advective flux. For the purposes of this study, 1) we obtain the velocity field by solving Stokes equations, with no-slip conditions on lateral boundaries, over the entire system, 2) we will only

consider a spheric diffusion tensor for the biofilm and water-phases 3) we fix $\mathscr{K} = 0.5$ and $D_\Sigma = \frac{D_\omega}{D_\gamma} = 0.3$ and take $l_\gamma = 0.5$.

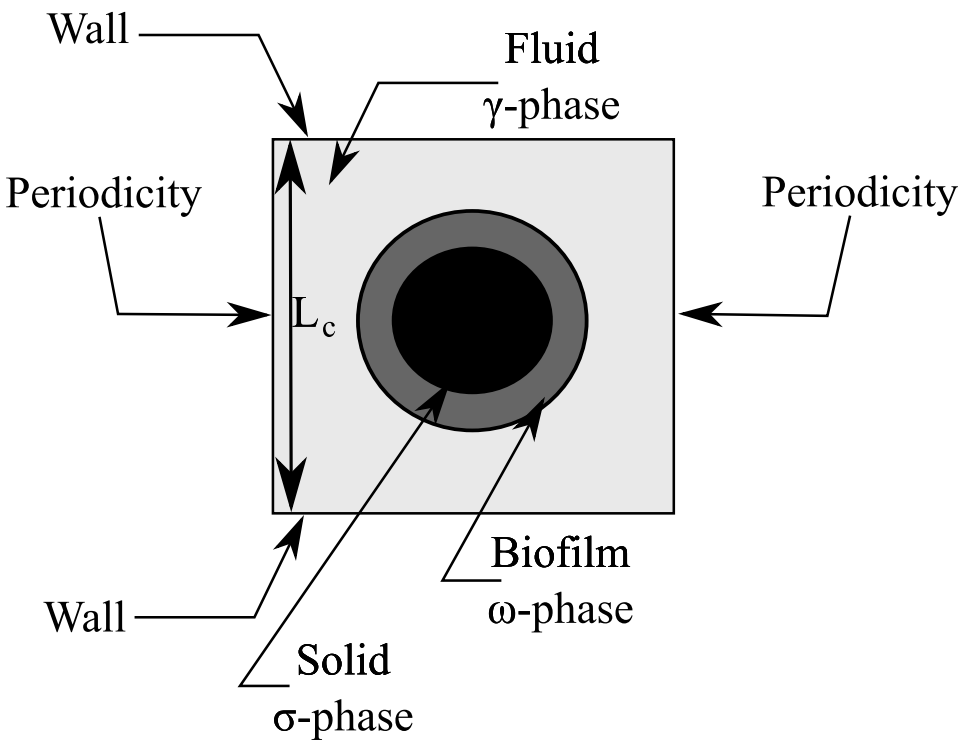

Figure 40: Representative cell

For these simulations, we have the following goals

1. To establish the behavior of the effective parameters as functions of Péclet and Damköhler numbers.

2. To compare these effective parameters with those of the local mass equilibrium model, as developed in [114].

3. To validate the model against pore-scale simulations both stationary and transient.

All the numerical calculations were performed using the COMSOL^{TM} Multiphysics package 3.5 based on a finite element formulation. For the resolution of Stokes equation, we use quadratic Lagrange elements for the velocities and linear elements for the pressure. For the resolution of the advection-diffusion equations, we use a quadratic Lagrange element formulation. Residuals are computed using a quadrature formula of order 2 for linear Lagrange elements and 4 for quadratic Lagrange elements. The linear systems are solved using the direct solver UMFPACK based on the Unsymmetric MultiFrontal method.

The problem Eqs (2.1)-(2.3) at the pore-scale can be rewritten under the following dimensionless form

$$\gamma-\mathrm{phase}: \qquad \frac{\partial c'_\gamma}{\partial t'}+\mathscr{P}e\,\boldsymbol{\nabla}\cdot\left(c'_\gamma \mathbf{v}'_\gamma\right)=\Delta c'_\gamma \tag{4.1}$$

$$\begin{aligned}
&\mathrm{BC1}: && -\mathbf{n}_{\gamma\sigma}\cdot\boldsymbol{\nabla}c'_\gamma=0 && \text{on } \mathscr{S}_{\gamma\sigma} && (4.2a)\\
&\mathrm{BC2}: && c'_\omega=c'_\gamma && \text{on } \mathscr{S}_{\gamma\omega} && (4.2b)\\
&\mathrm{BC3}: && -\mathbf{n}_{\gamma\omega}\cdot\boldsymbol{\nabla}c'_\gamma=-D_\Sigma\mathbf{n}_{\gamma\omega}\cdot\boldsymbol{\nabla}c'_\omega && \text{on } \mathscr{S}_{\gamma\omega} && (4.2c)\\
&\mathrm{BC4}: && -D_\Sigma\mathbf{n}_{\omega\sigma}\cdot\boldsymbol{\nabla}c'_\omega=0 && \text{on } \mathscr{S}_{\omega\sigma} && (4.2d)
\end{aligned}$$

$$\omega-\mathrm{phase}: \qquad \frac{\partial c'_\omega}{\partial t'}=\boldsymbol{\nabla}\cdot\left(D_\Sigma\boldsymbol{\nabla}c'_\omega\right)-\mathscr{D}aD_\Sigma\, c'_\omega \tag{4.3}$$

where the normalized concentrations and velocity are given by

$$c'_\omega = \frac{c_\omega}{c_0} \tag{4.4}$$

$$c'_\gamma = \frac{c_\gamma}{c_0} \tag{4.5}$$

$$\mathbf{v}'_\gamma = \frac{\mathbf{v}_\gamma}{\langle v_\gamma\rangle^\gamma} \tag{4.6}$$

The concentration c_0 is the input concentration. Notice that we impose $c_0 \ll \mathscr{K}$ which is a sufficient constraint for the linearization of the reaction rate. We have adopted the following additional definitions for dimensionless quantities

$$t' = \frac{t\langle v_\gamma\rangle^\gamma}{l_\gamma} \tag{4.7}$$

The ratio between the diffusion coefficients in the $\omega-\mathrm{phase}$ and $\gamma-\mathrm{phase}$ is

$$D_\Sigma = \frac{D_\omega}{D_\gamma} \tag{4.8}$$

The Péclet and Damköhler numbers are specified by

$$\mathscr{D}a = \frac{\alpha l_\gamma^2}{\mathscr{K}D_\omega} \tag{4.9}$$

$$\mathscr{P}e = \frac{\langle v_\gamma\rangle^\gamma l_\gamma}{D_\gamma} \tag{4.10}$$

The closure problems Eqs (3.13)-(3.18) take the form in dimensionless quantities

Problem I (s-problem)

$$\mathscr{P}e\,\boldsymbol{\nabla}\cdot\left(\mathbf{v}'_\gamma s_\gamma\right)=\Delta s_\gamma-\mathscr{D}a\,\frac{\varepsilon_\omega}{\varepsilon_\omega+\varepsilon_\gamma}-\mathscr{D}a\,\frac{\varepsilon_\gamma}{\varepsilon_\omega+\varepsilon_\gamma}\langle s_\gamma\rangle^\gamma \tag{4.11}$$

$$\begin{aligned}
&\text{BC1}: && -\mathbf{n}_{\gamma\sigma}\cdot\boldsymbol{\nabla} s_\gamma = 0 && \text{on } \mathscr{S}_{\gamma\sigma} && (4.12a)\\
&\text{BC2}: && s_\omega = s_\gamma && \text{on } \mathscr{S}_{\gamma\omega} && (4.12b)\\
&\text{BC3}: && -\mathbf{n}_{\gamma\omega}\cdot\boldsymbol{\nabla} s_\gamma = -\mathsf{D}_\Sigma \mathbf{n}_{\gamma\omega}\cdot\boldsymbol{\nabla} s_\omega && \text{on } \mathscr{S}_{\gamma\omega} && (4.12c)\\
&\text{BC4}: && -\{\mathsf{D}\}_\Sigma \mathbf{n}_{\omega\sigma}\cdot\boldsymbol{\nabla} s_\omega = 0 && \text{on } \mathscr{S}_{\omega\sigma} && (4.12d)\\
&\text{Periodicity}: && s_i(x+l_x) = s_i(x) && && (4.12e)
\end{aligned}$$

$$0 = \boldsymbol{\nabla}\cdot(\mathsf{D}_\Sigma \boldsymbol{\nabla} s_\omega) + \mathscr{D}a\,\frac{\varepsilon_\gamma}{\varepsilon_\omega+\varepsilon_\gamma} + \mathscr{D}a\,\frac{\varepsilon_\omega}{\varepsilon_\omega+\varepsilon_\gamma}\langle s_\omega\rangle^\omega - \mathscr{D}a\, s_\omega \tag{4.13}$$

Problem II (b-problem)

$$\begin{aligned}
\mathscr{P}e\,\left(\mathbf{v}'_\gamma\cdot\boldsymbol{\nabla}\mathbf{b}'_\gamma - \mathbf{v}'_\gamma s_\gamma + \tilde{\mathbf{v}}'_\gamma\right) = \;& \boldsymbol{\nabla}\cdot(\boldsymbol{\nabla}\mathbf{b}'_\gamma) - 2\boldsymbol{\nabla} s_\gamma && (4.14)\\
&- \mathscr{D}a\frac{\varepsilon_\gamma}{\varepsilon_\omega+\varepsilon_\gamma}\langle\mathbf{b}'_\gamma\rangle^\gamma - \frac{\mathscr{P}e}{\varepsilon_\omega+\varepsilon_\gamma}\langle s_\gamma\mathbf{v}'_\gamma\rangle\\
&+ \frac{\varepsilon_\omega}{\varepsilon_\gamma+\varepsilon_\omega}\mathsf{D}_\Sigma\langle\boldsymbol{\nabla} s_\omega\rangle^\omega + \frac{\varepsilon_\gamma}{\varepsilon_\gamma+\varepsilon_\omega}\langle\boldsymbol{\nabla} s_\gamma\rangle^\gamma
\end{aligned}$$

$$\begin{aligned}
&\text{BC1}: && -\mathbf{n}_{\gamma\sigma}\cdot\boldsymbol{\nabla}\mathbf{b}'_\gamma = \mathbf{n}_{\gamma\sigma}(1-s_\gamma) && \text{on } \mathscr{S}_{\gamma\sigma} && (4.15a)\\
&\text{BC2}: && \mathbf{b}'_\omega = \mathbf{b}'_\gamma && \text{on } \mathscr{S}_{\gamma\omega} && (4.15b)\\
&\text{BC3}: && -\mathbf{n}_{\gamma\omega}\cdot(\boldsymbol{\nabla}\mathbf{b}'_\gamma - \mathsf{D}_\Sigma\boldsymbol{\nabla}\mathbf{b}'_\omega) = -\mathbf{n}_{\gamma\omega}(\mathsf{D}_\Sigma - 1)(1-s_\gamma) && \text{on } \mathscr{S}_{\gamma\omega} && (4.15c)\\
&\text{BC4}: && -\mathbf{n}_{\omega\sigma}\cdot\boldsymbol{\nabla}\mathbf{b}'_\omega = \mathbf{n}_{\omega\sigma}(1-s_\omega) && \text{on } \mathscr{S}_{\omega\sigma} && (4.15d)\\
&\text{Periodicity}: && \mathbf{b}'_i(x+l_x) = \mathbf{b}'_i(x) && && (4.15e)
\end{aligned}$$

$$\begin{aligned}
0 = \;& \boldsymbol{\nabla}\cdot(\mathsf{D}_\Sigma\boldsymbol{\nabla}\mathbf{b}'_\omega) - 2\mathsf{D}_\Sigma\boldsymbol{\nabla} s_\omega && (4.16)\\
&+ \mathscr{D}a\frac{\varepsilon_\omega}{\varepsilon_\omega+\varepsilon_\gamma}\langle\mathbf{b}'_\omega\rangle^\omega - \mathscr{D}a\mathbf{b}'_\omega - \frac{\mathscr{P}e}{\varepsilon_\omega+\varepsilon_\gamma}\langle s_\gamma\mathbf{v}'_\gamma\rangle\\
&+ \frac{\varepsilon_\omega}{\varepsilon_\gamma+\varepsilon_\omega}\mathsf{D}_\Sigma\langle\boldsymbol{\nabla} s_\omega\rangle^\omega + \frac{\varepsilon_\gamma}{\varepsilon_\gamma+\varepsilon_\omega}\langle\boldsymbol{\nabla} s_\gamma\rangle^\gamma
\end{aligned}$$

where

$$\tilde{\mathbf{v}}'_\gamma = \frac{\tilde{\mathbf{v}}_\gamma}{\langle v_\gamma\rangle^\gamma} \qquad \mathbf{b}'_\gamma = \frac{\mathbf{b}_\gamma}{l_\gamma} \qquad \mathbf{b}'_\omega = \frac{\mathbf{b}_\omega}{l_\gamma} \tag{4.17}$$

Notice that, if one fixes D_Σ, the set of equations only depends upon $\mathscr{P}e$ and $\mathscr{D}a$.

4.1 DISPERSION, VELOCITY AND REACTIVE BEHAVIOR

In this section, we solve the closure parameters problems Eqs (4.11)-(4.16) over the cell Fig (40) for large ranges of $\mathscr{P}e$ and $\mathscr{D}a$. Then, the associated effective parameters are computed and presented Fig (41) for the longitudinal dispersion D^*_{xx} normalized with $\frac{\varepsilon_\gamma}{\varepsilon_\gamma+\varepsilon_\omega}\mathsf{D}_\gamma + \frac{\varepsilon_\omega}{\varepsilon_\gamma+\varepsilon_\omega}\mathsf{D}_\omega$; Fig (42) for the x-component of the effective velocity v^*_x normalized with $\frac{\varepsilon_\gamma}{\varepsilon_\gamma+\varepsilon_\gamma}\langle v_\gamma\rangle^\gamma$; Fig (43) for the effective kinetics α^* normalized with $\frac{\varepsilon_\omega}{\varepsilon_\gamma+\varepsilon_\gamma}\frac{\alpha}{\mathscr{K}}$.

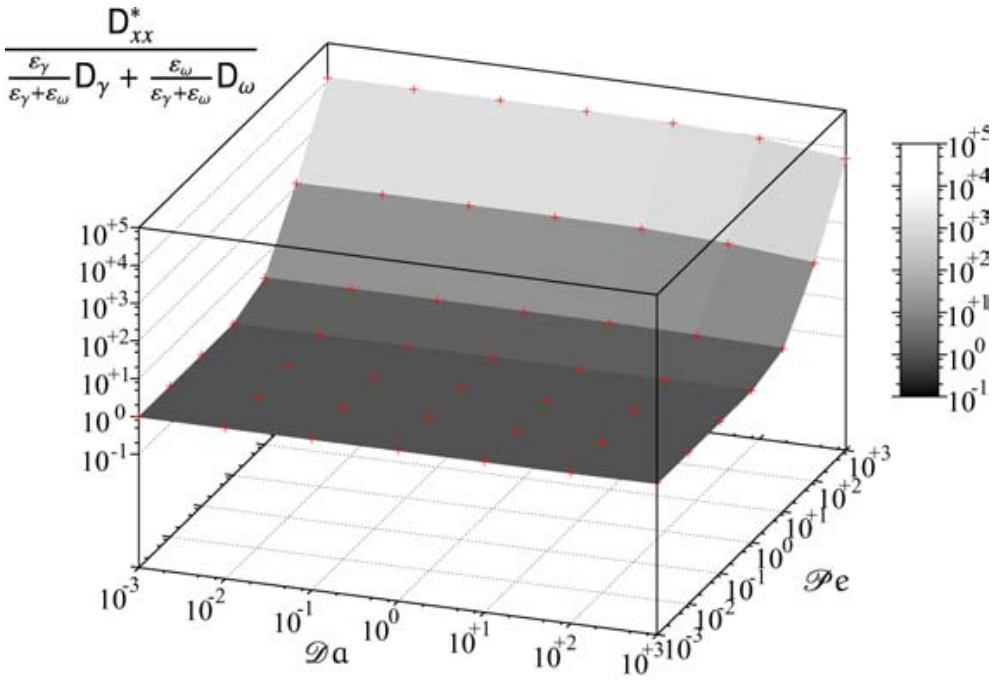

Figure 41: Normalized longitudinal dispersion of the non-equilibrium model as a function of $\mathscr{P}e$ and $\mathscr{D}a$ numbers

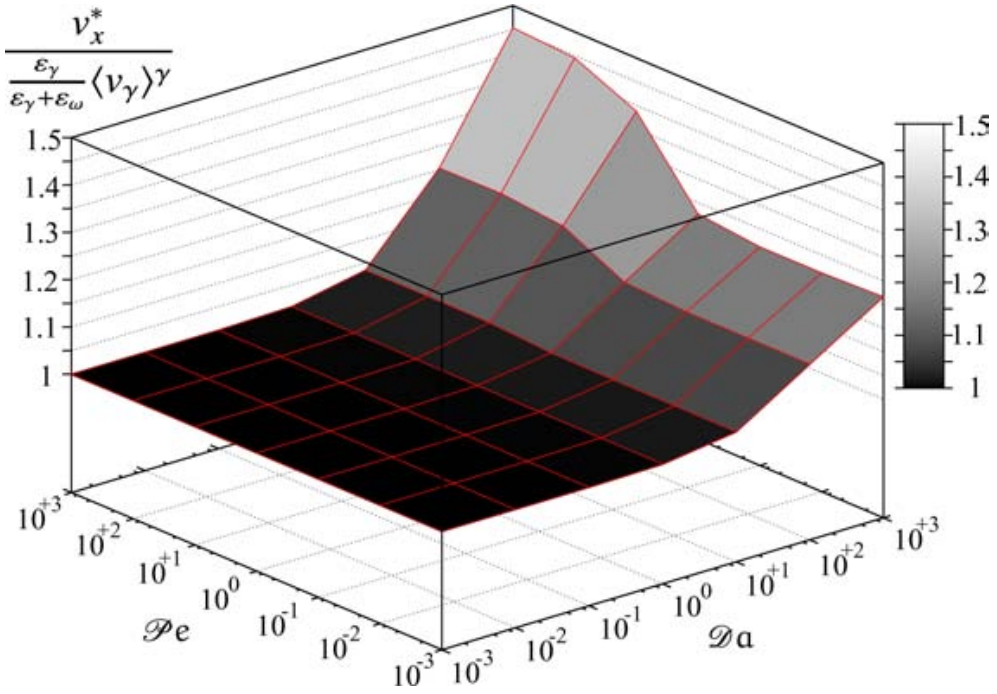

Figure 42: Normalized x-component of the effective velocity of the non-equilibrium model as a function of $\mathscr{P}e$ and $\mathscr{D}a$ numbers

As an aside, notice that for low $\mathscr{P}e$ and high $\mathscr{D}a$, the length scales constraints needed to develop the closed macroscopic equation are not satisfied. However, the

constraints are developed in terms of order of magnitudes so that it is not clear what is the exact limit between the homogenizable and non-homogenizable zones. Because of this, the entire space of $\mathscr{P}e$, $\mathscr{D}a$ parameters is kept and we do not clearly establish this frontier.

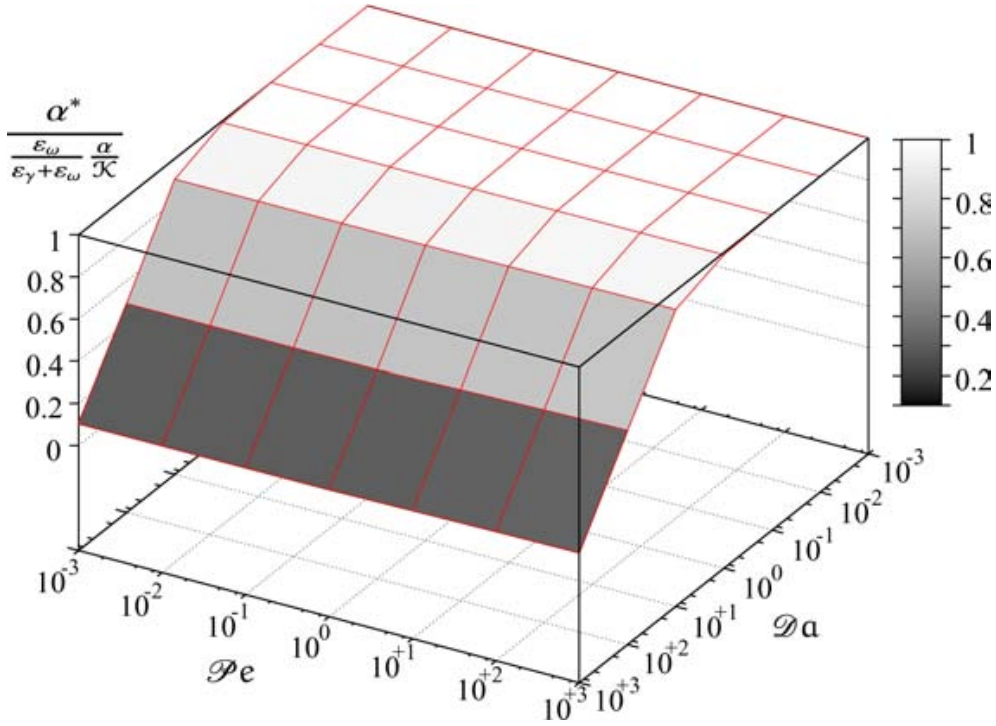

Figure 43: Normalized effective reaction rate of the non-equilibrium model as a function of $\mathscr{P}e$ and $\mathscr{D}a$ numbers

Effective parameters strongly depend upon the type of boundary conditions at the small scale, that is, the dispersion in a, say, Dirichlet bounded system or in a Neumann bounded problem may drastically change. In our case, for low $\mathscr{D}a$, the boundary between the biofilm-phase and the fluid-phase is a flux continuity whereas, as $\mathscr{D}a$ tends toward infinity, the concentration in the biofilm-phase and at the boundary tends toward zero, which can be interpreted, for conceptual purposes, as a Dirichlet boundary condition. In other words, when $\mathscr{P}e \gg 1$ and $\mathscr{D}a \gg 1$ the medium can conceptually be represented by a zero-concentration layer surrounding the biofilm, that is, the substrate reaches a limited interstitial space corresponding to the maxima of the local velocity field. It results in an increase of the apparent velocity with both $\mathscr{P}e$ and $\mathscr{D}a$ numbers. The dispersion exhibits the classical form, and increases mainly with the $\mathscr{P}e$ number as the hydrodynamic dispersion becomes predominant. However, the log scale hides the fact that D^* actually depends also on $\mathscr{D}a$ and this is presented in Fig (44). We observe a drastic reduction of the longitudinal dispersion at high $\mathscr{D}a$ and it is in agreement with previous studies [143, 92, 233]. The physics underlying this effect is reminiscent to the one causing an augmentation of the apparent velocity. As

a boundary layer in which $c_\gamma = 0$ surrounds the biofilm-phase, the solute is confined in a small portion of the fluid-phase or, more precisely, undertakes biodegradation as soon as it reaches the edges of this zone. The molecules of solute far away from the entrance have not visited the entire $\gamma - phase$ but rather a narrow central portion in which the fluctuations of the velocity field are limited. As a consequence, the substrate spreading due to hydrodynamic dispersion (reminiscent to the Taylor dispersion in a tube) is reduced. Additionally, it is important to keep in mind that our model porous medium does not exhibit any transverse dispersion. If it was to be considered, one would expect a different behavior for the transverse dispersion (see discussions in [143, 92, 233]).

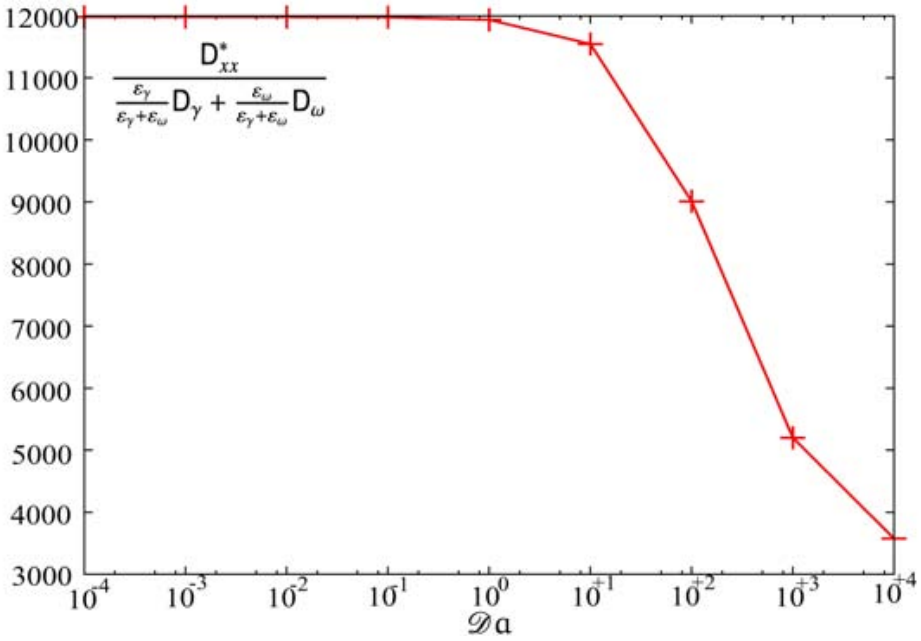

Figure 44: Normalized dispersion behavior of the non-equilibrium model for $\mathscr{P}e = 1000$ as a function of $\mathscr{D}a$ number

The effective reaction rate depends almost only on $\mathscr{D}a$ because the mass transfer through the boundary is mainly driven by diffusion. It seems that, for low $\mathscr{D}a$, the reaction rate is maximum and decreases when the consumption is too elevated compared to diffusion. It suggests that the reaction rate could be written under the form ηR_{max} with $\eta \leqslant 1$ a function of $\mathscr{D}a$. Notice that Dykaar and Kitanidis [92], following the work of Shapiro [233] for a surface reactive medium, also established a theoretical framework for this kind of effectiveness factor using the moments matching technique. However, their model describes an averaged concentration only on the water-phase rather than the total mass present in the porous medium at a given time. The reader is referred to the section 2.4 for an extensive discussion of this point.

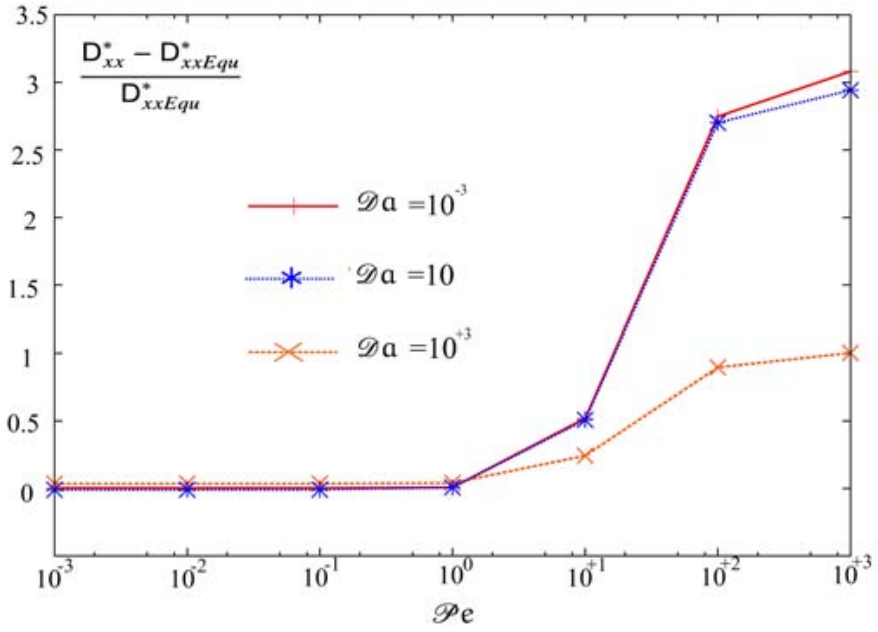

Figure 45: Relative differences of the longitudinal dispersion between local mass equilibrium and non-equilibrium models as functions of $\mathscr{P}e$ for different $\mathscr{D}a$ numbers

4.2 RELATIONSHIP WITH THE LOCAL MASS EQUILIBRIUM MODEL

In this part, we compare the local mass equilibrium model as developed in [114] with the non-equilibrium one-equation model. The local mass equilibrium model takes the form

$$\frac{\partial \langle c\rangle^{\gamma\omega}}{\partial t} + \mathbf{v}^*_{Equ} \cdot \boldsymbol{\nabla}\langle c\rangle^{\gamma\omega} = \boldsymbol{\nabla}\cdot\left(D^*_{Equ}\cdot\boldsymbol{\nabla}\langle c\rangle^{\gamma\omega}\right) - \alpha^*_{Equ}\langle c\rangle^{\gamma\omega} \tag{4.18}$$

where the effective parameters are given by

$$\mathbf{v}^*_{Equ} = \frac{\varepsilon_\gamma}{\varepsilon_\gamma+\varepsilon_\omega}\langle \mathbf{v}_\gamma\rangle^\gamma \tag{4.19}$$

$$D^*_{Equ} = \frac{\varepsilon_\gamma}{\varepsilon_\gamma+\varepsilon_\omega}\left[D_\gamma\langle\boldsymbol{\nabla}\mathbf{b}_{\gamma Equ}\rangle^\gamma\right] + \frac{\varepsilon_\omega}{\varepsilon_\gamma+\varepsilon_\omega}\left[D_\omega\langle\boldsymbol{\nabla}\mathbf{b}_{\gamma Equ}\rangle^\gamma\right] - \frac{1}{\varepsilon_\gamma+\varepsilon_\omega}\langle\tilde{\mathbf{v}}_\gamma\mathbf{b}_{\gamma Equ}\rangle \tag{4.20}$$

$$\alpha^*_{Equ} = \frac{\alpha}{\mathscr{K}}\frac{\varepsilon_\omega}{\varepsilon_\gamma+\varepsilon_\omega} \tag{4.21}$$

The closure parameters are solutions of the following problem

$$\gamma-phase: \qquad \mathscr{P}e\left(\mathbf{v}'_\gamma\cdot\boldsymbol{\nabla}\mathbf{b}'_{\gamma Equ} + \tilde{\mathbf{v}}'_\gamma\right) = \boldsymbol{\nabla}\cdot\{\boldsymbol{\nabla}\mathbf{b}'_{\gamma Equ}\} \tag{4.22}$$

$$\begin{aligned}
&\text{BC1}: && -\mathbf{n}_{\gamma\sigma}\cdot\boldsymbol{\nabla}\mathbf{b}'_{\gamma Equ} = \mathbf{n}_{\gamma\sigma} && \text{on } \mathscr{S}_{\gamma\sigma} && (4.23a)\\
&\text{BC2}: && \mathbf{b}'_{\omega Equ} = \mathbf{b}'_{\gamma Equ} && \text{on } \mathscr{S}_{\gamma\omega} && (4.23b)\\
&\text{BC3}: && -\mathbf{n}_{\gamma\omega}\cdot(\boldsymbol{\nabla}\mathbf{b}'_{\gamma} - D_\Sigma\boldsymbol{\nabla}\mathbf{b}'_{\omega Equ}) = -\mathbf{n}_{\gamma\omega}(D_\Sigma - 1) && \text{on } \mathscr{S}_{\gamma\omega} && (4.23c)\\
&\text{BC4}: && -\mathbf{n}_{\omega\sigma}\cdot\boldsymbol{\nabla}\mathbf{b}'_{\omega Equ} = \mathbf{n}_{\omega\sigma} && \text{on } \mathscr{S}_{\omega\sigma} && (4.23d)\\
&\text{Periodicity}: && \mathbf{b}'_{iEqu}(x+l_x) = \mathbf{b}'_{iEqu}(x) && && (4.23e)
\end{aligned}$$

$$\omega-phase: \qquad 0 = \boldsymbol{\nabla}\cdot\{D_\Sigma\boldsymbol{\nabla}\mathbf{b}'_{\omega Equ}\} - \mathscr{D}a\mathbf{b}'_{\omega Equ} \qquad (4.24)$$

where

$$\mathbf{b}'_{\gamma Equ} = \frac{\mathbf{b}_{\gamma Equ}}{l_\gamma} \qquad \mathbf{b}'_{\omega Equ} = \frac{\mathbf{b}_{\omega Equ}}{l_\gamma} \qquad (4.25)$$

In the local mass equilibrium model, the effective reaction rate and velocity are constant in terms of $\mathscr{P}e$ and $\mathscr{D}a$ numbers. Notice that, on Fig (42) and Fig (43) the effective parameters of the non-equilibrium model are directly normalized with those of the equilibrium one. Because of this, the comparison is straightforward and both are close to each other for $\mathscr{D}a \leqslant 1$.

For the dispersion, the relative differences between both models, in terms of $\mathscr{P}e$ and $\mathscr{D}a$ numbers, are presented in Fig (45). For $\mathscr{P}e \leqslant 1$, the relative difference is close to zero so that both models are equivalent for $\mathscr{D}a \leqslant 1$ and $\mathscr{P}e \leqslant 1$. It has been shown in [114] that this region of the $\mathscr{D}a$, $\mathscr{P}e$ space represents the entire region of validity of the local mass equilibrium model. As a direct consequence, it turns out that the non-equilibrium model includes the equilibrium one when this one is valid. A thorough study of the transient behavior for both models is performed and discussed in the next section.

4.3 COMPARISON WITH DIRECT NUMERICAL SIMULATION

The aim of this section is to provide direct evidences that the model allows a good approximation of the situation at the pore-scale, to catch its limits and to study some physics of the problem.

On the one hand, we solve the entire 2D microscopic problem on a total length of $120L_c$ (called DNS for Direct Numerical Simulation). On the other hand, we solve the 1D upscaled models on a total length of $120L_c$. First, we observe the stationary response of the system for different Péclet and Damköhler numbers. Notice that both boundary conditions at the output are free advective flux. Then, we study the breakthrough curves at $20L_c$, $60L_c$ and $100L_c$ for a square input of a width of $\delta t' = 5$ starting at $t' = 0$ for different Péclet and Damköhler numbers.

4.3.1 *Stationary analysis*

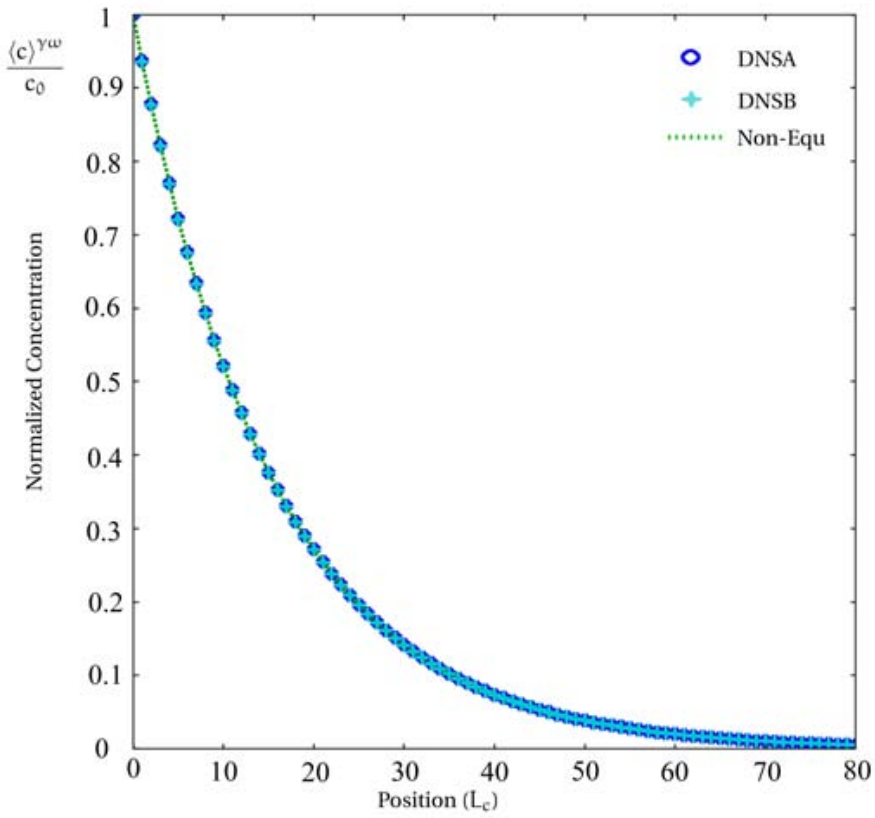

Figure 46: DNS and non-equilibrium model stationary concentration fields for $\mathscr{P}e = 10$ and $\mathscr{D}a = 10$ using normalization on the first cell (DNSB) and on the cell number 20 (DNSA)

The comparison of the concentration fields between the DNS and the non-equilibrium model is presented Fig (46) for $\mathscr{P}e = 10$, $\mathscr{D}a = 10$; Fig (47) for $\mathscr{P}e = 100$, $\mathscr{D}a = 100$ and Fig(48) for $\mathscr{P}e = 1000$, $\mathscr{D}a = 1000$. Notice that each circle, cross and square represents the value of $\langle c\rangle^{\gamma\omega}$ integrated on a cell.

We solve the stationary boundary value problem Eqs (2.1)-(2.3) with an input Dirichlet boundary condition of amplitude c_0. Then the results are normalized using the value of $\langle c\rangle^{\gamma\omega}$ calculated on the first cell (DNSB) and on the cell number 20 (DNSA) for Fig (46) and Fig (47); and on the first cell (DNSB), on the cell number 20 (DNSA) and 40 (DNSC). The origin of the spatial base is modified consequently to make them all start at 0.

For all the different situations, the model provides a very good approximation of the physics at the pore-scale. As previously discussed, the non-equilibrium model is time-constrained because of the hypothesis of quasi-stationarity on $\hat{c}_i$. Global stationarity represents a special time-constrained situation for which this hypothesis is very well satisfied.

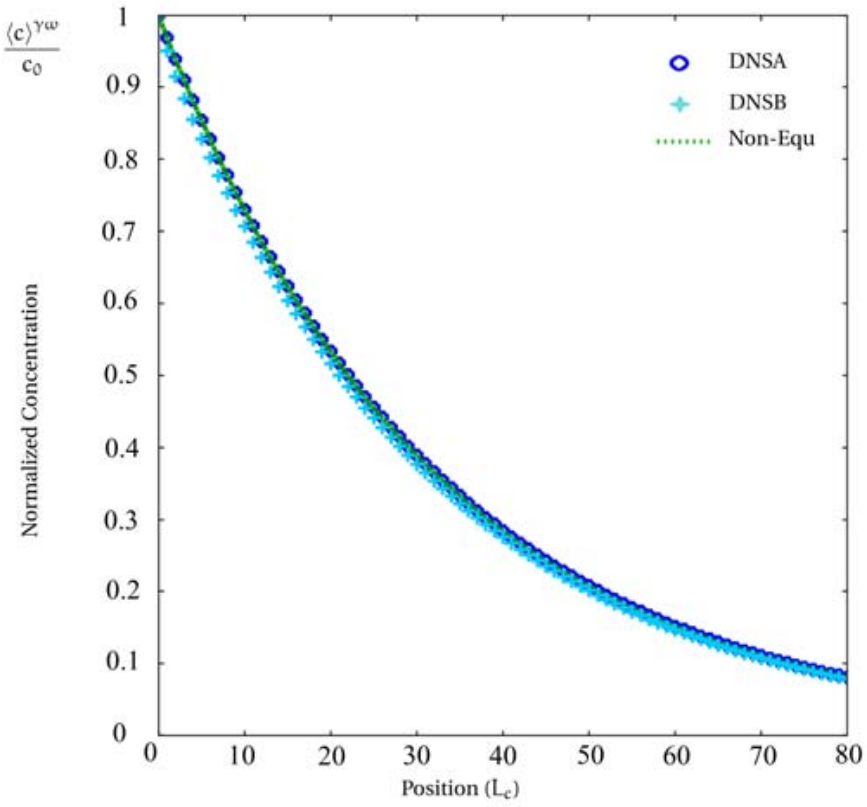

Figure 47: DNS and non-equilibrium model stationary concentration fields for $\mathscr{P}e = 100$ and $\mathscr{D}a = 100$ using normalization on the first cell (DNSB) and on the cell number 20 (DNSA)

However, for $\mathscr{P}e = 100$, $\mathscr{D}a = 100$ and $\mathscr{P}e = 1000$, $\mathscr{D}a = 1000$ some discrepancies arise between the different normalizations. If the concentration is normalized using $\langle c\rangle^{\gamma\omega}$ calculated on a cell far away from the input boundary, the results are closer between the DNS and the homogenized model. In the DNS, by imposing a Dirichlet boundary input, we impose $\tilde{c}_\gamma = 0$ and this can not be captured by the macroscopic model. As a consequence, the flux on $\mathscr{S}_{\gamma\omega}$ is overestimated in the DNS on the first cells compared to the homogenized model. When $\mathscr{P}e = 10$, $\mathscr{D}a = 10$, this overestimation does not even reach the second cell. For $\mathscr{P}e = 100$, $\mathscr{D}a = 100$, it start to exceed the first cell. For $\mathscr{P}e = 1000$, $\mathscr{D}a = 1000$, the discrepancy propagates very far from the boundary input as even the normalization on the cell number 20 does not give a satisfying result compared to the one on the cell number 40. These discrepancies appear because of the specific ordering of the porous medium and would not propagate so far from the input in a disordered medium. This question of the impact of boundary conditions on the comparison between direct numerical simulations and macroscopic predictions has received some attention in the literature [202, 17, 259]. Corrections of the macroscale boundary conditions, or mixed microscale/macroscale

approaches are available [17, 259, 40] but this is beyond the scope of this paper to develop such techniques.

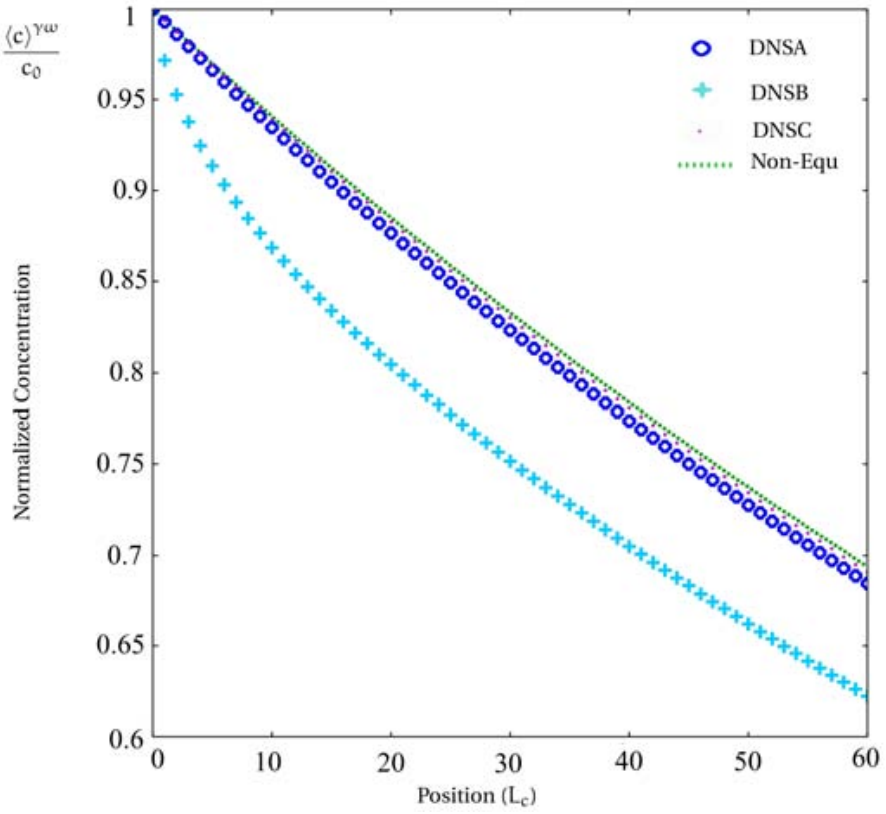

Figure 48: DNS and non-equilibrium model stationary concentration fields for $\mathscr{P}e = 1000$ and $\mathscr{D}a = 1000$ using normalization on the first cell (DNSB), on the cell number 20 (DNSA) and on the cell number 40 (DNSC)

4.3.2 *Transient analysis*

In this subsection, we study the transient behaviors of the one-equation non-equilibrium and equilibrium models for a square input of width $\delta t' = 5$ starting at $t' = 0$. Concentrations are normalized to the amplitude of the square input and the time t' is normalized with the characteristic time associated to the advective term. Notice that, in the transient case, we can not avoid the problem previously presented as the concentration can not be renormalized straightforwardly.

INFLUENCE OF THE PÉCLET NUMBER On Fig (49), the three homogenized models provide a very good approximation of the transport problem. At low Péclet, low Damköhler numbers, time and space non-locality tend to disappear because time and length scales are fully separated. Meanwhile, some very little discrepancy, proba-

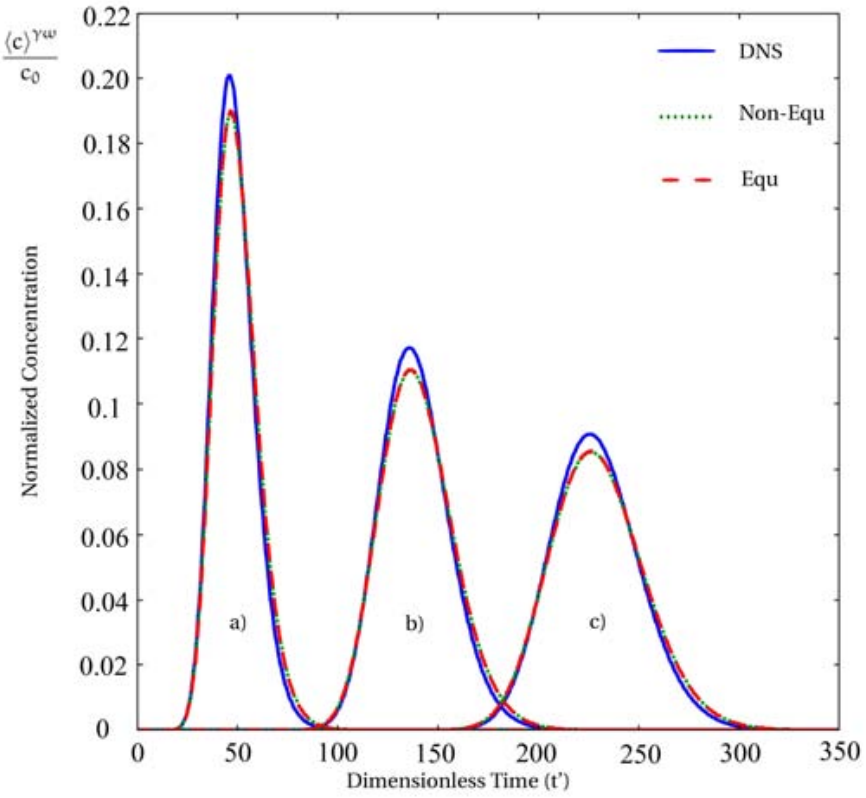

Figure 49: Transient breakthrough curves for the DNS, the local non-equilibrium and equilibrium models for a square input of $\delta t' = 5$ for $\mathscr{P}e = 1$ and $\mathscr{D}a = 10^{-5}$ after a) $20L_c$; b) $60L_c$; c) $100L_c$

bly due to the flux overestimation discussed in the section 4.3.1, exists at the peaks. The signal even propagates slowly enough for the local mass equilibrium assumption to be valid.

When the Péclet number reaches values around 100, the local mass equilibrium assumption becomes clearly inappropriate. Fig (50) shows that the local mass equilibrium model gives a poor approximation of the signal whereas the non-equilibrium one is still in good agreement. The fact that the peaks for $20L_c$ are not in such a good agreement is characteristic of non-locality. Memory functions (convolutions) or two-equation models should be considered in this case. However, when the signal spreads, non-locality tends to disappear and the breakthrough curves are in very good agreement.

For Péclet numbers around 1000, Fig (51), we show that there are some huge discrepancies between both homogenized model and the DNS, especially at $20L_c$ because of the strong non-locality. However, for long times, the non-equilibrium model seems to recover the tailing and the peak of the signal. Results suggest that the one-equation local non-equilibrium model might represent, in cases such as intermediate Péclet numbers or time-asymptotic regime, a good compromise, in

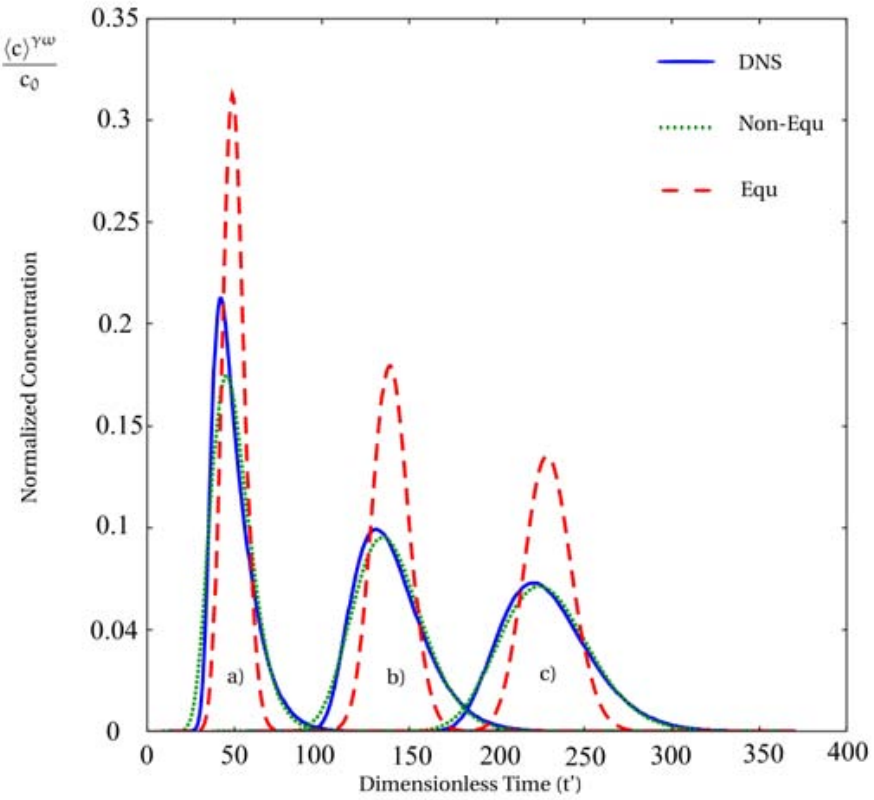

Figure 50: Transient breakthrough curves for the DNS, the local non-equilibrium and equilibrium models for a square input of $\delta t' = 5$ for $\mathscr{P}e = 100$ and $\mathscr{D}a = 10^{-5}$ after a) $20L_c$; b) $60L_c$; c) $100L_c$

terms of computational demand, between fully transient theories and the local mass equilibrium model. The importance of non-locality is also emphasized and becomes particularly obvious in the high Péclet number situation.

INFLUENCE OF THE DAMKÖHLER NUMBER When $\mathscr{P}e = 100$ and $\mathscr{D}a = 100$ Fig (52) and when $\mathscr{P}e = 1000$ and $\mathscr{D}a = 1000$ Fig (53), the local mass equilibrium model obviously does not recover the total mass of the system, that is, the reaction rate is overestimated. The non-equilibrium model is much more correct on this aspect. Meanwhile, at $20L_c$ it fails to capture non-locality and some discrepancies remain even when the signal spreads at $60L_c$ and $100L_c$ unlike for the low $\mathscr{D}a$ situation. This difference probably comes from the overestimation, in the DNS, of the flux on the first cells. In the non-reactive case, this effect has very little influence on the breakthrough curves whereas it is of special importance for high $\mathscr{D}a$ situation as the mass overexchanged disappears. However, notice that, unlike the situation $\mathscr{P}e = 1000$ and $\mathscr{D}a = 10^{-5}$, the one-equation non-equilibrium model recovers correctly the shape of the signal. It suggests that in the highly reactive case, the long-time regime

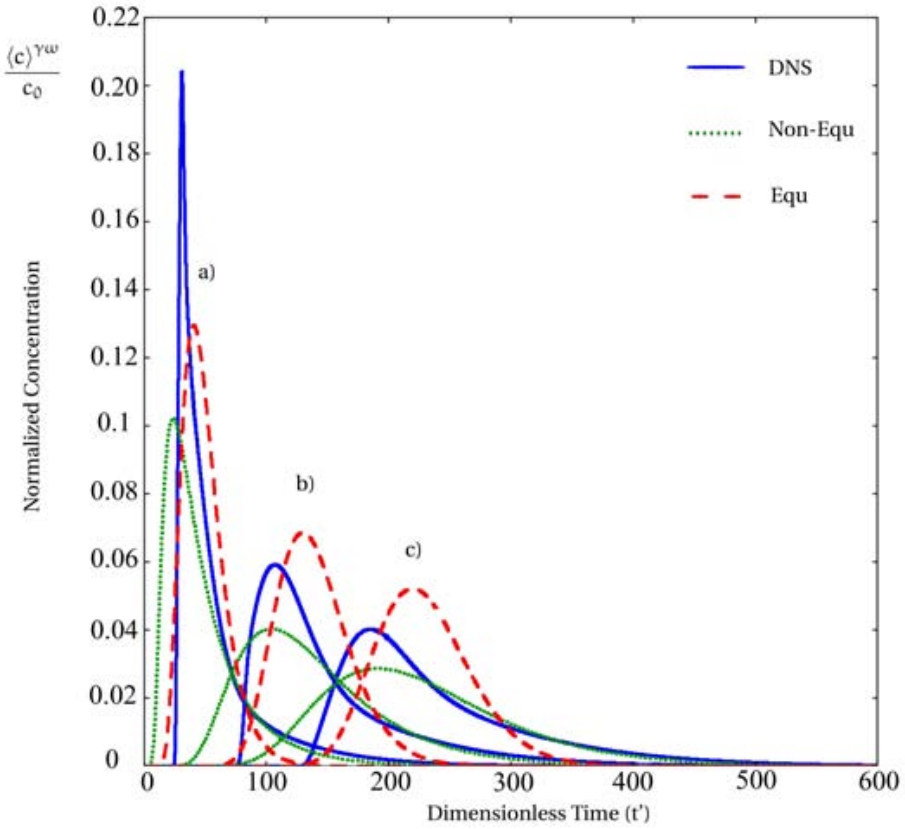

Figure 51: Transient breakthrough curves for the DNS, the local non-equilibrium and equilibrium models for a square input of $\delta t' = 5$ for $\mathscr{P}e = 1000$ and $\mathscr{D}a = 10^{-5}$ after a) $20L_c$; b) $60L_c$; c) $100L_c$

may be adhered quicker than in the low reactive case despite the shift coming from the input boundary discrepancies.

4.4 CONCLUSIONS CONCERNING THE NUMERICAL SIMULATIONS

First, we study all the effective parameters as functions of $\mathscr{P}e$ and $\mathscr{D}a$ numbers. We show that the dispersion exhibits differences between the reactive and the non-reactive case and this is coherent with other studies [143, 92, 233]. Effective reaction rate and velocities are also presented and we show that they mainly depend upon the $\mathscr{D}a$ number. We also show that the non-equilibrium model includes the local mass equilibrium one when the conditions of validity of this model are satisfied. From a theoretical point of view, one should realize that for this special case, the quasi-stationary analysis is the same for both the Gray decomposition and the non-zero averaged decomposition since the local mass equilibrium assumption means $\tilde{c}_\gamma = \hat{c}_\gamma$ and $\tilde{c}_\omega = \hat{c}_\omega$.

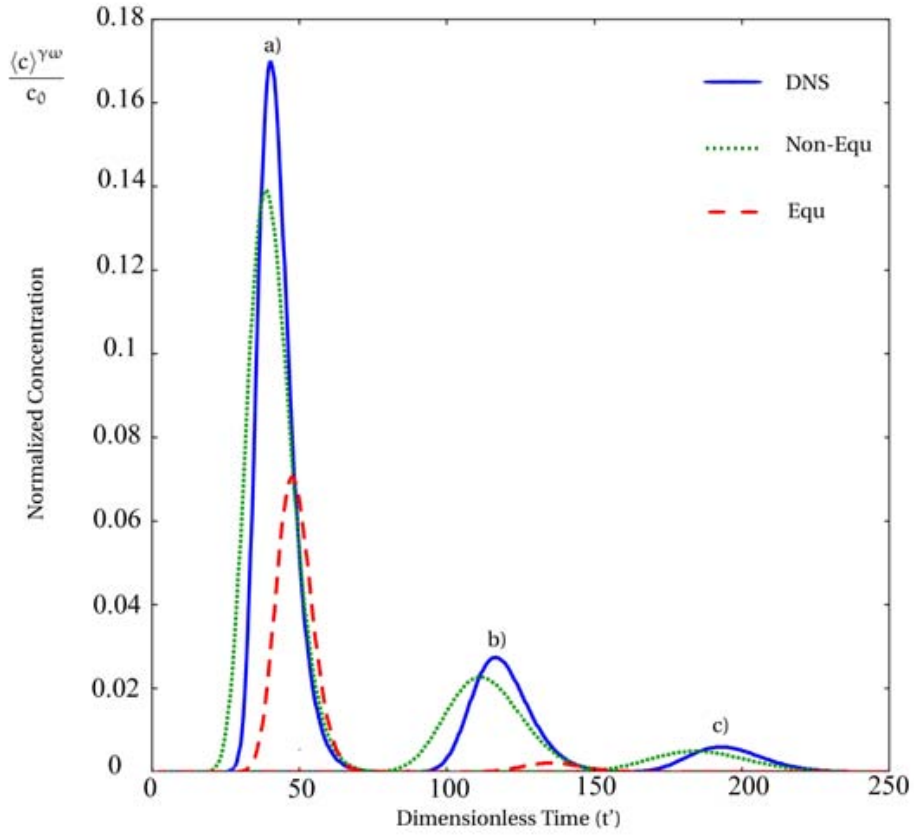

Figure 52: Transient breakthrough curves for the DNS, the local non-equilibrium and equilibrium models for a square input of $\delta t' = 5$ for $\mathscr{P}e = 100$ and $\mathscr{D}a = 100$ after a) $20L_c$; b) $60L_c$; c) $100L_c$

Then, by comparison with direct numerical simulations at the pore-scale, we show that the model is perfectly adapted to stationary analysis since this represents a special time-constrained case for which the quasi-stationarity on $\hat{c}_i$ is very well satisfied. We also establish the following limitations

- The model fails to capture very small time phenomena. Two-equations models or fully transient theories may be required in this case. The underlying consequence is that domains of validity for the different models must need a time dimension and not only dimensionless parameters such as $\mathscr{P}e$ and $\mathscr{D}a$ numbers.

- We emphasize that important discrepancies, coming from the boundary conditions, can propagate through the entire system for high $\mathscr{P}e$ and high $\mathscr{D}a$ numbers. Although, it might not propagate so far in disordered media, it requires further investigation.

There are two additional constraints which require supplementary research. The first one concerns the assumption on the reaction rate. Herein, we suppose that the

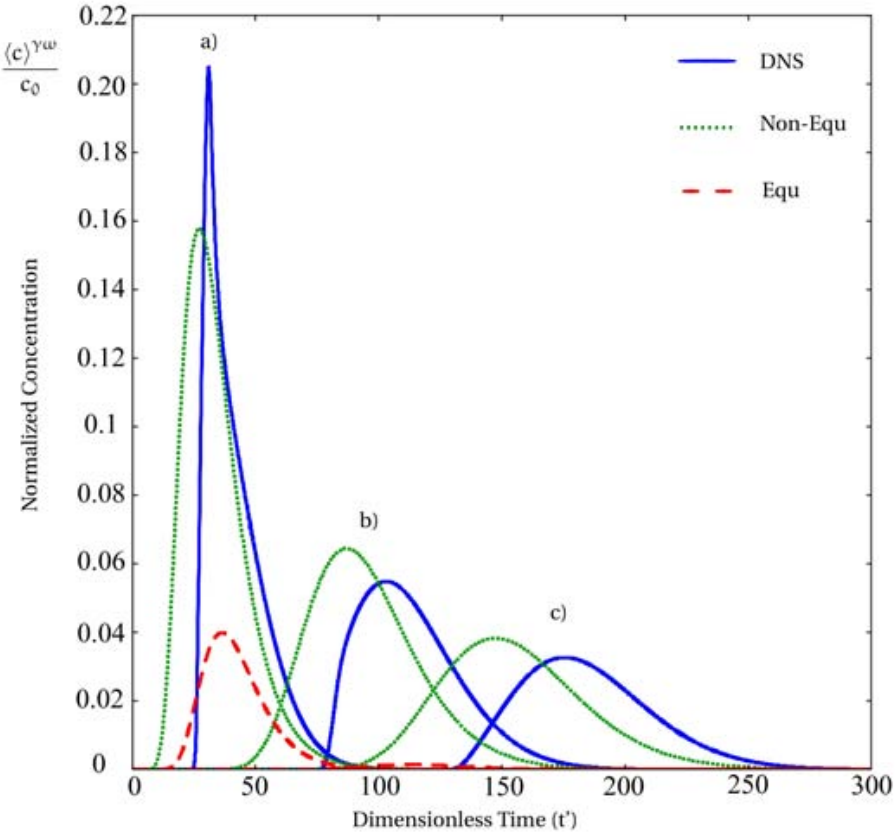

Figure 53: Transient breakthrough curves for the DNS, the local non-equilibrium and equilibrium models for a square input of $\delta t' = 5$ for $\mathscr{P}e = 1000$ and $\mathscr{D}a = 1000$ after a) $20L_c$; b) $60L_c$; c) $100L_c$

concentration of the solute is relatively small, that is, we can consider only linear kinetics. Upscaling of non-linear Monod type reaction rate in a general framework is an area of active research. The second one deals with the assumption that the effective parameters can be calculated on a REV in which the geometry of the biofilm is fixed. For example, in a real medium, one may have to consider fluctuations of the porosities or variations of the representative geometry and it is unclear how these would affect the domain of validity of the time-asymptotic model.

5

DISCUSSION AND CONCLUSIONS

5.1 RELATION TO OTHER WORKS

In this work, we derive a one-equation non-equilibrium model for solute transport in saturated and biologically reactive porous media. Undertaking the description of multiphase reactive transport using a single one equation approximation has been done countless times by experimenters. However, very few works have focused on developing a theoretical basis and on addressing the validity of this approach. Two situations allowing such a description have been identified in the past and are clarified in our study. On the one hand, when gradients within the bulk phases are relatively small, a single partial differential equation on the concentration in the water-phase can be used to described the mass transport. This situation is often referred to as the local mass equilibrium condition and has been extensively discussed in [114, 19]. On the other hand, it has been suggested that a completely different type of constraint can be formulated to allow a description with merely one equation. Cunningham and Mendoza-Sanchez in [65] have shown that the one-equation model is strictly equivalent to the multicontinuum approach under steady state conditions. This behavior has also been proved many years before in the non-reactive case by Zanotti and Carbonell in [295].

Our analysis can be seen as an extension and a complement of the works by Cunningham and Mendoza-Sanchez [65] and by Dykaar and Kitanidis [92]. In comparison with the work by Cunningham and Mendoza-Sanchez, we provide a direct link between the microscopic processes and the macroscale. Our development is based on the calculation of the effective parameters on a representative volume possibly accounting for very complex geometries. In addition to the approach by Dykaar and Kitanidis, we propose to take into account the total mass in the system rather than just the mass in the water-phase. The strategy adopted in [92] is clearly an extension of the work by Shapiro and Brenner [233] but additional constraints are necessary in the multiphase situation and this is not clearly emphasized. The domain of validity of our model is clearly established on the basis of (1) comparisons between the upscaled results and the direct numerical simulations at the pore-scale and (2) thorough discussions concerning the first-order closure and the quasi-stationarity of the problems on the perturbations.

Concerning the technique itself, we use a $\hat{c}$ decomposition for concentrations which is a more general case of the one introduced in [205] for mass transport and in [178] for heat transfer. We start our analysis with the microscale description of the medium and then average the equations to obtain a Darcy-scale description of the medium. In short times, the multidomain approach provides a better approximation of the transport processes because, the closure on the $\tilde{c}$ fluctuations captures more characteristic times and because, as previously discussed, the quasi-stationarity of the perturbation problem on $\hat{c}$ is much stronger than the one on $\tilde{c}$. In the non-reactive situation, these theoretical aspects have been extensively described in [295] and in [78] but this is the first application to a reactive situation.

5.2 GENERAL CONCLUSIONS

In past research, the calculation of effective parameters has been largely undertaken using tracer techniques and inverse optimization on the basis of simple heuristic models. The main problems with this approach are that (1) the macroscale equations are elaborated on the basis of simple conceptual schemes and it is unclear how much information these models are able to capture, (2) the effective parameters, say the dispersion, are often considered as intrinsic to a medium and not recalculated every time a physical parameter such as the Damköhler number is modified and (3) there is no clear relationship between the definition of the macroscopic concentrations and the concentration measured.

Given the advances in terms of imaging techniques and of understanding of the transport processes, we believe that deterministic upscaling represents an alternative in many cases. For example, the volume averaging theory lends itself very well for the exploration of the physics of the transport as well as for the expression of the effective parameters as a function of the microscale processes on a representative volume.

In conclusion, we provide a solid theoretical background for the one-equation model along with (1) constraints concerning its validity, (2) a method for the calculation of the effective parameters and (3) a precise definition of the macroscopic concentration. When applying the model to experimental results, these three points should be carefully examined.

Part V

CONCLUSIONS, ONGOING WORK AND PERSPECTIVES

1

CONCLUSIONS

Here, we only briefly summarize the different conclusions specific to each part of the thesis. We are primarily interested in the global strategy, and focus, in the next section, on ongoing work and perspectives.

In this thesis, our goal is to understand and model transport phenomena in porous media with biofilms. The work presented is based on experimental, theoretical and numerical analyses that provide an interesting novel framework for the study of these complex systems. First, we present a method for imaging biofilm within opaque porous media, in part II. This technical breakthrough, entirely developed during the thesis, uses X-ray computed microtomography, in conjunction with a selection of specific radiocontrast agents, to obtain a three-dimensional reconstitution of the biofilm/porous-structure (water-phase, biofilm-phase and grain-phase) with a voxel size down to 9 μm. This approach provides a promising framework to study the growth of biofilms within porous structures as well as the response of the microorganisms to different stimuli and environmental conditions.

On the basis of this information, we propose a modeling strategy for the transport of solutes in porous media with biofilms. As discussed in the part I, this MVMV approach follows four steps:

1. image pore-scale biofilms growth within porous structures and formulate equations that describe the various pore-scale phenomena.

2. incorporate these components in efficient pore-scale models based, for example, on Lattice–Boltzmann formulations (e.g., [116]) and validate the proposed mathematical descriptions.

3. upscale the set of differential equations (from the pore-scale to the Darcy-scale, eg. parts III and IV) in order to obtain different macroscale models and calculate effective parameters on the basis of 3-D realistic geometries.

4. develop the domains of validity of the various upscaled models, and validate the theoretical analysis against Darcy-scale experiments.

In this strategy, the equations that are used at the microscale are validated by comparing direct numerical results (cellular automata or individual-based modeling) against

three-dimensional observations. In addition, upscaled models are also studied and validated against Darcy-scale experiments. While such an approach would be extremely interesting, fully performing the four different steps remains very complex and this problem has not been tackled yet. In our study, we use a shortcut to this approach, that is, we consider a theoretical situation for which the pore-scale equations are well-known. On this basis, we devise a macrotransport theory for the transport of non-reactive as well as biodegraded solutes within porous media colonized by biofilms. To filter information from the pore-scale/biofilm-scale, we use the classical volume averaging with closure theory, a new average/fluctuation decomposition and the spatial moments matching technique. Various Darcy-scale models are developed, along with their domains of validity and numerical illustrations. If other microscale *linear* situations were to be considered, it would be possible to adapt this theory in order to develop the corresponding macroscale equations.

Ongoing works include the development of numerical tools to calculate the effective parameters on the 3-D image conjointly with other experimental and theoretical developments. These perspectives are presented in the next sections.

2

ONGOING WORK AND PERSPECTIVES

2.1 NUMERICAL PERSPECTIVES

2.1.1 *Calculation of effective properties*

While the X-ray tomography technique only captures the spatial distribution of phases with contrasted attenuation coefficients, numerical calculations can be used in order to recover more information. For example, one can directly solve Stokes equations on the images captured by the X-ray tomography technique to obtain the velocity field. Two examples are given on Fig. (54) . We use the images obtained before and after biofilm growth on a single polyamide bead. A finite volume formulation is used based on Uzawa's algorithm (e.g. [206]). Boundary conditions consist in a pressure gradient from the bottom to the top (z-direction) and periodic conditions for the others. The magnitude of the velocity field (arrows) Figs (54) (a) and (b) is found to be maximum along the edges parallel to the z-direction, essentially because this corresponds to the largest water-path within the bead array (periodic boundary conditions). Figs (54) (c) and (d) show the differences induced by the growth of biofilm within the vicinity of the surface of the bead.

On Fig. (55), we use a numerical configuration rather similar to our experimental device part II. We solve Stokes equation on images obtained after 10 days of biofilms growth. Both columns are alimented using the same water supply (identical microorganisms and nutrients thereof). However, the column corresponding to Fig. (55a) has a flow rate of approximately 0.85 ml/s while the one corresponding to Fig. (55b) is about 0.05 ml/s. As a consequence of the shear stress induced by the water flow, the porosity of column (a) is about 0.366 whereas the porosity of column (b) is about 0.240. Using these results, we can also compute the permeability of the two columns, respectively $1.630\ 10^{-5}$ and $1.437\ 10^{-5} m^2$ for columns (a) and (b). While the relative difference in permeability is only about 10 %, the pattern of biofilm growth is very different. In column (a) the growth is relatively uniform, that is, biofilm develops within area protected from the shear stress and the velocity field is poorly perturbed by the microbes Fig. (55a). Within column (b) the flow follows preferential pathways along the column Fig. (55b), that is, the biofilm is growing mainly in the center of the column. Initially, there is probably higher local velocities nearby the wall because,

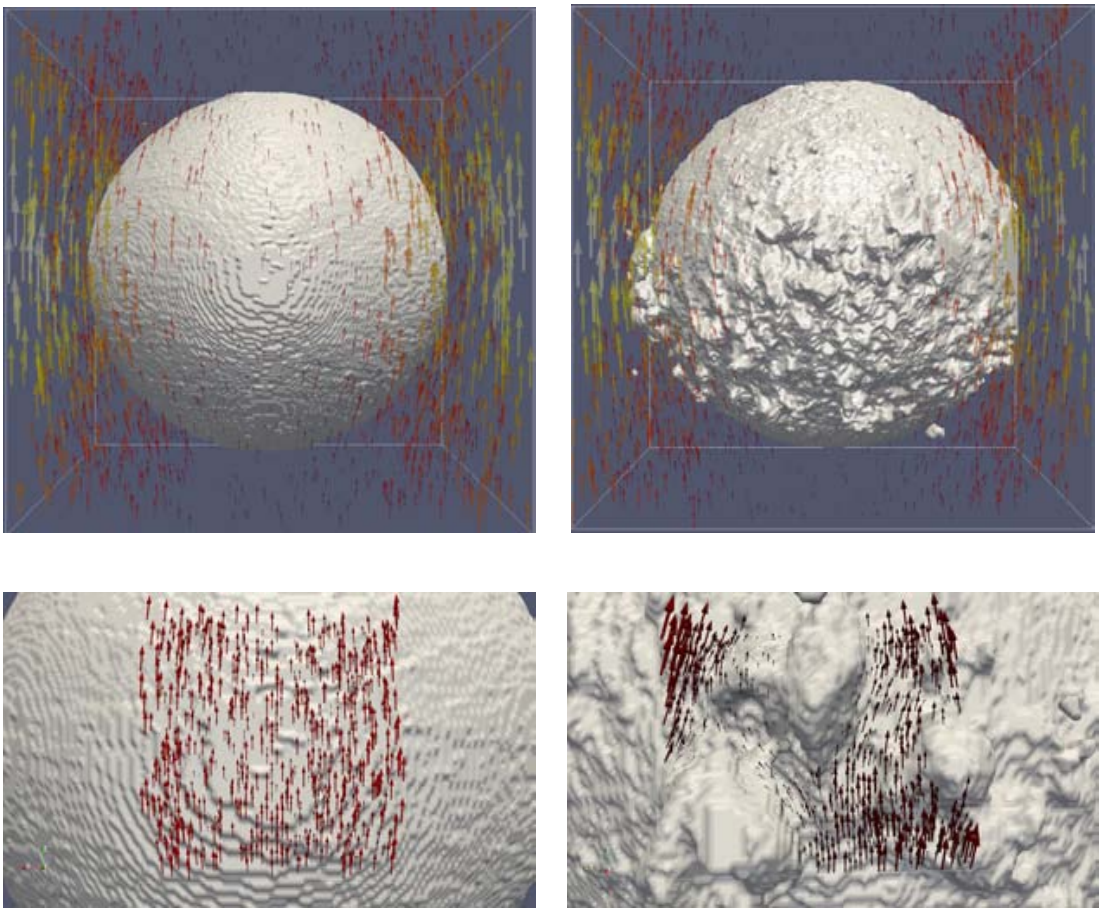

Figure 54: Calculation of the velocity field (resolution of Stokes equation) using a finite volume formulation (250x250x250 meshes).

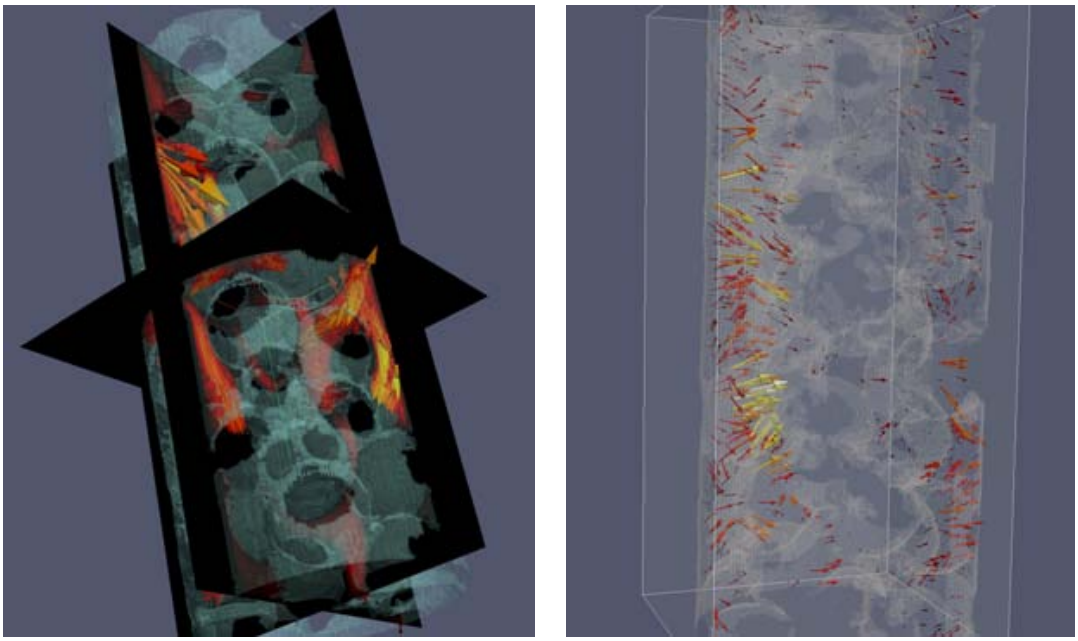

Figure 55: Calculation of the velocity field (resolution of Stokes equation) using a finite volume formulation (171x171x300 meshes).

locally, the bead packing is perturbed. Hence, the formation of biofilms might preferentially start in the center of the column, inducing the formation of preferential pathways for the flow. These results are given as an illustration of the effectiveness of this kind of calculations, and must be taken extremely precautiously. Generalization of such behaviors in rich nutrients conditions would require further experiments on various species and multiple replicates.

Following the same line, one could solve the closure problems developed in Parts III and IV, to obtain the effective parameters associated with the dispersive macroscale equations. The local mass equilibrium dispersion tensor as well as the one-equation non-equilibrium dispersion tensor or two-equations effective parameters can be solved directly on realistic porous media, and not only on simple 2-D geometries.

2.1.2 *Pore-network modeling ?*

One caveat when using directly images obtained through X-ray tomography is the potential size of the data. For example, on Figs. (54) and (55), we subsampled the data set to obtain a voxel size of 18 μm to compute the results within a reasonable amount of time. One solution to this issue would be to consider pore-network representation of the three-dimensional tomography image. A huge amount of image processing softwares have been developed to undertake this step, that is, to obtain the skeleton and a pore-network representation (often spheres connected by cylinders, see for

example [86]). Developing such algorithms for the biofilm problem is rather challenging as one would have to formulate algorithms that would be appropriate for the resolution of Navier-Stokes equations but also to the dual-phase closure problems. One could, for example, create two nested spheres and cylinders to delineate the fluid, the biofilm and the solid. One alternative could also be to develop a fully parallelized code than can be used to calculate effective parameters on extremely large data sets, using powerful CPU clusters.

2.1.3 *Adaptative macrotransport calculations*

Most of the numerical applications of upscaled models to experimental data use one single formulation that applies for one specific experiment. However, in many cases, the initial microscale problem that is considered is similar. It would be extremely interesting to develop codes that can adapt the formulation to the parameters of the problem. One could, for example, design a program that uses convolutions, three-equation, two-equation or one-equation models on the basis of internal constraints regarding the physical parameters at play. This would allow the development of one single code that can be used in, virtually, evey similar problem of mass transport (under the condition that the microscale formulation is identical).

2.2 EXPERIMENTAL PERSPECTIVES

2.2.1 *Controlling the microbial species in order to study responses to various environmental stresses*

While presenting the imaging work in various conferences, there has been some interest regarding the specific bacterial species and strains that were used. In our experiments, we amended water from the Garonne and used this to inoculate our porous systems. On the one hand this means that we do not control the species that are present in our system. On the other hand, it also means that our method is versatile and does not require an a priori staining of the cells. Anyways, working with specific species is required in order to draw conclusions regarding the behavior of specific biofilms. Recently, we started collaborations with E. Paul, Y. Pechaud from the LISBP (INSA Toulouse) and P. Creux, F. Guerton from the University of Pau, to tackle this issue.

A general view of the experimental device can be found on Fig . (56). E. Coli was introduced within the porous systems (packed glass beads to have an initial contrast between the solid phase and the water/biofilm phases) and set at rest for 24 hours. Then, various flow rates were imposed within the columns using peristaltic pumps as well as refrigerated (to avoid the formation of other organisms) and aerated (using an air pump) water mixed with nutrients. The nutrients were introduced in large excess

and consisted in a buffered solution of glucose. Oxygen consumption and pH were also followed at the output of the column.

One single test experiment has been performed and this still represents ongoing incomplete work. Full results are not available yet, but from observations made with the naked eye, it seemed that more biofilm has developed in the high flow rate experiment, as opposed to the experiment part II. Three-dimensional imaging has been done on a Skyscan 1172 (100kV), because glass materials require high energy beams. Several technical problems need to be tackled, before the reconstructed images can be used for quantitative analysis. For example, settling was observed within the barium sulfate suspension as a result of 20 times dilutions (to avoid an acquisition of several hours). The Micropaque (Guerbet) contains other components in small quantities that might avoid settling and might be inefficient in low concentrations.

2.2.2 *Imaging*

DYNAMIC GROWTH MONITORING The imaging technique as used in this thesis is not destructive, but still terminal as explained in detail in part II. Hence, it can not be used to follow the growth of the biomass within one single column. One could use various replicates, and sacrifice one column every given time step. However, such experiments would require an additional complexity and this is not necessarily simple to realize. In addition, following the same column would give more pore-scale information regarding the growth, even though the averaged parameters should be similar. Developing a dynamic imaging of biofilms growth within opaque porous media is still a problem that requires further attention.

SYNCHROTRON SOURCES While using benchmark tomograph is more accessible than synchrotron sources, materials such as glass or rock would be easier to image with high brilliance X-ray sources. In addition, one could use high concentration of contrast agents and avoid the settling problem. Such synchrotron experiments will be performed in November 2010, at the Argonne National Laboratory (Chicago) in collaboration with D. Wildenschild and G. Iltis from the Oregon State University.

2.2.3 *Darcy-scale experiments*

For the validation and test of the macroscale models as developed in part III and IV, it would be extremely useful to perform Darcy-scale experiments, in controlled environments. Such devices would also provide the information that is required in order to understand biofilm growth and to model it on a larger scale. On Fig (57), one can see a human-sized column that has been designed during this thesis, and that will be used for such purposes.

Figure 56: Experimental device used at the LISBP.

Figure 57: Human sized column filled with expanded polystyrene beads (IMFT)

2.3 THEORETICAL PERSPECTIVES

2.3.1 *Non-linearity*

One of the main approximation that has been made in part IV, is to assume a linear reaction rate within the biofilm matrix. While such an approximation is thoroughly discussed and has been used countless times, this is mainly a result of our incapacity to upscale non-linear terms. Developing upscaling techniques that apply to non-linear reaction rates would be extremely useful. One solution that can be adopted is to decompose the medium into virtual phases (for example three or four phases for the biofilm problem).

To understand this approach, we can simply express the reaction rate the following way

$$\mathscr{R}_i(c_i) = \mathscr{R}_i(\langle c_i\rangle^i + \tilde{c}_i) = \mathscr{R}_i(\langle c_i\rangle^i) + \dot{\mathscr{R}}_i(\langle c_i\rangle^i)\tilde{c}_i + \mathscr{O}\left(\tilde{c}_i^2\right)$$

The main problem, is that, in a general case, the terms $\dot{\mathscr{R}}_i(\langle c_i\rangle^i)\tilde{c}_i + \mathscr{O}\left(\tilde{c}_i^2\right)$ are non-linear and a closure to the perturbation problem is not straightforward. One has a solution to this issue when

1. the term $\mathscr{R}_i(c_i)$ is linear in relation to c_i.
2. the term $\mathscr{R}_i(c_i)$ is non-linear in relation to c_i and $\dot{\mathscr{R}}_i(\langle c_i\rangle^i)\tilde{c}_i + \mathscr{O}\left(\tilde{c}_i^2\right)$ can be neglected as compared to $\mathscr{R}_i(\langle c_i\rangle^i)$.

To satisfy the proposition number two, we need $\tilde{c}_i$ as small as possible, to approximate the reaction rate by its zeroth order Taylor approximation. One way to lower the pointwise values of $\tilde{c}_i$ is to create additional virtual phases. The obvious counterpart is that we filter less information from the microscale and, as a consequence, the problem will be more complex.

2.3.2 *Adaptative macrotransport theory*

Usually, the choice of using one-equation, two-equation models is rather intuitive. For example, even in a single-phase situation, one can consider two-equation models for momentum Darcy-scale transport, if dead-end pores represent a significative part of the pore space. In essence, this means that this is not the physical phases that are important, but rather the topology of the physical processes.

As an alternative to this heuristic fictive separation, one could, for example, solve numerically the microscale equations or a simpler problem (to be determined) on several REVs (rather than on the entire system), in order to obtain more information from the REV, that is, to get a view of the topology of the processes.

2.3.3 *Mobile interfaces and growth/transport coupling*

In all the different models presented during this thesis, interfaces are immobile. In other words, we assume that the characteristic times for biofilm growth is very large as compared to times associated with transport phenomena. This means that, at any given time, one can use effective properties that are constant over time (however, notice that this does not solve the problem of determining laws that apply to the effective parameters as functions of a larger time scale and this requires additional considerations).

Even though this approximation is verified in most cases (discussed extensively, especially in part IV), there certainly arise situations for which both times are of the same order of magnitude and a coupling would be mandatory. In such cases, it would be interesting to couple the biofilm motion with the mass transport phenomena, to understand the dynamics of effective parameters variations. One could, for example, couple cellular automata with upscaling techniques. Another possibility would be to image dynamically the porous medium with biofilm. One other way around would be to devise a downscaling technique that can recover the pore-scale geometry of the biofilm, in the condition that, say, the mass exchange coefficient is maximized and the averaged shear stress is minimized. One interest of the last proposition is that one would be able to identify what are the macroscopic parameters that drive biofilm growth.

2.3.4 *And the other scales ?*

In this work, we are particularly interested in upscaling from the pore-scale/biofilm-scale to the Darcy-scale, albeit we generalize the upscaling process in part III, in the case of non-reactive solute transport. As previously discussed, one of the main assumption of our developments is the form of the microscale problem that is used. Upscaling using volume averaging with closure necessarily requires that the boundary value problems that describes the phenomena of interest are well described at a given scale. One could start, for example, on a cellular or even on molecular-scale. The convection-diffusion problem considered in this thesis is known to be an excellent description of the processes as there has been substantial experimental support for this approximation.

However, there are many other scales that require further attention. For example, one could consider upscaling from the pore-scale to the Darcy-scale in a dual-phase configuration and then to a larger heterogeneous dual-region medium, to obtain four-equation models. One other interesting area of research concerns channeled biofilms. There has been some work regarding this physical problem [11]. However, this requires further investigation, and calculating effective parameters of biofilms on the basis of direct 3-D images of the channels, using for example X-ray microtomography, would considerably help in apprehending their function within biofilms.

Part VI

REFEREED PUBLICATIONS BY THE AUTHOR

Advances in Water Resources 33 (2010) 1075–1093

Contents lists available at ScienceDirect

Advances in Water Resources

journal homepage: www.elsevier.com/ locate/advwatres

Modeling non-equilibrium mass transport in biologically reactive porous media

Yohan Davit [a,c,*], Gérald Debenest [a,b], Brian D. Wood [d], Michel Quintard [a,b]

[a] Université de Toulouse; INPT, UPS; IMFT (Institut de Mécanique des Fluides de Toulouse) Allée Camille Soula F-31400 Toulouse, France
[b] CNRS; IMFT F-31400 Toulouse, France
[c] Université de Toulouse; INPT, UPS; ECOLAB Rue Jeanne Marvig F-31055 Toulouse, France
[d] School of Chemical, Biological, and Environmental Engineering, Oregon State University, Corvallis, OR 97331, United States

ARTICLE INFO

Article history:
Received 22 September 2009
Received in revised form 20 June 2010
Accepted 22 June 2010
Available online 30 June 2010

Keywords:
Porous media
Biofilms
Upscaling
Volume averaging
Non-equilibrium
One-equation model

ABSTRACT

We develop a one-equation non-equilibrium model to describe the Darcy-scale transport of a solute undergoing biodegradation in porous media. Most of the mathematical models that describe the macroscale transport in such systems have been developed intuitively on the basis of simple conceptual schemes. There are two problems with such a heuristic analysis. First, it is unclear how much information these models are able to capture; that is, it is not clear what the model's domain of validity is. Second, there is no obvious connection between the macroscale effective parameters and the microscopic processes and parameters. As an alternative, a number of upscaling techniques have been developed to derive the appropriate macroscale equations that are used to describe mass transport and reactions in multiphase media. These approaches have been adapted to the problem of biodegradation in porous media with biofilms, but most of the work has focused on systems that are restricted to small concentration gradients at the microscale. This assumption, referred to as the *local mass equilibrium* approximation, generally has constraints that are overly restrictive. In this article, we devise a model that does not require the assumption of local mass equilibrium to be valid. In this approach, one instead requires only that, at sufficiently long times, anomalous behaviors of the third and higher spatial moments can be neglected; this, in turn, implies that the macroscopic model is well represented by a convection–dispersion–reaction type equation. This strategy is very much in the spirit of the developments for Taylor dispersion presented by Aris (1956). On the basis of our numerical results, we carefully describe the domain of validity of the model and show that the *time-asymptotic constraint* may be adhered to even for systems that are not at local mass equilibrium.

1. Introduction

Biodegradation in porous media has been the subject of extensive studies from the environmental engineering point of view [1–5]. Reactions are mediated by microorganisms (primarily bacteria, fungi, archaea, and protists, although others may be present) aggregated and coated within an extracellular polymeric matrix; together, these which form are generically called biofilms. There has been significant interest for their role in bioremediation of soils and subsurfaces [6–12] and, more recently, for their application to supercritical CO_2 storage [13,14]. Numerous models for describing the transport of solutes, such as organic contaminants or injected nutrients, through geological formations as illustrated in Fig. 1, have been developed. Reviews of these mathematical and physical representations of biofilms processes can be found in [15] and [16].

1.1. One-equation local mass equilibrium model

In many applications, the macroscopic balance laws for mass transport in such hierarchical porous media with biofilms have been elaborated by inspection. For example, the advection–dispersion–reaction type Eq. (1) is commonly considered to describe the Darcy-scale transport of a contaminant/nutrient represented by a concentration $\langle c_\gamma \rangle^\gamma$ in the water γ-phase. Brackets notations are here as a reminder that this concentration must be defined in some averaged sense.

$$\frac{\partial \langle c_\gamma \rangle^\gamma}{\partial t} + \langle \mathbf{v}_\gamma \rangle^\gamma \cdot \nabla \langle c_\gamma \rangle^\gamma = \nabla \cdot \left(\mathbf{D} \cdot \nabla \langle c_\gamma \rangle^\gamma \right) + \mathcal{R} \tag{1}$$

In this expression, $\langle \mathbf{v}_\gamma \rangle^\gamma$ is the groundwater velocity and $\mathbf{D}$ is a dispersion tensor. The reaction rate $\mathcal{R}$ is usually assumed to have a Monod form $\mathcal{R} = -\alpha \frac{\langle c_\gamma \rangle^\gamma}{\langle c_\gamma \rangle^\gamma + \mathcal{K}}$, where α and $\mathcal{K}$ are parameters (discussed in Section 3.5). It is common to assume that the solute transport can be uncoupled from the growth process [17,18], that is, to consider that the characteristic times for these two processes are

* Corresponding author. Université de Toulouse; INPT, UPS; IMFT (Institut de Mécanique des Fluides de Toulouse) Allée Camille Soula F-31400 Toulouse, France.
E-mail addresses: davit@cict.fr (Y. Davit), debenest@imft.fr (G. Debenest), brian.wood@oregonstate.edu (B.D. Wood), quintard@imft.fr (M. Quintard).

0309-1708/$ – see front matter © 2010 Elsevier Ltd. All rights reserved.
doi:10.1016/j.advwatres.2010.06.013

International Journal of Heat and Mass Transfer 53 (2010) 4985–4993

Contents lists available at ScienceDirect

International Journal of Heat and Mass Transfer

journal homepage: www.elsevier.com/locate/ijhmt

Equivalence between volume averaging and moments matching techniques for mass transport models in porous media

Yohan Davit [a], Michel Quintard [a,b], Gérald Debenest [a,b,c,*]

[a] Université de Toulouse, INPT, UPS, IMFT (Institut de Mécanique des Fluides de Toulouse), Allée Camille Soula, F-31400 Toulouse, France
[b] CNRS, IMFT, F-31400 Toulouse, France
[c] Ecolab UMR 5245 (INP-ENSAT, UPS, CNRS), Equipe ECOGEN, Av. de l'Agrobiopole, BP 32607 Auzeville Tolosane, 31326 Castanet Tolosan Cedex, France

ARTICLE INFO

Article history:
Received 13 July 2009
Received in revised form 3 March 2010
Accepted 9 April 2010
Available online 14 June 2010

Keywords:
Porous media
Non-equilibrium
Two-equation model
Moments
Time-asymptotic
Volume averaging

ABSTRACT

This paper deals with local non-equilibrium models for mass transport in dual-phase and dual-region porous media. The first contribution of this study is to formally prove that the time-asymptotic moments matching method applied to two-equation models is equivalent to a fundamental deterministic perturbation decomposition proposed in Quintard et al. (2001) [1] for mass transport and in Moyne et al. (2000) [2] for heat transfer. Both theories lead to the same one-equation local non-equilibrium model. It has very broad practical and theoretical implications because (1) these models are widely employed in hydrology and chemical engineering and (2) it indicates that the concepts of volume averaging with closure and of matching spatial moments are equivalent in the one-equation non-equilibrium case. This work also aims to clarify the approximations that are made during the upscaling process by establishing the domains of validity of each model, for the mobile–immobile situation, using both a fundamental analysis and numerical simulations. In particular, it is demonstrated, once again, that the local mass equilibrium assumptions must be used very carefully.

1. Introduction

In this paper, we investigate the behavior of widely used models, especially in subsurface hydrology, for describing the transport of a tracer through dual-phase and dual-region porous media similar to those presented in Fig. 1. At the microscopic scale (pore-scale or Darcy-scale in this article), these two systems are usually thought as two continua, in which advection and Fickian diffusion/dispersion are dominant. Upscaling mass balanced equations from the pore-scale to the Darcy-scale in a dual-phase porous medium is, mathematically speaking, equivalent to upscaling from the Darcy-scale to the large-scale in a dual-region porous medium. Hence, in this work, we consider a general framework defined by the mathematical structure of the boundary-value problem at the small scale rather than by the scale itself and the corresponding physical phenomena.

A general solution to the dispersion problem at the macroscopic scale exhibits time and spatial convolutions (non-locality) [3–8]. Direct Numerical Simulations can be used to get an accurate response, but it is not often tractable for most of porous systems because of the complexity involved. Degraded models, but still rather accurate if one is concerned with the estimate of the flux exchanged between the different phases/regions, can be derived under the form of mixed models for mobile/immobile systems, i.e. systems with high diffusivity contrast and no advection in the low diffusivity phase/region [9–12]. In many practical applications, relevant constraints can be formulated concerning characteristic times and length scales [13], that is, when the different length scales of the system are separated by several orders of magnitude, non-local effects tend to disappear. One way of describing the transport while conserving partly the convolutions effects consists in using a two-equation quasi-stationary model (Eqs. (1) and (2)) involving two macroscopic concentrations, one for each phase/region γ and ω. Herein, the bracket notation is used as a reminder that concentrations appearing in the macroscopic equations are defined in a volume averaged sense. ε_i is the volume fraction of the *i-phase/region* and the star notation refers to the model effective parameters. In particular, α^{**} is a first order mass exchange coefficient.

Two-equation model:

$$\varepsilon_\gamma \partial_t \langle c_\gamma \rangle^\gamma + \mathbf{V}^{**}_{\gamma\gamma} \cdot \nabla \langle c_\gamma \rangle^\gamma + \mathbf{V}^{**}_{\gamma\omega} \cdot \nabla \langle c_\omega \rangle^\omega = \nabla \cdot \left\{ \mathbf{D}^{**}_{\gamma\gamma} \cdot \nabla \langle c_\gamma \rangle^\gamma \right\} + \nabla \cdot \left\{ \mathbf{D}^{**}_{\gamma\omega} \cdot \nabla \langle c_\omega \rangle^\omega \right\} - \alpha^{**} \left\{ \langle c_\gamma \rangle^\gamma - \langle c_\omega \rangle^\omega \right\} \quad (1)$$

* Corresponding author at: Université de Toulouse, INPT, UPS, IMFT (Institut de Mécanique des Fluides de Toulouse), Allée Camille Soula, F-31400 Toulouse, France.
E-mail addresses: davit@cict.fr (Y. Davit), quintard@imft.fr (M. Quintard), debenest@imft.fr (G. Debenest).

0017-9310/$ - see front matter © 2010 Elsevier Ltd. All rights reserved.
doi:10.1016/j.ijheatmasstransfer.2010.05.032

Journal of Microscopy, 2010
Received 29 October 2009, accepted 14 June 2010
doi: 10.1111/j.1365-2818.2010.03432.x

Imaging biofilm in porous media using X-ray computed microtomography

Y. DAVIT*‡,G. ILTIS||, G. DEBENEST*,†,
S. VERAN-TISSOIRES*, D. WILDENSCHILD||, M. GERINO‡,§
& M. QUINTARD*,†
*Université de Toulouse; INPT, UPS; IMFT(Institut de Mécanique des Fluides de Toulouse), Allée Camille Soula Toulouse, France
†CNRS; IMFT F-31400 Toulouse, France
‡Université de Toulouse; INPT, UPS; ECOLAB Rue Jeanne Marvig F-31055 Toulouse, France
§CNRS; ECOLAB F-31055 Toulouse, France
||School of Chemical, Biological, and Environmental Engineering, Oregon State University Corvallis, Oregon, U.S.A.

Key words: Biofilm, imaging, porous media, X-ray tomography.

Summary

In this study, a new technique for three-dimensional imaging of biofilm within porous media using X-ray computed microtomography is presented. Due to the similarity in X-ray absorption coefficients for the porous media (plastic), biofilm and aqueous phase, an X-ray contrast agent is required to image biofilm within the experimental matrix using X-ray computed tomography. The presented technique utilizes a medical suspension of barium sulphate to differentiate between the aqueous phase and the biofilm. Potassium iodide is added to the suspension to aid in delineation between the biofilm and the experimental porous medium. The iodide readily diffuses into the biofilm while the barium sulphate suspension remains in the aqueous phase. This allows for effective differentiation of the three phases within the experimental systems utilized in this study. The behaviour of the two contrast agents, in particular of the barium sulphate, is addressed by comparing two-dimensional images of biofilm within a pore network obtained by (1) optical visualization and (2) X-ray absorption radiography. We show that the contrast mixture provides contrast between the biofilm, the aqueous-phase and the solid-phase (beads). The imaging method is then applied to two three-dimensional packed-bead columns within which biofilm was grown. Examples of reconstructed images are provided to illustrate the effectiveness of the method. Limitations and applications of the technique are discussed. A key benefit, associated with the presented method, is that it captures a substantial amount of information regarding the topology of the pore-scale transport processes. For example, the quantification of changes in porous media effective parameters, such as dispersion or permeability, induced by biofilm growth, is possible using specific upscaling techniques and numerical analysis. We emphasize that the results presented here serve as a first test of this novel approach; issues with accurate segmentation of the images, optimal concentrations of contrast agents and the potential need for use of synchrotron radiation sources need to be addressed before the method can be used for precise quantitative analysis of biofilm geometry in porous media.

Correspondence to: Yohan Davit, Université de Toulouse; INPT, UPS; IMFT (Institut de Mécanique des Fluides de Toulouse), Allée Camille Soula F-31400 Toulouse, France. Tel: +33-5-3432-2882; fax: +33-5-3432-2993; e-mail: davit@cict.fr

Introduction

Microorganisms (primarily bacteria, fungi and algae), in wet or aqueous environments, tend to aggregate and grow on surfaces, embedded within extracellular polymeric substances (EPS) (Costerton *et al.*, 1995; Sutherland 2001). These sessile communities, termed biofilms, are ubiquitous in industry (Ganesh Kumar & Anand 1998), in medicine and natural environments (Hall-Stoodley *et al.*, 2004). Biofilm cells, when compared with planktonic cells, have been documented to be more resistant to antibiotics and biocides (Costerton *et al.*, 1999; Stewart, 2001; Davies, 2003; Hall-Stoodley *et al.*, 2004). Hence, the development of biofilms can have undesirable and potentially harmful consequences in medical applications (Diosi *et al.*, 2003; Lee & Kim, 2003), but can also be useful in natural or engineered systems such as wastewater treatment processes (Lazarova & Manem, 2000), bioremediation (Rittmann *et al.*, 2000) or CO_2 storage (Mitchell *et al.*, 2009). In medical, natural, as well as engineered systems, biofilm control strategies, based on a better understanding of biofilm growth characteristics as well

A Letters Journal Exploring the Frontiers of Physics

September 2008

EPL, **83** (2008) 64001
doi: 10.1209/0295-5075/83/64001

www.epljournal.org

Intriguing viscosity effects in confined suspensions: A numerical study

Y. Davit and P. Peyla[a]

Laboratoire de Spectrométrie Physique, Université Joseph Fourier - Grenoble 1, BP87, F-38402 Saint Martin d'Hères, France, EU

received 6 May 2008; accepted in final form 4 August 2008
published online 9 September 2008

PACS 47.57.E- – Suspensions
PACS 47.57.Qk – Rheological aspects
PACS 47.11.-j – Computational methods in fluid dynamics

Abstract – The effective viscosity of dilute and semi-dilute suspensions in a shear flow in a microfluidic configuration is studied numerically. The suspension is composed of monodisperse and non-Brownian hard spherical buoyant particles confined between two walls in a shear flow. An abrupt change of the viscosity behaviour occurs with strong confinements: when the wall-to-wall distance is below five times the radius of the particles, we obtain a change of the sign of the contribution of the hydrodynamic interactions to the effective viscosity. This effect is the macroscopic counterpart of the peculiar micro-hydrodynamics of confined suspensions due to the influence of walls. In addition, for higher concentrations (above 25%), we find that the viscosity meets a minimum when the inter-wall distance is around five times the sphere radius. This phenomenon is reminiscent of the Fahraeus-Lindqvist effect for blood confined in small capillaries. However, we show that for sheared confined semi-dilute suspensions, the physical origin of this minimum is not due to a migration effect but to the change of hydrodynamic interactions.

Introduction. – Solid particles suspended in a conventional liquid form a suspension. This composite fluid constitutes a widespread fluid material in nature as well as in industry [1]. The particles can be spatially confined in porous media, in biological capillaries or in microfluidic devices [2]. In these situations, rheological phenomena due to interactions between device boundaries and fluid constituents become much more important than in conventional cases. These interactions of hydrodynamic origin play a crucial role, particularly, they appear to affect notably the effective viscosity $\langle\eta\rangle_{eff}$ of confined sheared suspensions as shown in this letter. Of course, considering microfluidics devices, pressure-driven flows are very important. However, in order to understand the role of the walls on hydrodynamic interactions, it is preferable to study a suspension in a simple shear geometry in order to estimate its effective viscosity. In addition, it should allow rheologists to easily compare their experimental results with our numerical predictions.

It is well known that the relative viscosity of a semi-dilute sheared suspension follows a virial expansion:

$$\frac{\Delta\eta}{\eta_0} = \frac{\langle\eta\rangle_{eff} - \eta_0}{\eta_0} = [\eta]_1\phi + [\eta]_2\phi^2 + \mathcal{O}(\phi^3), \qquad (1)$$

where ϕ is the volume fraction defined as the volume of the particles normalized to the total volume of the suspension and η_0 is the viscosity of the fluid. For a non-confined suspension of hard spheres, the linear term (the intrinsic viscosity) is $[\eta]_{1,\infty} = 2.5$ as calculated by Einstein [3] for a strong dilution (*i.e.* particles are far enough not to interact with each other through hydrodynamics). Subscript ∞ indicates that we refer to non-confined suspensions. When increasing ϕ, the semi-dilute regime is reached, the particles get closer than in the dilute regime and start to interact hydrodynamically. Batchelor and Green [4] showed that the hydrodynamic interactions contribute to the second order in ϕ. They found $[\eta]_{2,\infty} = 5.2 \pm 0.3$ for a non-confined and non-Brownian suspension where the particles are uniformly distributed. Since then, a more precise estimation of $[\eta]_{2,\infty} = 5.0$ has been achieved by Cichoki and Felderhof [5].

We find that when the wall-to-wall distance (or gap) w decreases, the linear term $[\eta]_1$ (dominant for strongly dilute cases, *i.e.* $\phi \ll 1$) increases. This is due to dissipation which is enhanced for smaller gaps. However,

[a] E-mail: philippe.peyla@ujf-grenoble.fr

Part VII

APPENDIX

A

MATHEMATICAL DEVELOPMENT FOR THE TWO-EQUATION NON-REACTIVE MODEL

In this Appendix, we develop the volume averaged equations for each phase. We start with the microscale description of the medium associated with Fig (58).

$$\gamma-\text{phase}: \qquad \frac{\partial c_\gamma}{\partial t}+\boldsymbol{\nabla}\cdot(\mathbf{v}_\gamma c_\gamma)=\boldsymbol{\nabla}\cdot(\mathbf{D}_\gamma\cdot\boldsymbol{\nabla}c_\gamma) \tag{A.1}$$

$$\text{BC1}: \quad -(\mathbf{n}_{\gamma\sigma}\cdot\mathbf{D}_\gamma)\cdot\boldsymbol{\nabla}c_\gamma=0 \quad \text{on } \mathscr{S}_{\gamma\sigma} \tag{A.2a}$$

$$\text{BC2}: \quad c_\omega=c_\gamma \quad \text{on } \mathscr{S}_{\gamma\omega} \tag{A.2b}$$

$$\text{BC3}: \quad -(\mathbf{n}_{\gamma\omega}\cdot\mathbf{D}_\gamma)\cdot\boldsymbol{\nabla}c_\gamma=-(\mathbf{n}_{\gamma\omega}\cdot\mathbf{D}_\omega)\cdot\boldsymbol{\nabla}c_\omega \quad \text{on } \mathscr{S}_{\gamma\omega} \tag{A.2c}$$

$$\text{BC4}: \quad -(\mathbf{n}_{\omega\sigma}\cdot\mathbf{D}_\omega)\cdot\boldsymbol{\nabla}c_\omega=0 \quad \text{on } \mathscr{S}_{\omega\sigma} \tag{A.2d}$$

$$\omega-\text{phase}: \qquad \frac{\partial c_\omega}{\partial t}+\boldsymbol{\nabla}\cdot(\mathbf{v}_\omega c_\omega)=\boldsymbol{\nabla}\cdot(\mathbf{D}_\omega\cdot\boldsymbol{\nabla}c_\omega) \tag{A.3}$$

To develop equations governing mass transport at the macroscopic scale, we need to average each equation

$$\gamma-\text{phase}: \qquad \langle\frac{\partial c_\gamma}{\partial t}\rangle+\langle\boldsymbol{\nabla}\cdot(\mathbf{v}_\gamma c_\gamma)\rangle=\langle\boldsymbol{\nabla}\cdot(\mathbf{D}_\gamma\cdot\boldsymbol{\nabla}c_\gamma)\rangle \tag{A.4}$$

$$\omega-\text{phase}: \qquad \langle\frac{\partial c_\omega}{\partial t}\rangle+\langle\boldsymbol{\nabla}\cdot(\mathbf{v}_\omega c_\omega)\rangle=\langle\boldsymbol{\nabla}\cdot(\mathbf{D}_\omega\cdot\boldsymbol{\nabla}c_\omega)\rangle \tag{A.5}$$

Then, we are confronted to the classical problem of averaging time derivatives and spatial operators. For this purpose, we use the following theorems with **w** the velocity

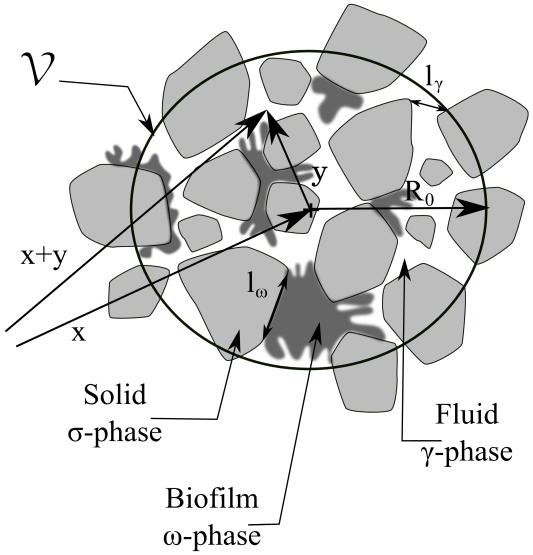

Figure 58: Pore-scale description of a Darcy-scale averaging volume

of the interface.
General transport theorem [273]

$$\langle \frac{\partial c_\gamma}{\partial t} \rangle = \frac{\partial \langle c_\gamma \rangle}{\partial t} - \frac{1}{V} \int_{\mathscr{S}_{\gamma\omega}(t)} (\mathbf{n}_{\gamma\omega} \cdot \mathbf{w})\, c_\gamma \, dS \tag{A.6}$$

$$\langle \frac{\partial c_\omega}{\partial t} \rangle = \frac{\partial \langle c_\omega \rangle}{\partial t} - \frac{1}{V} \int_{\mathscr{S}_{\omega\gamma}(t)} (\mathbf{n}_{\omega\gamma} \cdot \mathbf{w})\, c_\omega \, dS \tag{A.7}$$

Spatial Averaging theorems [129, 119]

$$\langle \nabla c_\gamma \rangle = \nabla \langle c_\gamma \rangle + \frac{1}{V} \int_{\mathscr{S}_{\gamma\omega}} \mathbf{n}_{\gamma\omega} c_\gamma \, dS + \frac{1}{V} \int_{\mathscr{S}_{\gamma\sigma}} \mathbf{n}_{\gamma\sigma} c_\gamma \, dS \tag{A.8}$$

$$\langle \nabla c_\omega \rangle = \nabla \langle c_\omega \rangle + \frac{1}{V} \int_{\mathscr{S}_{\omega\gamma}} \mathbf{n}_{\omega\gamma} c_\omega \, dS + \frac{1}{V} \int_{\mathscr{S}_{\omega\sigma}} \mathbf{n}_{\omega\sigma} c_\omega \, dS \tag{A.9}$$

Imposing $\mathbf{w} = 0$ leads to

$$\begin{aligned}\frac{\partial \varepsilon_\gamma \langle c_\gamma\rangle^\gamma}{\partial t} + \boldsymbol{\nabla}\cdot(\varepsilon_\gamma \langle c_\omega\rangle^\gamma \langle \mathbf{v}_\gamma\rangle^\gamma) = &\quad \boldsymbol{\nabla} \cdot\{\mathbf{D}_\gamma \cdot \left(\boldsymbol{\nabla}\{\varepsilon_\gamma \langle c_\gamma\rangle^\gamma\} + \frac{1}{V}\int_{\mathscr{S}_{\gamma\omega}} \mathbf{n}_{\gamma\omega} c_\gamma \, dS + \frac{1}{V}\int_{\mathscr{S}_{\gamma\sigma}} \mathbf{n}_{\gamma\sigma} c_\gamma \, dS\right)\} \\ &+ \frac{1}{V}\int_{\mathscr{S}_{\gamma\omega}} (\mathbf{n}_{\gamma\omega}\cdot\mathbf{D}_\gamma)\cdot\boldsymbol{\nabla} c_\gamma \, dS + \frac{1}{V}\int_{\mathscr{S}_{\gamma\sigma}} (\mathbf{n}_{\gamma\sigma}\cdot\mathbf{D}_\gamma)\cdot\boldsymbol{\nabla} c_\gamma \, dS \\ &- \boldsymbol{\nabla}\cdot\langle \tilde{c}_\gamma \mathbf{v}_\gamma\rangle \end{aligned} \tag{A.10}$$

$$\begin{aligned}\frac{\partial \varepsilon_\omega \langle c_\omega\rangle^\omega}{\partial t} + \boldsymbol{\nabla}\cdot(\varepsilon_\omega \langle c_\omega\rangle^\omega \langle \mathbf{v}_\omega\rangle^\omega) = &\quad \boldsymbol{\nabla} \cdot\{\mathbf{D}_\omega \cdot \left(\boldsymbol{\nabla}\{\varepsilon_\omega \langle c_\omega\rangle^\omega\} + \frac{1}{V}\int_{\mathscr{S}_{\omega\gamma}} \mathbf{n}_{\omega\gamma} c_\omega \, dS + \frac{1}{V}\int_{\mathscr{S}_{\omega\sigma}} \mathbf{n}_{\omega\sigma} c_\omega \, dS\right)\} \\ &+ \frac{1}{V}\int_{\mathscr{S}_{\omega\gamma}} (\mathbf{n}_{\omega\gamma}\cdot\mathbf{D}_\omega)\cdot\boldsymbol{\nabla} c_\omega \, dS + \frac{1}{V}\int_{\mathscr{S}_{\omega\sigma}} (\mathbf{n}_{\omega\sigma}\cdot\mathbf{D}_\omega)\cdot\boldsymbol{\nabla} c_\omega \, dS \\ &- \boldsymbol{\nabla}\cdot\langle \tilde{c}_\omega \mathbf{v}_\omega\rangle \end{aligned} \tag{A.11}$$

We use the following decompositions $c_\gamma = \langle c_\gamma\rangle^\gamma + \tilde{c}_\gamma$, $c_\omega = \langle c_\omega\rangle^\omega + \tilde{c}_\omega$ and

$$\langle c_\omega\rangle^\omega_{\mathbf{x}+\mathbf{y}} = \langle c_\omega\rangle^\omega_{\mathbf{x}} + \mathbf{y}\cdot\boldsymbol{\nabla}\langle c_\omega\rangle^\omega_{\mathbf{x}} + \cdots \tag{A.12}$$

$$\langle c_\gamma\rangle^\gamma_{\mathbf{x}+\mathbf{y}} = \langle c_\gamma\rangle^\gamma_{\mathbf{x}} + \mathbf{y}\cdot\boldsymbol{\nabla}\langle c_\gamma\rangle^\gamma_{\mathbf{x}} + \cdots \tag{A.13}$$

where $\mathbf{x}$ is the vector pointing the position of the center of the REV and $\mathbf{y}$ is the vector pointing inside the REV. Then we can neglect all the non-local terms involving y provided that $R_0^2 \ll L^2$ [274], where L is a characteristic field-scale length, and this is expressed by

$$\begin{aligned}\frac{1}{V}\int_{\mathscr{S}_{\gamma\omega}} \mathbf{n}_{\gamma\omega} c_\gamma \, dS + \frac{1}{V}\int_{\mathscr{S}_{\gamma\sigma}} \mathbf{n}_{\gamma\sigma} c_\gamma \, dS &= \frac{1}{V}\int_{\mathscr{S}_{\gamma\omega}} \mathbf{n}_{\gamma\omega} \langle c_\gamma\rangle^\gamma_{\mathbf{x}+\mathbf{y}} dS + \frac{1}{V}\int_{\mathscr{S}_{\gamma\sigma}} \mathbf{n}_{\gamma\sigma} \langle c_\gamma\rangle^\gamma_{\mathbf{x}+\mathbf{y}} dS \\ &\quad + \frac{1}{V}\int_{\mathscr{S}_{\gamma\omega}} \mathbf{n}_{\gamma\omega} \tilde{c}_\gamma \, dS + \frac{1}{V}\int_{\mathscr{S}_{\gamma\sigma}} \mathbf{n}_{\gamma\sigma} \tilde{c}_\gamma \, dS \\ &\simeq \langle c_\gamma\rangle^\gamma_{\mathbf{x}} \left(\frac{1}{V}\int_{\mathscr{S}_{\gamma\omega}} \mathbf{n}_{\gamma\omega} \, dS + \frac{1}{V}\int_{\mathscr{S}_{\sigma\omega}} \mathbf{n}_{\sigma\omega} \, dS\right) \\ &\quad + \frac{1}{V}\int_{\mathscr{S}_{\gamma\omega}} \mathbf{n}_{\gamma\omega} \tilde{c}_\gamma \, dS + \frac{1}{V}\int_{\mathscr{S}_{\gamma\sigma}} \mathbf{n}_{\gamma\sigma} \tilde{c}_\gamma \, dS \end{aligned} \tag{A.14}$$

$$\begin{aligned}\frac{1}{V}\int_{\mathscr{S}_{\omega\gamma}} \mathbf{n}_{\omega\gamma} c_\omega \, dS + \frac{1}{V}\int_{\mathscr{S}_{\omega\sigma}} \mathbf{n}_{\omega\sigma} c_\omega \, dS &= \frac{1}{V}\int_{\mathscr{S}_{\omega\gamma}} \mathbf{n}_{\omega\gamma} \langle c_\omega\rangle^\omega_{\mathbf{x}+\mathbf{y}} dS + \frac{1}{V}\int_{\mathscr{S}_{\omega\sigma}} \mathbf{n}_{\omega\sigma} \langle c_\omega\rangle^\omega_{\mathbf{x}+\mathbf{y}} dS \\ &\quad + \frac{1}{V}\int_{\mathscr{S}_{\omega\gamma}} \mathbf{n}_{\omega\gamma} \tilde{c}_\omega \, dS + \frac{1}{V}\int_{\mathscr{S}_{\omega\sigma}} \mathbf{n}_{\omega\sigma} \tilde{c}_\omega \, dS \\ &\simeq \langle c_\omega\rangle^\omega_{\mathbf{x}} \left(\frac{1}{V}\int_{\mathscr{S}_{\omega\gamma}} \mathbf{n}_{\omega\gamma} \, dS + \frac{1}{V}\int_{\mathscr{S}_{\omega\sigma}} \mathbf{n}_{\omega\sigma} \, dS\right) \\ &\quad + \frac{1}{V}\int_{\mathscr{S}_{\omega\gamma}} \mathbf{n}_{\omega\gamma} \tilde{c}_\omega \, dS + \frac{1}{V}\int_{\mathscr{S}_{\omega\sigma}} \mathbf{n}_{\omega\sigma} \tilde{c}_\omega \, dS \end{aligned} \tag{A.15}$$

Then, using spatial averaging theorems for the phase indicators gives

$$-\boldsymbol{\nabla}\varepsilon_\omega = \frac{1}{V}\int_{S_{\omega\gamma}} \mathbf{n}_{\omega\gamma} dS + \frac{1}{V}\int_{S_{\omega\sigma}} \mathbf{n}_{\omega\sigma} dS \tag{A.16}$$

$$-\boldsymbol{\nabla}\varepsilon_\gamma = \frac{1}{V}\int_{S_{\gamma\omega}} \mathbf{n}_{\gamma\omega} dS + \frac{1}{V}\int_{S_{\gamma\sigma}} \mathbf{n}_{\gamma\sigma} dS \tag{A.17}$$

Hence, we have

$$\frac{1}{V}\int_{\mathscr{S}_{\omega\gamma}} \mathbf{n}_{\omega\gamma} c_\omega \, dS + \frac{1}{V}\int_{\mathscr{S}_{\omega\sigma}} \mathbf{n}_{\omega\sigma} c_\omega \, dS \simeq -\boldsymbol{\nabla}\varepsilon_\omega \langle c_\omega\rangle^\omega_{\mathbf{x}} + \frac{1}{V}\int_{\mathscr{S}_{\omega\gamma}} \mathbf{n}_{\omega\gamma} \tilde{c}_\omega \, dS + \frac{1}{V}\int_{\mathscr{S}_{\omega\sigma}} \mathbf{n}_{\omega\sigma} \tilde{c}_\omega \, dS \tag{A.18}$$

$$\frac{1}{V}\int_{\mathscr{S}_{\gamma\omega}} \mathbf{n}_{\gamma\omega} c_\gamma \, dS + \frac{1}{V}\int_{\mathscr{S}_{\gamma\sigma}} \mathbf{n}_{\gamma\sigma} c_\gamma \, dS \simeq -\boldsymbol{\nabla}\varepsilon_\gamma \langle c_\gamma \rangle_{\mathbf{x}}^{\gamma} + \frac{1}{V}\int_{\mathscr{S}_{\gamma\omega}} \mathbf{n}_{\gamma\omega} \tilde{c}_\gamma \, dS + \frac{1}{V}\int_{\mathscr{S}_{\sigma\omega}} \mathbf{n}_{\sigma\omega} \tilde{c}_\gamma \, dS \quad \text{(A.19)}$$

Finally, injecting Eqs (B.18) and (B.19) into (B.10) and (B.11) and doing the same approximations for the macroscopic fluxes leads to

$$\begin{aligned}
\frac{\partial \varepsilon_\gamma \langle c_\gamma \rangle^\gamma}{\partial t} + \boldsymbol{\nabla}\cdot(\varepsilon_\gamma \langle c \rangle^\gamma \langle \mathbf{v}_\gamma \rangle^\gamma) = \quad & \boldsymbol{\nabla} \cdot \{\varepsilon_\gamma \mathbf{D}_\gamma \cdot \left(\boldsymbol{\nabla}\langle c_\gamma \rangle^\gamma + \frac{1}{V_\gamma}\int_{\mathscr{S}_{\gamma\omega}} \mathbf{n}_{\gamma\omega} \tilde{c}_\gamma \, dS + \frac{1}{V_\gamma}\int_{\mathscr{S}_{\gamma\sigma}} \mathbf{n}_{\gamma\sigma} \tilde{c}_\gamma \, dS \right)\} \\
+ \quad & \frac{1}{V}\int_{\mathscr{S}_{\gamma\omega}} (\mathbf{n}_{\gamma\omega}\cdot\mathbf{D}_\gamma)\cdot\boldsymbol{\nabla}\tilde{c}_\gamma \, dS + \frac{1}{V}\int_{\mathscr{S}_{\gamma\sigma}} (\mathbf{n}_{\gamma\sigma}\cdot\mathbf{D}_\gamma)\cdot\boldsymbol{\nabla}\tilde{c}_\gamma \, dS \\
- \quad & \boldsymbol{\nabla}\cdot\langle \tilde{c}_\gamma \mathbf{v}_\gamma \rangle
\end{aligned} \quad \text{(A.20)}$$

$$\begin{aligned}
\frac{\partial \varepsilon_\omega \langle c_\omega \rangle^\omega}{\partial t} + \boldsymbol{\nabla}\cdot(\varepsilon_\omega \langle c_\omega \rangle^\omega \langle \mathbf{v}_\omega \rangle^\omega) = \quad & \boldsymbol{\nabla} \cdot \{\varepsilon_\omega \mathbf{D}_\omega \cdot \left(\boldsymbol{\nabla}\langle c_\omega \rangle^\omega + \frac{1}{V_\omega}\int_{\mathscr{S}_{\omega\gamma}} \mathbf{n}_{\omega\gamma} \tilde{c}_\omega \, dS + \frac{1}{V_\omega}\int_{\mathscr{S}_{\omega\sigma}} \mathbf{n}_{\omega\sigma} \tilde{c}_\omega \, dS \right)\} \\
+ \quad & \frac{1}{V}\int_{\mathscr{S}_{\omega\gamma}} (\mathbf{n}_{\omega\gamma}\cdot\mathbf{D}_\omega)\cdot\boldsymbol{\nabla}\tilde{c}_\omega \, dS + \frac{1}{V}\int_{\mathscr{S}_{\omega\sigma}} (\mathbf{n}_{\omega\sigma}\cdot\mathbf{D}_\omega)\cdot\boldsymbol{\nabla}\tilde{c}_\omega \, dS \\
- \quad & \boldsymbol{\nabla}\cdot\langle \tilde{c}_\omega \mathbf{v}_\omega \rangle
\end{aligned} \quad \text{(A.21)}$$

B

MATHEMATICAL DEVELOPMENT FOR THE TWO-EQUATION NON-CLOSED REACTIVE MODEL

In this Appendix, we develop the volume averaged equations for each phase. We start with the pore-scale description of the medium

$$\gamma-\text{phase}: \qquad \frac{\partial c_\gamma}{\partial t}+\boldsymbol{\nabla}\cdot(c_\gamma \mathbf{v}_\gamma)=\boldsymbol{\nabla}\cdot(\mathbf{D}_\gamma\cdot\boldsymbol{\nabla}c_\gamma) \tag{B.1}$$

$$\text{BC1}: \quad -(\mathbf{n}_{\gamma\sigma}\cdot\mathbf{D}_\gamma)\cdot\boldsymbol{\nabla}c_\gamma=0 \quad \text{on } \mathscr{S}_{\gamma\sigma} \tag{B.2a}$$

$$\text{BC2}: \quad c_\omega=c_\gamma \quad \text{on } \mathscr{S}_{\gamma\omega} \tag{B.2b}$$

$$\text{BC3}: \quad -(\mathbf{n}_{\gamma\omega}\cdot\mathbf{D}_\gamma)\cdot\boldsymbol{\nabla}c_\gamma=-(\mathbf{n}_{\gamma\omega}\cdot\mathbf{D}_\omega)\cdot\boldsymbol{\nabla}c_\omega \quad \text{on } \mathscr{S}_{\gamma\omega} \tag{B.2c}$$

$$\text{BC4}: \quad -(\mathbf{n}_{\omega\sigma}\cdot\mathbf{D}_\omega)\cdot\boldsymbol{\nabla}c_\omega=0 \quad \text{on } \mathscr{S}_{\omega\sigma} \tag{B.2d}$$

$$\omega-\text{phase}: \qquad \frac{\partial c_\omega}{\partial t}=\boldsymbol{\nabla}\cdot(\mathbf{D}_\omega\cdot\boldsymbol{\nabla}c_\omega)+\mathscr{R}_\omega \tag{B.3}$$

To develop equations governing mass transport at the macroscopic scale, we need to average each equation

$$\gamma-\text{phase}: \qquad \langle\frac{\partial c_\gamma}{\partial t}\rangle+\langle\boldsymbol{\nabla}\cdot(c_\gamma\mathbf{v}_\gamma)\rangle=\langle\boldsymbol{\nabla}\cdot(\mathbf{D}_\gamma\cdot\boldsymbol{\nabla}c_\gamma)\rangle \tag{B.4}$$

$$\omega-\text{phase}: \qquad \langle\frac{\partial c_\omega}{\partial t}\rangle=\langle\boldsymbol{\nabla}\cdot(\mathbf{D}_\omega\cdot\boldsymbol{\nabla}c_\omega)\rangle+\langle\mathscr{R}_\omega\rangle \tag{B.5}$$

Then, we are confronted to the classical problem of averaging time derivatives and spatial operators. For this purpose, we use the following theorems
General transport theorem [273]

$$\langle\frac{\partial c_\gamma}{\partial t}\rangle=\frac{\partial\langle c_\gamma\rangle}{\partial t}-\frac{1}{V}\int_{\mathscr{S}_{\gamma\omega}(t)}(\mathbf{n}_{\gamma\omega}\cdot\mathbf{w})\,c_\gamma\,dS \tag{B.6}$$

$$\langle\frac{\partial c_\omega}{\partial t}\rangle=\frac{\partial\langle c_\omega\rangle}{\partial t}-\frac{1}{V}\int_{\mathscr{S}_{\omega\gamma}(t)}(\mathbf{n}_{\omega\gamma}\cdot\mathbf{w})\,c_\omega\,dS \tag{B.7}$$

with **w** the velocity of the interface.
Spatial Averaging theorems [129, 119]

$$\langle \boldsymbol{\nabla} c_\gamma \rangle = \boldsymbol{\nabla} \langle c_\gamma \rangle + \frac{1}{V} \int_{\mathscr{S}_{\gamma\omega}} \mathbf{n}_{\gamma\omega} c_\gamma \, dS + \frac{1}{V} \int_{\mathscr{S}_{\gamma\sigma}} \mathbf{n}_{\gamma\sigma} c_\gamma \, dS \tag{B.8}$$

$$\langle \boldsymbol{\nabla} c_\omega \rangle = \boldsymbol{\nabla} \langle c_\omega \rangle + \frac{1}{V} \int_{\mathscr{S}_{\omega\gamma}} \mathbf{n}_{\omega\gamma} c_\omega \, dS + \frac{1}{V} \int_{\mathscr{S}_{\omega\sigma}} \mathbf{n}_{\omega\sigma} c_\omega \, dS \tag{B.9}$$

It has already been emphasized [285] that characteristics times associated to biofilm motion are long compared to the one associated with the mass transport so that we can write

$$\begin{aligned} \frac{\partial \varepsilon_\gamma \langle c_\gamma \rangle^\gamma}{\partial t} + \boldsymbol{\nabla} \cdot (\varepsilon_\gamma \langle c \rangle^{\gamma\omega} \langle \mathbf{v}_\gamma \rangle^\gamma) = \quad & \boldsymbol{\nabla} \cdot \{ \mathbf{D}_\gamma \cdot \left(\boldsymbol{\nabla} \{ \varepsilon_\gamma \langle c_\gamma \rangle^\gamma \} + \frac{1}{V} \int_{\mathscr{S}_{\gamma\omega}} \mathbf{n}_{\gamma\omega} c_\gamma \, dS + \frac{1}{V} \int_{\mathscr{S}_{\gamma\sigma}} \mathbf{n}_{\gamma\sigma} c_\gamma \, dS \right) \} \\ & + \frac{1}{V} \int_{\mathscr{S}_{\gamma\omega}} (\mathbf{n}_{\gamma\omega} \cdot \mathbf{D}_\gamma) \cdot \boldsymbol{\nabla} c_\gamma \, dS + \frac{1}{V} \int_{\mathscr{S}_{\gamma\sigma}} (\mathbf{n}_{\gamma\sigma} \cdot \mathbf{D}_\gamma) \cdot \boldsymbol{\nabla} c_\gamma \, dS \\ & - \boldsymbol{\nabla} . \langle \hat{c}_\gamma \mathbf{v}_\gamma \rangle \end{aligned} \tag{B.10}$$

$$\begin{aligned} \frac{\partial \varepsilon_\omega \langle c_\omega \rangle^\omega}{\partial t} = \quad & \boldsymbol{\nabla} \cdot \{ \boldsymbol{D}_\omega \cdot \left(\boldsymbol{\nabla} \{ \varepsilon_\omega \langle c_\omega \rangle^\omega \} + \frac{1}{V} \int_{\mathscr{S}_{\omega\gamma}} \mathbf{n}_{\omega\gamma} c_\omega \, dS + \frac{1}{V} \int_{\mathscr{S}_{\omega\sigma}} \mathbf{n}_{\omega\sigma} c_\omega \, dS \right) \} \\ & + \frac{1}{V} \int_{\mathscr{S}_{\omega\gamma}} (\mathbf{n}_{\omega\gamma} \cdot \boldsymbol{D}_\omega) \cdot \boldsymbol{\nabla} c_\omega \, dS + \frac{1}{V} \int_{\mathscr{S}_{\omega\sigma}} (\mathbf{n}_{\omega\sigma} \cdot \boldsymbol{D}_\omega) \cdot \boldsymbol{\nabla} c_\omega \, dS \\ & + \varepsilon_\omega \langle \mathscr{R}_\omega \rangle^\omega \end{aligned} \tag{B.11}$$

We use the following decompositions $c_\gamma = \langle c_\gamma \rangle^\gamma + \tilde{c}_\gamma$, $c_\omega = \langle c_\omega \rangle^\omega + \tilde{c}_\omega$ and

$$\langle c_\omega \rangle^\omega_{\mathbf{x}+\mathbf{y}} = \langle c_\omega \rangle^\omega_{\mathbf{x}} + \mathbf{y} \cdot \boldsymbol{\nabla} \langle c_\omega \rangle^\omega_{\mathbf{x}} + \cdots \tag{B.12}$$

$$\langle c_\gamma \rangle^\gamma_{\mathbf{x}+\mathbf{y}} = \langle c_\gamma \rangle^\gamma_{\mathbf{x}} + \mathbf{y} \cdot \boldsymbol{\nabla} \langle c_\gamma \rangle^\gamma_{\mathbf{x}} + \cdots \tag{B.13}$$

where **x** is the vector pointing the position of the center of the REV and **y** is the vector pointing inside the REV. Then we can neglect all the non-local terms involving y provided that $R_0^2 \ll L^2$ [274], where L is a characteristic field-scale length, and this is expressed by

$$\begin{aligned} \frac{1}{V} \int_{\mathscr{S}_{\gamma\omega}} \mathbf{n}_{\gamma\omega} c_\gamma \, dS + \frac{1}{V} \int_{\mathscr{S}_{\gamma\sigma}} \mathbf{n}_{\gamma\sigma} c_\gamma \, dS &= \frac{1}{V} \int_{\mathscr{S}_{\gamma\omega}} \mathbf{n}_{\gamma\omega} \langle c_\gamma \rangle^\gamma_{\mathbf{x}+\mathbf{y}} \, dS + \frac{1}{V} \int_{\mathscr{S}_{\gamma\sigma}} \mathbf{n}_{\gamma\sigma} \langle c_\gamma \rangle^\gamma_{\mathbf{x}+\mathbf{y}} \, dS \\ &\quad + \frac{1}{V} \int_{\mathscr{S}_{\gamma\omega}} \mathbf{n}_{\gamma\omega} \tilde{c}_\gamma \, dS + \frac{1}{V} \int_{\mathscr{S}_{\gamma\sigma}} \mathbf{n}_{\gamma\sigma} \tilde{c}_\gamma \, dS \\ &\simeq \langle c_\gamma \rangle^\gamma_{\mathbf{x}} \left(\frac{1}{V} \int_{\mathscr{S}_{\gamma\omega}} \mathbf{n}_{\gamma\omega} \, dS + \frac{1}{V} \int_{\mathscr{S}_{\gamma\sigma}} \mathbf{n}_{\sigma\omega} \, dS \right) \\ &\quad + \frac{1}{V} \int_{\mathscr{S}_{\gamma\omega}} \mathbf{n}_{\gamma\omega} \tilde{c}_\gamma \, dS + \frac{1}{V} \int_{\mathscr{S}_{\gamma\sigma}} \mathbf{n}_{\gamma\sigma} \tilde{c}_\gamma \, dS \end{aligned} \tag{B.14}$$

$$\begin{aligned}\frac{1}{V}\int_{\mathscr{S}_{\omega\gamma}}\mathbf{n}_{\omega\gamma}c_\omega\,dS+\frac{1}{V}\int_{\mathscr{S}_{\omega\sigma}}\mathbf{n}_{\omega\sigma}c_\omega\,dS &= \frac{1}{V}\int_{\mathscr{S}_{\omega\gamma}}\mathbf{n}_{\omega\gamma}\langle c_\omega\rangle^\omega_{\mathbf{x}+\mathbf{y}}dS+\frac{1}{V}\int_{\mathscr{S}_{\omega\sigma}}\mathbf{n}_{\omega\sigma}\langle c_\omega\rangle^\omega_{\mathbf{x}+\mathbf{y}}dS\\ &\quad+\frac{1}{V}\int_{\mathscr{S}_{\omega\gamma}}\mathbf{n}_{\omega\gamma}\tilde{c}_\omega\,dS+\frac{1}{V}\int_{\mathscr{S}_{\omega\sigma}}\mathbf{n}_{\omega\sigma}\tilde{c}_\omega\,dS\\ &\simeq \langle c_\omega\rangle^\omega_{\mathbf{x}}\left(\frac{1}{V}\int_{\mathscr{S}_{\omega\gamma}}\mathbf{n}_{\omega\gamma}\,dS+\frac{1}{V}\int_{\mathscr{S}_{\omega\sigma}}\mathbf{n}_{\omega\sigma}dS\right)\\ &\quad+\frac{1}{V}\int_{\mathscr{S}_{\omega\gamma}}\mathbf{n}_{\omega\gamma}\tilde{c}_\omega\,dS+\frac{1}{V}\int_{\mathscr{S}_{\omega\sigma}}\mathbf{n}_{\omega\sigma}\tilde{c}_\omega\,dS \qquad \text{(B.15)}\end{aligned}$$

Then, using spatial averaging theorems for unity gives

$$-\boldsymbol{\nabla}\varepsilon_\omega = \frac{1}{V}\int_{\mathscr{S}_{\omega\gamma}}\mathbf{n}_{\omega\gamma}dS+\frac{1}{V}\int_{\mathscr{S}_{\omega\sigma}}\mathbf{n}_{\omega\sigma}dS \qquad \text{(B.16)}$$

$$-\boldsymbol{\nabla}\varepsilon_\gamma = \frac{1}{V}\int_{\mathscr{S}_{\gamma\omega}}\mathbf{n}_{\gamma\omega}dS+\frac{1}{V}\int_{\mathscr{S}_{\gamma\sigma}}\mathbf{n}_{\gamma\sigma}dS \qquad \text{(B.17)}$$

Hence, we have

$$\frac{1}{V}\int_{\mathscr{S}_{\omega\gamma}}\mathbf{n}_{\omega\gamma}c_\omega\,dS+\frac{1}{V}\int_{\mathscr{S}_{\omega\sigma}}\mathbf{n}_{\omega\sigma}c_\omega\,dS\simeq-\boldsymbol{\nabla}\varepsilon_\omega\langle c_\omega\rangle^\omega_{\mathbf{x}}+\frac{1}{V}\int_{\mathscr{S}_{\omega\gamma}}\mathbf{n}_{\omega\gamma}\tilde{c}_\omega\,dS+\frac{1}{V}\int_{\mathscr{S}_{\omega\sigma}}\mathbf{n}_{\omega\sigma}\tilde{c}_\omega\,dS \qquad \text{(B.18)}$$

$$\frac{1}{V}\int_{\mathscr{S}_{\gamma\omega}}\mathbf{n}_{\gamma\omega}c_\gamma\,dS+\frac{1}{V}\int_{\mathscr{S}_{\gamma\sigma}}\mathbf{n}_{\gamma\sigma}c_\gamma\,dS\simeq-\boldsymbol{\nabla}\varepsilon_\gamma\langle c_\gamma\rangle^\gamma_{\mathbf{x}}+\frac{1}{V}\int_{\mathscr{S}_{\gamma\omega}}\mathbf{n}_{\gamma\omega}\tilde{c}_\gamma\,dS+\frac{1}{V}\int_{\mathscr{S}_{\sigma\omega}}\mathbf{n}_{\sigma\omega}\tilde{c}_\gamma\,dS \qquad \text{(B.19)}$$

Finally, injecting Eqs (B.18) and (B.19) into (B.10) and (B.11) leads to

$$\begin{aligned}\frac{\partial\varepsilon_\gamma\langle c_\gamma\rangle^\gamma}{\partial t}+\boldsymbol{\nabla}\cdot(\varepsilon_\gamma\langle c\rangle^{\gamma\omega}\langle\mathbf{v}_\gamma\rangle^\gamma) = \;&\boldsymbol{\nabla}\cdot\{\varepsilon_\gamma\mathbf{D}_\gamma\cdot\left(\boldsymbol{\nabla}\langle c_\gamma\rangle^\gamma+\frac{1}{V_\gamma}\int_{\mathscr{S}_{\gamma\omega}}\mathbf{n}_{\gamma\omega}\tilde{c}_\gamma\,dS+\frac{1}{V_\gamma}\int_{\mathscr{S}_{\gamma\sigma}}\mathbf{n}_{\gamma\sigma}\tilde{c}_\gamma\,dS\right)\}\\ &+\frac{1}{V}\int_{\mathscr{S}_{\gamma\omega}}(\mathbf{n}_{\gamma\omega}\cdot\mathbf{D}_\gamma)\cdot\boldsymbol{\nabla}c_\gamma\,dS+\frac{1}{V}\int_{\mathscr{S}_{\gamma\sigma}}(\mathbf{n}_{\gamma\sigma}\cdot\mathbf{D}_\gamma)\cdot\boldsymbol{\nabla}c_\gamma\,dS\\ &-\boldsymbol{\nabla}.\langle\hat{c}_\gamma\mathbf{v}_\gamma\rangle \qquad \text{(B.20)}\end{aligned}$$

$$\begin{aligned}\frac{\partial\varepsilon_\omega\langle c_\omega\rangle^\omega}{\partial t} = \;&\boldsymbol{\nabla}\cdot\{\varepsilon_\omega\mathbf{D}_\omega\cdot\left(\boldsymbol{\nabla}\langle c_\omega\rangle^\omega+\frac{1}{V_\omega}\int_{\mathscr{S}_{\omega\gamma}}\mathbf{n}_{\omega\gamma}\tilde{c}_\omega\,dS+\frac{1}{V_\omega}\int_{\mathscr{S}_{\omega\sigma}}\mathbf{n}_{\omega\sigma}\tilde{c}_\omega\,dS\right)\}\\ &+\frac{1}{V}\int_{\mathscr{S}_{\omega\gamma}}(\mathbf{n}_{\omega\gamma}\cdot\mathbf{D}_\omega)\cdot\boldsymbol{\nabla}c_\omega\,dS+\frac{1}{V}\int_{\mathscr{S}_{\omega\sigma}}(\mathbf{n}_{\omega\sigma}\cdot\mathbf{D}_\omega)\cdot\boldsymbol{\nabla}c_\omega\,dS\\ &+\varepsilon_\omega\langle\mathscr{R}_\omega\rangle^\omega \qquad \text{(B.21)}\end{aligned}$$

C

MATHEMATICAL DEVELOPMENT FOR THE ONE-EQUATION PECULIAR DECOMPOSITION MODEL

In this part, we develop the macroscopic one-equation non-closed form of the model starting with the averaged equations for each phase

$$\begin{aligned}\frac{\partial \varepsilon_\gamma \langle c_\gamma\rangle^\gamma}{\partial t} + \boldsymbol{\nabla}\cdot(\varepsilon_\gamma \langle c\rangle^{\gamma\omega}\langle \mathbf{v}_\gamma\rangle^\gamma) = &\quad \boldsymbol{\nabla} \cdot\{\varepsilon_\gamma \mathbf{D}_\gamma \cdot \left(\boldsymbol{\nabla}\langle c_\gamma\rangle^\gamma + \frac{1}{V_\gamma}\int_{\mathscr{S}_{\gamma\omega}} \mathbf{n}_{\gamma\omega}\tilde{c}_\gamma \,dS + \frac{1}{V_\gamma}\int_{\mathscr{S}_{\gamma\sigma}} \mathbf{n}_{\gamma\sigma}\tilde{c}_\gamma \,dS\right)\} \\ &+ \frac{1}{V}\int_{\mathscr{S}_{\gamma\omega}} (\mathbf{n}_{\gamma\omega}\cdot\mathbf{D}_\gamma)\cdot\boldsymbol{\nabla} c_\gamma \,dS + \frac{1}{V}\int_{\mathscr{S}_{\gamma\sigma}} (\mathbf{n}_{\gamma\sigma}\cdot\mathbf{D}_\gamma)\cdot\boldsymbol{\nabla} c_\gamma \,dS \\ &- \boldsymbol{\nabla}.\langle \hat{c}_\gamma \mathbf{v}_\gamma\rangle \end{aligned} \tag{C.1}$$

$$\begin{aligned}\frac{\partial \varepsilon_\omega \langle c_\omega\rangle^\omega}{\partial t} = &\quad \boldsymbol{\nabla} \cdot\{\varepsilon_\omega \mathbf{D}_\omega \cdot \left(\boldsymbol{\nabla}\langle c_\omega\rangle^\omega + \frac{1}{V_\omega}\int_{\mathscr{S}_{\omega\gamma}} \mathbf{n}_{\omega\gamma}\tilde{c}_\omega \,dS + \frac{1}{V_\omega}\int_{\mathscr{S}_{\omega\sigma}} \mathbf{n}_{\omega\sigma}\tilde{c}_\omega \,dS\right)\} \\ &+ \frac{1}{V}\int_{\mathscr{S}_{\omega\gamma}} (\mathbf{n}_{\omega\gamma}\cdot\mathbf{D}_\omega)\cdot\boldsymbol{\nabla} c_\omega \,dS + \frac{1}{V}\int_{\mathscr{S}_{\omega\sigma}} (\mathbf{n}_{\omega\sigma}\cdot\mathbf{D}_\omega)\cdot\boldsymbol{\nabla} c_\omega \,dS \\ &+ \varepsilon_\omega \langle \mathscr{R}_\omega\rangle^\omega \end{aligned} \tag{C.2}$$

Then, we make the flux term disappear by summing equations over the $\gamma-\mathrm{phase}$ and the $\omega-\mathrm{phase}$ and by using the flux-continuity hypothesis at the interface between γ and ω.

$$\begin{aligned}\frac{\partial \langle c\rangle}{\partial t} + \boldsymbol{\nabla}\cdot(\varepsilon_\gamma \langle c\rangle^{\gamma\omega}\langle \mathbf{v}_\gamma\rangle^\gamma) = &\quad \boldsymbol{\nabla} \cdot\{\varepsilon_\omega \mathbf{D}_\omega \cdot \boldsymbol{\nabla}\langle c_\omega\rangle^\omega + \varepsilon_\gamma \mathbf{D}_\gamma \cdot \boldsymbol{\nabla}\langle c_\gamma\rangle^\gamma\} \\ &+ \boldsymbol{\nabla}\cdot\{\mathbf{D}_\omega \cdot \left(\frac{1}{V}\int_{\mathscr{S}_{\omega\gamma}} \mathbf{n}_{\omega\gamma}\tilde{c}_\omega \,dS + \frac{1}{V}\int_{\mathscr{S}_{\omega\sigma}} \mathbf{n}_{\omega\sigma}\tilde{c}_\omega \,dS\right)\} \\ &+ \boldsymbol{\nabla}\cdot\{\mathbf{D}_\gamma \cdot \left(\frac{1}{V}\int_{\mathscr{S}_{\gamma\omega}} \mathbf{n}_{\gamma\omega}\tilde{c}_\gamma \,dS + \frac{1}{V}\int_{\mathscr{S}_{\gamma\sigma}} \mathbf{n}_{\gamma\sigma}\tilde{c}_\gamma \,dS\right)\} \\ &+ \varepsilon_\omega \langle \mathscr{R}_\omega\rangle^\omega - \boldsymbol{\nabla}.\langle \hat{c}_\gamma \mathbf{v}_\gamma\rangle \end{aligned} \tag{C.3}$$

Then, we make intrinsic total average equation appear dividing by $\varepsilon_\gamma + \varepsilon_\omega$ (supposed constant over time and space) as it is the one used in the decompositions of concentrations.

$$\begin{aligned}
\frac{\partial \langle c\rangle^{\gamma\omega}}{\partial t} + \boldsymbol{\nabla}\cdot\left(\frac{\varepsilon_\gamma}{\varepsilon_\gamma+\varepsilon_\omega}\langle c\rangle^{\gamma\omega}\langle \mathbf{v}_\gamma\rangle^{\gamma}\right) = \quad & \boldsymbol{\nabla} \cdot\{\frac{\varepsilon_\omega}{\varepsilon_\gamma+\varepsilon_\omega}\mathbf{D}_\omega\cdot\boldsymbol{\nabla}\langle c_\omega\rangle^{\omega} + \frac{\varepsilon_\gamma}{\varepsilon_\gamma+\varepsilon_\omega}\mathbf{D}_\gamma\cdot\boldsymbol{\nabla}\langle c_\gamma\rangle^{\gamma}\} \\
+ \quad & \boldsymbol{\nabla}\cdot\{\frac{\varepsilon_\omega}{\varepsilon_\gamma+\varepsilon_\omega}\mathbf{D}_\omega\cdot\left(\frac{1}{V_\omega}\int_{\mathscr{S}_{\omega\gamma}}\mathbf{n}_{\omega\gamma}\hat{c}_\omega\,dS + \frac{1}{V_\omega}\int_{\mathscr{S}_{\omega\sigma}}\mathbf{n}_{\omega\sigma}\hat{c}_\omega\,dS\right)\} \\
+ \quad & \boldsymbol{\nabla}\cdot\{\frac{\varepsilon_\gamma}{\varepsilon_\gamma+\varepsilon_\omega}\mathbf{D}_\gamma\cdot\left(\frac{1}{V_\gamma}\int_{\mathscr{S}_{\gamma\omega}}\mathbf{n}_{\gamma\omega}\hat{c}_\gamma\,dS + \frac{1}{V_\gamma}\int_{\mathscr{S}_{\gamma\sigma}}\mathbf{n}_{\gamma\sigma}\hat{c}_\gamma\,dS\right)\} \\
+ \quad & \frac{\varepsilon_\omega}{\varepsilon_\gamma+\varepsilon_\omega}\langle\mathscr{R}_\omega\rangle^{\omega} - \frac{1}{\varepsilon_\gamma+\varepsilon_\omega}\boldsymbol{\nabla}.\langle\hat{c}_\gamma\mathbf{v}_\gamma\rangle
\end{aligned} \tag{C.4}$$

Finally, we use the following relations

$$\langle c_\gamma\rangle^{\gamma} = \langle c\rangle^{\gamma\omega} + \langle\hat{c}_\gamma\rangle^{\gamma} \tag{C.5}$$

$$\langle c_\omega\rangle^{\omega} = \langle c\rangle^{\gamma\omega} + \langle\hat{c}_\omega\rangle^{\omega} \tag{C.6}$$

$$\tilde{c}_\gamma = \hat{c}_\gamma - \langle\hat{c}_\gamma\rangle^{\gamma} \tag{C.7}$$

$$\tilde{c}_\omega = \hat{c}_\omega - \langle\hat{c}_\omega\rangle^{\omega} \tag{C.8}$$

which gives

$$\begin{aligned}
\frac{\partial \langle c\rangle^{\gamma\omega}}{\partial t} + \boldsymbol{\nabla}\cdot\left(\frac{\varepsilon_\gamma}{\varepsilon_\gamma+\varepsilon_\omega}\langle c\rangle^{\gamma\omega}\langle \mathbf{v}_\gamma\rangle^{\gamma}\right) = \quad & \boldsymbol{\nabla} \cdot\{\left(\frac{\varepsilon_\omega}{\varepsilon_\gamma+\varepsilon_\omega}\boldsymbol{D}_\omega + \frac{\varepsilon_\gamma}{\varepsilon_\gamma+\varepsilon_\omega}\boldsymbol{D}_\gamma\right)\cdot\boldsymbol{\nabla}\langle c\rangle^{\gamma\omega}\} \\
+ \quad & \boldsymbol{\nabla} \cdot\{\frac{\varepsilon_\omega}{\varepsilon_\gamma+\varepsilon_\omega}\boldsymbol{D}_\omega\cdot\boldsymbol{\nabla}\langle\hat{c}_\omega\rangle^{\omega} + \frac{\varepsilon_\gamma}{\varepsilon_\gamma+\varepsilon_\omega}\boldsymbol{D}_\gamma\cdot\boldsymbol{\nabla}\langle\hat{c}_\gamma\rangle^{\gamma}\} \\
+ \quad & \boldsymbol{\nabla}\cdot\{\frac{\varepsilon_\omega}{\varepsilon_\gamma+\varepsilon_\omega}\boldsymbol{D}_\omega\cdot\left(\frac{1}{V_\omega}\int_{\mathscr{S}_{\omega\gamma}}\mathbf{n}_{\omega\gamma}\hat{c}_\omega\,dS + \frac{1}{V_\omega}\int_{\mathscr{S}_{\omega\sigma}}\mathbf{n}_{\omega\sigma}\hat{c}_\omega\,dS\right)\} \\
+ \quad & \boldsymbol{\nabla}\cdot\{\frac{\varepsilon_\gamma}{\varepsilon_\gamma+\varepsilon_\omega}\boldsymbol{D}_\gamma\cdot\left(\frac{1}{V_\gamma}\int_{\mathscr{S}_{\gamma\omega}}\mathbf{n}_{\gamma\omega}\hat{c}_\gamma\,dS + \frac{1}{V_\gamma}\int_{\mathscr{S}_{\gamma\sigma}}\mathbf{n}_{\gamma\sigma}\hat{c}_\gamma\,dS\right)\} \\
- \quad & \boldsymbol{\nabla}\cdot\{\frac{\varepsilon_\omega}{\varepsilon_\gamma+\varepsilon_\omega}\boldsymbol{D}_\omega\cdot\left(\frac{1}{V_\omega}\int_{\mathscr{S}_{\omega\gamma}}\mathbf{n}_{\omega\gamma}\langle\hat{c}_\omega\rangle^{\omega}\,dS + \frac{1}{V_\omega}\int_{\mathscr{S}_{\omega\sigma}}\mathbf{n}_{\omega\sigma}\langle\hat{c}_\omega\rangle^{\omega}\,dS\right)\} \\
- \quad & \boldsymbol{\nabla}\cdot\{\frac{\varepsilon_\gamma}{\varepsilon_\gamma+\varepsilon_\omega}\boldsymbol{D}_\gamma\cdot\left(\frac{1}{V_\gamma}\int_{\mathscr{S}_{\gamma\omega}}\mathbf{n}_{\gamma\omega}\langle\hat{c}_\gamma\rangle^{\gamma}\,dS + \frac{1}{V_\gamma}\int_{\mathscr{S}_{\gamma\sigma}}\mathbf{n}_{\gamma\sigma}\langle\hat{c}_\gamma\rangle^{\gamma}\,dS\right)\} \\
+ \quad & \frac{\varepsilon_\omega}{\varepsilon_\gamma+\varepsilon_\omega}\langle\mathscr{R}_\omega\rangle^{\omega} - \frac{1}{\varepsilon_\gamma+\varepsilon_\omega}\boldsymbol{\nabla}.\langle\hat{c}_\gamma\mathbf{v}_\gamma\rangle
\end{aligned} \tag{C.9}$$

Then, using spatial averaging theorems for unity gives

$$\begin{aligned}
-\boldsymbol{\nabla}\varepsilon_\omega &= \frac{1}{V}\int_{\mathscr{S}_{\omega\gamma}}\mathbf{n}_{\omega\gamma}dS + \frac{1}{V}\int_{\mathscr{S}_{\omega\sigma}}\mathbf{n}_{\omega\sigma}dS \\
-\boldsymbol{\nabla}\varepsilon_\gamma &= \frac{1}{V}\int_{\mathscr{S}_{\gamma\omega}}\mathbf{n}_{\gamma\omega}dS + \frac{1}{V}\int_{\mathscr{S}_{\gamma\sigma}}\mathbf{n}_{\gamma\sigma}dS
\end{aligned} \tag{C.10}$$

So that we can write

$$
\begin{aligned}
\frac{\partial \langle c\rangle^{\gamma\omega}}{\partial t} + \boldsymbol{\nabla}\cdot\left(\frac{\varepsilon_\gamma}{\varepsilon_\gamma+\varepsilon_\omega}\langle c\rangle^{\gamma\omega}\langle \mathbf{v}_\gamma\rangle^{\gamma}\right) = \quad & \boldsymbol{\nabla} \quad \cdot\{\left(\frac{\varepsilon_\omega}{\varepsilon_\gamma+\varepsilon_\omega}\boldsymbol{D}_\omega + \frac{\varepsilon_\gamma}{\varepsilon_\gamma+\varepsilon_\omega}\boldsymbol{D}_\gamma\right)\cdot\boldsymbol{\nabla}\langle c\rangle^{\gamma\omega}\} \\
& + \quad \boldsymbol{\nabla}\cdot\left(\frac{\varepsilon_\omega}{\varepsilon_\gamma+\varepsilon_\omega}\boldsymbol{D}_\omega\cdot\boldsymbol{\nabla}\langle \hat{c}_\omega\rangle^{\omega} + \frac{\varepsilon_\gamma}{\varepsilon_\gamma+\varepsilon_\omega}\boldsymbol{D}_\gamma\boldsymbol{\nabla}\langle \hat{c}_\gamma\rangle^{\gamma}\right) \\
& + \quad \boldsymbol{\nabla}\cdot\{\frac{\varepsilon_\omega}{\varepsilon_\gamma+\varepsilon_\omega}\boldsymbol{D}_\omega\cdot\left(\frac{1}{V_\omega}\int_{\mathscr{S}_{\omega\gamma}}\mathbf{n}_{\omega\gamma}\hat{c}_\omega\,dS + \frac{1}{V_\omega}\int_{\mathscr{S}_{\omega\sigma}}\mathbf{n}_{\omega\sigma}\hat{c}_\omega\,dS\right)\} \\
& + \quad \boldsymbol{\nabla}\cdot\{\frac{\varepsilon_\gamma}{\varepsilon_\gamma+\varepsilon_\omega}\boldsymbol{D}_\gamma\cdot\left(\frac{1}{V_\gamma}\int_{\mathscr{S}_{\gamma\omega}}\mathbf{n}_{\gamma\omega}\hat{c}_\gamma\,dS + \frac{1}{V_\gamma}\int_{\mathscr{S}_{\gamma\sigma}}\mathbf{n}_{\gamma\sigma}\hat{c}_\gamma\,dS\right)\} \\
& + \quad \boldsymbol{\nabla}\cdot\left(\frac{1}{\varepsilon_\gamma+\varepsilon_\omega}\boldsymbol{D}_\omega\cdot\boldsymbol{\nabla}\varepsilon_\omega\langle \hat{c}_\omega\rangle^{\omega}\right) \\
& + \quad \boldsymbol{\nabla}\cdot\left(\frac{1}{\varepsilon_\gamma+\varepsilon_\omega}\boldsymbol{D}_\gamma\cdot\boldsymbol{\nabla}\varepsilon_\gamma\langle \hat{c}_\gamma\rangle^{\gamma}\right) \\
& + \quad \frac{\varepsilon_\omega}{\varepsilon_\gamma+\varepsilon_\omega}\langle \mathscr{R}_\omega\rangle^{\omega} - \frac{1}{\varepsilon_\gamma+\varepsilon_\omega}\boldsymbol{\nabla}.\langle \hat{c}_\gamma\mathbf{v}_\gamma\rangle \qquad \text{(C.11)}
\end{aligned}
$$

D

INTRODUCTION ET CONCLUSION EN FRANÇAIS

D.1 CONTEXTE - BIODÉGRADATION EN MILIEUX POREUX

L'eau est un élément indispensable à toute forme de vie, et particulièrement aux hommes. Les activités humaines requièrent déjà des quantités d'eau considérables et, de manière évidente, la consommation a tendance à augmenter avec la croissance de la population mondiale. Malheureusement, l'eau douce est relativement rare sur Terre, et la quantité de produits chimiques qui la polluent est aussi positivement corrélée à la taille de la population. Quelques exemples d'une telle pollution sont illustrés ci-dessous :

- L'agriculture génère des quantités considérables de polluants organiques et inorganiques tels que des insecticides, des herbicides, des nitrates ou des phosphates.
- Des produits chimiques, comme des solvants, des détergents, des métaux lourds, des huiles qui sont présents sur des déchetteries illégales peuvent atteindre les réserves d'eau souterraine. Par exemple, de grandes quantités de systèmes électroniques en provenance d'Europe ou des Etats-Unis sont envoyés en Afrique [228, 185]. Ces déchets y sont rarement traités et contiennent des composés extrêmement toxiques (plomb, mercure, arsenique et autres). Ces "e-waste" représentent une source de pollution importante et une menace directe de santé publique [102].
- Certains médicaments se retrouvent en grande concentration dans les écosystèmes d'eau douce. Par exemple, les hormones présentes dans les pilules contraceptives, en particulier les estrogènes, affectent profondément les poissons, menant à un phénomène de féminisation et à l'apparition d'espèces "intersex"[136].

Par conséquent, la gestion des réserves en eau nécessite une attention particulière. Comprendre comment se comporte les polluants dans les écosystèmes d'eau douce est devenu une priorité. La zone contaminée, c'est-à-dire, le site de pollution original et la zone qui a été touchée à travers des phénomènes de transport doit être clairement

identifiée parce-qu'elle nécessite un traitement particulier. Pour atteindre cet objectif, il est nécessaire de :

1. comprendre les processus qui sont impliqués dans ces phénomènes de transport. En premier lieu, on peut imaginer que les molécules toxiques sont transportées dans les rivières et les lacs, mais il s'agit d'une image très imprécise. L'eau douce liquide se trouve principalement dans les sols et les aquifères. Le transport des polluants à travers ces formations géologiques met en jeu des phénomènes complexes incluant de la diffusion moléculaire, des mouvements de convection, des phénomènes de sorption, des réactions hétérogènes et de la dispersion.

2. mettre au point et optimiser des techniques pour la récupération et le traitement de ces polluants. Par exemple, les polluants organiques peuvent être dégradés par de nombreux microorganismes (endogènes ou exogènes). Ce phénomène, que l'on nomme habituellement biodégradation, décrit la capacité des microbes, et des bactéries en particulier, à modifier la spéciation chimique des éléments présents dans le milieu. Ces minuscules organismes peuvent rompre les chaines moléculaires de composés toxiques pour produire d'autres espèces chimiques. Quand les produits de cette réaction sont inertes ou moins toxiques, les microbes peuvent être utilisés directement pour purifier l'eau. Par exemple, les huiles pétrolières, composées de molécules aromatiques toxiques, peuvent être dégradées par une classe de bactéries hydrocarbonoclastiques (HCB) [292]. La biodégradation peut aussi produire des composés extrêmement toxiques et cela doit être pris soigneusement en considération. Par exemple, la dégradation anaérobie du perchloroethylène (PCE) peut mener à une production de trichloroethène (TCE), dichloroéthène (DCE) and chloride de vinyl (VC).

Pour réaliser ces deux tâches, les phénomènes de transport doivent être décrits quantitativement en utilisant une modélisation mathématique. Cette modélisation requiert, en général, certaines simplifications. Dans ce travail de thèse, les polluants sont traités en tant que solutés. Cela signifie qu'il y a toujours une partie de ces polluants qui est dissoute dans l'eau, même relativement peu et que les processus significatifs, en terme de transport, sont ceux associés à la portion miscible. Par exemple, les liquides denses formant une phase non-aqueuse (NAPLs) forment des blobs persistants, piégés dans la matrice poreuse, qui se dissolvent peu à peu dans l'eau. De plus, ces solutés seront considérés comme des traceurs (potentiellement réactifs). On entend par là que le contaminant est présent en relativement faibles concentrations, i.e., la densité et la viscosité de l'eau ne soit pas modifiés. C'est généralement le cas pour une large quantité de polluants, pour les NAPLs par exemple.

On a aussi besoin de caractériser l'aquifère lui-même. Pour ce faire, on peut utiliser certains traceurs non-réactifs. L'introduction de ces solutés dans les milieux aquatiques permet d'observer les courbes d'élution en effectuant des prélèvements à partir

de puits répartis autour de la zone d'introduction. On peut en tirer des informations concernant la direction de l'écoulement et l'organisation générale du milieu. Cependant, une interprétation correcte des ces données et des développements théoriques de modèles de transport requièrent des informations sur la topologie du système à une plus petite échelle. On peut, par exemple, utiliser la microtomographie à rayons X pour obtenir une images en trois dimensions de la structure poreuse à petite échelle sur des volumes relativement larges.

D.2 CONCLUSIONS GÉNÉRALES

Dans cette partie, nous proposons une synthèse des différentes conclusions propres à chaque partie. Nous souhaitons tout particulièrement replacer ce travail dans le cadre d'une stratégie plus globale. La section suivante est réservée aux différentes perspectives, et aux travaux en cours de réalisation.

Dans cette thèse, nous nous sommes intéressés aux phénomènes de transport dans des milieux poreux colonisés par du biofilm. Le travail présenté est basé sur des analyses expérimentales, théoriques et numériques qui forment une base nouvelle pour l'étude des ces systèmes complexes. Dans un premier temps, partie II, nous présentons une technique d'imagerie du biofilm dans des milieux poreux opaques. Cette avancée technique, développée entièrement durant ce travail de doctorat, utilise la microtomographie à rayons X (ou tomodensitométrie) assistée par ordinateur, en conjonction avec un choix spécifique d'agents de contraste, pour obtenir une image en trois dimensions de la répartition spatiale des trois phases (biofilm, eau et solide) avec une taille de voxel d'environ 9 µm. Cette approche s'avère très prometteuse pour étudier la croissance de biofilms dans des structures poreuses ainsi que la réponse des microorganismes à différents stimuli et conditions environnementales.

En utilisant cette information, on peut construire une stratégie de modélisation pour le transport de solutés dans des milieux poreux colonisés par du biofilm. Dans la partie I, nous présentons cette approche (MVMV) qui peut se décomposer en quatre étapes :

1. imager la croissance de biofilm dans des structures poreuses et formuler les équations qui décrivent les différents phénomènes à l'échelle du pore.

2. incorporer ces composantes dans des modèles efficaces à l'échelle du pore, par exemple, en utilisant des formulations de type Lattice-Boltzmann (e.g., [116]) et valider la description mathématique proposée.

3. moyenner les équations différentielles à l'échelle du pore pour obtenir des équations à l'échelle de Darcy (eg. parties III et IV) et calculer les propriétés effectives associées à ces modèles sur la base de la géométrie 3-D capturée par la technique d'imagerie.

4. développer les domaines de validité des différents modèles macroscopiques, et valider l'analyse théorique par des mesures à l'échelle de Darcy.

Dans cette stratégie, les équations qui sont utilisées à la petite échelle sont validées en comparant des résultats numériques directs (automates cellulaires ou modélisation cellulaire individuelle) avec les observations tri-dimensionnelles. De plus, les modèles macroscopiques sont aussi étudiés et validés avec des expériences à l'échelle de Darcy. Une telle approche, bien que fondamentale, est extrêmement complexe à appliquer. Dans notre étude, on simplifie la démarche en considérant une situation théorique pour laquelle le système d'équations décrivant les processus à l'échelle du pore est bien connu. Sur cette base, on développe un théorie pour le transport macroscopique de solutés non-réactifs et/ou biodégradés dans des milieux poreux colonisés par des biofilms. Pour filtrer l'information à l'échelle du pore, on utilise la méthode de prise de moyenne volumique, une nouvelle décomposition en moyenne plus perturbation et des analyses en terme de moments spatiaux. De nombreux modèles à l'échelle de Darcy sont présentés, ainsi que leurs domaines de validité et des illustrations numériques. Si d'autres configurations décrites par un jeu d'équations différentielles *linéaires* devaient être considérées, il serait tout à fait possible d'adapter la théorie développée dans ce manuscrit. Les travaux en cours incluent le développements d'outils numériques pour calculer les propriétés effectives sur les images 3-D obtenues.

BIBLIOGRAPHY

[1] Ahmadi, A., Quintard, M., and Whitaker, S. (1996). Large-scale properties for two-phase flow in random porous media. *J. Hydrol.*, 183:69–99. (Cited on page 125.)

[2] Ahmadi, A., Quintard, M., and Whitaker, S. (1998). Transport in chemically and mechanically heterogeneous porous media, v, two-equation model for solute transport with adsorption. *Advances in Water Resources*, 22:59–86. (Cited on pages 70, 73, 114, 119, 125, and 135.)

[3] Allegrucci, M., Hu, F., Shen, K., Hayes, J., Ehrlich, G., Post, J., and Sauer, K. (2006). Phenotypic characterization of streptococcus pneumoniae biofilm development. *Journal of Bacteriology*, 188:2325–2335. (Cited on pages 13 and 21.)

[4] Anderson, J. and McCarty, P. (1994). Model for treatment of trichloroethylene by methanotrophic biofilms. *Journal of Environmental Engineering, American Society of Civil Engineers*, 120(2):379–400. (Cited on page 34.)

[5] Andrews, J., Mason, V., Thompson, I., Stephens, G., and Marckx, G. (2006). Construction of artificially structured microbial consortia (asmc) using dielectrophoresis: Examining bacterial interactions via metabolic intermediates within environmental biofilms. *Journal of Microbiological Methods*, 64:96–106. (Cited on page 21.)

[6] Applegate, D. and Bryers, J. (1990). *Bacterial biofilm sloughing. Nutrient limitation effects. In: Physiology of immobilized cells.* Amsterdam: Elsevier. (Cited on page 15.)

[7] Arbogast, T. (1985). Derivation of the double porosity model of single phase flow via homogenization theory. *SIAM Journal on applied Mathematics*, 21:3087–3098. (Cited on pages 63 and 135.)

[8] Arbogast, T. (1988). *The double porosity model for single phase flow in naturally fractured reservoirs, in Numerical Simulation in Oil Recovery, IMA Volumes in Mathematics and Its Applications.* Springer Verlag, New York. (Cited on pages 68 and 135.)

[9] Aris, R. (1956). On the dispersion of a solute in a fluid flowing through a tube. *Proceedings of the Royal Society of London. Series A, Mathematical and Physical Sciences (1934-1990)*, 235(1200):67–77. (Cited on pages 32 and 74.)

[10] Aronson, J. (2006). Iodinated contrast media. *Meyler's Side Effects of Drugs: The International Encyclopedia of Adverse Drug Reactions and Interactions*, pages 1848–1896. (Cited on page 48.)

[11] Aspa, Y., Debenest, G., and Quintard, M. (2008). Effective dispersion in channeled biofilms. *in review for International Journal of Environment and Waste Management*. (Cited on pages 65 and 185.)

[12] Auriault, J. and Adler, P. (1995). Taylor dispersion in porous media: Analysis by multiple scale expansions. *Advances in Water Resources*, 18:217–226. (Cited on page 76.)

[13] Bakke, R., Kommedal, R., and Kalvenes, S. (2001). Quantification of biofilm accumulation by an optical approach. *Journal of Microbiology Methods*, 44(1):13–26. (Cited on page 43.)

[14] Bakke, R. and Olsson, P. (1986). Biofilm thickness measurements by light-microscopy. *Journal of Microbiology Methods*, 5(22):93–08. (Cited on page 43.)

[15] Bakonyi, S. (1931). Method of carrying out biochemical processes. (Cited on page 6.)

[16] Bardy, S., Ng, S., and Jarrell, K. (2003). Prokaryotic motility structures. *Microbiology*, 149:295–304. (Cited on page 13.)

[17] Batsale, J., Gobbé, C., and Quintard, M. (1996). *Local Non-Equilibrium Heat Transfer in Porous Media, In: Recent Research Developments in Heat, Mass and Momentum Transfer*. Research Signpost. (Cited on pages 163 and 164.)

[18] Baveye, P. (2010). Comment on comparison of bioclogging effects in saturated porous media within one- and two-dimensional flow systems by martin thullner. *Ecological Engineering*, doi:10.1016/j.ecoleng.2009.11.025. (Cited on pages 37 and 43.)

[19] Baveye, P. and Valocchi, A. (1989). An evaluation of mathematical models of the transport of biologically reacting solutes in saturated soils and aquifers. *Water Resources Research*, 25(6):1413–1421. (Cited on pages 134 and 171.)

[20] Beachey, E. (1981). Bacterial adherence: adhesin-receptor interactions mediating the attachment of bacteria to mucosal surfaces. *The Journal of infectious diseases*, 143(3):325–345. (Cited on page 15.)

[21] Beech, I., Cheung, C., Johnson, D., and Smith, J. (1996). Comparative studies of bacterial biofilms on steel surfaces using atomic force microscopy and environmental scanning electron microscopy. *Biofouling*, 10(1–3):65–77. (Cited on page 43.)

[22] Beloin, C., Valle, J., Latour-Lambert, P., Faure, P., Kzieminski, P., Balestrino, D., Haagensen, J., Molin, S., Prensier, G., Arbeille, B., and Ghigo, J. (2004). Global impact of mature biofilm lifestyle on escherichia coli k-12 gene expression. *Molecular Microbiology*, 51:659–665. (Cited on page 21.)

[23] Bensoussan, A., Lions, J., and Papanicolau, G. (1978). *Asymptotic Analysis for Periodic Structures*. North-Holland, Amsterdam. (Cited on page 35.)

[24] Bishop, P. and Rittmann, B. (1995). Modelling heterogeneity in biofilms: Report of the discussion session. *Water Science Technology*, 32:263–265. (Cited on page 25.)

[25] Blair, K., Turner, L., Winkelman, J., Berg, H., and Kearns, D. (2008). A molecular clutch disables flagella in the *Bacillus subtilis* biofilm. *Science*, 320:1636. (Cited on page 7.)

[26] Blake, G. (1963). The incidence and control of bacterial infection of dental units and ultrasonic scalers. *British Dental Journal*, 115:413. (Cited on page 6.)

[27] Böckelmann, U., Janke, A., Kühn, R., Neu, T., Wecke, J., Lawrence, J., and Szewzyk, U. (2006). Bacterial extracellular dna forming a defined network-like structure. *FEMS Microbiology Letters*, 262:31–38. (Cited on page 19.)

[28] Bonner, J. T. (2006). *Why size matters - From bacteria to blue whales*. Princeton University Press. (Cited on page 24.)

[29] Borden, R. and Bedient, P. (1986a). Transport of dissolved hydrocarbons influenced by oxygen-limited biodegradation 1. theoretical development. *Water Resources Research*, 22(13):1973–1982. (Cited on pages 33 and 132.)

[30] Borden, R., Bedient, P., Lee, M., Ward, C., and Wilson, J. (1986b). Transport of dissolved hydrocarbons influenced by oxygen-limited biodegradation 2. field application. *Water Resources Research*, 22(13):1983–1990. (Cited on pages 33 and 132.)

[31] Bourgeat, A., Quintard, M., and Whitaker, S. (1988). Comparison between homogenization theory and volume averaging method with closure problem. *Comptes Rendus de l'Académie des Sciences. Série 2*, 306:463–466. (Cited on page 76.)

[32] Boyle, E. and Finlay, B. (2003). Bacterial pathogenesis: exploiting cellular adherence. *Current Opinion in Molecular Biology*, 15(5):633–639. (Cited on page 15.)

[33] Brenner, H. (1980). Dispersion resulting from flow through spatially periodic porous media. *Philos. Trans. R. Soc. London Ser. A*, 297(1430):81–133. (Cited on pages 108, 118, and 119.)

[34] Bruijs, M., Venhuis, L., Jenner, H., Da, D., and Licine, G. (2001). Biocide optimisation using an on-line biofilm monitor. *Journal of Power Plan Chemistry*, 3(7):http://www.environmental–expert.com/Filesiogeorge.pdf. (Cited on page 7.)

[35] Brusseau, M., Jessup, R., and Rao, P. (1989). Modeling the transport of solutes influenced by multiprocess nonequilibrium. *Water Resources Research*, 25(9):1971–1988. (Cited on page 72.)

[36] Brusseau, M., Jessup, R., and Rao, P. (1992). Modeling solute transport influenced by multiprocess nonequilibrium and transformation reactions. *Water Resources Research*, 28(1):175–182. (Cited on page 145.)

[37] Bryers, J. and Characklis, W. (1982). Processes governing early biofilm formation. *Biotechnology and Bioengineering*, 24:2451–2476. (Cited on page 15.)

[38] Busscher, H., Handley, P., Rouxhet, P., Hesketh, L., and Van der Mei, H. (1991). *The relationship between structural and physico-chemical surface properties of tufted Steptococcus sanguis strains, in Microbial Surface Analysis: Structural and physico-chemical methods*. VCH Publishers Inc., New York. (Cited on page 15.)

[39] Carslaw, H. and Jaeger, J. (1946). *Conduction of Heat in Solids*. Clarendon Press, Oxford. (Cited on pages 88 and 90.)

[40] Chandesris, M. and Jamet, D. (2006). Boundary conditions at a planar fluid-porous interface for a poiseuille flow. *International Journal of Heat and Mass Transfer*, 49:2137–2150. (Cited on page 164.)

[41] Chang, C., Kemblowski, M., and Urroz, G. (1999). Transient stochastic analysis of biodegradable contaminant transport: First-order decay. *Transport in Porous Media*, 35:1–14. (Cited on page 145.)

[42] Characklis, W. (1973). Attached microbial growths-ii. frictional resistance due to microbial slimes. *Water Research*, 7:1249–1258. (Cited on page 6.)

[43] Chastanet, J. and Wood, B. (2008). The mass transfer process in a two-region medium. *Water Resources Research*, 44(doi:10.1029/2006WR005553):W05413. (Cited on pages 63, 66, 68, 72, and 125.)

[44] Chen, B. and Li, Y. (1999). Numerical modeling of biofilm growth at the pore scale. In *Proceedings of the Conference on Hazardous Waste Research*. (Cited on page 32.)

[45] Chen, V., Li, H., and Fane, A. (2004). Non-invasive observation of synthetic membrane processes - a review of methods. *Journal of Membrane Science*, 241(1):23–44. (Cited on page 48.)

[46] Chen, Y., Abriola, L., Alvarez, P., Anid, P., and Vogel, T. (1992). Modeling transport and biodegradation of benzene and toluene in sandy aquifer material: Comparisons with experimental measurements. *Water Resources Research*, 28(7):1833–1847. (Cited on page 132.)

[47] Cherblanc, F., Ahmadi, A., and Quintard, M. (2003). Two-medium description of dispersion in heterogeneous porous media: Calculation of macroscopic properties. *Water Resources Research*, 39(6):6–1. (Cited on pages 63, 70, and 135.)

[48] Cherblanc, F., Ahmadi, A., and Quintard, M. (2007). Two-domain description of solute transport in heterogeneous porous media: Comparison between theoretical predictions and numerical experiments. *Advances in Water Resources*, 30(5):1127–1143. (Cited on pages 63, 70, 72, 125, and 135.)

[49] Choi, Y. and Morgenroth, E. (2003). Monitoring biofilm detachment under dynamic changes in shear stress using layer-based particle size analysis and mass fractionation. *Water Science and Technology*, 47(5):69–76. (Cited on page 17.)

[50] Cholodny, N. (1930). Uber eine methode zur untersuchung der bodenmikroflora. *Archives of Microbiology*, 1:620. (Cited on page 5.)

[51] Chrysikopoulos, C., Kitanidis, P., and Roberts, P. (1992). Generalized Taylor-Aris moment analysis of the transport of sorbing solutes through porous media with spatially-periodic retardation factor. *Transport in Porous Media*, 7(2):163–185. (Cited on page 151.)

[52] Cirpka, O. and Kitanidis, P. (2000). An advective-dispersive streamtube approach for the transfer of conservative-tracer data to reactive transport. *Water Resources Research*, 36(5):1209–1220. (Cited on page 37.)

[53] Cirpka, O. and Kitanidis, P. (2001). Travel-time based model of bioremediation using circulation wells. *Ground Water*, 39(3):422–432. (Cited on page 37.)

[54] Clement, T., Peyton, B., Skeen, R., Jennings, D., and Petersen, J. (1997). Microbial growth and transport in porous media under denitrification conditions: experiments and simulations. *Journal of Contaminant Hydrology,*, 24:269–285. (Cited on page 32.)

[55] Coats, K. and Smith, B. (1964). Dead end pore volume and dispersion in porous media. *Society Of Petroleum Engineers Journal*, 4:73–84. (Cited on page 72.)

[56] Conn, H. (1932). The cholodny technic for the microscopic study of the soil microflora. *Zentr. Bakt. Parasitenk., Abt. II*, 87:233–239. (Cited on page 5.)

[57] Correa, A., Pande, K., Ramey, H., and Brigham, W. (1990). Computation and interpretation of miscible displacement performance in heterogeneous porous media. *SPE (Society of Petroleum Engineers) Reservoir Engineering*, 5(1). (Cited on page 72.)

[58] Cortis, A. and Birkholzer, J. (2008). Continuous time random walk analysis of solute transport in fractured porous media. *Water Resources Research*, 44:W06414. (Cited on page 135.)

[59] Costerton, J. and Lappin-Scott, H. (1995). *Microbial Biofilms*, chapter Introduction to microbial biofilms, pages 1–11. Cambridge University Press, Cambridge, UK. (Cited on page 7.)

[60] Costerton, J. W. (2007). *The Biofilm Primer - Springer series on biofilms*. Springer-Verlag Berlin Heidelberg. (Cited on pages 5, 6, 7, 11, 12, 15, 18, 20, 21, and 31.)

[61] Cowan, M., Mikx, F., and Busscher, H. (1994). Electrophoretic miobility and hemagglutination of *Treponema denticola* atcc 33520. *Colloids and Surfaces B: Biointerfaces*, 2:407–410. (Cited on page 15.)

[62] Cumberland, D. (1977). Optimum viscosity of barium suspension for use in the double contrast barium meal. *Abdominal Imaging*, 2:169–174. (Cited on page 47.)

[63] Cunningham, A., Characklis, W., Abedeen, F., and Crawford, D. (1991). Influence of biofilm accumulation on porous media hydrodynamics. *Environmental Science & Technology*, 25(7):1305–1311. (Cited on page 32.)

[64] Cunningham, A., Gerlach, R., Spangler, L., and Mitchell, A. (2009). Microbially enhanced geologic containment of sequestred supercritical CO_2. *Energy Procedia*, 1(1):3245–3252. (Cited on page 132.)

[65] Cunningham, J. and Mendoza-Sanchez, I. (2006). Equivalence of two models for biodegradation during contaminant transport in groundwater. *Water Resources Research*, 42:W02416. (Cited on pages 73, 134, 135, 145, and 171.)

[66] Cusack, F., Singh, S., McCarthy, C., Grieco, J., de Rocco, M., Nguyen, D., Lappin-Scott, H., and Costerton, J. (1992). Enhanced oil recovery: three dimensional sandpack simulation of ultramicrobacteria resuscitation in reservoir formations. *Journal of General Microbiology*, 138:647–655. (Cited on page 12.)

[67] Cushman, J. (1997). *The Physics of Fluids in Hierarchical Porous Media: Angstroms to Miles*. Kluwer Acad., Norwell, Mass. (Cited on page 35.)

[68] Cushman, J. and Ginn, T. (1993). Nonlocal dispersion in media with continuously evolving scales of heterogeneity. *Transport in Porous Media*, 13(1):123–138. (Cited on page 66.)

[69] Dagan, G. (1989). *Flow and Transport in Porous Formations*. Springer-Verlag, New York. (Cited on page 35.)

[70] Dagan, G. (1990). Transport in heterogeneous porous formations: spatial moments, ergodicity and effective dispersion. *Water Resources Research*, 26(6):1281–1290. (Cited on page 68.)

[71] Dagan, G. (1991). Dispersion of a passive solute in non-ergodic transport by steady velocity fields in heterogeneous formations. *Journal of Fluid Mechanics*, 223:197–210. (Cited on page 68.)

[72] Dahlem Workshop on Structure and Function of Biofilms (1989). *Structure and Function of Biofilms Characklis, WG, Wilderer, PA, 1989*. John Wiley and Sons, Chichester. (Cited on page 19.)

[73] Davarzani, H., Marcoux, M., and Quintard, M. (2010). Theoretical predictions of the effective thermodiffusion coefficients in porous media. *International Journal of Heat and Mass Transfer*, 53:1514–1528. (Cited on pages 76 and 127.)

[74] Davies, D. and Geesey, G. (1995). Regulation of the alginate biosynthesis gene *algC* in *Pseudomonas aeruginosa* during biofilm development in continuous culture. *Applied Evironmental Microbiology*, 61:860–867. (Cited on page 24.)

[75] Davies, D., Parsek, M., Pearson, J., Iglewski, B., Costerton, J., and Greenberg, E. (1998). The involvement of cell-to-cell signals in the development of a bacterial biofilm. *Science*, 280:295–298. (Cited on page 15.)

[76] Davit, Y., Debenest, G., Gerino, M., and Quintard, M. (2010a). Imaging biofilm in porous media using X-ray computed microtomography. *Journal of Microscopy*. (Cited on page 153.)

[77] Davit, Y., Debenest, G., Wood, B. D., and Quintard, M. (2010b). Modeling non-equilibrium mass transport in biologically reactive porous media. *Advances in Water Resources*, 33:1075–1093. (Cited on pages 102 and 110.)

[78] Davit, Y., Quintard, M., and Debenest, G. (2010c). Equivalence between volume averaging and moments matching techniques for mass transport models in porous media. *International Journal of Heat and Mass Transfer*, 53:4985–4993. (Cited on pages 109, 110, 115, 136, 148, and 172.)

[79] de Blanc, P., McKinney, D., and Speitel, G. (1996). *Advances in Porous Media, Vol. 3*. Elsevier. (Cited on page 132.)

[80] De Josselin de Jong, G. (1958). Longitudinal and transverse diffusion in granular deposits. *American Geophysical Union*, 39:67–74. (Cited on page 32.)

[81] De Smedt, F. and Wierenga, P. (1979). Mass transfer in porous media with immobile water. *Journal of Hydrology*, 41:59–67. (Cited on pages 72 and 135.)

[82] deBeer, D., Stoodley, P., Roe, F., and Lewandowski, Z. (1994). Effects of biofilm structures on oxygen distribution and mass transport. *Biotechnology Bioengineering*, 43:1131–1138. (Cited on page 21.)

[83] Debenest, G. and Quintard, M. (2008). Transport in highly heterogeneous porous media: From direct simulation to macro-scale two-equation models or mixed models. *Chemical Product and Process Modeling*, 3 : Iss. 1:Article 19. (Cited on pages 68 and 135.)

[84] Decho, A., Visscher, P., and Reid, P. (2005). Production and cycling of natural microbial extracellular polymers (eps) within a marine stromatolite. *Palaeogeography Palaeoclimatology Palaeoecology*, 219:71–88. (Cited on page 20.)

[85] Derlon, N., Massé, A., Escudié, R., Bernet, N., and Paul, E. (2007). Stratification in the cohesion of biofilms grown under various environmental conditions. *Water Research*, 42:2102–2110. (Cited on page 17.)

[86] Dong, H. and Blunt, M. (2009). Pore-network extraction from micro-computerized-tomography images. *Physical Review E*, 80(3):036307. (Cited on page 180.)

[87] Drury, W., Characklis, W., and Stewart, P. (1993). Interactions of 1 ÎŒm latex particles with pseudomonas aeruginosa biofilms. *Water Research*, 27(7):1119–1126. (Cited on page 48.)

[88] Dupin, H., Kitanidis, P., and McCarty, P. (2001). Pore-scale modelling of biological clogging due to aggregate expansion: a material mechanics approach. *Water Research*, 37(12):2965–2979. (Cited on page 32.)

[89] Dupraz, C., Visscher, P., Baumgartner, L., and Reid, R. (2004). Microbe-mineral interactions: early carbonate precipitation in a hypersaline lake (eleuthera island, bahamas). *Sedimentology*, 51:745–776. (Cited on page 20.)

[90] Dutta, L., Nuttall, H., Cunningham, A., James, G., and Hiebert, R. (2005). In situ biofilm barriers: case study of a nitrate groundwater plume. *Remediation Journal*, 15(4):101–111. (Cited on page 12.)

[91] Duval, F., Fichot, F., and Quintard, M. (2004). A local thermal non-equilibrium model for two-phase flows with phase-change in porous media. *International Journal of Heat and Mass Transfer*, 47(3):613–639. (Cited on page 135.)

[92] Dykaar, B. and Kitanidis, P. (1996). Macrotransport of a biologically reacting solute through porous media. *Water Resources Research*, 32(2):307–320. (Cited on pages 136, 145, 158, 159, 167, and 171.)

[93] Eames, I. and Bush, J. (1999). Longitudinal dispersion by bodies fixed in a potential flow. *Proceedings of the Royal Society A: Mathematical, Physical and Engineering Sciences*, 455(1990):3665–3686. (Cited on page 151.)

[94] Ebrahimi, S., Picioreanu, C., Xavier, J., Kleerebezm, R., Kreutzer, M., Kapteijn, F., Moulijn, J., and van Loosdrecht, M. (2005). Biofilm growth pattern in honeycomb monolith packings: Effect of shear rate and substrate transport limitations. *Catalysis Today*, 105:448–454. (Cited on page 16.)

[95] Elenter, D., Milferstedt, K., Zhang, W., Hausner, M., and Morgenroth, E. (2007). Influence of detachment on substrate removal and microbial ecology in a heterotrophic/autotrophic biofilm. *Water Research*, 41(20):4657–4671. (Cited on page 17.)

[96] Farhadian, M., Vachelard, C., Duchez, D., and Larroche, C. (2008). In situ bioremediation of monoaromatic pollutants in groundwater : A review. *Bioresource Technology*, 99:5296–5308. (Cited on page 21.)

[97] Field, J., Stams, A., Kato, M., and Schraa, G. (1995). Enhanced biodegradation of aromatic pollutants in cocultures of anaerobic and aerobic bacterial consortia. *Antonie van Leeuwenhoek*, 67(1):47–77. (Cited on page 132.)

[98] Fiori, A. and Bellin, A. (1999). Non-ergodic transport of kinetically sorbing solutes. *Journal of contaminant hydrology*, 40(3):201–219. (Cited on page 68.)

[99] Flemming, H. (1995). Biofouling and biocorrosion. *Chemie Ingenieur Technik*, 67:1425–1430. (Cited on page 7.)

[100] Flemming, H., Neu, T., and Wozniak, D. (2007). The eps matrix: The house of biofilm cells. *Journal of Bacteriology*, 189(22):7945–7947. (Cited on page 20.)

[101] Frankel, R., Bazylinski, D., Johnson, M., and Taylor, B. (1997). Magneto-aerotaxis in marine coccoid bacteria. *Biophysics Journal*, 73(2):994–1000. (Cited on page 13.)

[102] Frazzoli, C., Orisakwe, O., Dragone, R., and Mantovani, A. (2010). Diagnostic health risk assessment of electronic waste on the general population indeveloping countries scenarios. *Environmental Impact Assessment Review*, Article in Press, doi:10.1016/j.eiar.2009.12.004. (Cited on pages 3 and 207.)

[103] FrΦlund, B., Palmgren, R., Keiding, K., and Nielsen, P. (1996). Extraction of extracellular polymers from activated sludge using a cation exchange resin. *Water Research*, 30(8):1749–1758. (Cited on page 21.)

[104] Fujikawa, H. (1994). Diversity of the growth patterns of bacillus subtilis colonies on agar plates. *FEMS Microbiology Ecology*, 13(3):159–167. (Cited on page 26.)

[105] Furumai, H. and Rittmann, B. (1994). Interpretation of bacterial activities in nitrification filters by a biofilm model considering the knetics of soluble microbial products. *Water Science Technology*, 30(11):147–156. (Cited on page 16.)

[106] Geesey, G., Richardson, W., Yeomans, H., Irvin, R., and J. W.Costerton (1977). Microscopic examination of natural sessile bacterial populations from an alpine stream. *Canadian Journal of Microbiology*, 23:1733–1736. (Cited on page 6.)

[107] Gelhar, L., Welty, C., and Rehfeldt, K. (1992). A critical review of data on field-scale dispersion in aquifers. *Water Resources Research*, 28(7). (Cited on page 33.)

[108] Ghigo, J. (2001). Natural conjugative plasmids induce biofilm development. *Nature*, 412:442–445. (Cited on page 13.)

[109] Ghigo, J. (2003). Are there biofilm-specific physiological pathways beyond a reasonable doubt ? *Research in Microbiology*, 154:1–8. (Cited on page 13.)

[110] Gibbons, R. and van Houte, J. (1975). Dental caries. *Annual Review of Medicine*, 26:121–136. (Cited on page 6.)

[111] Gilbert, P., Maira-Litran, T., McBain, A., Rickard, A., and Whyte, F. (2002). The physiology and collective recalcitrance of microbial biofilm communities. *Advances in Microbiology and Physiology*, 46:2002–2056. (Cited on page 21.)

[112] Ginn, T., Wood, B., Nelson, K., Scheibe, T., Murphy, E., and Clement, T. (2002). Processes in microbial transport in the natural subsurface. *Advances in Water Resources*, 25(8-12):1017–1042. (Cited on pages 13 and 27.)

[113] Golfier, F., Quintard, M., Cherblanc, F., Harvey, C., Zinn, B., and Wood, B. (2007). Comparison of theory and experiment for solute transport in highly heterogeneous porous medium. *Advances in Water Resources*, 30:2235–2261. (Cited on pages 77 and 125.)

[114] Golfier, F., Wood, B., Orgogozo, L., Quintard, M., and Buès, M. (2009). Biofilms in porous media: Development of macroscopic transport equations via volume averaging with closure for local mass equilibrium conditions. *Advances in Water Resources*, 32(3):463–485. (Cited on pages 111, 135, 154, 160, 161, and 171.)

[115] Goltz, M. and Roberts, P. (1986). Three-dimensional solutions for solute transport in an infinite medium with mobile and immobile zones. *Water Resources Research*, 22(7):1139–1148. (Cited on pages 72 and 135.)

[116] Graf von der Schulenburg, D., Pintelon, T., Picioreanu, C., Van Loosdrecht, M., and Johns, M. (2008). Three-dimensional simulations of biofilm growth in porous media. *AIChE Journal*, 55(2):494–504. (Cited on pages 37, 38, 39, 175, and 209.)

[117] Graves, N., Halton, K., and Lairson, D. (2007). Economics and preventing hospital-acquired infection: broadening the perspective. *Infection Control and Hospital Epidemiology*, 28(2):178–184. (Cited on page 7.)

[118] Gray, W. (1975). A derivation of the equations for multiphase transport. *Chemical Engineering Science*, 30(3):229–233. (Cited on page 136.)

[119] Gray, W., Leijnse, A., Kolar, R., and Blain, C. (1993). *Mathematical Tools for Changing Spatial Scales in the Analysis of Physical Systems*. CRC Press: Boca Raton, FL. (Cited on pages 196 and 200.)

[120] Haggerty, R. and Gorelick, S. (1995). Multiple-rate mass transfer for modeling diffusion and surface reactions in media with pore-scale heterogeneity. *Water Resources Research*, 31(10):2383–2400. (Cited on page 71.)

[121] Haggerty, R., Harvey, C., Freiherr von Schwerin, C., and Meigs, L. (2004). What controls the apparent timescale of solute mass transfer in aquifers and soils? a comparison of experimental results. *Water Resources Research*, 40:W01510. (Cited on page 68.)

[122] Hall-Stoodley, L., Costerton, J., and Stoodley, P. (2004). Bacterial biofilms: From the natural environment to infectious diseases. *Nature Review of Microbiology*, 2:95–108. (Cited on pages 16, 18, 19, and 23.)

[123] Harvey, R., Metge, D., Kinner, N., and Mayberry, N. (1996). Physiological considerations in applying laboratory-determined buoyant densities to predictions of bacterial and protozoan transport in groundwater: Results of in-situ and laboratory tests. *Environmental Science & Technology*, 31(1):289–295. (Cited on page 27.)

[124] Hausner, M. and Wuertz, S. (1999). High rates of conjugation in bacterial biofilms as determined by quantitative in situ analysis. *Applied and Environmental Microbiology*, 65(8):3710–3713. (Cited on page 21.)

[125] Henrici, A. (1933). Studies of freshwater bacteria. i. a direct microscopic technique. *Journal of Bacteriology*, 25:277–286. (Cited on page 5.)

[126] Hentschel, E. (1925). Anwasserbiologie. *Abderhalden's Handb. der biol. Arbeitsmethod*, Abt. 9:266. (Cited on page 5.)

[127] Hilen, E. (1923). *Report on a bacteriological study of ocean slime. Report Bureau Construction and Repair*. United States Navy Department, Washington. (Cited on page 5.)

[128] Hood, S. and Zottola, E. (1995). Biofilms in food processing. *Food Control*, 6:8–18. (Cited on page 15.)

[129] Howes, F. and Whitaker, S. (1985). The spatial averaging theorem revisited. *Chemical engineering science*, 40(8):1387–1392. (Cited on pages 196 and 200.)

[130] Iltis, G., Armstrong, R., Jansik, D., Wildenschild, D., and Wood, B. (2009). Imaging biofilm architecture within porous media using synchrotron based x-ray computed microtomography. *In preparation*. (Cited on page 153.)

[131] Iltis, G., Armstrong, R., Jansik, D., Wood, B., and Wildenschild, D. (2010). Imaging biofilm architecture within porous media using synchrotron based x-ray computed microtomography. *Submitted to Water Resources Research*. (Cited on pages 44 and 59.)

[132] J. W.Costerton, Geesey, G., and Cheng, K. (1978). How bacteria stick. *Scientific American*, 238:86–95. (Cited on page 6.)

[133] James, G., Beaudette, L., and Costerton, J. (1995). Interspecies bacterial interactions in biofilms. *Journal of Industrial Microbiology*, 15:257–262. (Cited on page 21.)

[134] Jefferson, K. (2004). What drives bacteria to produce a biofilm? *FEMS Microbiology Letters*, 236:163–173. (Cited on pages 22 and 23.)

[135] Jeong, D. and Frank, J. (1994). Growth of *Listeria monocytogenes* at 10°c in biofilms with microorganisms isolated from meat and dairy processing environments. *Journal of Food Protection*, 57:576–586. (Cited on page 15.)

[136] Jobling, S., Nolan, M., Tyler, C., Brighty, G., and Sumpter, J. (1998). Widespread sexual disruption in wild fish. *Environmental Science & Technology*, 32(17):2498–2506. (Cited on pages 3 and 207.)

[137] Kadurugamuwa, J. and Beveridge, T. (1998). Delivery of the non-membrane-permeative antibiotic gentamicin into mammalian cells by using shigella flexneri membrane vesicles. *Antimicrobial Agents and Chemotherapy*, 42:1476–1483. (Cited on page 19.)

[138] Kapellos, G., Alexiou, T., and Payatakes, A. (2007). A multiscale theoretical model for diffusive mass transfer in cellular biological media. *Mathematical Biosciences*, 210:177–237. (Cited on pages 26 and 32.)

[139] Kildsgaard, J. and Engesgaard, P. (2001). Numerical analysis of biological clogging in two-dimensional sand box experiments. *Journal of Contaminant Hydrology,*, 50:261–285. (Cited on page 32.)

[140] Kindred, J. and Celia, M. (1989). Contaminant transport and biodegradation, 2, conceptual model and test simulations. *Water Resources Research*, 25(6):1149–1159. (Cited on page 33.)

[141] Kjelleberg, S. (1993). *Starvation in Bacteria*. Plenum, New York. (Cited on page 11.)

[142] Knutson, C., Valocchi, A., and Werth, C. (2006). Comparison of continuum and porescale models of nutrient biodegradation under transverse mixing conditions. *Advances in Water Resources*, 30(6–7):1421–1431. (Cited on page 32.)

[143] Knutson, C., Valocchi, A., and Werth, C. (2007). Comparison of continuum and pore-scale models of nutrient biodegradation under transverse mixing conditions. *Advances in Water Resources*, 30(6-7):1421–1431. (Cited on pages 158, 159, and 167.)

[144] Koch, D. and Brady, J. (1987). A non-local description of advection-diffusion with application to dispersion in porous media. *Journal of Fluid Mechanics Digital Archive*, 180:387–403. (Cited on pages 66 and 67.)

[145] Koch, J. and Brady, J. (1988). Anomalous diffusion in heterogeneous porous media. *Physics of Fluids*, 31:965–073. (Cited on page 66.)

[146] Kolodkin-Gal, I., Romero, D., Cao, S., Clardy, J., Kolter, R., and Losick, R. (2010). D-amino acids trigger biofilm disassembly. *Science*, 328:627. (Cited on page 7.)

[147] Kosakowski, G., Berkowitz, B., and Scher, H. (2001). Analysis of field observations of tracer transport in a fractured till. *Journal of Contaminant Hydrology*, 47:29–51. (Cited on page 72.)

[148] Kuehn, M., Hausner, M., Bungartz, H., Wagner, M., Wilderer, P., and Wuertz, S. (1998). Automated confocal laser scanning microscopy and semiautomated image processing for analysis of biofilms. *Applied Environmental Microbiology*, 64:4115–4127. (Cited on page 43.)

[149] Labbate, M., andK. S. Koh, S., Rice, S., Givskov, M., and Kjelleberg, S. (2004). Quorum sensing-controlled biofilm development in *Serratia liquefaciens* mg 1. *Journal of Bacteriology*, 186:692–698. (Cited on page 18.)

[150] Lake, L. and Hirasaki, G. (1981). Taylor's dispersion in stratified porous media. *SPE Journal*, pages 459–468. (Cited on pages 72, 73, and 113.)

[151] Landereau, P., Noetinger, B., and Quintard, M. (2001). Quasi-steady two-equation models for diffusive transport in fractured porous media: large-scale properties for densely fractured systems. *Adv. Water Resour.*, 24:863–876. (Cited on page 118.)

[152] Lappin-Scott, H. (1999). Claude e. zobell - his life and contributions to biofilm microbiology. In *8th International Symposium on Microbial Ecology*. (Cited on page 6.)

[153] Laspidou, C., Kungolos, A., and Samaras, P. (2010). Cellular-automata and individual-based approaches for the modeling of biofilm structures: Pros and cons. *Desalination*, 250:390–394. (Cited on pages 26 and 43.)

[154] Laspidou, C. and Rittmann, B. (2002). A unified theory for extracellular polymeric substances, soluble microbial products, and active and inert biomass. *Water Research*, 36:2711–2720. (Cited on page 19.)

[155] Lawrence, J., Hoyle, D. K., Costerton, J., and Caldwell, D. (1991). Optical sectioning of microbial biofilms. *Journal of Bacteriology*, 173:6558–6567. (Cited on pages 6 and 43.)

[156] Lawrence, J., Swerhone, G., Leppard, G., Araki, T., Zhang, X., West, M., and Hitchcock, A. (2003). Scanning transmission x-ray, laser scanning, and transmission electron microscopy mapping of the exopolymeric matrix of microbial biofilms. *Applied Environmental Microbiology*, 69:5543–5554. (Cited on page 7.)

[157] Leeuwenhoek, A. V. (1932). *Antony Van Leeuwenhoek and His "Little Animals"*. Dover Publications Inc. (Cited on page 5.)

[158] Lewandowksi, Z. and Stoodley, P. (1995). Flow induced vibrations, drag force, and pressure drop in conduits covered with biofilm. *Water Science Technology*, 32:19–26. (Cited on page 21.)

[159] Lewandowska, J., Szymkiewicz, A., Burzyński, K., and Vauclin, M. (2004). Modeling of unsaturated water flow in double-porosity soils by the homogenization approach. *Advances in Water Resources*, 27:283–296. (Cited on page 68.)

[160] Lewandowski, Z., Altobelli, S., and Fukushima, E. (1993). Nmr and microelectrode studies of hydrodynamics and kinetics in biofilms. *Biotechnology Progress*, 9:40–45. (Cited on page 21.)

[161] Lewandowski, Z., Altobelli, S., Majors, P., and Fukushima, E. (1992). NMR imaging of hydrodynamics near microbially colonized surfaces. *Water Science and Technology*, 26:577–584. (Cited on page 43.)

[162] Licina, G. (2001). Monitoring biofilms on metallic surfaces in real time. *CORROSION*, Paper No. 1442, NACE, Houston, TX. (Cited on page 7.)

[163] Luo, J., Cirpka, O., Fienen, M., Wu, W., Mehlhorn, T., Carley, J., Jardine, P., Criddle, C., and Kitanidis, P. (2006). Accurate predictions based on mechanistic models require knowledge of the spatial distribution of the hydraulic, chemical, and biological properties. *Journal of Contaminant Hydrology*, 83:27–41. (Cited on page 37.)

[164] Lux, R. and Shi, W. (2004). Chemotaxis-guided movements in bacteria. *Critical Reviews in Oral Biology and Medicine*, 15(4):207–220. (Cited on page 13.)

[165] Lynch, J. and Hobbie, J. (1988). *Micro-organisms in Action: Concepts and Applications in Microbial Ecology*. Blackwell Scientific Publications. (Cited on page 21.)

[166] Marle, C., Simandoux, P., Pacsirszky, J., and Gaulier, C. (1967). Etude du déplacement de fluides miscibles en milieu poreux stratifié. *Revue de l'Institut Francais du Pétrole*, 22:272–294. (Cited on pages 73 and 113.)

[167] Marsh, E., Luo, H., and Wang, H. (2003). A three-tiered approach to differentiate listeria monocytogenes biofilm-forming abilities. *FEMS Microbiology Letters*, 228:203–210. (Cited on page 20.)

[168] Marshall, K., Stout, R., and Mitchell, R. (1971). Mechanisms of the initial events in the sorbtion of marine bacteria to surfaces. *Journald of General Microbiology*, 68:337–348. (Cited on page 15.)

[169] McLean, J., Majors, P., Reardon, C., Bilskis, C., Reed, S., Romine, M., and Fredrickson, J. (2008). Investigations of structure and metabolism within *Shewanella oneidensis* mr-1 biofilms. *Journal of Microbiological Methods*, 74(1):47–56. (Cited on page 10.)

[170] Megee, R., Kinoshita, S., Fredrickson, A., and Tsuchiya, H. (1970). Differentiation and product formation in molds. *Biotechnology and Bioengineering*, 12(5):771–801. PMID: 5489783. (Cited on page 145.)

[171] Mermillod-Blondin, F., Gaudet, J., Gerino, M., Desrosiers, G., José, J., and Creuzé des Châtelliers, M. (2004). Relative influence of bioturbation and predation on organic matter processing in river sediments: a microcosm experiment. *Freshwater Biology*, 49(7):895–912. (Cited on page 32.)

[172] Meunier, A. and Williamson, K. (1981). Packed bed biofilm reactors: Simplified model. *Journal of the Environmental Engineering Division*, 107(2):307–317. (Cited on page 132.)

[173] Miller, C., Poirier-McNeill, M., and Mayer, A. (1990). Dissolution of trapped nonaqueous phase liquids : Mass transfer characteristics. *Water Resources Research*, 26(11):2783–2796. (Cited on page 33.)

[174] Mitchell, A., Phillips, A., Hiebert, R., Gerlach, R., Spangler, L., and Cunningham, A. (2009). Biofilm enhanced geologic sequestration of supercritical CO_2. *International Journal of Greenhouse Gas Control*, 3(1):90–99. (Cited on page 132.)

[175] Molz, F., Widdowson, M., and Benefield, L. (1986). Simulation of microbial growth dynamics coupled to nutrient and oxygen transport in porous media. *Water Resources Research*, 22(8):1207–1216. (Cited on page 134.)

[176] Morgenroth, E. and Wilderer, P. (2000). Influence of detachment mechanisms on competition in biofilms. *Water Research*, 34(2):417–426. (Cited on page 17.)

[177] Moyne, C. (1997). Two-equation model for a diffusive process in porous media using the volume averaging method with an unsteady-state closure. *Advances in Water Resources*, 20(2-3):63–76. (Cited on pages 66, 71, 75, 87, and 109.)

[178] Moyne, C., Didierjean, S., Amaral Souto, H., and da Silveira, O. (2000). Thermal dispersion in porous media: one-equation model. *International Journal of Heat and Mass Transfer*, 43:3853–3867. (Cited on pages 74, 81, 85, 109, 110, and 172.)

[179] MΦller, S., Korber, D., Wolfaardt, G., Molin, S., and Caldwell, F. (1997). Impact of nutrient composition on a degradative biofilm community. *Applied Environmental Microbiology*, 63:2432–2438. (Cited on page 21.)

[180] Murga, R., Foster, T., Brown, E., Pruckler, J., Fields, B., and Donlan, R. (2001). The role of biofilms in the survival of *Legionella pneumophilia* in a model potable water system. *Microbiology*, 147:3121–3126. (Cited on page 21.)

[181] Murphy, E. and Ginn, T. (2000). Modeling microbial processes in porous media. *Hydrogeology Journal*, 8:142–158. (Cited on page 132.)

[182] Muto, Y. and Goto, S. (1986). Transformation by extrecellular DNA produced by *Pseudomonas Aeruginosa*. *Microbiology and Immunology*, 30(7):621–628. (Cited on page 19.)

[183] Nichols, W. (1991). Biofilms, antibiotics, and penetration. *Review Medical Microbiology*, 2:177–181. (Cited on page 21.)

[184] Nivens, D., Chambers, J., Anderson, T., Tunlid, A., Smit, J., and White, D. (1993). Monitoring microbial adhesion and biofilm formation by attenuated total reflection fourier-transform infrared-spectroscopy. *Journal of Microbiology Methods*, 17(3):199–213. (Cited on page 43.)

[185] Nnorom, I. and Osibanjo, O. (2008). Electronic waste (e–waste): Material flows and management practices in nigeria. *Waste Management*, 28(8):1472–1479. (Cited on pages 3 and 207.)

[186] Noetinger, B., Estebenet, T., and Quintard, M. (2001). Up-scaling flow in fractured media: Equivalence between the large scale averaging theory and the continuous time random walk method. *Transport in Porous Media*, 43:581–596. (Cited on pages 76 and 118.)

[187] Nuñez, M., Martin, M., Chan, P., and Spain, E. (2005). Predation, death, and survival in a biofilm: *Bdellovibrio* investigated by atomic force microscopy. *Colloids and Surfaces B: Biointerfaces*, 42:263–271. (Cited on page 21.)

[188] Ochoa, J., Stroeve, P., and Whitaker, S. (1986). Diffusion and reaction in cellular media. *Chemical Engineering Science*, 41(12):2999–3013. (Cited on pages 70 and 141.)

[189] Ochoa Chaves, J. (2009). *Analyse de l'influence de l'hydrodynamique locale sur le détachement des biofilms*. PhD thesis, INSA Toulouse. (Cited on page 16.)

[190] Ochoa-Tapia, J., Stroeve, P., and Whitaker, S. (1994). Diffusive transport in two-phase media: Spatially periodic models and maxwell's theory for isotropic and anisotropic systems, chem. *Engineering Science*, 49:709–726. (Cited on pages 82 and 151.)

[191] Orgogozo, L., Golfier, F., Buès, M., and Quintard, M. (2010). Upscaling of transport processes in porous media with biofilms in non-equilibrium conditions. *Accepted for publication in Advances in Water Resources*. (Cited on page 135.)

[192] Parker, J. and Valocchi, A. (1986). Constraints on the validity of equilibrium and first-order kinetic transport models in structured soils. *Water Resources Research*, 22(3):399–407. (Cited on page 71.)

[193] Parry, J. (2005). Sugarcoated bacteria: wolves in sheeps' clothing? *Microbiology Today*, February:18–21. (Cited on page 17.)

[194] Patti, J., Allen, B., McGavin, M., and Hook, M. (1994). Mscramm-mediated adherence of microorganisms to host tissues. *Annual Review of Microbiology*, 48:585–617. (Cited on page 23.)

[195] Picioreanu, C. (1999). *Multidimensional modeling of biofilm structure*. PhD thesis, Polytechnic Institute, Bucharest, Romania. (Cited on page 16.)

[196] Picioreanu, C., Loosdrecht, M. V., and Heijnen, J. (1999). Discrete-differential modelling of biofilm structure. *Water Science and Technology*, 39(7):115–122. (Cited on page 16.)

[197] Picioreanu, C., van Loosdrecht, M., and Heijnen, J. (1998). Mathematical modeling of biofilm structure with a hybrid differential-discrete cellular automaton approach. *Biotechnology and Bioengineering*, 58(1):101–116. (Cited on page 16.)

[198] Picioreanu, C., Van Loosdrecht, M., and Heijnen, J. (2000). Effect of diffusive and convective substrate transport on biofilm structure formation: A two-dimensional modeling study. *Biotechnology and Bioengineering*, 69(5):504–515. (Cited on pages 132 and 141.)

[199] Pickup, G., Ringrose, P., Jensen, J., and Sorbie, K. (1994). Permeability tensors for sedimentary structures. *Mathematical Geology*, 26(2):227–250. (Cited on page 151.)

[200] Plouraboué, F., Cloetens, P., Fonta, C., Steyer, A., Lauwers, F., and Marc-Vergnes, J. (2004). X-ray high-resolution vascular network imaging. *Journal of Microscopy*, 215:139–148. (Cited on page 47.)

[201] Potter, K., Kleinberg, R., McFarland, E., and Brockman, F. (1996). Assay for bacteria in porous media by diffusion-weighted NMR. *Journal of Magnetic Resonance B*, 113(1):9–15. (Cited on page 43.)

[202] Prat, M. (1989). On the boundary conditions at the macroscopic level. *Transport in Porous Media*, 4:259–280. (Cited on page 163.)

[203] Priester, J., Horst, A., Van De Werfhorst, L., Saleta, J., Mertes, L., and Holden, P. (2007). Enhanced visualization of microbial biofilms by staining and environmental scanning electron microscopy. *Journal of Microbiology Methods*, 68(3):577–587. (Cited on page 43.)

[204] Prigent-Combaret, C. and Lejeune, P. (1999). Monitoring gene expression in biofilms. *Methods in Enzymology*, 310:56–79. (Cited on pages 15 and 23.)

[205] Quintard, M., Cherblanc, F., and Whitaker, S. (2001). Dispersion in heterogeneous porous media: One-equation non-equilibrium model. *Transport in Porous Media*, 44(1):181–203. (Cited on pages 72, 73, 74, 109, 110, 111, 112, 115, 144, 148, and 172.)

[206] Quintard, M. and Whitaker, S. (1994a). Convection, dispersion, and interfacial transport of contaminants: Homogeneous porous media. *Advances in Water Resources*, 17(4):221–239. (Cited on page 177.)

[207] Quintard, M. and Whitaker, S. (1994b). Transport in ordered and disordered porous media i: The cellular average and the use of weighting functions. *Transport in Porous Media*, 14(2):163–177. (Cited on page 80.)

[208] Quintard, M. and Whitaker, S. (1994c). Transport in ordered and disordered porous media ii: Generalized volume averaging. *Transport in Porous Media*, 14(2):179–206. (Cited on pages 80 and 144.)

[209] Quintard, M. and Whitaker, S. (1994d). Transport in ordered and disordered porous media iii: Closure and comparison between theory and experiment. *Transport in Porous Media*, 15(1):31–49. (Cited on page 80.)

[210] Quintard, M. and Whitaker, S. (1994e). Transport in ordered and disordered porous media iv: Computer generated porous media for three-dimensional systems. *Transport in Porous Media*, 15(1):51–70. (Cited on page 80.)

[211] Quintard, M. and Whitaker, S. (1994f). Transport in ordered and disordered porous media v: Geometrical results for two-dimensional systems. *Transport in Porous Media*, 15(2):183–196. (Cited on page 80.)

[212] Quintard, M. and Whitaker, S. (1995). Aerosol filtration: An analysis using the method of volume averaging. *Journal of Aerosol Science*, 26:1227–1255. (Cited on page 27.)

[213] R. M.Donlan and Costerton, J. (2002). Bioflms: survival mechanisms of clinically relevant microorganisms. *Clinical Microbiology Review*, 15:167–193. (Cited on pages 13 and 16.)

[214] Ram, R., VerBerkmoes, N., Thelen, M., Tyson, G., Baker, B., Blake, R., Shah, M., Hettich, R., and Banfield, J. (2005). Community proteomics of a natural microbial biofilm. *Science*, 308:1915. (Cited on page 7.)

[215] Rasmussen, B. (2000). Filamentous microfossils in a 3,235-millionyear-old volcanogenic massive sulphide deposit. *Nature*, 405:676–679. (Cited on page 12.)

[216] Renard, P. and de Marsily, G. (1997). Calculating equivalent permeability: a review. *Advances in Water Resources*, 20(5-6):253–278. (Cited on page 151.)

[217] Reysenbach, A. and Cady, S. (2001). Microbiology of ancient and modern hydrothermal systems. *Trends in Microbiology*, 9:79–86. (Cited on page 12.)

[218] Rifai, H. and Bedient, P. (1990). Comparison of biodegradation kinetics with an instantaneous reaction model for groundwater. *Water Resources Research*, 26(4):637–645. (Cited on page 34.)

[219] Rittmann, B. (1993). The significance of biofilms in porous media. *Water Resources Research*, 29(7):2195–2202. (Cited on pages 32 and 134.)

[220] Rittmann, B. and McCarty, P. (1980). Model of steady-state-biofilm kinetics. *Biotechnology and Bioengineering*, 22(11):2343–2357. (Cited on page 132.)

[221] Rittmann, B. and McCarty, P. (2001). *Environmental Biotechnology: Principles and Aplications*. McGraw-Hill, New York. (Cited on pages 24 and 134.)

[222] Riva, M., Guadagnini, A., Bodin, J., and Delay, F. (2009). Characterization of the hydrogeological experimental site of poitiers (france) by stochastic well testing analysis. *Journal of Hydrology*, 369:154–164. (Cited on page 37.)

[223] Rockhold, M., Yarwood, R., Niemet, M., Bottomley, P., Brockman, F., and Selker, J. (2007). Visualization and modelling of the colonization dynamics of a bioluminescent bacterium in variably saturated, translucent quartz sand. *Advances in Water Resources*, 30:1593–1607. (Cited on page 32.)

[224] Saffman, P. (1959). A theory of dispersion in porous media. *Journal of Fluid Mechanics*, 6:321–349. (Cited on page 32.)

[225] Sauer, K. and Camper, A. (2001). Characterization of phenotypic changes in pseudomonas putida in response to surface-associated growth. *Journal of Bacteriology*, 183:6579–6589. (Cited on pages 13 and 21.)

[226] Sauer, K., Camper, A., Ehrlich, G., Costerton, J., and Davies, D. (2002). Pseudomonas aeruginosa displays multiple phenotypes during development as a biofilm. *Journal of Bacteriology*, 184:1140–1154. (Cited on pages 13, 16, and 21.)

[227] Scow, K. and Hicks, K. (2005). Natural attenuation and enhanced bioremediation of organic contaminants in groundwater. *Current Opinion in Biotechnology*, 16(3):246–253. (Cited on page 132.)

[228] Selva, M. (Thursday, 21 September 2006). Toxic shock: How western rubbish is destroying africa. *The Independent*. (Cited on pages 3 and 207.)

[229] Seymour, J., Codd, S., Gjersing, E., and Stewart, P. (2004a). Magnetic resonance microscopy of biofilm structure and impact on transport in a capillary bioreactor. *Journal of Magnetic Resonance*, 167(2):322–327. (Cited on pages 43 and 153.)

[230] Seymour, J., Gage, J., Codd, S., and Guerlach, R. (2004b). Anomalous fluid transport in porous media induced by biofilm growth. *Physical Review Letters*, 93(19):198103. (Cited on page 43.)

[231] Seymour, J., Gage, J., Codd, S., and Guerlach, R. (2007). Magnetic resonance microscopy of biofouling induced scale dependent transport in porous media. *Advances in Water Resources*, 30(6–7):1408–1420. (Cited on page 43.)

[232] Shafahi, M. and Vafai, K. (2009). Biofilm affected characteristics of porous structures. *International Journal of Heat and Mass Transfer*, 52(3–4):574–581. (Cited on page 32.)

[233] Shapiro, M. and Brenner, H. (1986). Taylor dispersion of chemically reactive species: Irreversible first-order reactions in bulk and on boundaries. *Chemical Engineering Science*, 41:1417. (Cited on pages 158, 159, 167, and 171.)

[234] Shemesh, H., Goertz, D., van der Sluis, L., de Jong, N., Wu, M., and Wesselink, P. (2007). High frequency ultrasound imaging of a single-species biofilm. *Journal of Dentistry*, 35(8):673–678. (Cited on page 43.)

[235] Singh, R., Paul, D., and Jain, R. (2006). Biofilms: implications in bioremediation. *Trends in Microbiology*, 14(9):389–397. (Cited on page 132.)

[236] Smoot, L. and Pierson, M. (1998). Effect of environmental stress on the ability of *Listeria monocytogenes* scott a to food contact surfaces. *Journal of Food Protection,*, 61(10):1293–1298. (Cited on page 15.)

[237] Souadnia, A., Didierjean, S., and Moyne, C. (2002). Transient dispersion in porous media: A comparison between exact and approximate solutions in a case study. *Transport in Porous Media*, 47:245–277. (Cited on pages 71, 75, 81, 85, 87, and 109.)

[238] Stewart, P. (1993). A model of biofilm detachment. *Biotechnology Bioengineering*, 41:111–117. (Cited on pages 16 and 17.)

[239] Stewart, P. and Costerton, J. (2001a). Antibiotic resistance of bacteria in biofilms. *The Lancet*, 358:135–138. (Cited on page 13.)

[240] Stewart, P. and Costerton, J. (2001b). Antibiotic resistance of bacteria in biofilms. *Lancet*, 358:135–138. (Cited on page 21.)

[241] Stoodley, P., deBeer, D., and Lewandowski, Z. (1994). Liquid flow in biofilm systems. *Applied Environmental Microbiology*, 60:2711–2716. (Cited on pages 21 and 48.)

[242] Stoodley, P., Dodds, I., De Beer, D., Scott, H., and Boyle, J. (2005). Flowing biofilms as a transport mechanism for biomass through porous media under laminar and turbulent conditions in a laboratory reactor system. *Biofouling*, 21(3–4):161–168. (Cited on page 32.)

[243] Suci, P., Mittelman, M., Yu, F., and Geesey, G. (1994). Investigation of ciprofloxacin penetration into pseudomonas aeruginosa biofilms. *Antimicrobial Agents and Chemotherapy*, 38:2125–2133. (Cited on page 21.)

[244] Sun, Y. and Lu, X. (2005). A screening model for evaluating the degradation and transport of mtbe and other fuel oxygenates in groundwater. *Transport in Porous Media*, 60:75–88. (Cited on page 145.)

[245] Sutherland, I. (2001a). Biofilm exopolysaccharides: A strong and sticky framework. *Microbiology*, 147:3–9. (Cited on page 19.)

[246] Sutherland, I. (2001b). The biofilm matrix - an immobilized but dynamic microbial environment. *Trends in Microbiology*, 9:222–227. (Cited on page 19.)

[247] Sykes, J., Soyupak, S., and Farquhar, G. (1982). Modeling of leachate organic migration and attenuation in groundwaters below sanitary landfills. *Water Resources Research*, 18(1):135–145. (Cited on page 33.)

[248] Taylor, G. (1953). Dispersion of soluble matter in solvent flowing slowly through a tube. *Proceedings of the Royal Society of London. Series A, Mathematical and Physical Sciences (1934-1990)*, 219(1137):186–203. (Cited on pages 32 and 74.)

[249] Taylor, G. (1954). Conditions under which dispersion of a solute in a stream of solvent can be used to measure molecular diffusion. *Proceedings of the Royal Society A: Mathematical and PhysicalSciences*, 225:473–477. (Cited on page 74.)

[250] Taylor, S. and Jaffé, P. (1990). Biofilm growth and the related changes in the physical properties of a porous medium, 1, experimental investigation. *Water Resources Research*, 26(9):2153–2159. (Cited on page 32.)

[251] Telgmann, U., Horn, H., and Morgenroth, E. (2004). Influence of growth history on sloughing and erosion from biofilms. *Water Research*, 38(17):3671–3684. (Cited on pages 17 and 32.)

[252] Thar, R. and Kü, M. (2002). Conspicuous veils formed by vibroid bacteria in sulfidic mine sediment. *Applied Environmental Microbiology*, 68:6310–6320. (Cited on page 20.)

[253] Thomasson, H. (1925). Methoden zur untersuchung der mikrophyte, usw. *Abderhalden's Handb. der biol. Arbeitsmethod*, Abt. 9:266. (Cited on page 5.)

[254] Thullner, M. (2010a). Comparison of bioclogging effects in saturated porous media within one- and two-dimensional flow systems. *Ecological Engineering*, 36(2):176–196. (Cited on page 43.)

[255] Thullner, M. (2010b). Response to comment on comparison of bioclogging effects in saturated porous media within one- and two-dimensional flow systems by martin thullner by philippe baveye. *Ecological Engineering*, doi:10.1016/j.ecoleng.2009.12.015. (Cited on page 43.)

[256] Thullner, M., Schroth, M., Zeyer, J., and Kinzelbach, W. (2004). Modeling of a microbial growth experiment with bioclogging in a two-dimensional saturated porous media flow field. *Journal of Contaminant Hydrology,*, 70:37–62. (Cited on page 32.)

[257] Tiwari, S. and Bowers, K. (2001). Modeling biofilm growth for porous media applications. *Mathematical and Computer Modelling,*, 33:299–319. (Cited on page 32.)

[258] Tolker-Nielsen, T., Brinch, U., Ragas, P., Andersen, J., Jacobsen, C., and Molin, S. (2000). Development and dynamics of *Pseudomonas* sp. biofilms. *Journal of Bacteriology*, 182:6482–6489. (Cited on page 18.)

[259] Valdès-Parada, F., Goyeau, B., and Ochoa-Tapia, J. (2006). Diffusive mass transfer between a microporous medium and an homogeneous fluid: Jump boundary conditions. *Chemical Engineering Science*, 61:1692–1704. (Cited on pages 163 and 164.)

[260] Valocchi, A. (1985). Validity of the local equilibrium assumption for modeling sorbing solute transport through homogeneous soils. *Water Resources Research*, 21(6). (Cited on page 111.)

[261] Van der Mei, H., Handley, P., Bos, R., and Busscher, H. (1998). *Structural and physico-chemical factors in oral microbial adhesive mechanisms. In Oral Biofilms and Plaque Control.* Harwood Academic Publishers, Amsterdam, The Netherlands. (Cited on page 15.)

[262] van Loosdrecht, M., Eikelboom, D., Gjaltema, A., Mulder, A., Tijhuis, L., and Heijnen, J. (1995). Biofilm structures. *Water Science Techonlogy*, 8:35–43. (Cited on pages 16 and 17.)

[263] van Loosdrecht, M., Picioreanu, C., and Heijnen, J. (1997). A more unifying hypothesis for the structure of microbial biofilms. *FEMS Microbiology Ecology*, 24:181–183. (Cited on page 17.)

[264] Vandevivere, P. and Baveye, P. (1992). Saturated hydraulic conductivity reduction caused by aerobic bacteria in sand columns. *Soil Science Society of America Journal*, 156:1–13. (Cited on page 32.)

[265] Velimirov, B. (2001). Nanobacteria, ultramicrobacteria and starvation forms: A search for the smallest metabolizing bacterium. *Microbes and Environments*, 16:67–77. (Cited on page 12.)

[266] Vieira, M., Melo, L., and Pinheiro, M. (1993). Biofilm formation: Hydrodynamic effects on internal diffusion and structure. *Biofouling*, 7(1):67–80. (Cited on page 32.)

[267] Walker, J. and Marsh, P. (2004). A review of biofilms and their role in microbial contamination of dental unit water systems (duws). *International Biodeterioration and Biodegradation*, 54:87–98. (Cited on pages 6 and 15.)

[268] Wang, J. and Kitanidis, P. (1999). Analysis of macrodispersion through volume averaging: comparison with stochastic theory. *Stochastic Environmental Research and Risk Assessment (SERRA)*, 13(1):66–84. (Cited on page 151.)

[269] Wanner, O., Cunningham, A., and Lundman, R. (1995). Modeling biofilm accumulation and mass transport in a porous medium under high substrate loading. *Biotechnology Bioengineering*, 47:703–712. (Cited on page 27.)

[270] Wanner, O., Eberl, H., Morgenroth, E., Noguera, D., Picioreanu, C., Rittmann, B., and Loosdrecht, M. V. (2006). *Mathematical Modeling of Biofilms*. IWA Scientific and Technical Report No.18, IWA Publishing. (Cited on page 36.)

[271] Wanner, O. and Gujer, W. (1986). A multispecies biofilm model. *Biotechnology Bioengineering*, 28:314–328. (Cited on page 27.)

[272] Westall, F., de Wit, M., Dann, J., van der Gaast, S., de Ronde, C., and Gerneke, D. (2001). Early archean fossil bacteria and biofilms in hydrothermally-influenced sediments from the barberton greenstone belt, south africa. *Precambrian Research*, 106(1):93–116. (Cited on page 12.)

[273] Whitaker, S. (1981). *Introduction to fluid mechanics*. Malabar, FL, USA:R.E. Krieger. (Cited on pages 196 and 199.)

[274] Whitaker, S. (1999). *The method of volume averaging*. Kluwer Academic Publishers. (Cited on pages 35, 82, 111, 118, 135, 151, 197, and 200.)

[275] Whitchurch, C., Tolker-Nielsen, T., Ragas, P., and Mattick, J. (2002). Extracellular dna required for bacterial biofilm formation. *Science*, 295(5559):1487. (Cited on page 19.)

[276] White, D., Flemming, C., Leung, K., and Macnaughton, S. (1998). In situ microbial ecology for quantitative appraisal, monitoring, and risk assessment of pollution remediation in soils, the subsurface, the rhizosphere and in biofilms. *Journal of Microbiological Methods*, 32(2):93–105. (Cited on page 132.)

[277] Williamson, K. and McCarty, P. (1976a). A model of substrate utilization by bacterial films. *Journal of the Water Pollution Control Federation*, 48(1):9–24. (Cited on pages 32 and 132.)

[278] Williamson, K. and McCarty, P. (1976b). Verification studies of the biofilm model for bacterial substrate utilization. *Journal of the Water Pollution Control Federation*, 48(2):281–296. (Cited on page 132.)

[279] Wimpenny, J. and Colasanti, R. (1997a). A unifying hypothesis for the structure of microbial biofilms based on cellular automaton models. *FEMS Microbiology Ecology*, 22:1–16. (Cited on page 16.)

[280] Wimpenny, J. and Colasanti, R. (1997b). A unifying hypothesis for the structure of microbial biofilms based on cellular automaton models. *FEMS Microbiology Letters*, 22:1–16. (Cited on page 26.)

[281] Winogradsky, S. (1928). The direct method in soil microbiology and its application to the study of nitrogen fixation. *Soil Science*, 25:37–43. (Cited on page 5.)

[282] Wood, B. (2009). The role of scaling laws in upscaling. *Advances in Water Resources*, 32:723–736. (Cited on pages 36, 68, 77, 81, and 149.)

[283] Wood, B., Cherblanc, F., Quintard, M., and Whitaker, S. (2003). Volume averaging for determining the effective dispersion tensor: Closure using periodic unit cells and comparison with ensemble averaging. *Water Resources Research*, 39(1210):1029. (Cited on page 76.)

[284] Wood, B., Quintard, M., and Whitaker, S. (2002). Calculation of effective diffusivities for biofilms and tissues. *Biotechnology and Bioengineering*, 77(5):495–516. (Cited on pages 27, 135, and 139.)

[285] Wood, B. and Whitaker, S. (1998). Diffusion and reaction in biofilms. *Chemical Engineering Science*, 53(3):397–425. (Cited on pages 27, 66, 70, 132, 133, 141, and 200.)

[286] Wood, B. and Whitaker, S. (1999). Cellular growth in biofilms. *Biotechnology and Bioengineering*, 64(6):656–670. (Cited on pages 27 and 145.)

[287] Wood, B. and Whitaker, S. (2000). Multi-species diffusion and reaction in biofilms and cellular media. *Chemical Engineering Science*, 55(17):3397–3418. (Cited on pages 27, 66, 111, 133, and 139.)

[288] Wu, J., Gui, S., Stahl, P., and Zhang, R. (1997). Experimental study on the reduction of soil hydraulic conductivity by enhanced biomass growth. *Soil Science*, 162(10):741–748. (Cited on page 32.)

[289] Xavier, J., Picioreanu, C., Rani, S., van Loosdrecht, M., and Stewart, P. (2005). Biofilm-control strategies based on enzymic disruption of the extracellular polymeric substance matrix - a modelling study. *Microbiology*, 151:3817–3832. (Cited on page 16.)

[290] Xi, C., Marks, D., Schlachter, S., Luo, W., and Boppart, S. (2006). High-resolution three-dimensional imaging of biofilm development using optical coherence tomography. *Journal of Biomedical Optics*, 11(3):034001. (Cited on page 43.)

[291] Xie, H., Cook, G., Costerton, J., Bruce, G., Rose, T., and Lamont, R. (2000). Intergeneric communication in dental plaque biofilms. *Journal of Bacteriology*, 182:7067–7069. (Cited on page 15.)

[292] Yakimov, M., Timmis, K., and Golyshin, P. (2007). Obligate oil–degrading marine bacteria. *Current Opinion in Biotechnology*, 18(3):257–266. (Cited on pages 4 and 208.)

[293] Yawata, Y., Toda, K., Setoyama, E., Fukuda, J., Suzuki, H., Uchiyam, H., and Nomura, N. (2010). Monitoring biofilm development in a microfluidic device using modified confocal reflection microscopy. *Journal of Bioscience and Bioengineering*, In press. (Cited on page 11.)

[294] Young, J. and McCarty, P. (1969). The anaerobic filter for waste treatment. *Water Pollution Control Federation*, 41. PMID: 5791941. (Cited on page 132.)

[295] Zanotti, F. and Carbonell, R. (1984). Development of transport equations for multiphase system–1 : General development for two phase system. *Chemical Engineering Science*, 39(2):263–278. (Cited on pages 73, 93, 94, 101, 109, 113, 119, 135, 148, 171, and 172.)

[296] ZoBell, C. and Meyer, K. (1931). Reduction of nitrates by representatives of the brucella group. *Proceedings of the Society for Experimental Biology and Medicine*, 29:116–118. (Cited on page 5.)

[297] Zottola, E. and Sasahara, K. (1994). Microbial biofilms in the food processing. should they be a concern? *International Journal Food Microbiology*, 23:125–148. (Cited on page 15.)